THE
PHYSICAL REVIEW
A journal of experimental and theoretical physics established by E. L. Nichols in 1893

VOL. 61, NOS. 7 AND 8 APRIL 1 AND 15, 1942 SECOND SERIES

A Hypothesis as to the Origin of Cosmic Rays and Its Experimental Testing in India and Elsewhere

ROBERT A. MILLIKAN, H. VICTOR NEHER, AND WILLIAM H. PICKERING
California Institute of Technology, Pasadena, California

(Received February 9, 1942)

The hypothesis here adopted as to the mode of origin of the cosmic rays makes possible the prediction of five definite cosmic-ray bands, each of which should reach the earth in a particular latitude, and of four plateaus of unchanging cosmic-ray intensity, these plateaus being delimited by the latitudes of entrance of the successive bands. These bands will be designated as (1) a silicon band of energy 13.2 Bev, (2) an oxygen-nitrogen band of mean energy 7.1 Bev, (3) a carbon band of energy 5.6 Bev, and (4) a helium band of energy 1.9 Bev. The experimental evidence that has been so far obtained in India and elsewhere for the existence of these five bands and four plateaus may be thus summarized: The evidence seems to be excellent for the existence of the silicon band and the joint nitrogen-oxygen band, and some indications have appeared for the existence of the carbon band and the helium band. Also all of these bands are found, roughly at least, in the predicted latitudes and of right order of intensities. The evidence also appears to be good for the existence of at least three of the four above-mentioned plateaus of constant cosmic-ray intensity.

I. THE PREDICTION OF FIVE COSMIC-RAY BANDS AND FOUR PLATEAUS OF CONSTANT COSMIC-RAY INTENSITY

IT was suggested more than ten years ago, in view of the two most surprising properties of the cosmic rays, namely, (1) their enormous energies, and (2) their uniform distribution over the celestial dome, that it was difficult to conceive of any mode of origin that was at all capable of yielding such energies and such directions save the one that had been so successfully invoked since about 1905 in accounting for the otherwise inexplicably large evolution of energy by the sun and stars. Thus, for at least thirty-five years astronomers have recognized the fact that there is no way of accounting for the known evolution of heat by the sun save through the assumption that it is actually somehow radiating away its mass. Einstein in the development in 1905 of his equation $mc^2 = E$ gave quantitative expression to this hypothesis. The successes of this equation have not only now made it a universally accepted basis for astronomical calculations but the equation has not yet failed in any of the nuclear transformation phenomena, like those involved in radioactive change, in which it has been found possible to subject it to careful test. *The transformation of rest mass into other forms of energy is now the corner stone of practically all work in the field of nuclear physics.*

In 1928 Millikan and Cameron[1] used the Einstein equation, as applied to the partial annihilation of mass in the atom-building process, for the interpretation of cosmic-ray energies. This was before those energies had

[1] R. A. Millikan and G. H. Cameron, Proc. Nat. Acad. Sci. **14**, 637 (1928); Phys. Rev. **32**, 533 (1928).

become definitely known through direct measurement, and when their indirectly estimated values seemed to make the loss of mass through the building up of the heavier elements out of the lighter elements yield adequate energies from the known values of so-called "packing fractions." Beginning in 1931 this possibility was eliminated for two reasons: First, the largest energy obtainable from packing fractions in the case of any element of appreciable abundance namely, iron, was 0.48 g per g-atom, or about half a billion electron volts, but in the fall of 1931 Anderson and Millikan first measured *directly*[2] the energies of cosmic rays and found them running up above 6 Bev, much higher than could be accounted for by any possible packing fractions. This alone was definite and final. Second, precisely these same atom-building processes involving the same "packing fractions" seem now to be successfully accounting for the sun's heat.[3] If this be so one must now assume that those very processes, of *partial* annihilation through atom building, which were assumed going on *outside* the stars to account for cosmic rays, are instead going on *inside* the sun to account for its evolution of heat. But since the cosmic rays do not come from the sun or the stars one is now debarred also from using these same processes to account for them. In other words, there is abundant reason for retaining the principle, beautifully illustrated by Bowen's interpretation of the nebulium lines, that the conditions existing in interstellar space make possible at least some sorts of atomic energy transformations that are forbidden within the stars. There is, of course, no doubt about it at all in the case of the origin of the nebulium lines.

Both of the foregoing difficulties—namely, that occasioned by the enormous energies and that by the uniformity of distribution of the apparent sources—disappear if one simply reverses the former suggestions and assumes that the sun's heat is due to atom building going on in its interior while cosmic rays are due to the complete annihilation process going on in inter-

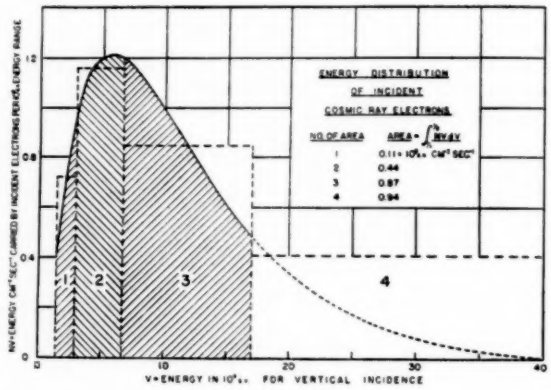

FIG. 1. The rectangular area 4 is made proportional to the total cosmic-ray energy that enters the earth at the equator. It is, in fact, the area underneath a complete cosmic-ray curve taken up to the top of the atmosphere at Madras. It is the sum of the energies of all non-field sensitive cosmic rays, no matter whether this non-field sensitiveness arises from the fact that incoming charged particles have too high an energy to be blocked off by the earth's magnetic field or whether some of the incoming rays consist of photons or neutrons which cannot, because of their nature (no matter what the energies), be affected by a magnetic field. Rectangle 4 then represents the total cosmic-ray background that is uniform all over the earth's surface. The sum of the rectangular areas 1, 2, 3 represents the total energy of the field-sensitive cosmic rays. This sum is more than 60 percent of the total incoming cosmic-ray energy. This means that the cosmic rays cannot have come through an appreciable amount of matter in getting from their place of origin to the earth.

stellar space, or better to the *complete*, instead of the partial, transformation of the rest mass of the atoms into cosmic-ray energy. The question which one then faces is, how well does this last suggestion work quantitatively?

There are two definite quantitative facts that have been established, namely, (1) Fig. 1, reproduced from Phys. Rev. **53**, 859 (1938), shows a maximum of incoming "charged-particle"[4] energy somewhere between 5 Bev and

[2] R. A. Millikan and C. D. Anderson, Phys. Rev. **40**, 325 (1932); also **41**, 405 (1932) and **45**, 352 (1934); also *Electrons (+ and −), Protons, Photons, Neutrons, and Cosmic Rays* (University of Chicago Press, 1935).

[3] H. A. Bethe, Phys. Rev. **55**, 103, 434 (1939); Phys. Soc. Reports pp. 1–15 (1939).

[4] It would make no difference so far as all the results considered in this paper are concerned whether the "charged particles" are electrons, mesotrons, or protons, for at the very large energies here involved, the effect of a magnetic field is essentially the same upon them all. What is known with certainty about incoming particles is that, as shown by Bowen, Millikan and Neher [Phys. Rev. **52**, 83 (1937), and **53**, 218 (1938)], even when they have energies as high as 10 billion electron volts they *are very rapidly absorbed as soon as they get into the atmosphere*, not 1/500 of their energy being able to get down to sea level. This is as it should be for *electrons* but not normally for heavier particles, for the former, because of their extreme lightness, must be quickly "bremsed" in collisions with nuclei and thus have their energy almost completely transformed into photons which, in turn, in succeeding collisions transform their energy into electron pairs, etc., and thus proceed to fritter it away in showers. Particles like protons (2000 times heavier) on the other

10 Bev; and (2) certainly not less than, and probably much more than, 60 percent of the total incoming cosmic-ray energy is carried by these charged particles, for this is the ratio of the sum of the areas of the blocks 1, 2, 3 to that of 1, 2, 3, 4. (See table in Fig. 1.)

But now, to carry through the desired computation one must know what are the most common elements in interstellar space where the cosmic rays seem to originate. Here again another of Bowen's remarkable discoveries is ready to be called upon, for Bowen and Wise,[5] by spectroscopic observations on the ring nebulae, have recently made determinations of the relative abundance of the atoms in the spaces between the stars. Since the ring nebula studied is a light year, 6,000 billion miles or more, from the exciting star, one can scarcely fail to take their estimates of relative abundance as applying to interstellar space. Here are their results. They find that hydrogen atoms and helium atoms stand first and second in abundance, hydrogen being about ten times as abundant as helium. They find, further, four other atoms all having about the same abundance, which, however, in each case is only about one-tenth the abundance of helium. No other atoms have more than a tenth of the abundance of any of these four, and most of the rest have less than a hundredth. These four most abundant atoms are *carbon*, *nitrogen*, *oxygen*, and *silicon*.[5] The predominant abundance of these four atoms is also in line with their known structures and stabilities.

Now, the rest mass energy of the hydrogen atom comes out by Einstein's equation just a little less than one Bev (accurately, 938 million). If, then, this rest mass is capable of being transformed completely into cosmic rays, since the momentum principle must in any case be satisfied, the only way these two conditions can be met is through the appearance of a pair of electrons or photons (in the case of hydrogen, though not in the case of the heavy atoms, deficiency in mass would bar out protons or neutrons) starting out from the point of annihilation of the rest mass of H_1 in opposite directions each of energy of about 500,000 ev. Epstein[6] has shown that an electron endowed with this energy could not get through the sun's magnetic field and reach the earth so there is no use expecting to find it here. Even if the sun's magnetic field were not strong enough to prevent its reaching the earth it could get through the earth's magnetic field only quite close to the

---

hand cannot be thus suddenly bremsed, the absorption coefficient of air for such particles being inversely proportional to the square of the mass of the particles. For this reason protons, for example, should be millions of times more penetrating than electrons. It is then impossible to reconcile the observed high absorbability of the incoming particles with masses many times greater than the mass of the electron, *unless one assumes the existence of some new kind of absorption utterly different from the bremsung-pair-formation process.*

That there must indeed be other types of absorption than that due to the shower process has been clearly pointed out (see R. A. Millikan, *Cosmic Rays* (Macmillan Company, 1939), p. 100), but we have in the past thought it much simpler to get the existing very high absorbability by adding one or more of the effects of these new processes to the large normal absorbability of electrons, rather than to violate so completely the normal and theoretically necessary high penetrability of heavier particles. This argument, however, will have to be abandoned in case it can be shown that the energy of hypothetical incoming protons is practically completely transformed into mesotrons in the upper layers of the atmosphere by one of these other types of absorption; but that, we think, involves more knowledge than is as yet available as to the relative frequencies of collisions giving rise to mesotrons and to showers.

It may be pointed out that our own curve shown in Fig. 10 (reference 7), has not the right shape at high altitudes to be due alone to the absorption of electrons by shower-production, for this would require it to be concave upward near the top of the atmosphere instead of nearly straight. In any case, however, the well established facts of mesotron formation near the top of the atmosphere must cause a marked departure from such a theoretical curve.

[5] Bowen and Wise have recently made by spectroscopic means a determination of the abundance of the elements in the nebulae and published the same in the Bull. Lick Observatory **19**, 1 (1939). Their results are shown in the accompanying table in which the figures given in the abundance columns are the exponents required to indicate the number of atoms in a given volume of space. Thus the number 11 following hydrogen means 10^{11} hydrogen atoms, while the number 9 opposite carbon means 10^9 carbon atoms, etc. The uncertainty sign $\leqslant$ associated

Element	Abundance	Element	Abundance	Element	Abundance
H	11 −	Ne	8	K	6 +
He	10	Na	$\leqslant$7 +	Ca	7 −
Li	<8 −	Mg	7 +	Sc	<6 +
Be	<8 −	Al	$\leqslant$8 −	Ti	<7 −
B	<9	Si	$\leqslant$9	V	<8
C	9	P	<8	Cr	<7
N	9 −	S	8	Mn	<7
O	9	Cl	7 +	Fe	7 +
Fl	6	A	7		

with Si in the table is due, Bowen says, to a slight uncertainty as to whether one of the critical lines used is surely a silicon line or not, but in any case, since aluminum has an atomic weight of 27 its cosmic-ray influence would be inseparable by our tests from that of silicon (at. wt. 28), and similarly any possible effects due to phosphorus or sulphur would be so close to those of silicon as to be separately distinguishable with great difficulty. This composite influence may then for simplicity be called the hypothetical silicon band.

[6] P. S. Epstein, Phys. Rev. **53**, 862 (1938). See also L. Janossy, Zeits. f. Physik **104**, 430 (1937).

pole and, in view of its low energy, would be absorbed in the upper regions of the atmosphere where it would be undetectable by our electroscopes or counters. Again, if the rest mass of a hydrogen *molecule*, instead of a hydrogen atom, underwent such a complete transformation, it would produce two oppositely directed one-Bev electrons. This radiation also could not be detected here for the reason just given even if one makes the *very unlikely* assumption that hydrogen molecules have sufficient abundance to produce such rays in detectable amounts; but the case of a molecule is here considered since, if the possibility of the complete transformation in interstellar space of rest mass into cosmic-ray energy exists at all, there is probably no more reason for excluding molecules, or even larger aggregates, from the operation of the principle than there is for excluding such aggregates from the operation of the equipartition principle applied so successfully by their inclusion to the interpretation of the Brownian movements.

By the foregoing procedure one finds that helium atoms of atomic weight 4 would produce 2 (more accurately 1.9) billion volt cosmic rays. According to Epstein, if one takes the value of the general magnetic field of the sun at not over 16 gauss—an assumption in line with most recent work—then 2 Bev charged-particle-rays would not be barred by the sun's field from reaching the earth, and further they would be able to get through the earth's magnetic field vertically at all latitudes north of about Bismarck (Mag. lat 56.7° N). Also, if there were any incoming rays of energy between 1.9 Bev and 1.4 Bev, which is the energy required to penetrate vertically through the earth's magnetic field at Saskatoon, (Mag. lat 60° N) such rays would not be barred by the aforementioned sun's field from reaching the earth, and the total cosmic-ray energy reaching the earth at the latitude of Saskatoon and higher should be larger than that entering at the latitude of Bismarck. But if the rays found at Bismarck are in fact the hypothetical helium band then there should be no increase in cosmic-ray intensity in going north from Bismarck, and in fact there appears to be none, though still further checks on this point are being sought.

Altogether similarly, carbon rays of energy 6 (accurately 5.6) Bev would begin to get through the earth's field at about latitude 42° N, a little north of San Antonio, for at San Antonio the voltage required to get electrons down to earth vertically is 6.7 Bev. This is also very close to the latitude at which nitrogen rays of energy 7 (better 6.6) Bev would first be found as the observer moves northward from the equator. A few degrees farther south, say at about 33° or 34°, the southern edge of the oxygen cosmic-ray plateau corresponding to an energy of 8 (better 7.5) Bev would be found. Another southern edge of a wide cosmic-ray plateau corresponding to the entrance of silicon rays would be expected to appear, as one moves northward from the equator, at a magnetic latitude at which the energy required to break through the earth's magnetic field vertically is 14 (13.2) Bev and from that point down to the magnetic equator, where in India the energy required to get through vertically is 17 Bev, there should be no further change in the intensity of the incoming vertical cosmic rays. The observed edges of this succession of overlapping cosmic-ray plateaus corresponding to the energies 2, 6, 7, 8, and 14 Bev would not be expected to be sharp so long as one uses for the detecting instruments electroscopes, which respond to rays from all directions (see Fig. 2), for the computed energies correspond only to vertically incoming rays.

II. THE EXPERIMENTAL TESTING IN INDIA OF THE ABOVE PREDICTIONS

In order to test the foregoing predictions with any sort of accuracy it was obviously necessary to measure directly *vertical* incoming cosmic-ray energies as a function of latitude. It was also obvious that, if equipment for so doing were available, India was the best, indeed the only suitable, place in the world for the most significant of the tests. For while in India it takes 17 billion-volt, vertical, charged-particle rays to break through the blocking effect of the earth's magnetic field at the equator, it takes but about 13 billion to do so on the other side of the earth, i.e., in Peru, so that only in India was there any possibility of finding the latitude north of which the hypothetical silicon rays, of energy 13.2 Bev,

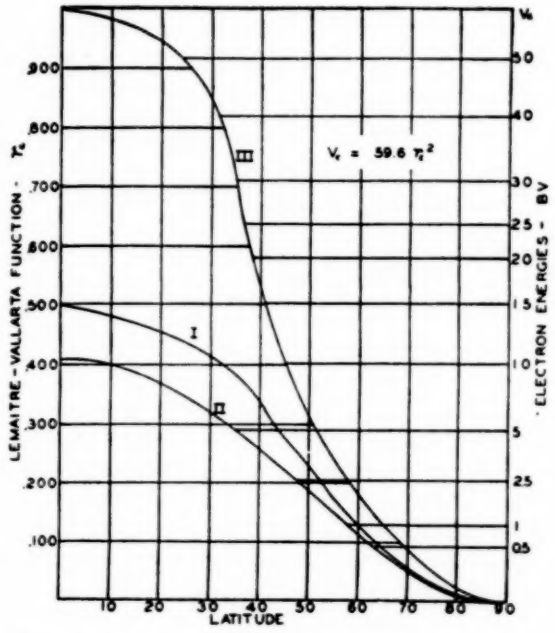

FIG. 2. The Lemaitre-Vallarta function γ_c for three directions plotted against latitude. Curve I is for the vertical direction, curve II is for the western horizon, and curve III is for the eastern horizon. Electron energies are given along the right margin. (Lemaitre and Vallarta.)

would be found and south of which they would be absent. Since, according to Bowen, there were no atoms of atomic weight between oxygen and silicon sufficiently abundant to send into the earth any appreciable cosmic-ray energy, and similarly none of atomic weight higher than silicon and of comparable abundance, one might expect to find in India a perfectly flat cosmic-ray plateau for vertical rays extending from Madura on the magnetic equator clear up to about latitude 20° where silicon rays should be able to break through vertically, and then on going still farther north one should find a sudden rise to a new plateau-level at the latitude at which this break through for silicon rays occurs.

From the Lemaitre-Vallarta curves it was estimated that the vertical energy necessary to get through at Agra (Mag. lat 17.3° N) was 15.4 Bev, and that at Peshawar, only 7.7° farther north, at 12.4 Bev. On account of some uncertainty as to the accuracy of these computations Agra was chosen as the most northerly point at which it was safe to make the test and still be fairly sure that the point of observation would be south of the latitude of entrance of the silicon band of energy 13.2 Bev and still on the hypothetical equatorial plateau. Peshawar, the most northerly city in India, was chosen as the best available place for getting north of the latitude of entrance of the hypothetical silicon band and upon the plateau between the latitudes of entrance of the silicon and the oxygen bands. For reasons of convenience Bangalore was chosen instead of Madura for making the observations on the equator, since the approximate law of change of incoming energy with latitude φ, namely, $\cos^4\varphi$ differed for $\varphi=3°$ quite immeasurably from the value for $\varphi=0$. These considerations then determined the choice of locations in India for making the tests on the incoming energies of the vertical rays.

When the measuring instruments sent to the top of the atmosphere are electroscopes or single counters which respond to rays reaching them from all directions instead of merely from the vertical, the analysis becomes much more complicated, especially in equatorial latitudes, for the Lemaitre-Vallarta curves (see Fig. 2) show that the hypothetical silicon rays of energy 13.2 Bev would be shooting through the top of the atmosphere to some extent even at the equator, and that the atmospheric ionization due to these rays would therefore increase continuously up to the latitude at which the vertical rays get down to earth, and even beyond that to some extent, clear up to a latitude of about 40° N.

As shown in the accompanying paper by Neher and Pickering[7] (see especially Figs. 1, 4, and 6), both of the foregoing predictions as to the behavior of electroscopes, single and double counters, were precisely what was found in the India experiments between the magnetic equator and magnetic latitude 25° N, so that, so far as India is concerned, the hypothetical silicon band may properly be said to predict the thus far observed latitude effects satisfactorily.

III. THE INTERPRETATION OF EARLIER SEA-LEVEL EXPERIMENTS IN THE LIGHT OF THE PRESENT HYPOTHESIS

In 1933 it was first observed[8] that there was a marked increase in the sea-level intensity of

[7] H. V. Neher and W. H. Pickering, Phys. Rev. **61**, 407 (1942).

[8] R. A. Millikan and H. V. Neher, Phys. Rev. **47**, 205 (1935).

cosmic rays in sending a recording electroscope around the world in the equatorial belt from India to Peru. Since according to the hypothesis here being tested the only one of the five hypothetical bands of cosmic rays that has the energy to get into the equatorial belt at all is the silicon band, the foregoing observation can only mean that these silicon rays that have not sufficient energy to get to earth at the equator in India, *are able to do so in Peru*. Furthermore, the energy of these rays is 13.2 Bev, while the energy needed to get in vertically in Peru has been taken for years as only 13 Bev, according to Epstein somewhat less. Hence there is nothing in the observed longitude effect that is out of line with the hypothesis under test; the decrease in the blocking effect of the earth's magnetic field in going from India to Peru is sufficient to permit the hypothetical silicon rays to get in in full strength vertically in Peru.

But again, on account of the strong absorption of the atmosphere, sea-level observations made with electroscopes certainly correspond very roughly to vertically incoming cosmic rays and should therefore exhibit, though somewhat less sharply, the series of bands and plateaus characteristic of vertical rays rather than the very gradual changes with latitude in the equatorial belt that are characteristic of electroscopes when sent up to the top of the atmosphere where rays can pass through them from all directions.

TABLE I. Electroscope discharge rates at eight-hour intervals between latitude 28° N. magnetic and 0° N. magnetic. The readings of electroscope No. 3 are more significant than those of No. 1 since in these electroscopes the sea level ionization due to the cosmic rays themselves is only about 1.6 ions, the rest being background which is seen to be much larger in No. 1 than in No. 3.

SS. Mongolia enroute Los Angeles to Balboa		SS. Ebro enroute Balboa to Mollendo	
No. 1	No. 3	No. 1	No. 3
8.70	3.86	8.64	3.82
8.84	4.02	8.51	3.85
8.97	3.88	8.39	4.19
8.73	3.79	8.92	3.77
8.63	3.78	8.37	3.80
9.02	3.76	8.43	4.15
8.57	3.68	8.66	3.99
8.57	3.96	8.38	3.93
8.60	3.85	8.66	3.91
8.70	3.96	8.53	3.95
8.53	4.18	8.54	3.97
8.93	4.33	8.84	3.99
9.09	3.84	9.18	3.89
8.54	4.18	8.37	3.86
9.14	4.02	8.35	3.90
8.69	4.18	8.61	3.97
9.03	3.94		3.81
8.64	4.23		3.92
8.80			3.85
Mean 8.77	3.97	8.586	3.92

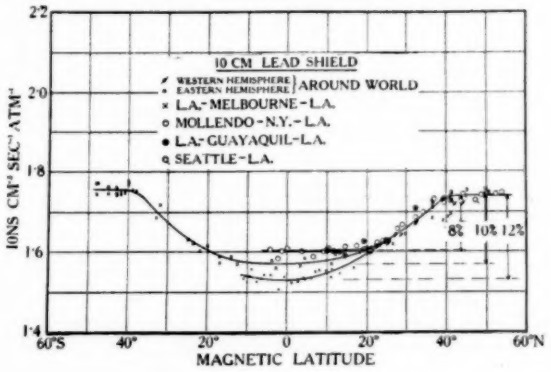

FIG. 3. The longitude effect taken with a shielded electroscope. The 12 percent equatorial dip is found in the neighborhood of India (eastern hemisphere). The 10 percent equatorial dip is found in going from Los Angeles to Melbourne. The 8 percent or 7 percent equatorial dip is found in going from Los Angeles to Guayaquil.

Since, then, the hypothetical silicon rays are already reaching the earth in Peru one may expect, in going north from Mollendo, to find at least indications of the long plateau that should exist for vertical rays between the latitude at which the silicon rays of energy 13.2 Bev can get through the earth's magnetic field and the latitude at which the next possible band of rays of lower energy, namely, oxygen rays of only 7.5 Bev, begin to get through.

In fact, Millikan and Cameron appear to have brought to light this plateau with the use of their sea-level electroscope measurements in the very first trip to South America that was undertaken in August 1926 to test for a latitude effect in cosmic rays; for they found no change at all in sea-level cosmic-ray intensity in going from about magnetic latitude 28° N, where they first got their observations under way in the wireless room of the SS. Mongolia, and the end of their journey at Mollendo just below the magnetic equator. Table I, not heretofore published, and not included at all in the data graphed in Fig. 3, gives the actual day by day series of continuous readings taken in 1926 at eight-hour intervals between about latitude 28° and latitude 0°.

But the existence of this predicted sea-level plateau is more significantly indicated by the much more careful readings shown in Fig. 3, which is reproduced here from a preceding publication[9] prepared when the authors were guided by no theory at all, but were merely trying to get as accurate observations as they could on the variation of sea-level intensities as their electroscopes were taken from Los Angeles to Mollendo, the Allan Hancock yacht, Vallero III, stopping, according to instructions, for days at a time enroute so as to get accurate observations at a given latitude.

From the results of at least the five different sea-level expeditions between Los Angeles and Mollendo recorded in Table I and the upper curve of Fig. 3 the conclusion seems justified that from the magnetic equator clear up to 20° N, or possibly even 25° N, there is a plateau of unchanging cosmic-ray intensity as measured by an electroscope at sea level. This contrasts strikingly, as the lower curve of Fig. 3 shows, with the rise between 0° and 25° found on the India side of the earth where the hypothetical silicon band should come in between these latitudes.

There is indeed in the upper curve of Fig. 3, as it is drawn, the beginning of a rise between 20° and 25° but it is, in any case, very slight and from the point of view of this hypothesis would not be there were it not for the imperfectness with which electroscopes at sea level isolate vertical rays. Indeed, for strictly vertical rays the plateau should extend up to about latitude 33° or 34° N. It is hoped in the near future to be able to present experimental tests in Mexico of this prediction.

The sea-level observations made in 1932 both by Bowen, Millikan, and Neher and by A. H. Compton brought to light with great definiteness the "cosmic-ray shelf" shown so strikingly in Fig. 3 and *which is in exactly the latitude in which it should be to indicate the entrance into the atmosphere of the hypothetical oxygen and nitrogen bands of energies 7.5 Bev and 6.6 Bev.* From the Lemaitre-Vallarta curves reproduced in Fig. 2 it is estimated that these two bands should have been able to get to the earth vertically at magnetic latitudes between 33–36 and 37–39, respectively.

However, it is to be especially noted that the flatness of the cosmic-ray sea-level plateau, which is actually found above magnetic latitude 41°, cannot be taken as indicating the absence of incoming cosmic rays of energies immediately lower than 6 Bev, since there is every evidence that 6 Bev is about the lower limit of the energy of incoming rays which have the capacity to throw appreciable influences of any kind down to sea level through the absorbing effect of the atmosphere. Other evidence from higher up in the atmosphere must then be sought for the existence of bands of carbon and of helium rays, as well as for the theoretical cosmic-ray plateau between these hypothetical carbon rays of energy 5.5 Bev and helium rays of energy 1.9 Bev.

IV. THE BEARING OF THE 1932 AIRPLANE FLIGHTS UPON THE HYPOTHESIS

Much stronger evidence for the existence of the long plateau of constant cosmic-ray intensities between the latitudes of entrance of the

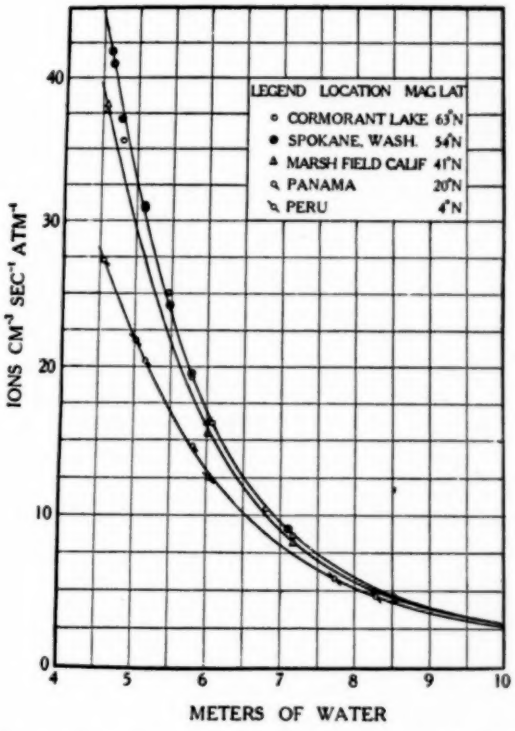

FIG. 4. The striking element in these curves is that the intensities at 4° N and at 20° N are identical all the way up, as are also those at 54° N and 63° N.

[9] R. A. Millikan and H. V. Neher, Phys. Rev. **47**, 207 (1935).

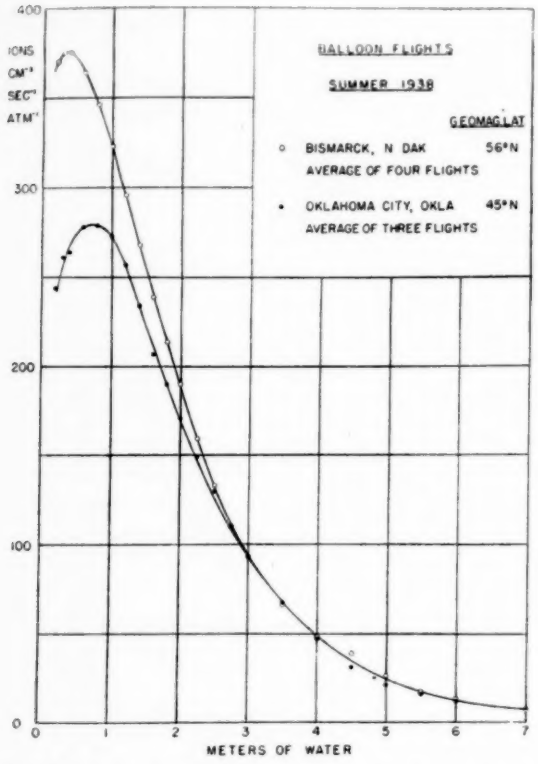

FIG. 5. The most significant element in these curves is that they seem to coincide below about 2.5 m of water, but it is to be remembered that these are electroscope readings, not double counter readings. This introduces an element of some uncertainty.

hypothetical silicon and oxygen bands is found in the records of airplane flights made in both Peru and Panama in the fall of 1932 and reproduced[10] in Fig. 4. The lower of the three curves shows that even up to the altitude of 22,000 feet one could find no difference between cosmic-ray intensities in the latitude 0° and 20° for one and the same curve is nicely fitted by the points taken at both latitudes. This is not only in marked contrast with what is found in India with electroscopes at these altitudes in going only from 0° up to 17.3° instead of from 0° to 20° (see Fig. 1 reference 7, the Agra curve being consistently above the Bangalore curve), but it could not exist if there were any rays of any appreciably larger energy than the oxygen rays coming in between the hypothetical silicon and oxygen bands. For the Lemaitre-Vallarta curves (Fig. 2) show that oxygen rays of energy 7.5 Bev could not get in at all at 20°, while any rays of energy much closer to that of the 13.2 Bev band should have been able to do so, hence arguing merely by analogy with the behavior of the silicon band in India there should certainly have been a difference between the readings in Panama and Peru, especially at 22,000-foot altitudes. *These Panama-Peru observations are, in fact, in all respects consistent with the hypothesis as to the existence of the long plateau between the latitudes of entrance of the hypothetical silicon and oxygen bands.*

Again, the readings reproduced in Fig. 4 furnish some uncertain evidence for the existence of the hypothetical carbon band. This is found in the difference between the upper curve and the intermediate one. The difference between the lower curve and the intermediate one is due to the fact that the latter is taken at a latitude (Mag. lat 41° N) a little farther north than those latitudes at which the hypothetical oxygen and nitrogen bands have been able to get through the earth's magnetic field. The fact that the differences between these curves extend down to sea level (Fig. 4) shows that these two bands have enough energy to extend their ionizing influences in small measure down that far. The fact that careful sea-level observations made by two different observers with two different instruments in the same month, September, 1932, in which the curves of Fig. 4 were taken, revealed no sea-level changes at all between Los Angeles and Vancouver, shows that no incoming rays of lower energy than those represented by the intermediate curve of Fig. 4 are able to extend any measurable influences to sea level. But the upper curve, also taken in September, 1932 at Spokane, reveals unambiguously other entering rays of sufficient energy to throw their influences between eight-tenths and nine-tenths of the way down to sea level. This is just what the hypothetical carbon rays of energy 5.5 Bev should be able to do. This is some little evidence for the existence of the carbon band which is supplemented by further data given below. It is significant, too, that all these data were taken and the curves of Fig. 4 drawn years before any such interpretations as those here given were thought of.

[10] Bowen, Millikan, and Neher, Phys. Rev. **46**, 642 (1934).

V. EVIDENCE FOR THE EXISTENCE OF HELIUM RAYS

The hypothetical helium rays could not be brought to light by any such observations as those recorded in Fig. 4, for such rays of energy but 1.9 Bev could not possibly be expected to throw their influences more than from a third to a fourth of the way through the atmosphere if nitrogen rays of energy 6.6 Bev can just extend a measurable influence to sea level. There is, then, nothing significant in the fact that the points taken at Cormorant Lake (Mag. lat 63) and Spokane (see Fig. 4) all lie on one and the same curve for the airplane flights involved extended only to 22,000 feet or to a pressure of 4.5 meters of water, so that no rays whatever that could get in north of Spokane could possibly extend their influences down far enough to be here observed. Higher altitudes must be reached before any effects of helium rays are to be expected.

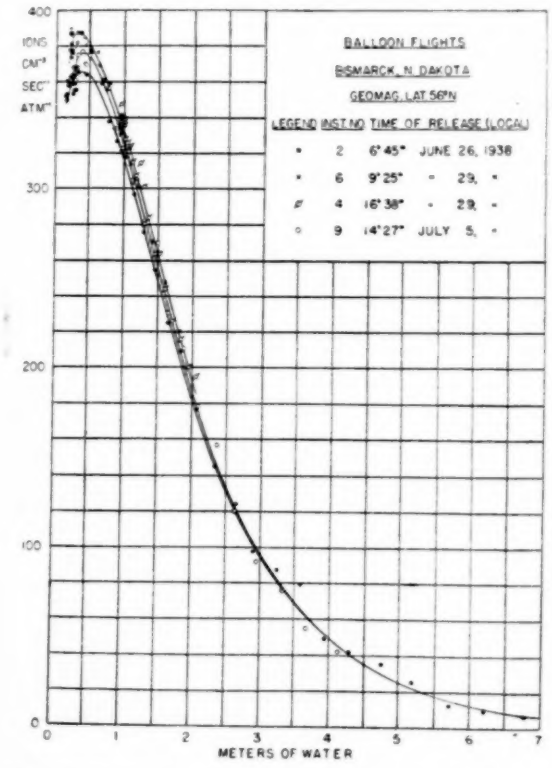

FIG. 6. These curves, all taken in the same week, reveal fluctuations in the hypothetical helium rays coming in at Bismarck. In later experiments we have found that these fluctuations, *in the case of these particular rays*, may introduce differences in readings taken *in different years* amounting to as much as 30 percent.

The best evidence for the existence of a band of helium rays is found in observations taken by Millikan and Neher in Saskatoon in the summer of 1937, and in other observations taken at Bismarck, North Dakota, and Oklahoma City in the summer of 1938. The results of the 1938 flights are presented in Fig. 5. As indicated, the points through which these curves are drawn are the mean values at each altitude obtained from the four flights at Bismarck and the three flights at Oklahoma City taken within two weeks of one another. Their consistency indicates a good degree of reliability in the curves. The curves show that somewhere between Oklahoma City, Mag. lat 45°, where we estimate that it takes 4.3 Bev to get through the earth's magnetic field vertically, and Bismarck, where it takes about 1.9 Bev to get through vertically (see the Lemaitre-Vallarta curves in Fig. 2) a new group of rays does get in which is capable, however, of

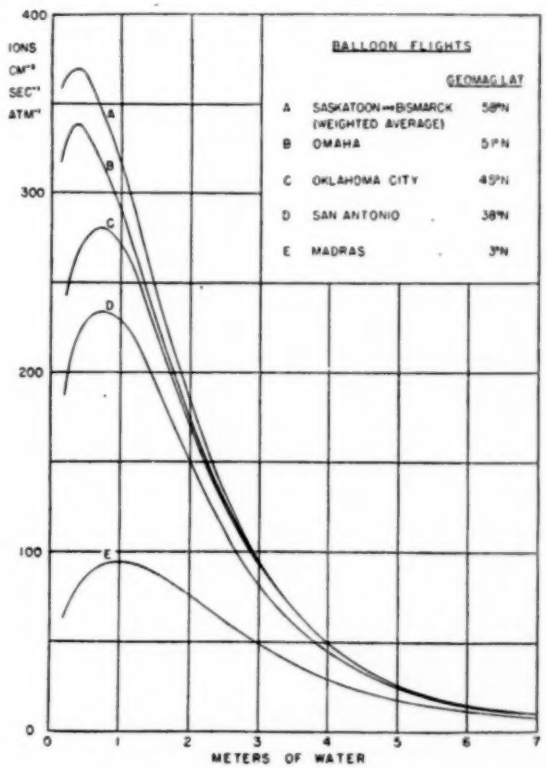

FIG. 7. The differences in the areas underneath the successive curves *A*, *B*, *C*, *D*, *E* represent the energies coming in between the corresponding latitude limits. These energies are the blocks 1, 2, 3, 4, of Fig. 8. Blocks 5 and 6 (Fig. 8) are obtained similarly from the Peshawar, Agra, and Bangalore curve in the accompanying paper by Neher and Pickering.

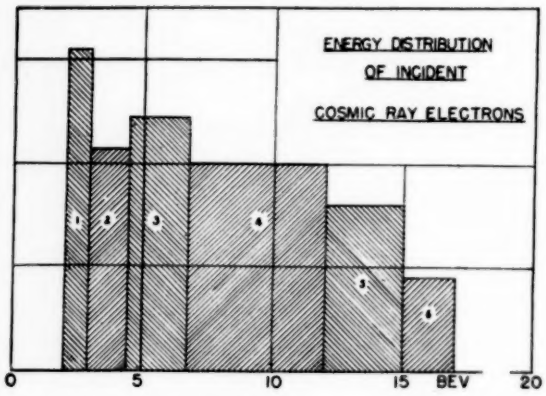

FIG. 8. The above energy blocks correspond to electroscope readings not double counter readings.

penetrating not more than a fourth of the way through the atmosphere for the two curves coalesce at a depth of but between 2 and 3 meters of water below the top. For the reason just advanced the hypothetical helium rays of energy 1.9 Bev would fit this specification admirably, and no rays of very much larger energy would fit it.

Nor is that all the evidence. For in comparing the 1938 readings at Bismarck with those obtained at Saskatoon (Mag. lat 60° N) in 1937 we wrote as follows: "It is found that in the upper fifth of the atmosphere, i.e., about 2 m of water, the readings at Bismarck are consistently about 4 percent or 5 percent *higher* than those at Saskatoon. *For the lower four-fifths of the atmosphere the readings at Bismarck are identical with those at Saskatoon.*" To understand how the readings near the top of the atmosphere at Bismarck can be *higher* than those at Saskatoon we must of course postulate some sort of a cause which produces differences at different times in the cosmic-ray intensity over the whole polar cap made by those electronic energies which according to the Lemaitre-Vallarta curves should get through the earth's magnetic field at about the latitude of Bismarck, but in any case, since it is the Bismarck readings that are the higher, the conclusion seems fairly well justified that there are no electrons entering the atmosphere of energies lower than those that normally can just get through vertically at the latitude of Bismarck. In other words, the theory of a helium cosmic-ray band enables the prediction of the observed plateau of constant cosmic-ray intensities north of Bismarck. The best of present evidence is that the sun's magnetic field cannot be greater than 16 gauss and this would mean that it could not be the cause of the absence of less energetic rays than those of helium north of Bismarck.

But also since the Bismarck-Saskatoon curves are identical in the lower four-fifths of the atmosphere their difference must be due to fluctuations in incoming 1.9-Bev rays, such as seem to be shown in Fig. 6, and since the Bismarck-Oklahoma City curves also are identical in the lower three-fourths of the atmosphere, it appears that the difference between the Oklahoma City and Bismarck curves of Fig. 5 must also be due primarily to the hypothetical helium rays, the argument being merely that these observed rays do not penetrate far enough into the atmosphere to be due to rays of higher energy than helium rays. This argument is strengthened by a glance at the curves in Fig. 7, which show that the rays which cause the difference between the curves taken at San Antonio and Oklahoma City and which must be largely the carbon rays of energy 5.5 Bev, do penetrate far down toward sea level, as they should. It should be said, however, that this evidence is somewhat less certain than that furnished by the data of Fig. 4 which were all taken in one summer (1932), while, though the Oklahoma City-Omaha-Bismarck data were also all taken in a single summer (that of 1938), those at San Antonio were taken in the summer of 1936.

VI. RELATIVE ENERGIES IN DIFFERENT BANDS

In a word, then, the hypothesis here made has had some measure of success in predicting four cosmic-ray bands, namely, a silicon band at about 13.2 Bev, a nitrogen-oxygen band at 6.6 Bev and 7.5 Bev, a carbon band at about 5.6 Bev, a helium band at about 1.9 Bev, and four cosmic-ray plateaus, one between 17 Bev and 13.2 Bev, one between 13.2 and 7.5 billion, one between 5.6 Bev and 1.9 Bev, and one extending in all probability from about magnetic latitude 58° to the pole.

Has it had any success in predicting the amounts of energy in these bands? Bowen gives

carbon, nitrogen, oxygen, and silicon about the same abundance. The silicon has twice the energy per ray of the mean of carbon, nitrogen, and oxygen, so that it might be expected to carry about 40 percent of the energy of the four bands. That is not very much more than what it does carry if one attributes to it all the increase in electroscope readings between Bangalore and Peshawar (blocks 5 and 6 Fig. 8). Again, if the band between San Antonio and Oklahoma City (block 3) is taken as the contribution of carbon rays it comes out reasonably close to half of what is left of the energy carried by carbon, nitrogen, oxygen, and silicon after the carbon and silicon have been deducted. Also, if the helium band is responsible for all the new rays added above carbon its energy is a little more than the mean of the carbon, nitrogen, and oxygen bands. It ought to carry roughly twice as much energy as any of them, since each ray has about one-fourth as much energy as the mean of these three, but Bowen gives it ten times their abundance. He probably would not regard his estimates as sufficiently quantitative to make the discrepancy serious.

In conclusion, it may properly be asserted that there is already a reasonable amount of evidence for the actual existence of the five predicted bands and the four predicted plateaus, and the relative energies brought in by the five bands are in every case at least of the predicted order of magnitude.

This comparison of prediction and experiment has been made possible largely through the generous support of the investigation by the Carnegie Corporation of New York and the Carnegie Institution of Washington. The success of the work in India was made possible by the extraordinarily generous and complete cooperation of the British Indian Meteorological Service.

APRIL 1 AND 15, 1942 PHYSICAL REVIEW VOLUME 61

Results of a High Altitude Cosmic-Ray Survey Near the Magnetic Equator

H. V. NEHER AND W. H. PICKERING
California Institute of Technology, Pasadena, California

(Received February 9, 1942)

Electroscope and Geiger counter observations have been taken with free balloons at geomagnetic latitudes of 3°, 17°, and 25°N. The most important results are as follows: (1) The Geiger counter technique with a single counter will give results very close to those obtained with the electroscope and of comparable accuracy. (2) Vertical coincidence measurements give rise to markedly different values for the relative amounts of incident energy at various latitudes, as compared with the electroscope or single counter data. (3) Within the experimental error, no difference was obtained between the vertical coincidence curves at 3° and 17°, and thus no new energy lies in the primary energy spectrum between the limits of 17 and 15 Bev. (4) This is direct evidence for a banded structure in the primary cosmic-ray spectrum. (5) Flights made with triple and quadruple coincidences, and also with counters arranged to record showers, showed that showers do not significantly affect the vertical coincidence measurements.

INTRODUCTION

IN order to measure the primary energy distribution of the cosmic radiation, observations of the incident energy at the top of the atmosphere in different parts of the earth are necessary. These data, in conjunction with the analysis of the effect of the magnetic field of the earth upon incoming charged particles, can yield the required information. During the last few years Millikan and Neher have taken such data with self-recording electroscopes in several different magnetic latitudes. Although this technique is entirely satisfactory in most respects, there are two limitations inherent in the method. These are: (1) the electroscopes can be released only in such places and at such times that the chance of

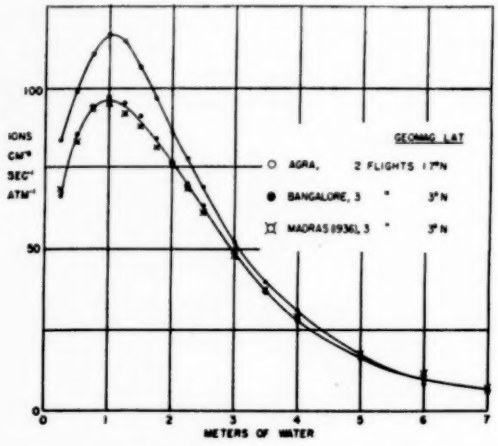

FIG. 1. Average data for electroscope flights at magnetic latitudes 17°, and 3° north.

recovery is reasonably good, and (2) the electroscope gives the integrated intensity over the whole dome of the sky and thus cannot be used for any "fine structure" analysis of the incident energies.

A procedure which surmounts these difficulties at the expense of considerably increased experimental complication is the use of Geiger counters to record the radiation. Such a record can be readily adapted to radio transmission to the ground. An apparatus suitable for this is described in a paper which will appear in *The Review of Scientific Instruments*. By arranging two or more counters as a cosmic-ray telescope, only the radiation from a selected part of the sky is recorded, and thus the energies recorded are delimited with considerably greater accuracy than in the case of the electroscope.

This paper is a report of high altitude free balloon observations with both electroscope and counter techniques in latitudes near the magnetic equator. The observations were made in India by R. A. Millikan and the authors during the period from November, 1939 to February, 1940.

ELECTROSCOPE FLIGHTS

The electroscopes used for these flights were similar to those used previously, and have been described elsewhere.[1] Flights were made at two latitudes—Bangalore, magnetic latitude 3° north; and Agra, magnetic latitude 17° north. Three good records were obtained at Bangalore and two at Agra. In 1936, one of us (H. V. N.) made a series of flights in Madras in almost the same magnetic latitude as Bangalore. For comparison the average values of these flights are shown together with the averages for the new flights in Fig. 1. The curves give the intensity of the radiation as a function of the barometric pressure reduced to meters of water. Comparing the Bangalore curve with the Madras curve made three years earlier, it is apparent that no appreciable change in the radiation at the magnetic equator has taken place in that period. The two curves are within about 2 percent of each other at all points. The two groups of flights were also made at different seasons—October, 1936 and January, 1940—and the close fit of the curves shows that there is no equatorial seasonal effect, at least for these particular seasons. Hence the comparison made below of the data taken at Agra with that at Bangalore two months later, will not be complicated by seasonal effects.

The Agra curve shows a greater intensity than that at Bangalore, the integrated area under the curve being some 8 percent greater. As previously shown,[2] this area is proportional to the incident energy per square centimeter per second at the top of the atmosphere, and thus some 8 percent more of the primary energy can penetrate the earth's magnetic field at Agra than at Bangalore, which, for all practical purposes can be regarded as on the magnetic equator. In passing from the equator to the latitude of Agra the energy necessary for vertical incidence decreases[3] from 17 to about 15 Bev. However, the minimum energy necessary to reach the earth at very oblique incidence decreases from about 11 to 9 Bev. Clearly then, the 8 percent increase in incident energy at Agra can be caused by new incoming particles which might have any energy value between 9 and 17 Bev.

SINGLE COUNTER FLIGHTS

The Geiger counters used were of the "fast" type, having a mixture of argon and organic

[1] Millikan, Neher, and Haynes, Phys. Rev. **50**, 992 (1936).

[2] Bowen, Millikan, and Neher, Phys. Rev. **53**, 855 (1938).

[3] From curves appearing in Lemaitre and Vallarta, Phys. Rev. **49**, 719 (1936), and **50**, 503 (1936). We obtained the values 17.0, 15.4, and 12.4×10^9 ev for the energies of vertically incoming rays at 0°, 17.3° (Agra), and 25° (Peshawar).

vapor as the gas. The cylinders were 15 cm long, the diameters varied somewhat, but on the average were about 3.5 cm. The gas pressure was about 10 cm of mercury and the operating voltage about 1200 to 1300 volts. The counters were tested by exposure to high temperatures and high counting rates, and were required to have a reasonably good plateau several hundred volts long. By using these "fast" counters in the appropriate circuits, no correction for a decrease in counter efficiency at high counting rates is necessary.

In order to calibrate the counters used on the single counter flights they were exposed to the radiation from a source of Th C″ filtered through about 2 cm of lead. This gave a counting rate somewhat larger than that reached during the flights in the equatorial region. The background counting rate inside the lead shield used above was also measured. Thus the net counting rate due to a constant radiation was found for each counter, and accordingly all counting rates observed during actual flights could be reduced to the rate of a standard counter. Upon our return from India the calibration of several of these counters was repeated and no changes greater than 5 percent were found. As an approximate check on the relationship between the ionization and the counting rate of the standard counter, the ionization corresponding to the

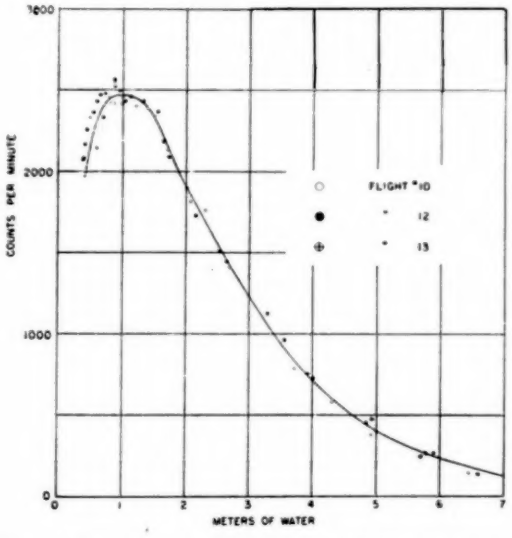

FIG. 2. Data from single counter flights at magnetic latitude (Agra) 17° north. Corrected to standard counter and for background counting rate.

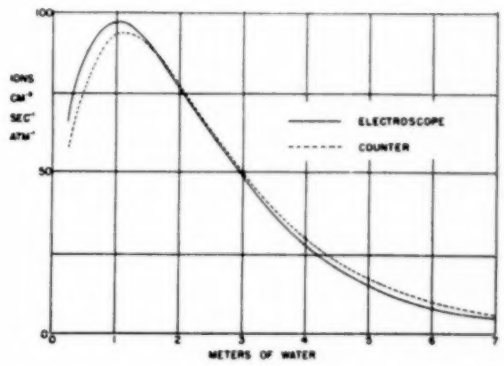

FIG. 3. Comparison of electroscope and single counter flights at the magnetic equator. The counter curve is fitted to the electroscope curve to give approximately the same area under each curve.

Th C″ source used above was measured with one of the balloon electroscopes placed in the lead shield in the same location as the counters. This, of course, would not be expected to give an accurate reduction of the counts observed on the flights because of the very different geometry in the two cases. Actually it was found that the flight counting rates had to be lowered by a further 19 percent to give good agreement with the ionization measured in the electroscope flights.

For these counter flights, the single counter was mounted on top of the amplifier unit with its axis at an angle of 45° with the horizontal. This was done in order to give a somewhat more uniform response to the total radiation than would be obtained with the counter horizontal. Flights were made in three locations: Bangalore and Agra, and in addition, Peshawar in magnetic latitude 25° north. The data obtained are plotted as a function of barometric pressure by taking four-minute averages of the counting rate and pressure. The consistency between the various flights in each latitude is quite good. As an example the data from the Agra flights are shown in Fig. 2. The agreement between the electroscope and the counter data is very satisfactory provided one makes the 19 percent additional geometrical correction mentioned above. Figure 3 shows this comparison for Bangalore. It will be noted that the two curves fit very well up to an altitude of about 1.5 meters of water. Above this the counter curve falls below the other. This is to be expected, because at high

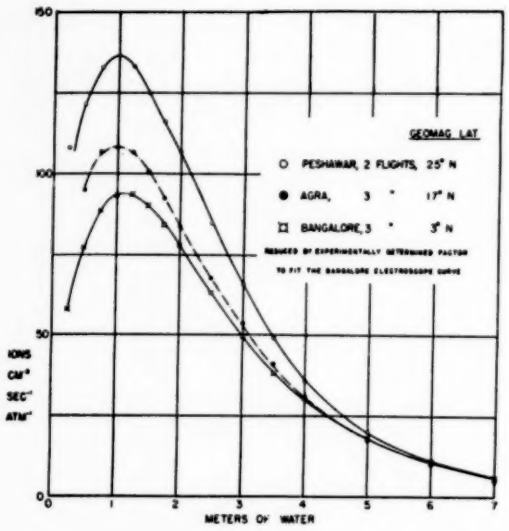

FIG. 4. Data from single counter flights. If the area under the Bangalore curve is taken as 100, then the areas under the other curves are 111 and 136, respectively.

altitudes groups of particles must become increasingly prevalent, and these register but once in the counter whereas they give their true value in the electroscope.

The averages of all the single counter flights are shown in Fig. 4, plotted in terms of ionization calculated as above. If the area under the Bangalore curve is taken as 100, then the other areas are 111 and 136, respectively. There is thus a marked increase in the primary intensity between the two latitudes of 17° and 25° north. The energies required for vertical incidence at these latitudes are 15 and 12.5 Bev, respectively.

VERTICAL COINCIDENCE FLIGHTS

In addition to the amplifier units that could be used for single counter flights, other units were built to use for double, triple, or quadruple coincidence observations. Vertical coincidence measurements, as stated above, have the significant advantage over single counter or electroscope measurements that they narrow down the band of primary energies that are recorded. Thus, in principle, these flights should give a much more satisfactory analysis of the primary energy distribution.

Double coincidence measurements were taken at the three locations of Bangalore, Agra, and Peshawar. The counter sets used for these flights consisted of two pairs of counters mounted with the members of each pair separated about 7.5 cm, and the vertical distance between the pairs about 14.0 cm. Hence the solid angle over which at least half the counter area was effective, measured about 45×25 degrees. The counting rates of the different sets were reduced to the rate of a standard set by taking calibration runs immediately before the flights. This was done by comparing the counting rate with that of the standard set when placed in some fixed position at the ground station. At least 15,000 counts were used for these calibrations. Some of the sets used were also recalibrated in Pasadena after our return. A further check on the calibration was obtained by calculation from the geometry of the sets which varied somewhat due to variations in counter diameter and spacing. The results of the flights were then weighed with due regard to the consistency of these three calibrations.

The results of the vertical coincidence flights are shown in Figs. 5 and 6. Again four-minute averages are used to obtain the curves. Figure 5 shows the actual data obtained on a flight at Peshawar after reduction to the standard counter set. The averages of all the flights are shown in Fig. 6. This includes three flights at Peshawar, four at Agra, and six at Bangalore. The comparison between the data at the different latitudes gives the following result. If the area under the Bangalore curve is taken as 100, then that under the Agra curve is also 100, and that under the Peshawar curve is 121.

By a similar analysis to that of the electroscope and single counter curves, it is possible to show that the area under the vertical coincidence curves is proportional to the vertical energy incident at the top of the atmosphere, provided that one makes the following assumptions:—(1) secondaries produced along the path of the incident particle do not diverge appreciably from the direction of the primary; (2) the passage of several secondaries through the counters simultaneously is a relatively rare event; (3) the contribution to the observed counting rate of showers arising from primaries making a large angle with the vertical can be neglected. Assumption (1) is justified from theoretical considerations,[4] assumption (2) is verified experi-

[4] T. H. Johnson, Phys. Rev. **56**, 226 (1939).

mentally by the close agreement between the single counter and the electroscope curves, and (3) is verified experimentally by the results discussed in the next section. Hence the area under the vertical counter curves can be taken as giving a measure of the incident energy per square cm, per second, per unit solid angle at the vertical, at the top of the atmosphere. A numerical value can be obtained for this energy by using the known counting rate of the standard set at sea level in high latitudes where the number of particles per square cm, per second, per unit solid angle is known,[5] and an average value of the ionization per cm of path of the cosmic-ray particles in the air. Using a value of 80 ion pairs per cm,[6] one finds the vertical energy incident at the magnetic equator to be 2.2×10^8 ev/sq. cm/sec./unit solid angle.

The agreement between the Bangalore and Agar curves is considered to be well established within the limits of error of the data. On a statistical basis alone, the probable error of each point on the average curves is less than 1 percent in the region of the maximum. The internal consistency of the data is not this good, but indicates an error of about 3 percent in each curve at the maximum. Since the single counter and electroscope flights were made at the same time as these flights, the results show clearly that a real and marked difference exists between the change in the vertical radiation and the change in the integrated radiation. This difference must be ascribed to low energy particles which fail to reach the vertical counters at the higher latitude because of the gradual opening of the cones of permitted directions. In view of the complicated nature of the expressions for the effect of the earth's magnetic field on the radiation, it is clear that the vertical coincidence data are more satisfactory for the determination of the primary energy spectrum than the single counter or electroscope data. The limiting energies for vertical incidence at the three latitudes at which observations were made, are approximately as follows: —Bangalore, 17 Bev, Agra, 15 Bev, and Peshawar, 12.5 Bev. Hence, our experimental result leads to the conclusion that there is no new energy lying in the primary energy range from 17 to 15 Bev but that there is a new energy band that gets in between 15 and 12.5.

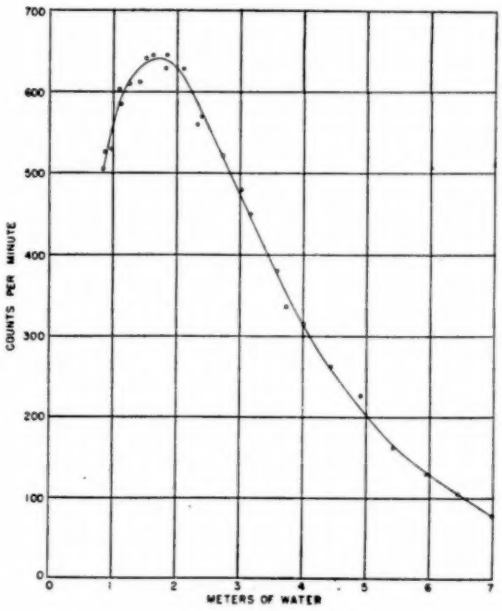

FIG. 5. Example of the data obtained from one vertical coincidence flight at Peshawar (doubles).

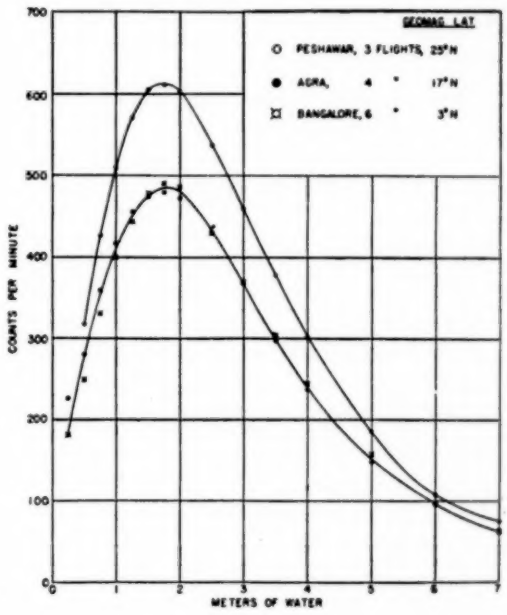

FIG. 6. Summary of vertical counter data. No detectable increase in intensity is observed between latitudes 3° and 17°, but there is a 21 percent increase in going from latitude 17° to 25°.

[5] J. C. Street and R. H. Woodward, Phys. Rev. **46**, 1029 (1934).
[6] R. B. Brode, Rev. Mod. Phys. **11**, 222 (1939).

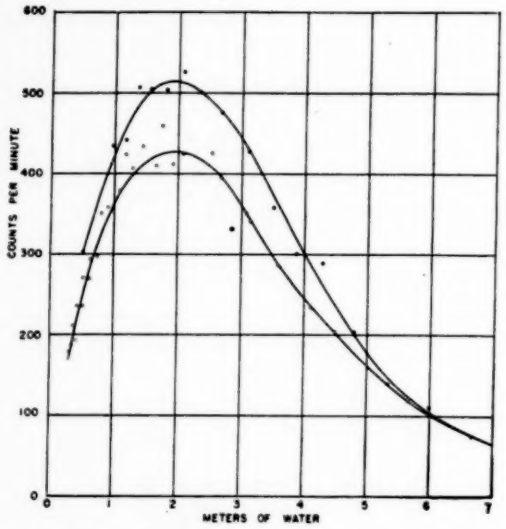

FIG. 7. Two triple vertical coincidence flights. Solid circles, Peshawar; open circles, Bangalore. The difference shown at these two latitudes is about the same as was found in the case of double coincidences; however, the maxima of the curves are about 15 percent lower than the corresponding double coincidence curves.

AIR SHOWERS

The contribution of air showers to the vertical coincidence counting rate was estimated by the following experiments. At Bangalore and at Peshawar triple coincidence flights were made in addition to the double coincidence flights. In each case the observed counting rates were lower for the triple coincidences (Fig. 7). At the maxima of the curves the difference is about 15 percent. However, the areas under the curves obtained for the two cases are not very different. The difference between the double and triple coincidences can be caused only by showers since experiments showed that the accidental counting rate, even in the case of the double coincidences, was only about 1.5 percent of the real coincidences at the highest counting rates. The triple coincidences are lower because of the decreased proability that a shower will operate three counters. These flights accordingly show that the effect of showers is small, and that we are justified in using the double coincidence counting rate as a measure of the vertical intensity. Because of the greater accuracy of these double flights, our conclusions are based upon them.

An interesting check on the above results is afforded by a quadruple coincidence flight made at Agra (Fig. 8). Within the quite large experimental error in this particular flight in which the counting-rate is of course very much reduced, we obtained the same result as the triple coincidence flight at Bangalore.

The difference curves between the double and triple coincidence flights rise rapidly to a maximum at about 1.5 meters water equivalent depth below the top of the atmosphere. They then fall to zero at a depth of about 4.0 meters. This behavior is similar to that observed in a flight made at Bangalore with three pairs of counters out of line in the usual shower arrangement, except that in this case the curve does not fall so rapidly. From the ground to the maximum the showers observed in this flight increased by a factor of about 50 (Fig. 9).

ABSORPTION OF 13.7 BEV PARTICLES

In Fig. 10 is shown the difference curve obtained by subtracting the Agra vertical coincidence data from the Peshawar data. This curve gives the absorption of the primary particles lying in the energy range from 12.5 to 15 Bev. The average energy of these particles will be approximately 13.7 Bev. The general character of the curve is in good agreement with others of this type obtained both theoretically and experimentally. It exhibits the well-known departure from theory at depths below about 3 meters, and is accordingly further evidence for the production of mesotrons in the atmosphere. The depth of the maximum of the curve, 1.6 meters, is somewhat larger than that predicted from theory.[7] Extra-

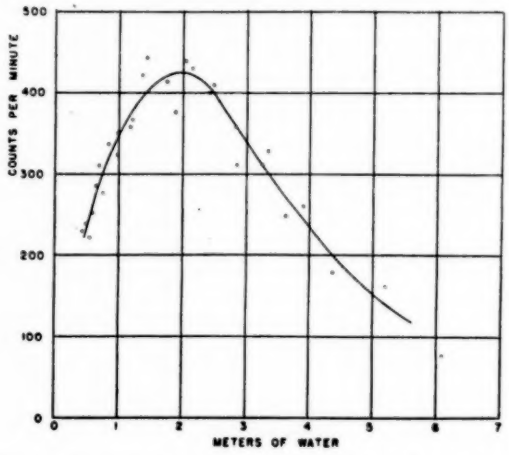

FIG. 8. A quadruple coincidence flight made at Agra.

[7] R. Serber, Phys. Rev. **54**, 317 (1938).

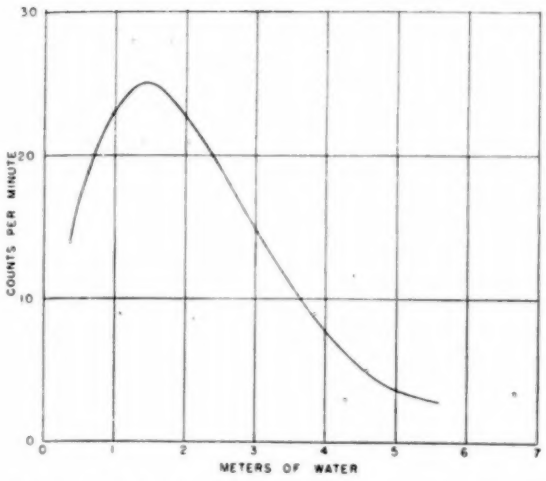

FIG. 9. A flight showing the increase of air showers at the magnetic equator. At the ground, altitude 3000 feet, the rate was 0.5 per minute.

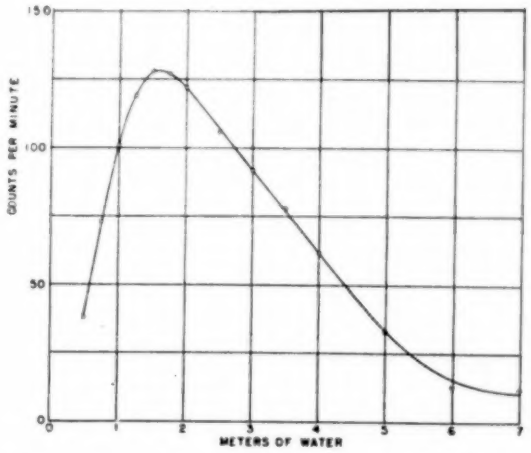

FIG. 10. The difference curve for vertical double coincidences. Peshawar minus Agra-Bangalore average. This curve gives the absorption of the incoming charged particles which have an energy of about 13.7 Bev.

polating the curve to zero depth gives a value which approximately checks the theoretical decrease from the maximum. It is significant to note, however, that the increase in the first half meter below the top of the atmosphere is much more rapid than can be accounted for by the usual shower theory.

CONCLUSION

The results of these flights may be summarized as follows:

(1) The vertical coincidence technique with Geiger counters gives a satisfactory picture of the behavior of the vertically incident radiation, without the necessity of correcting for the effect of showers.

(2) The latitude effects measured with this technique may be significantly different from those obtained with electroscopes or single Geiger counters.

(3) For the determination of the primary energy distribution from the latitude effect, the vertical coincidence data are more significant than the electroscope or single counter data.

(4) The identity of the coincidence curves at Bangalore and at Agra 14° farther north, is direct evidence that the primary radiation spectrum shows a banded structure with little or no energy lying in the range from 15 to 17 Bev.

In conclusion the authors wish to express their appreciation for the invaluable aid rendered by R. A. Millikan in the planning of these experiments, the observations in the field, and the discussion of the results. They sincerely thank the Carnegie Corporation of New York for the financial assistance which made this expedition possible, and they remember with great pleasure their many friends in the Indian Meteorological Service without whose help it would have been impossible to have made so many successful flights.

Cosmic-Ray Electrons of Low Energy in the Atmosphere

BRUNO ROSSI, *Cornell University, Ithaca, New York*

AND

S. J. KLAPMAN, *Utah Radio Products Company, Chicago, Illinois*

(Received January 26, 1942)

The track length of shower electrons above 10^7 ev energy in air has been calculated as a function of the primary energy, for both electron- and photon-initiated showers. The results obtained have been used to evaluate the number of electrons of energy larger than 10^7 ev arising from collision processes and from the disintegration of mesotrons in the atmosphere.

I. INTRODUCTION

THE theory of multiplicative showers can be developed analytically only if certain approximations are made. These include (a) using the asymptotic formulae for complete screening in the description of pair production and radiation processes, (b) neglecting Compton effect, (c) neglecting the production of high energy secondary electrons by collision processes of electrons, and (d) either neglecting the energy loss of electrons by collision or considering it as independent of the electron energy. With these approximations one can solve the shower problem completely in the field of large energies; i.e., one can find a closed expression for the number $\Pi(E, \eta, x)$ of electrons of energy larger than η produced in the thickness x by a primary electron (or photon) of energy E, provided η is large compared with the critical energy. Also, a method has been developed, which gives fairly accurately the "total" number of electrons irrespective of energy; i.e., the function $\Pi(E, \eta, x)$ for $\eta=0$. However, on account of mathematical difficulties, it has not been possible, so far, to obtain an expression for the number of electrons with energy larger than η if η is smaller than the critical energy, but different from zero. Even if such an expression could be derived from the present theory, its meaning would be doubtful because the simplifying assumptions on which the theory is based are certainly not valid in the field of low energies.

The lack of theoretical information regarding low energy electrons is particularly serious in the interpretation of counter experiments on the soft component of cosmic rays in the atmosphere, where one records all the electrons which have sufficient energy to penetrate the walls of the counters. With the ordinary arrangements, this energy is of the order of 10^7 ev; i.e., about ten times smaller than the critical energy in air.

In principle, of course, one could treat the shower problem by numerical methods, without introducing any simplifications or limiting the range of energies. However, the determination of $\Pi(E, \eta, x)$ by such numerical methods is an almost hopeless task. A problem which can be handled somewhat more easily is the determination of the integral of $\Pi(E, \eta, x)$ with respect to x; i.e., of the quantity

$$z(E, \eta)=\int_0^\infty \pi(E, \eta, x)dx.$$

The function $z(E)$ is called the "electron track length" and represents the total distance traveled by all shower electrons while their energy is larger than η. Knowledge of the track length as a function of E is sufficient to determine the number $n(\eta)$ of electrons with energy larger than η in equilibrium with a harder radiation. Indeed, if $X(E)dE$ electrons of energy (E, dE) are produced per unit thickness and if the rate of production does not change appreciably over a distance in which the secondary showers are completely absorbed, $n(\eta)$ is given by,[1]

$$n(\eta)=\int_\eta^\infty X(E)z(E, \eta)dE. \qquad (1)$$

In the present paper we propose to calculate the electron track length *in air* for $\eta=10^7$ ev and

[1] See B. Rossi and K. Greisen, "Cosmic-ray theory," Section 40, Rev. Mod. Phys. **13**, 240 (1941). This article will be referred to as (CRT).

for electron-initiated as well as for photon-initiated showers. We shall take into consideration all phenomena which are of importance in the production or in the absorption of shower particles, and shall use the accurate theoretical expressions for the probabilities of these processes. These expressions are summarized and discussed in (CRT), Part I, where the references to the original papers are also given. For the convenience of the reader, we list in the following section the formulae which will enter in our calculations.

II. THEORETICAL FORMULAE FOR THE ELEMENTARY PROCESSES

In the formulae below, N is Avogadro's number, μ_e is the rest energy and r_0 the classical radius of the electron, A is the atomic weight, and Z the atomic number. Since the energies under consideration are all large compared with μ_e, no distinction is made between total energy and kinetic energy of electrons. All probabilities are expressed in cm^2/g.

(a) Pair Production

The probability of a positive electron of energy (E', dE') and a negative electron of energy $(E-E', dE')$ being produced by the materialization of a photon of energy E is

$$\Psi(E, E')dE' = \frac{4}{137}\frac{N}{A}Z^2r_0^2\frac{dE'}{E^3}\left\{[(E')^2+(E-E')^2]\left[\frac{f_1(\gamma)}{4}-\frac{\log Z}{3}\right]+\tfrac{2}{3}E'(E-E')\left[\frac{f_2(\gamma)}{4}-\frac{\log Z}{3}\right]\right\} \quad (2)$$

or

$$\Psi(E, E')dE' = \frac{4}{137}\frac{N}{A}Z^2r_0^2\frac{dE'}{E^3}[(E')^2+(E-E')^2+\tfrac{2}{3}E'(E-E')]\left[\log\frac{2E'(E-E')}{E\mu_e}-\tfrac{1}{2}-c(\gamma)\right], \quad (2')$$

according to whether $\gamma<2$ or $\gamma>2$. $\gamma=100\mu_eE/E'(E-E')Z^{\frac{1}{3}}$. The functions $f_1(\gamma)$, $f_2(\gamma)$, and $c(\gamma)$ have been given by Bethe and Heitler and are reproduced in (CRT), Section 11.

The total probability for pair production is

$$\sum_p(E)=\int_0^E\Psi(E, E')dE'. \quad (3)$$

(b) Radiation Processes

The probability of a photon of energy (E', dE') being produced by an electron of energy E is

$$\Phi(E, E')dE' = B(E, E')dE'/E', \quad (4)$$

where

$$B(E, E') = \frac{4}{137}\frac{N}{A}Z^2r_0^2\frac{1}{E^2}\left\{[E^2+(E-E')^2]\left[\frac{f_1(\gamma)}{4}-\frac{\log Z}{3}\right]-\tfrac{2}{3}E(E-E')\left[\frac{f_2(\gamma)}{4}-\frac{\log Z}{3}\right]\right\} \quad (5)$$

or

$$B(E, E') = \frac{4}{137}\frac{N}{A}Z^2r_0^2\frac{1}{E^2}[E^2+(E-E')^2-\tfrac{2}{3}E(E-E')]\left[\log\frac{2E(E-E')}{E'\mu_e}-\tfrac{1}{2}-c(\gamma)\right], \quad (5')$$

according to whether $\gamma<2$ or $\gamma>2$. $\gamma=100\mu_eE'/E(E-E')Z^{\frac{1}{3}}$; $f_1(\gamma)$, $f_2(\gamma)$ and $c(\gamma)$ are as in (a).

(c) Compton Effect

The probability of a scattering process in which the energy E of the photon is reduced to (E', dE'), and a recoil electron of energy $(E-E', dE')$ is produced, is given by

$$\kappa(E, E')dE' = \pi\frac{N}{A}Zr_0^2\frac{\mu_e}{E}\frac{dE'}{E'}\left[1+\left(\frac{E'}{E}\right)^2\right]. \quad (6)$$

The total probability of Compton scattering is

$$\sum_c(E)=\pi\frac{N}{A}Zr_0^2\frac{\mu_e}{E}\left[\log\frac{2E}{\mu_e}+\frac{1}{2}\right]. \tag{7}$$

(d) Collision Processes

If $E'>\eta$, the probability of an electron of energy (E', dE') being ejected from an atom by an electron or a positron is

$$\chi(E')dE'=2\pi\frac{N}{A}Zr_0^2\mu_e\frac{dE'}{(E')^2}. \tag{8}$$

The accurate expression for $\chi(E')$ contains additional terms, different for primary electrons and positrons and depending on their energy. These terms are only important when E' approaches the primary energy, and neglecting them does not introduce any appreciable error in the results, because of the rarity of collision processes in which the secondary electron acquires a large energy.

(e) Collision Loss

The energy loss of electrons and positrons caused by collision processes resulting in excitation or ejection of electrons of energy smaller than η is

$$k(E,\eta)=2\pi(N/A)Zr_0^2\mu_e[\log(2E^2\eta/\mu_eI^2Z^2)-1], \tag{9}$$

where $I=13.5$ ev.

As pointed out by Fermi,[2] for very large energies Eq. (9) ceases to be valid and $k(E,\eta)$ becomes practically independent of E. In air, according to Fermi, this happens in the neighborhood of 10^8 ev. In our calculations we shall use Eq. (9) for $E<E_0$, where $E_0=2\times10^8$ ev, and shall take $k(E,\eta)=k(E_0,\eta)=k_0$, for $E>E_0$.

III. EQUATIONS FOR THE TRACK LENGTHS

In what follows we shall use the notation $z(E)$ for the electron track length of electron-produced showers and introduce the notation $\zeta(E)$ for the electron track length of photon-produced showers. For simplicity of writing, we shall drop the η, which is a constant in our problem.

Let us consider a photon of energy E. This produces electrons either by materialization or by Compton effect. The fractional number of cases in which the photon is absorbed by materialization and produces a pair of electrons with energies (E', dE') and $(E-E', dE)$ is given by

$$\Psi(E,E')dE'/[\textstyle\sum_p(E)+\sum_c(E)].$$

In these cases the original photon is equivalent to two electrons, of energies E' and $E-E'$. The fractional number of cases in which the photon undergoes Compton scattering and the scattered photon has the energy (E', dE') is given by

$$\kappa(E,E')dE'/[\textstyle\sum_p(E)+\sum_c(E)].$$

In these cases the original photon is equivalent to an electron of energy $E-E'$ and a photon of

[2] E. Fermi, Phys. Rev. **57**, 485 (1940).

energy E'. It follows that the electron track length of a photon-initiated shower is

$$\zeta(E)=\{1/[\textstyle\sum_p(E)+\sum_c(E)]\}\left\{\int_0^E\Psi(E,E')[z(E')+z(E-E')]dE'+\int_{\mu_e/2}^{\infty}\kappa(E,E')[\zeta(E')+z(E-E')]dE'\right\}$$

or

$$\zeta(E)=\{1/[\textstyle\sum_p(E)+\sum_c(E)]\}\left\{2\int_\eta^E\Psi(E,E')z(E')dE'+\int_{\mu_e/2}^{\infty}\kappa(E,E')[\zeta(E')+z(E-E')]dE'\right\}. \quad (10)$$

Let us consider next an electron of energy E and let us indicate by $P_{\Delta x}(E')dE'$ the probability that its energy is reduced to $(E-E', dE')$ while traversing a thickness of Δx g/cm^2. $P_{\Delta x}(E')$ tends to infinity at the limit for $E'=0$ and $\Delta x=0$, and obviously satisfies the condition

$$\int_0^E P_{\Delta x}(E')dE'=1. \quad (11)$$

For any given value of η, if Δx is sufficiently small, the probability that a loss $E'>\eta$ occurs in more than one process is negligible. Hence, for $E'>\eta$, we can always take

$$P_{\Delta x}(E')=[\Phi(E,E')+\chi(E')]\Delta x. \quad (12)$$

From (11) and (12) it follows that

$$\int_0^\eta P_{\Delta x}(E')dE'=1-\Delta x\int_\eta^E[\Phi(E,E')+\chi(E')]dE'. \quad (13)$$

Moreover, the total energy given to electrons or photons *of energy smaller than* η in the layer Δx by the electron under consideration is

$$\int_0^\eta E'P_{\Delta x}(E')dE'=[k(E,\eta)+b(E,\eta)]\Delta x, \quad (14)$$

where $k(E,\eta)$ represents the collision loss already defined and

$$b(E,\eta)=\int_0^\eta E'\Phi(E,E')dE'=\int_0^\eta B(E,E')dE' \quad (15)$$

is the corresponding radiation loss.

When the electron loses in an amount $E'<\eta$ of energy, the track length of the original electron is $\Delta x+z(E-E')$ because the track lengths of secondary electrons or photons of energy smaller than η are zero. When, however, an electron or a photon of energy $E'>\eta$ is produced, the track length becomes $\Delta x+z(E-E')+z(E')$ or $\Delta x+z(E-E')+\zeta(E')$, respectively. If we consider the probabilities of these various events, we can write the following equation:

$$z(E)=\int_0^\eta P_{\Delta x}(E')[\Delta x+z(E-E')]dE'+\Delta x\int_\eta^E\Phi(E,E')[\Delta x+z(E-E')+\zeta(E')]dE'+\Delta x\int_\eta^E\chi(E')[\Delta x+z(E-E')+z(E')]dE'$$

or, taking Eq. (11) into consideration, we may write

$$z(E)=\Delta x+\int_0^{\eta}P_{\Delta x}(E')z(E-E')dE'+\Delta x\int_{\eta}^{E}\Phi(E,E')[z(E-E')+\zeta(E')]dE'$$
$$+\Delta x\int_{\eta}^{E}\chi(E')[z(E-E')+z(E')]dE'. \quad (16)$$

The quantity $z(E)$, by its nature, must be a smoothly increasing function of E. We will assume that it can be approximated by a linear function in any energy interval of magnitude η. Accordingly, we shall put in our equations

$$z(E-E')=z(E)-s(E)E' \quad \text{for} \quad E'<\eta.$$

One then obtains, considering (13) and (14),

$$\int_0^{\eta}P_{\Delta x}(E')z(E-E')dE'=z(E)\left\{1-\Delta x\int_{\eta}^{E}[\Phi(E,E')+\chi(E')]dE'\right\}-s(E)[k(E,\eta)+b(E,\eta)]\Delta x$$

and Eq. (16) becomes

$$[k(E,\eta)+b(E,\eta)]s(E)=1-\int_{\eta}^{E}\Phi(E,E')[z(E)-z(E-E')-\zeta(E')]dE'$$
$$-\int_{\eta}^{E}\chi(E')[z(E)-z(E-E')-z(E')]dE'. \quad (17)$$

Equations (10) and (17), together with the condition

$$z(E)=\zeta(E)=0 \quad \text{for} \quad E<\eta,$$

determine the track lengths $z(E)$ and $\zeta(E)$ completely.

IV. INTEGRATION OF THE EQUATIONS FOR THE TRACK LENGTHS

Equations (10) and (17) were integrated step by step in the following way. The energy scale was divided into equal intervals of magnitude η. The quantities $\Psi(E,E')$, $B(E,E')$ and the derivatives of $z(E')$ and $\zeta(E')$ with respect to E', which are all slowly varying functions of E', were considered as constant within each of these intervals. Accordingly, the following substitutions were made in Eqs. (10) and (17): For $n\eta<E'<(n+1)\eta$

$$\begin{aligned}\Psi(E,E')&=\Psi(E,(n+\tfrac{1}{2})\eta),\\ B(E,E')&=B(E,(n+\tfrac{1}{2})\eta),\\ z(E')&=z_n+s_n\cdot(E'-n\eta),\\ \zeta(E')&=\zeta_n+\sigma_n\cdot(E'-n\eta),\end{aligned} \quad (18)$$

where $z_n=z(n\eta)$, $\zeta_n=\zeta(n\eta)$, $s_n=(dz/dE)_{E=n\eta}$, $\sigma_n=(d\zeta/dE)_{E=n\eta}$.

Let us suppose that z_n, ζ_n, s_{n-1} and σ_{n-1} are known for $n\leqslant n_1$. Then s_{n_1} can be calculated directly from Eq. (17) because the arguments of z and ζ in the right-hand side of this equation range from η to $n_1\eta$. After s_{n_1} has been calculated, one obtains $z_{n_1+1}=z_{n_1}+s_{n_1}\eta$. Subsequently one can calculate ζ_{n_1+1}, using Eq. (10). In the right-hand side of this equation the arguments of z and ζ range from η to $(n_1+1)\eta$. z is already known up to $E=(n_1+1)\eta$, while ζ is supposed to be known only up to $E=n_1\eta$. However, no appreciable error will be made by putting in the right-hand side of Eq. (10) $\zeta(E')=\zeta_{n_1}+\sigma_{n_1-1}(E'-n_1\eta)$ for $n_1\eta<E'<(n_1+1)\eta$, because the term affected by this approximation is very small. Finally one obtains $\sigma_{n_1}=(\zeta_{n_1+1}-\zeta_{n_1})/\eta$.

It is thus proved that z_n, ζ_n, s_{n-1} and σ_{n-1} can be calculated for $n=n_1+1$ if the same quantities are known for $n\leqslant n_1$. Since $z_1=\zeta_1=s_0=\sigma_0=0$, repeated application of the procedure described above gives z_n and ζ_n for any desired value of n.

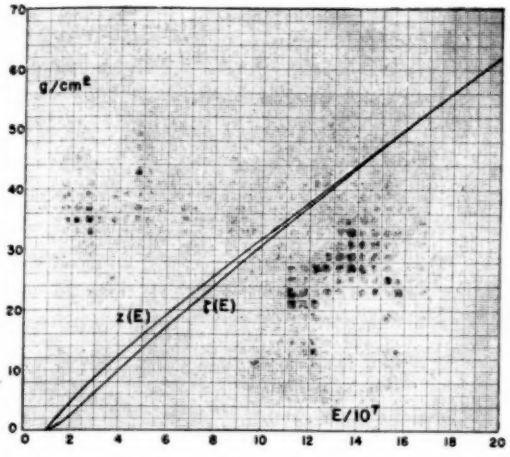

FIG. 1. Electron track lengths for electron-initiated (z) and for photon-initiated (ζ) showers, as functions of the primary energy.

The calculations become more and more lengthy as n is increased. They were carried out as far as $n=20$ ($E=E_0=2\times10^8$ ev) and the results are graphically represented in Fig. 1.

It is seen that, for $E=2\times10^8$, $z(E)$ and $\zeta(E)$ are practically coincident. It is seen, also, that the curves representing $z(E)$ and $\zeta(E)$ approach more and more a straight line as E is increased. This suggests that, for $E>2\times10^8$, $z(E)$ and $\zeta(E)$ may be approximated by a function of the following form:

$$z(E)=\zeta(E)=s_\infty E+l+m/E+h/E^2, \quad (19)$$

where the coefficients s_∞, l, m, and h are determined by the condition that $z(E)$ as well as its derivative with respect to E are continuous at $E=E_0=2\times10^8$ and that $s_\infty=\lim_{E=\infty}(dz/dE)$. These conditions yield

$$z_{20}=s_\infty E_0+l+m/E_0+h/E_0^2,$$

$$s_{20}=s_\infty-m/E_0^2-2h/E_0^3,$$

$$s_\infty=\lim_{E=\infty}\{1/[k(E,\eta)+b(E,\eta)]\} \quad (20)$$

$$\times\left\{1-\int_\eta^E\Phi(E,E')[z(E)-z(E-E')-\zeta(E')]dE'\right.$$

$$\left.-\int_\eta^E\chi(E')[z(E)-z(E-E')-z(E')]dE'\right\}.$$

According to Section II and Eq. (15) the last equation becomes

$$[k_0+\eta B_0]s_\infty$$

$$=1-B_0\lim_{E=\infty}\int_\eta^E[z(E)-z(E-E')-\zeta(E')]dE'/E'$$

$$-C\lim_{E=\infty}\int_\eta^E[z(E)-z(E-E')-z(E')]dE'/(E')^2,$$

where

$$k_0=k(E_0,\eta),$$

$$C=2\pi(N/A)Zr_0^2\mu_c,$$

$$B_0=\lim_{E'/E=0}B(E,E')$$

$$=\frac{4}{137}\frac{N}{A}Z^2r_0^2\left\{2\left[\frac{f_1(0)}{4}-\frac{\log Z}{3}\right]\right.$$

$$\left.-\frac{2}{3}\left[\frac{f_2(0)}{4}-\frac{\log Z}{3}\right]\right\}.$$

Using Fig. 1 and Eq. (19), one readily obtains

$$l=0,$$

$$[k_0+\eta B_0]s_\infty=1+B_0H-B_0s_\infty(E_0-\eta)+CL$$

$$-Cs_\infty\log(E_0/\eta)+B_0m/E_0$$

$$+B_0h/2E_0^2+Cm/2E_0^2+Ch/3E_0^3, \quad (21)$$

where

$$H=\int_\eta^{E_0}\zeta(E')dE'/E'=52.9,$$

$$L=\int_\eta^{E_0}z(E')dE'/(E')^2=7.64/\eta.$$

The two first Eqs. (20), together with Eq. (21), form a system of linear equations which can be solved for s_∞, m, and h. The result is

$$s_\infty\eta=3.06, \quad m/\eta=7.0, \quad h/\eta^2=216.$$

Thus the constant term in Eq. (19) is identically zero, while the contribution of the terms in $1/E$ and $1/E^2$ is already less than 2 percent at $E=E_0=2\times10^8$ and decreases rapidly with increasing energy. If these terms are neglected, Eq. (19) becomes

$$z(E)=\zeta(E)=s_\infty E=3.06(E/10^7)\ \text{g/cm}^2. \quad (19')$$

s_∞ turns out to be very slightly different from $s_{20}(s_{20}\eta=2.99)$, and this justifies the procedure which has been followed in calculating $z(E)$ for $E>20\eta$. The values of $z(E,\eta)$ and $\zeta(E,\eta)$ for $\eta=10^7$ ev given by Eq. (19′) may be compared with the values of the same functions for $\eta=0$. Under the simplifying assumption that the energy loss of electrons is a constant k, the track lengths $z(E,0)$ and $\zeta(E,0)$ are obviously equal to E/k. If one takes for k the value generally used in the shower theory (see CRT, Section 25) one obtains.

$$z(E,0)=\zeta(E,0)=4.3(E/10^7).$$

V. ELECTRONS ARISING FROM COLLISION PROCESSES OF MESOTRONS IN AIR

As a first application of the results obtained, we want to calculate the number of electrons of energy larger than 10^7 ev arising from collision processes of mesotrons in the atmosphere and subsequent multiplication of the electrons thus produced.

The number of collision electrons of energy (E, dE) produced in 1 g/cm² by mesotrons of a given energy will be taken as equal to

$$X(E)dE=2\pi\frac{N}{A}Zr_0^2\mu_e\frac{dE}{\beta^2E^2}\left[1-\beta^2\frac{E}{E_m}\right]M, \quad (22)$$

where M is the number of mesotrons, β is their velocity, and E_m the maximum transferable energy. E_m is given, as a function of the mass μ and the momentum p of the mesotrons, by the equation (see CRT, Section 1)

$$E_m=2\mu_e p^2/[\mu_e^2+\mu^2+2\mu_e(p^2+\mu^2)^{\frac{1}{2}}]. \quad (23)$$

Equation (22) is valid for mesotrons of all energies if the spin of mesotrons is zero, and practically so if the spin is $\frac{1}{2}$. It is valid only for mesotrons of energy small compared with 6×10^{10} ev if the spin is 1 (see CRT, Section 2).

Under the assumption that the mesotron mass is $\mu=10^8$ ev/c^2, Eq. (23) shows that the maximum transferable energy is 10^7 ev for mesotrons of momentum equal to 3.16×10^8 ev/c. Therefore only mesotrons above 3.16×10^8 ev/c need to be taken into consideration and for these particles β is practically equal to 1. If we neglect the variation of the mesotron momentum over a distance in which the showers produced by the secondary electrons are completely absorbed, the fractional number of electrons of energy larger than 10^7 ev in equilibrium with mesotrons of momentum p is given by the following equation [see Eq. (1)]

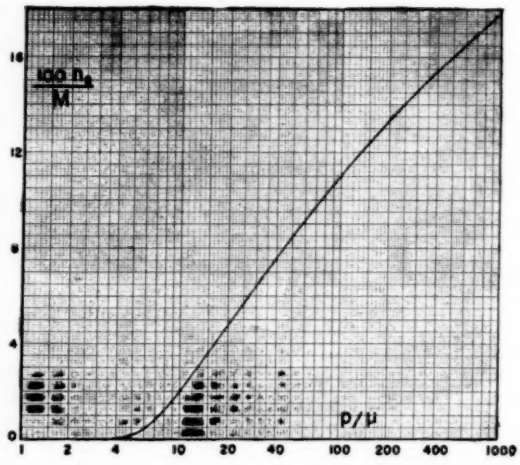

FIG. 2. Fractional number of collision electrons of energy larger than 10^7 ev/c in equilibrium with mesotrons, as a function of the mesotron momentum.

$$n_c/M=2\pi(N/A)Zr_0^2\mu_e \times\int_\eta^{E_m}[1-(E/E_m)]z(E)dE/E^2, \quad (24)$$

where p enters implicitly in E_m, according to Eq. (23).

The integral can be evaluated by taking $z(E)$ from Fig. 1 for $E<2\times10^8$ ev and using Eq. (19′) for $E>2\times10^8$ ev. One thus obtains for n_c/M the values plotted in Fig. 2. For $E_m>2\times10^8$ ev the following equation holds very closely:

$$n_c/M=0.035+0.0234\log(E_m/2\times10^8).$$

By averaging n_c over the momentum spectrum of mesotrons[3] one calculates that *the number of collision electrons with energy larger than 10^7 ev at sea level is 0.067 per incident mesotron of momentum larger than 3×10^8 ev/c.*

VI. ELECTRONS ARISING FROM THE DISINTEGRATION OF MESOTRONS IN THE ATMOSPHERE

As a second application, we want to calculate the number of electrons of energy larger than 10^7 ev arising from the disintegration of meso-

[3] See P. M. S. Blackett, Proc. Roy. Soc. **159**, 1 (1937).

trons in the atmosphere. We shall assume that the mesotrons disintegrate into an electron and a neutrino. The probability that a mesotron of momentum p disintegrates in a layer of 1 g/cm² of air, producing an electron of energy (E, dE), is then given by

$$(\mu/\tau_0\rho)(dE/p^2),$$

where μ is the mass, τ_0 the lifetime of the mesotrons, and ρ the density of air.[4] Hence the number of electrons of energy greater than 10^7 in equilibrium with M mesotrons of momentum p is [from Eq. (1)]

$$n_d=(M\mu/\tau_0\rho p^2)\int_{\eta'}^{E_{\max}} z(E)dE, \qquad (25)$$

where η' is the smallest of the two energies η and $E_{\min}\cdot E_{\max}$ and $E_{\min}$ are the maximum and the minimum energies of the decay electrons, respectively, and are given by (see reference 4)

$$E_{\max}=\tfrac{1}{2}[(p^2+\mu^2)^{\frac{1}{2}}+p],$$

$$E_{\min}=\tfrac{1}{2}[(p^2+\mu^2)^{\frac{1}{2}}-p].$$

For $p>3\times10^8$ ev/c, and if terms of the order of $(p/\mu)^4$ are neglected, Eq. (25) yields

$$n_d=\tfrac{1}{2}(M\mu/\tau_0\rho)s_\infty[1+57\eta^2/p^2]. \qquad (25')$$

The term $57\mu^2/p^2$ amounts to only 6 percent for $p=3\times10^8$ ev/c and decreases rapidly with increasing momentum. Hence, no appreciable error will be made by dropping this term and writing

$$n_d=\tfrac{1}{2}(M\mu/\tau_0\rho)s_\infty. \qquad (25'')$$

The quantity $\frac{1}{2}(M\mu/\tau_0\rho)$ represents the energy going into decay electrons per g/cm². If this quantity is indicated by K_0, Eq. (25′) becomes

$$n_d=K_0s_\infty=3.06(K_0/10^7). \qquad (25''')$$

It will be noted that the expression (25″) does not contain the momentum p of the mesotrons. Hence it also applies to a non-monoenergetic beam of mesotrons.

In the above calculations we have neglected the variation of the rate of production of electrons with depth. This approximation does not introduce any appreciable error in the results of the previous section because the average energy of the collision electrons is very small and the showers to which they give rise are, therefore, absorbed in a very short distance. The error is much larger in the present case both because the average energy of the decay electrons is larger than that of the collision electrons and because the rate of production of decay electrons increases with height as M/ρ; i.e., more rapidly than the number M of mesotrons.

In order to see how this error can be corrected, let K be the energy dissipated in one g/cm² of air by the shower electrons which accompany the mesotron beam at a certain level. K may be taken as a measure of the ionization produced by these electrons in the layer under consideration. If the variation of the rate of production of decay electrons with depth could be neglected, K would be equal to the total energy K_0 of the decay electrons generated in the same layer. Actually K is larger than K_0 because the electrons present at a certain level originate from decay processes which have occurred at a higher altitude where the number M of mesotrons is larger and the density ρ of air is smaller. It has been shown by Rossi and Greisen (see reference 4) that K is equal to K_0 calculated at a distance of 130 g/cm² above the place of observation. It is safe to assume that the variation of the rate of production of decay electrons with depth affects the number of electrons above 10^7 ev energy very nearly in the same way as it affects the quantity K. Under this assumption, Eq. (25‴) is still valid, provided one substitutes K for K_0. According to Rossi and Greisen (see reference 4), at the altitude of Ithaca (259 m above sea level) $K/M=0.61\times10^6$ ev per g/cm², if only mesotrons with momentum larger than 3×10^8 ev/c are taken into consideration. It follows that *the number of electrons of energy larger than 10^7 arising from the decay of mesotrons of momentum larger than 3×10^8 ev/c is 0.19 per incident mesotron above 3×10^8 ev/c.* The number of electrons arising from the decay of mesotrons below 3×10^8 ev/c is practically negligible (see reference 4).

[4] See, for instance, B. Rossi and K. Greisen, Phys. Rev. **61**, 121 (1942).

The Production of Neutrons and Protons by the Cosmic Radiation at 14,125 Feet

S. A. KORFF
Bartol Research Foundation and New York University, New York, New York

AND

E. T. CLARKE
Bartol Research Foundation and Massachusetts Institute of Technology, Cambridge, Massachusetts

(Received February 9, 1942)

The production of neutrons and protons in various substances by the cosmic radiation was investigated with proportional counters at the Mt. Evans Laboratory (barometer 46 cm). Neutrons were studied with counters filled with BF_3 and cadmium absorbers. The neutron counter was surrounded by water, so that nearly all the neutrons should be slow, and also so that the neutrons measured should nearly all have been produced in the water, very few of those produced elsewhere reaching the counter. Protons were observed in counters filled with CH_4. The size distribution of ionizing events was determined. Coincidences between neutron counts and shower counts were observed, suggesting a connection between the neutrons and the soft component. Estimates are given of the rates of production in various substances, these being of the order of 10^{-3} to 10^{-4} per gram per second on Mt. Evans.

INTRODUCTION

THE presence of neutrons and protons in the cosmic radiation has been the subject of much investigation. The neutrons have been studied with the aid of photographic plates,[1] proportional counters,[2] and induced radioactivity,[3] while the protons have been investigated with cloud chambers,[4] photographic plates,[5] and proportional counters.[6] The particles are believed in the main to be of secondary origin, and to have been produced by the cosmic radiation. Some theories regarding the origin of these particles have been put forward.[7,8] In an attempt to throw further light on the process of production, the several experiments described below were performed during August, 1941, at the Mount Evans Cosmic Ray Laboratory. This laboratory is located at 14,125 feet, just below the 14,260 foot summit of Mount Evans, Colorado. The mean barometer during our stay was 46 cm, and the altitude may be taken as roughly six meters of water equivalent below the top of the atmosphere.

NEUTRON OBSERVATIONS

Neutrons were observed with the aid of a proportional counter, filled with boron trifluoride gas. Several counter tubes were used, of various sizes and various gas-pressures. Those to be discussed here, had volumes of 3551 cc and 1450 cc, with pressures of 41.5 and 75 cm, respectively, of BF_3. Several smaller counters were used as checks. The counter of volume 3551 cc and pressure 41.5 cm was also equipped with a thin glass window, through which alpha- and beta-particles could be projected into the gas of the counter, for the purpose of calibrating the pulse sizes. It will be recalled that proportional counters can be calibrated through the use of particles of known specific ionization,[9] and that the pulse sizes obtained under certain conditions can be computed,[10] and related to the size and gas-pressure of the counter and the amount of energy lost by the particle as ionization within

[1] L. H. Rumbaugh and G. L. Locher, Phys. Rev. **44**, 855 (1936); E. and L. Schopper, Physik. Zeits. **40**, 22 (1939); also see reference 4 below.
[2] E. Fünfer, Zeits. f. Physik **111**, 351 (1938); S. A. Korff, Rev. Mod. Phys. **11**, 211 (1939); Proc. Am. Phil. Soc. **84**, 589 (1941).
[3] H. v. Halban, L. Kowarski, and M. Magat, Comptes rendus **208**, 572 (1939).
[4] M. Blau and H. Wambacher, Nature **140**, 585 (1937); A. Widhalm, Zeits. f. Physik **115**, 481 (1940); further bibliography, see M. M. Schapiro, Rev. Mod. Phys. **13**, 58 (1941).
[5] G. Herzog and W. H. Bostick, Phys. Rev. **59**, 122 (1941); W. F. Powell, Phys. Rev. **58**, 474 (1940); S. H. Neddermeyer and C. D. Anderson, Phys. Rev. **54**, 88 (1938).
[6] S. A. Korff, Phys. Rev. **59**, 949 (1941).
[7] H. A. Bethe, S. A. Korff, and G. Placzek, Phys. Rev. **57**, 573 (1940).
[8] E. Bagge, Ann. d. Physik **39**, 512 (1941).
[9] S. A. Korff, Rev. Sci. Inst. **12**, 94 (1941).
[10] M. E. Rose and S. A. Korff, Phys. Rev. **59**, 850 (1941).

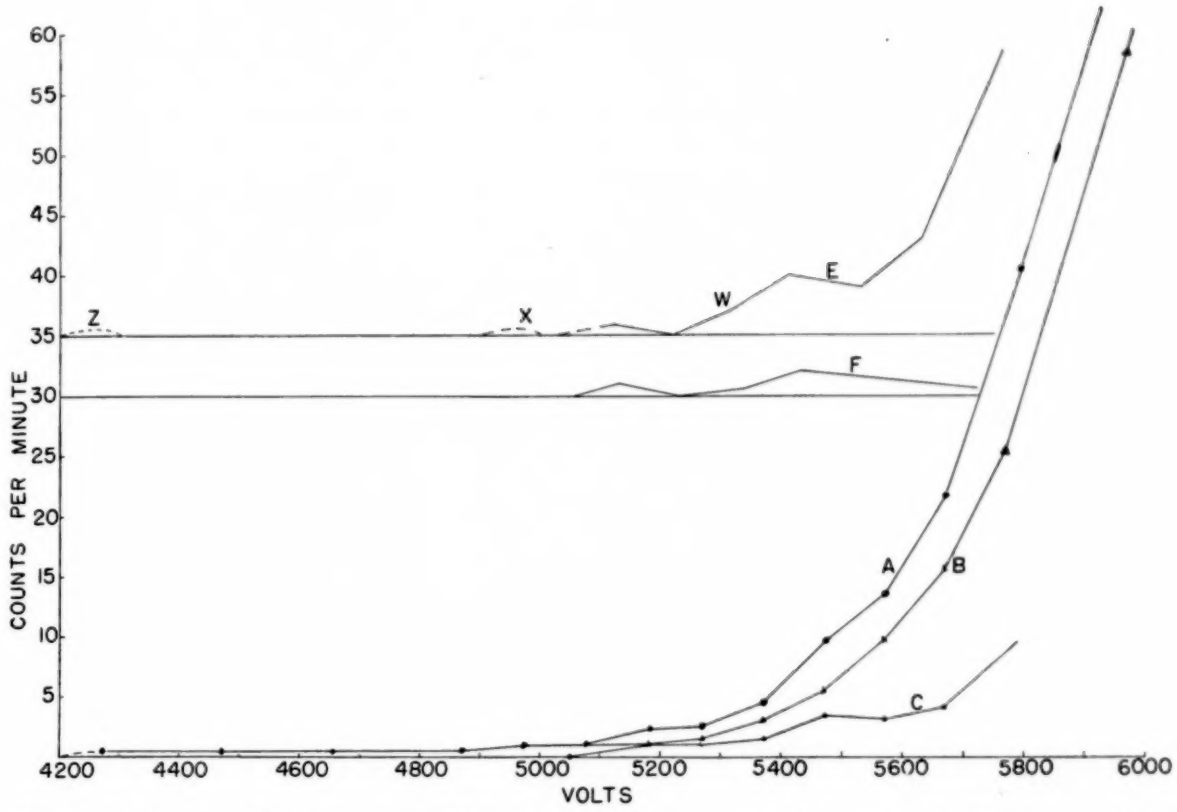

FIG. 1. Counting rate of neutron counter filled with BF_3 at 74 cm on Mt. Evans. Curve *A* without, curve *B* with cadmium shield over counter. Curve *C* is difference due to cadmium shield. Curves *E* and *F* are pulse-size distributions, being differentials of *A* and *C*, respectively, *E* representing the total number of pulses observed, and *F* due to neutrons. The very largest pulses are due to giant showers and contamination alphas, and hence are not affected by the cadmium.

the counter. It will also be recalled[9] that at any voltage, the counter and recording circuit detect all pulses greater than a certain minimum size, and that therefore the differential with respect to voltage of the curve of counting-rate as a function of the voltage gives the pulse-size distribution.

The neutron counters were surrounded with water. This was accomplished by standing a sufficient number of 5-gallon cans filled with water around the counter, so that any particle from the outside had to pass through 30 to 80 cm of water. Whereas the amount and geometrical arrangement of the water were by no means ideal, the arrangement of the water has been found by several observers to make little experimentally detectible difference, a fact again noted in the present work. The purpose of the water was to insure that most of the neutrons reaching the counter would be slow, and further, the thickness was such that practically no neutrons reached the counter from the outside, all those counted having been produced in the water. A thin (0.7 mm) cadmium shield could be slipped over the counter, and the counting rates were determined with and without this cadmium shield. Such a thin shield had a very small mass compared to the other matter around the counter, and presumably only had the effect of absorbing slow neutrons from the water. It would have no appreciable effect on other components of the radiation.

The observed counting rates as a function of voltage found with the counter of 1450 cc mentioned above, are shown in Fig. 1, with and without cadmium, in curves *A* and *B*. Curve *C* is the difference between *A* and *B*, and hence represents the neutrons which did not get through the cadmium. Curve *E* is the pulse size distribution, being the differential of *A*, for all the pulses. It will be seen that there are a few (*z*) very large pulses (mostly giant showers), a

few pulses (x) somewhat larger than those due to neutron-disintegration alphas (mostly contamination alphas from the counter cylinder), and quite a number of about the size of the neutron induced pulses (w) and smaller. Curve F is the differential of C, or the pulse-size distribution among the neutrons. Unfortunately the process of differentiation tends to accentuate errors, and hence the accuracy of the pulse-size distribution curve is not as good as that of the integral counting-rate curve.

The same counter was also operated at Denver University, barometer 63.1 cm, for the purpose of obtaining comparable data to permit the estimation of the increase of the neutron intensity as a function of elevation. The same geometrical arrangement was used. The cadmium shield reduced the counting rate from 12.0 to 8.5 counts per minute, thus indicating about 3.5 ± 0.5 counts per minute owing to slow neutrons at this elevation compared to 15 ± 1 at the top of Mount Evans. Since the difference in elevation corresponds to nearly 2 meters of water equivalent, the neutrons are seen to increase with elevation by a factor of about 2 per meter of water in this interval. This increase is faster than that of the total intensity of the radiation, but roughly equal to that of the soft component. It may be pointed out again that because the neutrons do not travel through large fractions of the atmosphere before they are absorbed, one would expect the altitude dependence of the neutrons to be the same as that of the producing agency. Hence the altitude dependence suggests an association of the neutrons with the soft component.

COINCIDENCE EXPERIMENTS

The second experiment consisted of observing coincident discharges between the neutron counter and a tray of ordinary Geiger counters arranged to detect showers. The tray comprised 25 counters 1 cm in diameter and 30 cm long, arranged side by side in a horizontal plane and so connected[11] that at least two had to discharge simultaneously in order to record as a shower. The neutron counter could also be connected, and neutron-shower coincidences were recorded. The resolving time was adjusted to 10^{-4} second, so that neutrons formed in any process could have time to be slowed down before being captured. Because of the slow counting rate, accidentals within this time-limit were negligible. Water was arranged around the neutron counter in the same way as described above, and a cadmium shield could be slipped over the neutron counter. Directly above the shower tray were two 1-cm Pb slabs, for the purpose of producing additional showers. The neutron counter was placed above the lead, to minimize the counts due to large showers produced in the lead which might cause the neutron counter to discharge. The counting rates of neutron-shower coincidences were observed, with and without the cadmium shield.

It was found that the coincidence counting rate with the cadmium shield was 0.22 per minute while without the shield it was 0.396 ± 0.03 per minute. It appears improbable that the cadmium shield could influence the counting rate in any way except through absorption of slow neutrons, and the count with the cadmium in place thus permitted the background rate to be determined. The background will evidently include accidentals, contributions due to large showers, counts produced by faster neutrons, and other highly ionizing events. The difference between the two observed counting rates is therefore that due to neutrons which were actually produced in some process connected with the shower.

PROTON OBSERVATIONS

Several proportional counters were also operated, with methane, for the purpose of studying the protons produced by the cosmic radiation. One counter was identical with the large neutron counter described above, being 3551 cc in volume and filled to 41.5 cm with CH_4. The other two counters had cylinders 25.4 cm long and 9 cm in diameter, and were filled to 21.4 cm with CH_4. Each was equipped with a thin window for the admission of alpha- and beta-particles for calibration. The cylinders of the latter two were made of lead and of aluminum, all other counter cylinders being of copper. These elements were used in order to ascertain whether any difference in the rates of production of particles in the various different elements could be observed. Since the lead and aluminum counters are otherwise identical, their counting rates can be compared directly. The quantitative interpre-

[11] W. E. Ramsey, Phys. Rev. **57**, 106 (1940).

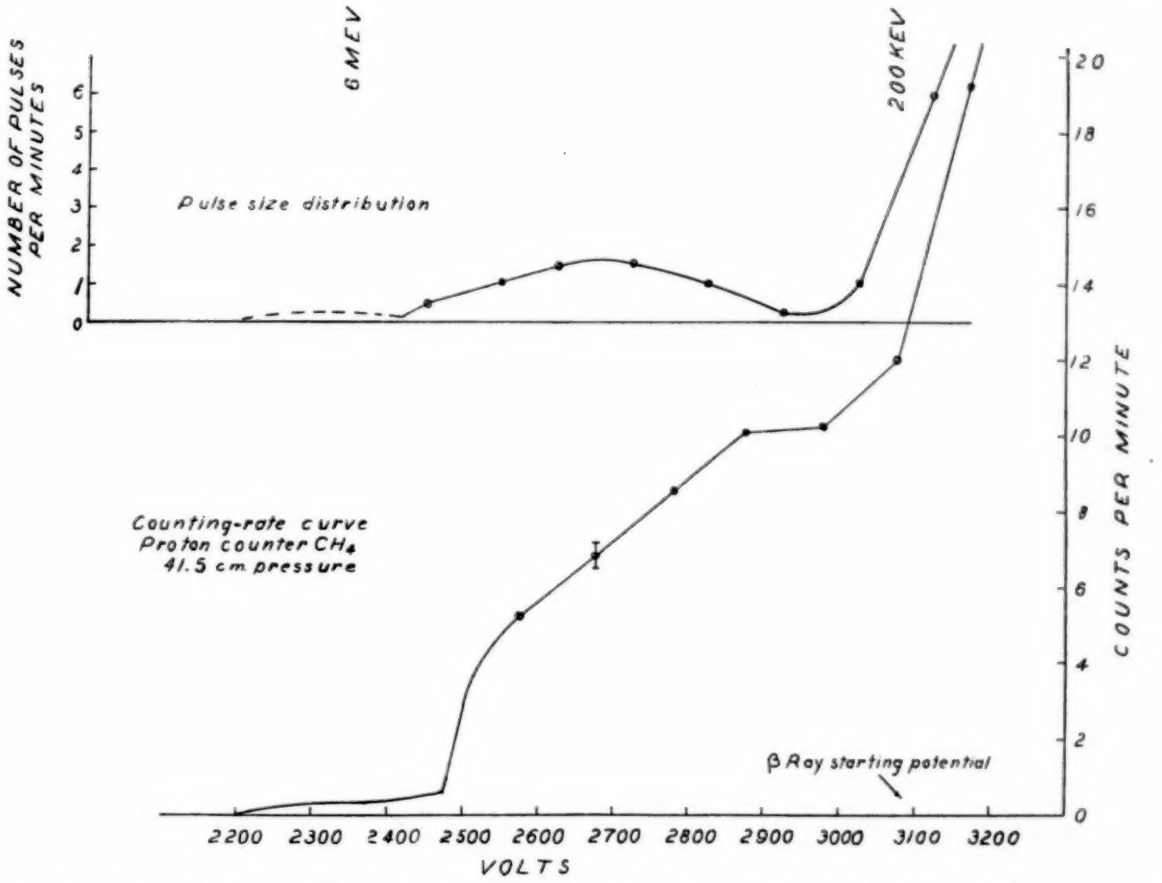

FIG. 2. Counting rate of proton counter, filled with CH_4 on Mt. Evans. Upper curve is differential of observed curve below, and shows size distribution of ionizing events. This counter does not detect slow neutrons.

tation in terms of rates of production is discussed below.

The counting rate of the copper cylinder counter is shown in Fig. 2, as is the pulse-size distribution observed in this counter. Because of the different counter lengths, the counting rate of the copper cylinder counter was reduced to a value per unit length before comparing with the other counters. Under comparable conditions, the counting rates of the several counters were

$$n_{Al} : n_{Cu} : n_{Pb} = 7 : 4.5 : 7$$
$$\pm 0.5 \text{ counts per minute,}$$

where the metal of which the cylinder is made is indicated by the subscript. The cylinder, about 1 mm of lead or equivalent, was thick compared to the range for most of the protons observed.

DISCUSSION

It will be recalled[7] that a detector surrounded by water will be activated at a rate n counts per second, related to q_w, the rate of production of neutrons per gram per second in the water, through

$$q_w = (n/V)(\sigma_w/\sigma_D)(1245/p), \qquad (1)$$

where V is the volume of the counter, p the pressure of the gas in it, 1245 is a constant equal to the standard volume $2.24\times10^4/18$, the 18 being the molecular weight of water, σ_w is the capture cross section of water for slow neutrons, and σ_D that of boron. Using this relationship, and the observed counting rate of the counter $n=0.1$ counts per second (corresponding to the difference between the counts with and without cadmium), $V=1450$ cc, $p=74/76$ atmos., and taking σ_w and σ_D as 0.5 and 550×10^{-24}, respectively, we find the rate of production of neutrons in water at the level of the top of Mount Evans to be 2×10^{-4} per gram per second; while at Denver it is 5×10^{-5} per gram per second. It must be pointed out that Eq. (1) assumes that all the

disintegrations occurring in the volume V are recorded. Thus V is the effective volume of the counter, a quantity smaller than the volume of the cylinder by an amount equal to the end and side corrections, since alpha-particles produced near the ends or sides may collide with the walls before expending all their energy as ionization in the gas. Thus the effective volume corrections depend on the pressure and may be calculated for any given arrangement. By applying this active volume correction, V in the case cited is about 900 cc, and the values of q for neutrons become 3×10^{-4} and 8×10^{-5} per gram per second in water at Mount Evans and Denver, respectively.

The coincidence experiments also indicate a connection between the neutrons and the soft component. We may inquire what fraction of the total showers S are showers in which a neutron is produced. Let E_n be the efficiency of the neutron counter, which counts neutrons at the rate C_n. Then the total number of neutrons will be C_n/E_n, passing through the counter per unit time. If neutron-shower coincidences are observed at a rate C_c, and if Z is the total number of events in which both a shower and a neutron was produced, then

$$Z/S=C_c/E_nC_s. \tag{2}$$

In this case, C_c was 0.2, C_s, the counting rate for showers, was 100, and E_n, for thermal neutrons, is given by

$$E_n=Np\sigma L, \tag{3}$$

where N is the Loschmidt number, p the gas pressure in atmos., L the average path length for neutrons passing through the counter, and σ the capture cross section of the detecting gas molecule for the neutrons to be measured. In the counters used, L was 7 cm, σ was taken as 550×10^{-24}, a figure which has the isotope ratio already included, and which assumes, as is the case here, that substantially all the neutrons are thermal, E_n was about 0.1. Hence Z/s is about 0.02, or about two percent of all the showers are events in which a neutron is produced also.

The rate of production of the protons Q per gram per second can be related, as has been shown,[6] to the counting rate N_p, through the expression

$$N_p=S\int_0^{E_{\max}} I(E)dE=SQR(E_{\max}), \tag{4}$$

where S is the effective area of the counter, $I(E)$ is the flux of protons per cm sq. per sec. with energies in the interval dE, and $R(E_{\max})$ is the range corresponding to the maximum value of the proton energy E which can be detected in the particular counter used. It is evident that if Q is to be in grams, R must be in grams. There were about 0.1 count per second due to protons in the counter and its cross-sectional area S was about 500 sq. cm. In this case, $R(E_{\max})$ was about 400 cm of standard air, or dividing by the density, 0.4 g; and hence Q is about 5×10^{-4} per gram, which is of the same order of magnitude as the rate of production of neutrons.

In the counters with lead and aluminum cylinders, the rates of production per gram in Pb and Al, Q_{Pb} and Q_{Al}, will be related to the respective counting rates N in the ratio

$$Q_{\mathrm{Al}}/Q_{\mathrm{Pb}}=(N_{\mathrm{Al}}/N_{\mathrm{Pb}})\cdot(S_{\mathrm{Al}}/S_{\mathrm{Pb}})\cdot(\mu_{\mathrm{Pb}}/\mu_{\mathrm{Al}})$$
$$=1.86\pm0\,3, \tag{5}$$

where μ is the atomic weight and S the relative stopping power per atom of each substance indicated by its subscript. Hence Q_{Pb} and Q_{Al} may be expressed in terms of production cross section σ which will have the ratio

$$\sigma_{\mathrm{Al}}/\sigma_{\mathrm{Pb}}=(N_{\mathrm{Al}}/N_{\mathrm{Pb}})\cdot(S_{\mathrm{Al}}/S_{\mathrm{Pb}})=0.3. \tag{6}$$

The counting rate of the copper cylinder counter may be similarly considered, and the ratio of $\sigma_{\mathrm{Al}}:\sigma_{\mathrm{Cu}}$ obtained. It is found that the results may be expressed in the ratio

$$\sigma_{\mathrm{Al}}:\sigma_{\mathrm{Cu}}:\sigma_{\mathrm{Pb}};\quad 1:1\pm0.2:3\pm0.3. \tag{7}$$

It will be noted that σ increases more slowly than Z, the ratios of the Z's being roughly 1 : 2.2 : 6.5, which suggests that possibly in heavier nuclei some screening occurs, decreasing the probability of proton emission below a direct proportionality with the number of protons Z.

Some protons will also be produced in the gas (CH_4) of the counters. If the volume of gas within the cylinder is 1416 cc at 0.28 atmos. pressure, the s.t.p. density of CH_4 being 0.00072

g/cc, then the total mass of gas is 0.285 gram, and if Q is about 10^{-3} per gram, we would expect a contribution of about 1.7×10^{-2} count per minute, or about one percent of the observed counting rate. Most of the protons will be produced in the walls or gas, for it would require a proton of about 80 Mev to penetrate through the thick cylinder and glass envelope to reach the interior from any region of production outside the counter. The protons producing the counts must be within the last 30 Mev of the ends of their ranges in passing through the counters in order to lose enough energy per traversal to count.

Giant showers will trip the neutron-shower coincidence arrangement, since they cause two or more of the shower counters to discharge, and might easily also cause several hundred electrons to pass through the neutron counter, thus producing as much ionization as a disintegration-alpha. In order to set a limit to the number of counts due to such showers, we took advantage of the opportunity provided by the presence on Mt. Evans of a cloud chamber belonging to Wilson Powell. The neutron-shower arrangement was set up directly above his cloud chamber and neutron-shower coincidences caused to trip the chamber. The resulting photographs showed one to two giant showers per hour, a figure which may be seen to account for ten to twenty percent of the observed "neutron-shower coincidence" counts.

The background counting rate of the neutron-shower coincidences, found when cadmium surrounded the neutron counter was 0.22 per min. But the giant shower rate, capable of tripping this arrangement was found to be of the order of 0.03 per min. It is clear that there are some additional processes taking place in which large amounts of ionization are liberated but a small number of particles are involved, which may possibly be protons produced by events connected with the soft component.

Some attempts have been made to explain the production of heavy particles by the cosmic radiation on the basis of various hypotheses. The possibility that the neutrons are in part produced by photons has been discussed.[7] Such processes are known for photons of 17 Mev and less,[12] but the cross sections at these energies are not large enough to enable the known density of photons in the cosmic radiation to be considered as having produced all the observed neutrons. Yet it must be recalled that the cross section for the production of photo-neutrons is known to increase with energy up to the present observable limit at 17 Mev and may reasonably be assumed to increase further up to several times this energy. A cross section of about 10^{-26} sq. cm will suffice to explain all the neutrons on this basis.

The suggestion has been made[8] that electrons produce "star" explosion processes, and that these may be the origin of the neutrons. While it is quite evident that an electron of, say 10^9 ev has ample energy to penetrate a nucleus and cause it to "explode," yet it is necessary to postulate a fairly large cross section if this process is to account for all the neutrons. We are aware of no process by which the abundant low energy cosmic-ray electrons may produce nuclear disintegrations; yet the equally abundant low energy photons are known so to do. It seems probable that in actuality several processes are involved and that the cross section for each is a different function of the energy.

ACKNOWLEDGMENTS

It is a pleasure to acknowledge the helpful assistance received from J. C. Stearns and the University of Denver in connection with the use of the Mount Evans Cosmic Ray Laboratory and the operation of the counter at Denver. Financial support was received from the Carnegie Institution of Washington. We are indebted to Wilson Powell for extensive collaboration in connection with the cloud-chamber study. The counters and thin windows were constructed by Austin Nester. The investigation was started while the authors were on the staff of the Bartol Research Foundation and concluded at New York University.

[12] H. Bothe and W. Gentner, Naturwiss. **25**, 90, 126, 191, and 284 (1937).

The Radioactive Isotopes of Nickel and Their Assignments

MARTIN E. NELSON, M. L. POOL, AND J. D. KURBATOV
The Ohio State University, Columbus, Ohio

(Received January 16, 1942)

As a result of discrepancies in the reported methods of production and in the assignments of the radioactive isotopes of nickel the following reactions were investigated: Fe(α, n), Co(d, $2n$), Ni(d, p), Ni(n, γ), and Ni(n, $2n$). The relative yields of the known 2.6-hour and 36-hour periods from fast and slow neutrons on nickel were compared with other neutron reactions. The results obtained are in agreement with the assignment of the 2.6-hour period to Ni^{63} and the 36-hour period to Ni^{57}. The possible existence of a short period in nickel, reported as a result of an Fe(α, n) reaction, is not established since it would be masked by the 2.1-minute oxygen period formed from the carbon present in iron. In the attempted separation of the O^{15} activity it was observed that under the prevailing experimental conditions the rate of removal of oxygen from bombarded iron approached the rate of decay of O^{15}.

INTRODUCTION

THREE radioactive isotopes of nickel of periods 2.6 hours, 36 hours and 2 minutes have been reported. The 2.6-hour period was first produced by activation of nickel with slow neutrons,[1] and later by activation of zinc, copper, and nickel with fast neutrons.[2] The 2.6-hour period was also observed by other investigators after the bombardment of nickel with slow and fast neutrons and with deuterons.[3]

In addition a 36-hour period in nickel was obtained from the bombardment of iron with alpha-particles and nickel with fast neutrons.[3] However, the 36-hour activity was not produced by either a deuteron or slow neutron bombardment of nickel and so was assigned to Ni^{57} as shown in Fig. 1. In contradiction to these results, the 36-hour period was recently reported to be observed after slow neutron and deuteron bombardment of nickel.[4] The activity was consequently assigned to Ni^{59}.

A 2-minute period was also reported as a result of the bombardment of iron with alpha-particles and nickel with fast neutrons. This activity was assigned to Ni^{57}. Observations of the regularities in families of odd nuclei differing by alpha-particle units led to the expectation of periods of approximately 2 minutes, 30 hours, and several years in nickel.[5,6] These periods were assigned to Ni^{57}, Ni^{59}, and Ni^{63}, respectively, leaving the 2.6-hour period to be assigned to Ni^{65}.

Because of these predictions and the discrepancies in the experimental data, a reinvestigation of the various nickel activities was thought justifiable.

THE 2.6-HOUR PERIOD

Hilger No. 5477 H.S. nickel metal was bombarded with 10-Mev deuterons. Spectroscopic analysis indicates the presence of 0.015 percent iron, 0.03 percent carbon, and traces of copper and oxygen. After bombardment the metal was dissolved, carriers of the above-mentioned impurities and of other elements commonly present in nickel were added, and separation of nickel was made with dimethylglyoxime. The nickel precipitate was redissolved and after another addition of carriers was again precipitated. This procedure was repeated several times until the filtrates from nickel showed no activity when measured with an immersion type G-M tube.

The purified nickel fraction was then measured with a Wulf electrometer and an ionization chamber filled with Freon under two atmospheres pressure. The decay curve shown in Fig. 2 is the simple 2.6-hour period which was followed through 18 half-lives to one-tenth of background. Since this period has also been produced

[1] J. Rotblat, Nature **136**, 515 (1935).
[2] F. A. Heyn, Physica **4**, 1224 (1937).
[3] J. J. Livingood and G. T. Seaborg, Phys. Rev. **53**, 756 (1938).
[4] R. L. Doran and W. J. Henderson, Phys. Rev. **60**, 411 (1941).
[5] G. R. Dickson, P. W. McDaniel, and E. J. Konopinski, Phys. Rev. **57**, 351 (1940).
[6] G. R. Dickson and E. J. Konopinski, Phys. Rev. **58**, 949 (1940).

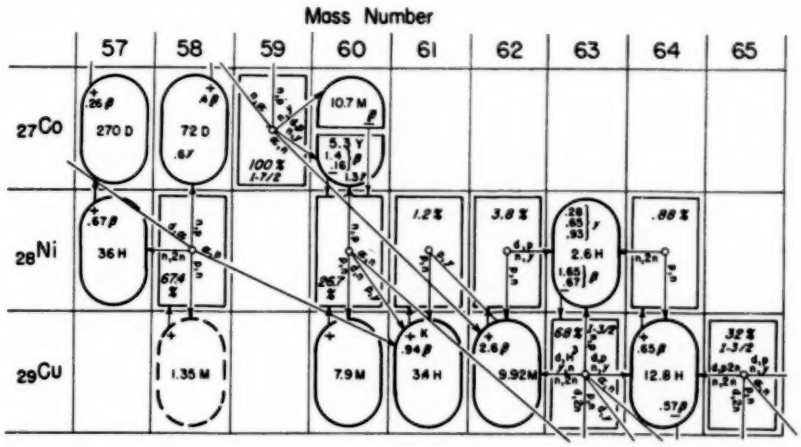

FIG. 1. Isotopic chart of the region studied.

by Zn(n, α) and Cu(n, p) reactions, its assignment to either Ni^{63} or Ni^{65} is possible. Definite assignment can best be based on the relative production of the activity by slow and fast neutrons on nickel.

In order to determine whether the apparent production by fast neutrons might actually be due to slow neutrons present in the fast neutron radiation, the yields of activity produced by slow and fast neutron bombardments were compared. These comparisons were made under the assumption that the capture cross section averaged over the slow neutron energies was nearly the same for the slow neutrons present in the paraffin as for the slow neutrons present in the fast neutron radiation.

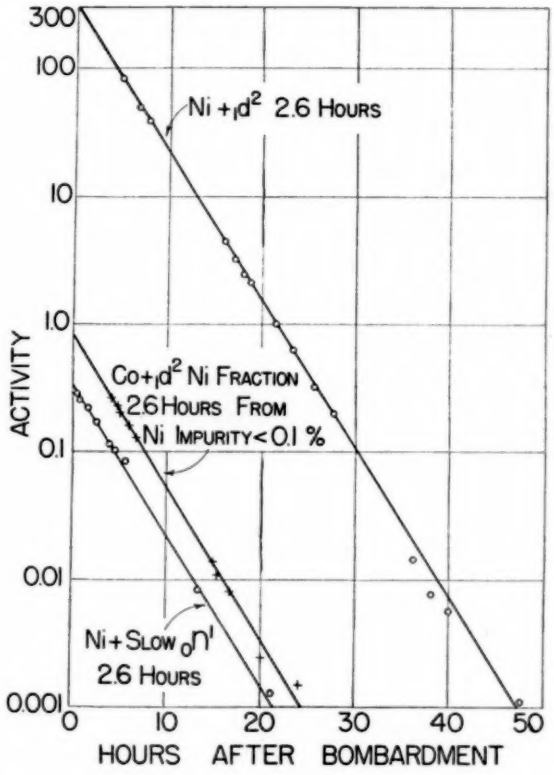

FIG. 2. Decay curves resulting from Ni+d, Co+d, and Ni+slow n bombardments.

Two similar sets of samples of manganese, silver, copper, and nickel were simultaneously bombarded with slow and fast neutrons. The samples to be activated by fast neutrons were placed directly behind a lithium target in the cyclotron tank (position A). The slow neutron samples were imbedded in paraffin blocks outside the tank (position B). The ratio of the yield obtained at position A to the yield obtained at position B for each element is given in Table I along with the type of reaction by which each of the activities was produced.

The ratio of the yield at A to the yield at B for the 2.6-hour nickel period is greater by a factor of 36 than that for the 2.59-hour manganese period which is produced by an (n, γ) reaction. However, the ratio is of the same order of magnitude as that for the 12.8-hour copper period which is produced by both (n, γ) and (n, $2n$) reactions. These comparisons indicate that the 2.6-hour nickel period is not produced by an (n, γ) reaction alone but by an (n, $2n$) reaction as well. This conclusion would necessitate the assignment of the activity to Ni^{63}.

THE 36-HOUR PERIOD

In the previously described bombardment of nickel with deuterons no 36-hour activity was found. If the 36-hour period had also been pro-

duced, its initial activity must have been less than 0.01 percent of that of the 2.6-hour period, otherwise it would have been detected. The ratio of the activities (36-hour : 2.6-hour) which would have been produced from an infinitely long bombardment was calculated to be less than 1 : 1200. In addition, it was found that during deuteron bombardments activities apparently due to deuterons were actually due to secondary neutrons produced at the target. Samples of nickel and cobalt were placed behind the primary nickel target. A weak activity was produced in the nickel sample, indicating the presence of the 2.6-hour period, and the known 2.59-hour period of Mn^{56} resulting from the $Co^{59}(n, \alpha)Mn^{56}$ reaction was observed in the cobalt sample. The intensity of the latter activity was about 1 percent of that produced by lithium neutrons.

Nickel was also bombarded with slow neutrons. No 36-hour activity was found but a 2.6-hour period was followed for seven half-lives to less than one-tenth of background. The ratio of the activities (36-hour : 2.6-hour) which would have been produced from an infinitely long bombardment was calculated to be less than 1 : 25.

To investigate a possible $Co(d, 2n)Ni$ reaction, Hilger No. 11045 V.P.S. cobalt metal was bombarded with deuterons. Spectroscopic analysis shows that its main impurities are nickel in a concentration less than 0.1 percent and traces of calcium, chromium, iron, copper, zinc, silver, and lead totaling about 0.1 percent. After bombardment, nickel was separated from iron, chromium, phosphorus, and other elements by precipitating the latter with ammonium hydroxide and filtering off the ammoniacal complex containing nickel. Since copper, cobalt, and other elements were still present, nickel was repeatedly separated from them with dimethylglyoxime as previously described. The decay curve of the nickel fraction again showed no 36-hour period but only the 2.6-hour period due to the nickel impurity. Thus no 36-hour activity was produced from a $Co(d, 2n)Ni$ reaction with 10-Mev deuterons.

TABLE I. Comparison of yields.

Reaction	Period	Yield at position A / Yield at position B
(n, γ)	2.59 hr. Mn	0.33
$(n, 2n)$	25 min. Ag	>5000
(n, γ) and $(n, 2n)$	12.8 hr. Cu	10
——	2.6 hr. Ni	12
——	36 hr. Ni	>200

The 36-hour period was produced by the known $Fe(\alpha, n)$ and $Ni(n, 2n)$ reactions, in which cases chemical separations similar to those previously described were made. However, the activity was not produced by $Co(d, 2n)$, $Ni(d, p)$ or $Ni(n, \gamma)$ reactions. All these data can be interpreted by assigning this period to Ni^{57}. The absence of activity from a $Co(d, 2n)$ reaction is consistent with the recently reported non-existence of stable Co^{57}.[7]

THE 2-MINUTE PERIOD

The 2-minute period has been previously reported as a result of $Fe(\alpha, n)Ni$, and $Ni(n, 2n)Ni$ reactions. However, the definite possibility of the presence of the 2.1-minute oxygen period which might complicate the identification of the nickel was not indicated. The 2.1-minute oxygen should always be formed by the $C^{12}(\alpha, n)O^{15}$ reaction after activation of iron with alpha-particles since even the purest iron samples contain some carbon. Therefore, an attempt was made to remove oxygen in order to observe the possible existence of a short period in nickel.

An independent alpha-particle bombardment of carbon in the form of sodium carbonate was made. After dissolving the activated substance in water a part was measured immediately with an immersion type G-M tube. Another part was treated with hydrochloric acid and evaporated. The procedure was repeated three times before measurement. The presence of a 2.2 ± 0.1-minute activity in both parts showed that the radioactive O^{15} was not entirely removed. The difficulty lies in the fact that the removal of oxygen is never complete in the procedure mentioned and that the rate of removal approached the rate of decay of the oxygen period.

Iron was bombarded with alpha-particles and then dissolved in nitric acid. The activity in one part was measured immediately and was found to decay with a 2.2-minute period. Another part of the same solution was treated with hydrochloric acid and evaporated. The solid salt of

[7] J. J. Mitchell, H. S. Brown, and R. D. Fowler, Phys. Rev. **60**, 359 (1941).

iron was converted into the oxide by ignition. The oxide was again dissolved and the operation repeated. Measurements on the G-M counter showed that a weak 2.2-minute period remained just as in the case of the carbon bombardment.

Nickel was also bombarded with fast neutrons, but no 2-minute period was observed. However, the production of such a period by fast neutron bombardment of oxygen in the form of sodium carbonate was confirmed.

These results indicate that the 2-minute activity reported as a result of the bombardment of iron with alpha-particles may be due to O^{15}. However, the results do not necessarily exclude the possibility of the existence of a short period in nickel, the presence of which is not evident from the above described experiments. The development of an experimental technique for the rapid removal of oxygen is necessary before the question of the existence of a short period in nickel can be settled.

It is a pleasure to acknowledge the support received from the University Development Fund and from Mr. Julius F. Stone. Valuable assistance through the W.P.A. cyclotron project No. 65-1-42-89 is also acknowledged.

APRIL 1 AND 15, 1942 PHYSICAL REVIEW VOLUME 61

Forbidden Transitions in β-decay and Orbital Electron Capture and Spins of Nuclei

R. E. MARSHAK
University of Rochester, Rochester, New York

(Received January 16, 1942)

A general formula giving minimum lifetimes for forbidden β-transitions of arbitrary order or forbidden orbital electron capture is derived. Exact Coulomb wave functions are used for the electron. It is shown that the observed electron emission of K^{40} requires Gamow-Teller selection rules. Combined with the Konopinski-Uhlenbeck result that only the tensor and vector interactions are compatible with the energy spectra of the β-rays from Na^{24}, P^{32}, and RaE, it follows that the tensor interaction alone can explain both the lifetimes and energy spectra of forbidden β-transitions. The application of the tensor interaction to K^{40} and to the other long-lived β-emitters, Rb^{87}, Lu^{176}, Be^{10}, C^{14}, and to existing data on orbital electron capture, leads to certain spin and parity predictions about parent and product nuclei—e.g., neither Be^{10} nor C^{14} can have a spin greater than $3\hbar$, the 2-Mev γ-ray from K^{40} is associated with K-electron capture to an excited state of A^{40} having even parity, etc. The stability of the known neighboring isobars and the conditions under which L-electron capture becomes more probable than K-electron capture are also discussed.

I. INTRODUCTION

EXPERIMENTS on β-radioactive nuclei have tended in recent years to confirm Gamow and Teller's[1] modification of Fermi's theory of β-decay according to which an "allowed" transition may involve a spin change of as much as one unit of $\hbar$. In particular, the strikingly large probability of the reaction $He^6 \rightarrow Li^6 + e^-$, was presumed to provide strong support for the correctness of the Gamow-Teller selection rules since the transition from He^6 with a spin zero to Li^6 with a spin one involves a spin change of one unit. The Li^6 spin has been measured but the spin of He^6 was based on the argument from nuclear theory that all nuclei, whether stable or unstable, with an even number of protons and an even number of neutrons, have spin zero. It is certainly true that all known *stable* even-even nuclei have spin zero but the extrapolation to unstable even-even nuclei has been rendered extremely dubious by the fact that certain homologues of He^6, such as Be^{10} and C^{14}, decay very slowly and cannot therefore have the same

[1] G. Gamow and E. Teller, Phys. Rev. **49**, 895 (1936); there is a good deal of indirect evidence for the Gamow-Teller selection rules [cf. especially E. P. Wigner, Phys. Rev. **56**, 519 (1939); and White, Creutz, Delsasso, and Wilson, Phys. Rev. **59**, 63 (1941)] but none can be as conclusive as the type discussed below.

spin as He^6.[2] If not *all* unstable even-even nuclei have spin zero, it becomes a little difficult to decide whether any have, and the evidence for the Gamow-Teller selection rules becomes more shaky. Thus the decay of He^6 and C^{10} would be compatible with the original Fermi selection rules if the spins of both He^6 and C^{10} are one; furthermore, the slow reactions involving Be^{10} and C^{14} could be explained by assuming even larger spins than one. It therefore becomes of interest to find some independent test of the validity of the Gamow-Teller selection rules.

A test of the Gamow-Teller selection rules is, in principle, possible if the lifetime and spin of the β-radioactive nucleus, the spin of the product nucleus, and the maximum energy of the β-ray are all known. A knowledge of all these quantities enables one to calculate a lower limit to the lifetime for a given spin change and given maximum energy of the β-ray. An interaction between the nuclear particles and the electron-neutrino field, which contains an explicit dependence on the spin (to be referred to as a Gamow-Teller type of interaction), will in general permit a change of spin of one unit more—for approximately the same lifetime—than will be allowed by an interaction containing no explicit dependence on the spin (to be referred to as a Fermi type of interaction). To put it another way, corresponding to a known spin change the minimum lifetime predicted by a Fermi type of interaction is greater—by a factor of about one thousand—than the minimum lifetime predicted by a Gamow-Teller type of interaction. If the observed lifetime lies between the Fermi and Gamow-Teller minimum values then the Fermi type of interaction is definitely excluded and the Gamow-Teller type of interaction is strongly supported. The most difficult to obtain but at the same time the crucial piece of information required to make this kind of decision is knowledge of the spin of the β-radioactive nucleus. To determine the spin of the β-emitter it is necessary that the lifetime be long compared to the experimental time and the only β-emitters satisfying this condition will be those undergoing "forbidden" transitions. This requires an extension of the theory of β-decay to a calculation of the lifetimes for forbidden transitions of arbitrary order; this calculation is carried out in Section II and the general formulae are given by Eqs. (11), (17a), (17b), and (19c).

Until very recently only the spins of the fairly abundant naturally β-radioactive nuclei Rb^{87} and Lu^{176} [3] had been measured. But now Zacharias[4] has measured the spin of the very rare naturally β-radioactive isotope K^{40}. It is to be expected that existing techniques could be employed to measure the spins of the artifically produced long-lived nuclei such as Be^{10} and C^{14}, but it will be shown that knowledge of the spins of the natural β-emitters—in particular of K^{40}—is sufficient to decide for the Gamow-Teller selection rules in β-decay. A preliminary calculation on K^{40} which did not take account of the Coulomb field for the electron has been reported on[5] but in the present paper exact wave functions are used for both the electron and neutrino. Since recent improved experiments supply convincing evidence[6] for a theory of β-decay which does not involve derivatives of the light particle wave functions, one must make a decision among five possible independent formulations—the scalar, pseudo-scalar, vector, pseudo-vector, and tensor interactions. Of these the first three are Fermi type interactions whereas the last two are Gamow-Teller type interactions. As far as lifetime calculations are concerned the last two cannot be distinguished. However in the meantime Konopinski and Uhlenbeck[7] have tried to decide among the various possible formulations on the basis of the observed energy spectra of Na^{24}, P^{32}, and RaE. They conclude that the scalar, pseudo-scalar, and pseudo-vector interactions can be eliminated. This, combined with our result that only the pseudo-vector and tensor interactions are possible, leads to the unique result that the tensor interaction is the correct one.

[2] For a discussion of this point, see J. R. Oppenheimer, Phys. Rev. **59**, 908 (1941).

[3] M. Heyden and H. Kopfermann, Zeits. f. Physik **108**, 232 (1938) and H. Schüler and H. Gollnow, Zeits. f. Physik **113**, 1 (1939).

[4] J. R. Zacharias, Phys. Rev. **60**, 168 (1941).

[5] R. E. Marshak, Phys. Rev. **59**, 937A (1941).

[6] For a discussion of this evidence, cf. R. D. Evans, "Introduction to the Atomic Nucleus," M. I. T. Course Notes; I am indebted to Professor Evans for placing his manuscript at the disposal of our laboratory.

[7] E. J. Konopinski and G. E. Uhlenbeck, Phys. Rev. **60**, 308 (1941); I wish to thank the authors for sending me their paper prior to publication.

In Section III the tensor interaction is applied to the known long-lived β-emitters Rb^{87}, Lu^{176}, Be^{10}, C^{14}, with half-lives of the order or greater than one thousand years, to determine the nature of the forbidden transition taking place. Table I gives the experimental data and Table II lists the theoretical lifetimes obtained under different assumptions as to the spin and parity changes of the nuclei involved. It is found, for example, that neither Be^{10} nor C^{14} can have a spin larger than $3\hbar$, that the Rb^{87} decay involves a parity change, and so on.

Finally in Section IV the tensor interaction is used to find a general formula [cf. Eq. (20)] for allowed and forbidden orbital electron capture. It is shown that for allowed transitions and sufficiently negative energy differences between initial and final nuclei, L_{I}-electron capture becomes comparable to K-electron capture. Under favorable circumstances it should be possible to observe these long-lived allowed transitions. Moreover, the presence or absence of appreciable x-radiation associated with L_{I} capture will distinguish long-lived allowed transitions from first forbidden transitions. Again, in principle, for first- or higher-order forbidden transitions and sufficiently negative energy differences between initial and final nuclei, $L_{\text{II, III}}$-electron capture becomes comparable to K capture; but it is likely that such activities will escape detection because of the small intensities involved. An attempt is made to classify the type of the transition (i.e., allowed or forbidden) for the better known long-lived unstable nuclei decaying by orbital electron capture, e.g., V^{47}, Mn^{54}, K^{40}. The stability of the known neighboring isobars is also discussed on the basis of Eq. (20).

II. THE CALCULATION OF LIFETIMES FOR FORBIDDEN β-EMISSION

It is well known from the theory of atomic spectra that the lifetime of an excited state is independent of the magnetic quantum number of the state for a given total angular momentum change and provided that the summation is taken over all possible magnetic quantum numbers of the final state. A similar rule holds for β-ray emission and we can therefore choose the magnetic quantum number of the initial state in such a way that the least amount of calculation is required. Let j_i be the spin of the initial nucleus and j_f the spin of the final nucleus. Then the maximum contribution to the transition probability comes from that part of the electron-neutrino field which has associated with it a total angular momentum $k=|j_i-j_f|$. We assume first that $j_i>j_f$; then if we choose the maximum value of m_i (equal to j_i), there is only one possible transition, namely, $j_i,\ m_i=j_i\rightarrow j_f,\ m_f=m_i-\mu$ where $\mu=k$ is the maximum magnetic quantum number associated with the field. The transition probability T may therefore be calculated in a unique way by considering the emission of an electron-neutrino pair with total angular momentum quantum number k and total magnetic quantum number $\mu=k$; the lifetime τ will be $1/T$. If $j_i<j_f$, the transition probably T found for the emission of an electron-neutrino pair with total quantum numbers k and $\mu=k$, must be multiplied by the statistical factor $(2j_f+1)/(2j_i+1)$ to give the reciprocal lifetime, i.e.,

$$1/\tau=[(2j_f+1)/(2j_i+1)]\cdot T.$$

We are interested in the shortest lifetime which is compatible with the emission of an electron-neutrino pair of total angular momentum $k=|j_i-j_f|$. This will clearly be given by the Gamow-Teller type of interaction of which there are two kinds,[8] the tensor and pseudo-vector interactions. Since Konopinski and Uhlenbeck have excluded the pseudo-vector interaction on the basis of energy spectra considerations, we perform our calculation for the tensor interaction. However, this is no real restriction since the axial vector interaction leads to essentially the same result. The tensor interaction may be written as:

$$H=G\{(\Psi^*\beta\sigma\Phi)\cdot(\psi^*\beta\sigma\phi)+(\Psi^*\beta\alpha\Phi)\cdot(\psi^*\beta\alpha\phi)\}. \quad (1)$$

In this expression G is the coupling constant of the nuclear particle with the electron-neutrino field, Ψ and Φ are the quantized Dirac wave functions of the nuclear particle; if Ψ represents a proton, then Φ represents a neutron and

[8] Cf. H. A. Bethe and R. F. Bacher, Rev. Mod. Phys. **8**, 82 (1936).

conversely. The quantities ψ, ϕ are the quantized wave functions of the electron and anti-neutrino, respectively, normalized to one particle in a sphere of unit radius, and evaluated at the position of the nuclear particle; ψ is a solution of the Dirac equation in the Coulomb field of the nucleus, and ϕ is a solution of the Dirac equation in the field-free case. The operators β, α are the usual Dirac operators, and we have $\sigma=-i\alpha_x\alpha_y\alpha_z\alpha$. The probability of the emission of an electron with energy[9] between W and $W+dW$ is:

$$P(W)dW=\frac{2}{\pi}\sum_{(j_1l_1m_1)}\sum_{(j_2l_2m_2)}|H_{ab}|^2\frac{W}{(W^2-1)^{\frac{1}{2}}}dW. \quad (2)$$

The first summation is over the angular momentum quantum numbers of the electron, the second over the angular momentum quantum numbers of the neutrino; H_{ab} is the matrix element of a transition for the interaction (1) taken over the nuclear volume. Since the de Broglie wave-length of the electron and neutrino are large compared to nuclear dimensions, this matrix element can be evaluated in successive approximations corresponding to increasingly larger values of the total angular momentum of the electron-neutrino pair. For a given spin change, $k=|j_i-j_f|$ of the nucleus, by far the largest contribution to the transition probability will come from the part of (1) containing the four-component operator $\beta\sigma$; therefore we first neglect the second term in the expression (1). We consider the single matrix element:

$$H_{ab}=\int d\tau(\Psi_b^*\beta\sigma\Phi_a)\cdot(\psi^*\beta\sigma\phi). \quad (3)$$

It is convenient to use only the positive energy solutions of the Dirac equation; if we use an ordering between solutions of positive and negative energy which is both Lorentz invariant and invariant with respect to all reflections, we may write for H_{ab}:

$$H_{ab}=\int d\tau(\Psi_b^*\beta\sigma\Phi_a)\cdot(\psi C\beta\sigma\phi)^*. \quad (4)$$

[9] All quantities are given in relativistic units: unit of energy is mc^2, of time is $\hbar/mc^2$, and of length is $\hbar/mc$; m is the electron mass.

The operator C can be written as $\beta\alpha_y$[10] and the ψ, ϕ are now positive energy solutions of the following forms:[11]

Type (a): $j=l+\frac{1}{2}$

$$\left.\begin{aligned}
\psi_1&=i\left(\frac{l-m+\frac{3}{2}}{2l+3}\right)^{\frac{1}{2}}Y_{l+1,\,m-\frac{1}{2}}f_l(r),\\
\psi_2&=i\left(\frac{l+m+\frac{3}{2}}{2l+3}\right)^{\frac{1}{2}}Y_{l+1,\,m+\frac{1}{2}}f_l(r),\\
\psi_3&=\left(\frac{l+m+\frac{1}{2}}{2l+1}\right)^{\frac{1}{2}}Y_{l,\,m-\frac{1}{2}}g_l(r),\\
\psi_4&=-\left(\frac{l-m+\frac{1}{2}}{2l+1}\right)^{\frac{1}{2}}Y_{l,\,m+\frac{1}{2}}g_l(r).
\end{aligned}\right\} \quad (5a)$$

Type (b): $j=l-\frac{1}{2}$

$$\left.\begin{aligned}
\psi_1&=i\left(\frac{l+m-\frac{1}{2}}{2l-1}\right)^{\frac{1}{2}}Y_{l-1,\,m-\frac{1}{2}}f_{-l-1}(r),\\
\psi_2&=-i\left(\frac{l-m-\frac{1}{2}}{2l-1}\right)^{\frac{1}{2}}Y_{l-1,\,m+\frac{1}{2}}f_{-l-1}(r),\\
\psi_3&=\left(\frac{l-m+\frac{1}{2}}{2l+1}\right)^{\frac{1}{2}}Y_{l,\,m-\frac{1}{2}}g_{-l-1}(r),\\
\psi_4&=\left(\frac{l+m+\frac{1}{2}}{2l+1}\right)^{\frac{1}{2}}Y_{l,\,m+\frac{1}{2}}g_{-l-1}(r).
\end{aligned}\right\} \quad (5b)$$

The functions f, g are defined in reference 11 and involve confluent hypergeometric functions of (pr) where p is the electron momentum. The neutrino wave functions are of exactly the form (5a), (5b) except that the f's and g's are now Bessel functions and the energy is equal to the momentum which is denoted by q. Thus we have:

$$\left.\begin{aligned}
f_l&=(\pi q/2r)^{\frac{1}{2}}J_{l+3/2}(qr),\\
g_l&=-(\pi q/2r)^{\frac{1}{2}}J_{l+\frac{1}{2}}(qr),
\end{aligned}\right\} \quad (6a)$$

$$\left.\begin{aligned}
f_{-l-1}&=(\pi q/2r)^{\frac{1}{2}}J_{l-1}(qr),\\
g_{-l-1}&=(\pi q/2r)^{\frac{1}{2}}J_{l+\frac{1}{2}}(qr).
\end{aligned}\right\} \quad (6b)$$

[10] The operator C is different from the $\delta=\beta\alpha_x\alpha_z$ originally used by Fermi (Zeits. f. Physik **88**, 161 (1934)); C satisfies the conditions: (a) $\alpha^*C=C\alpha$, (b) $\beta^*C=-C\beta$, whereas δ satisfies condition (a) but requires a positive sign in (b). In the standard representation of the Dirac matrices C must be used instead of δ. Cf. W. Pauli, Rev. Mod. Phys. **13**, 203 (1941).

[11] Cf. M. E. Rose, Phys. Rev. **51**, 484 (1937); we use his notation throughout. This also follows the notation of Konopinski and Uhlenbeck (cf. reference 7 above).

If the neutrino rest mass m_0 were not taken as zero the f functions would have an additional factor $[(\epsilon-m_0)/\epsilon]^{\frac{1}{2}}$ and the g functions a factor $[(\epsilon+m_0)/\epsilon]^{\frac{1}{2}}$ where ϵ is the total energy measured in units of mc^2 and m_0 the rest mass measured in the same units. Moreover, it is to be remembered that all wave functions are normalized to one particle in a sphere of unit radius. Since $qr \ll 1$, we shall always use the asymptotic expansions of the Bessel functions for small values of the argument, namely:

$$J_{n+\frac{1}{2}}(z) \backsimeq \left(\frac{2}{\pi}\right)^{\frac{1}{2}} \frac{z^{n+\frac{1}{2}}}{1\cdot 3\cdots(2n+1)}. \tag{6c}$$

We shall also expand the hypergeometric functions and always keep the first non-vanishing term in (pr). These approximations are extremely good in all cases in which we are interested.

We can now calculate $P(W)dW$ for the various forbidden transitions, but as an illustration of the method we shall first calculate the transition probability when the electron-neutrino pair has a total angular momentum quantum number $k=1$ and a total magnetic quantum number $\mu=1$. If we then consider terms involving only the lowest powers of (pr) and (qr) and substitute for $(\psi c\beta\sigma\phi)^*$ the appropriate expressions, namely:

$$A_x=(\psi C\beta\sigma_x\phi)^*=i(-\psi_1\phi_3+\psi_2\phi_4-\psi_3\phi_1+\psi_4\phi_2)^*,$$

$$A_y=(\psi C\beta\sigma_y\phi)^*=-(\psi_1\phi_3+\psi_2\phi_4+\psi_3\phi_1+\psi_4\phi_2)^*,$$

$$A_z=(\psi C\beta\sigma_z\phi)^*=i(\psi_1\phi_4+\psi_2\phi_3+\psi_3\phi_2+\psi_4\phi_1)^*,$$

the double summation in (2) reduces to two terms, namely, when

$$\text{(a)} \quad \begin{cases} j_1=\frac{1}{2}, & l_1=1, & m_1=\frac{1}{2}, \\ j_2=\frac{1}{2}, & l_2=0, & m_2=\frac{1}{2}, \end{cases}$$

and when

$$\text{(b)} \quad \begin{cases} j_1=\frac{1}{2}, & l_1=0, & m_1=\frac{1}{2}, \\ j_2=\frac{1}{2}, & l_2=1, & m_2=\frac{1}{2}. \end{cases}$$

Consider the combination (a); if the electron wave functions (5b) corresponding to $j_1=\frac{1}{2}$, $l_1=1$, $m_1=\frac{1}{2}$ and the neutrino functions (6a) corresponding to $j_2=\frac{1}{2}$, $l_2=0$, $m_2=\frac{1}{2}$ are inserted, we get for the operators:

$$A_x=i[-iY^{*2}{}_{00}(\pi q/2r)^{\frac{1}{2}}f_{-2}(pr)J_1(qr)] = +Y^2{}_{00}\pi^{\frac{1}{2}}qf_{-2}(pr),$$

$$A_y=-iA_x,$$

$$A_z=0.$$

It is seen that we have only retained the terms coming from $\psi_1\phi_3$ and used (6c); the other combinations either vanish or bring in products of higher order Bessel functions (such as $J_{3/2}(qr)\sim(qr)^{\frac{1}{2}}$ instead of $J_1(qr)\sim(qr)^{\frac{1}{2}}$) and higher order hypergeometric functions which may be neglected. In a similar fashion combination (b) gives

$$A_x=i[+iY^{*2}{}_{00}(\pi q/2r)^{\frac{1}{2}}g_0(pr)J_1(qr)] = -Y^2{}_{00}\pi^{\frac{1}{2}}qg_0(pr),$$

$$A_y=-iA_x,$$

$$A_z=0.$$

These expressions must be substituted into (4) and then H_{ab} inserted into (2) with the result:

$$P(W)dW=\frac{G^2}{4\pi^3}\left|\int d\tau\Psi_b^*\beta\left(\frac{\sigma_x-i\sigma_y}{\sqrt{2}}\right)\Psi_a\right|^2(g_0^2+f_{-2}^2)\frac{q^2W}{p}dW. \tag{7}$$

The functions g_0 and f_{-2} are evaluated at the nuclear radius R and to a good approximation we have:

$$g_0^2+f_{-2}^2=2p^2F_0(Z,W)\left(\frac{1+s_0}{2}\right)$$

where

$$F_0(Z,W)=\frac{4}{\Gamma^2(1+2s_0)}(2pR)^{2s_0-2}e^{\pi\alpha ZW/p}\left|\Gamma\left(s_0+\frac{i\alpha ZW}{p}\right)\right|^2,$$

and $s_0=(1-\alpha^2Z^2)^{\frac{1}{2}}$. The quantity α is the fine structure constant, and R is the nuclear radius meas-

ured in units of $\hbar/mc$; also $F(0, W_0)=1$. For the lifetime $\tau_T^{(0)}$ we may write:

$$\frac{1}{\tau_T^{(0)}}=\frac{1}{\tau_0}|M_0|^2B_0(Z, W_0); \quad \tau_0=\frac{2\pi^3}{G^2}, \tag{8}$$

where

$$M_0=\int d\tau\Psi^*_b\left(\frac{\sigma_x-i\sigma_y}{\sqrt{2}}\right)\Psi_a, \tag{8a}$$

and

$$B_0(Z, W_0)=\int_1^{W_0}(W^2-1)^{\frac{1}{2}}W(W_0-W)^2F_0(Z, W)\left(\frac{1+s_0}{2}\right)dW. \tag{8b}$$

W_0 is the maximum energy of the electron. If the initial state of the nucleus has a spin j_i smaller than the spin j_f of the final state, the theoretical lifetime is smaller by a factor $(2j_i+1)/(2j_f+3)$. In the matrix element M_0 the operator $(\sigma_x-i\sigma_y)/\sqrt{2}$ which corresponds to $(x-iy)/\sqrt{2}$ in atomic spectra refers to the nucleus alone and can be considered now as the usual combination of Pauli two-component spin operators[12] which has the effect of lowering the order of a spherical harmonic by one. When there is a nuclear spin change of one unit in an allowed transition the nuclear wave functions will contain a spherical harmonic of the first order and $(\sigma_x-i\sigma_y)/\sqrt{2}$ will lower it to one of zero order; this zero-order harmonic combines with one of the zero-order harmonics contributed by the electron and neutrino wave functions which do not appear explicitly in (8b) because they have been absorbed into the constant in (8). The matrix element M_0 is of the order of magnitude unity, becoming an order of magnitude smaller for heavier nuclei (cf. Section III below), provided the parities of the initial and final states are the same.

If the parities of the initial and final states are different, the matrix element M_0 will vanish; to get a spin change of one unit it will then be necessary to include the terms in A_x, A_y, A_z which had previously been neglected and moreover to include the contributions from the "small" term in (1). The transition probability arising from the "small" $\beta\alpha$ term can easily be calculated in the manner outlined above. The same two angular momentum combinations (a) and (b) occur as before and we get:

$$P_1(W)dW=\frac{G^2R^2}{4\pi^3}|M'_0|^2(g_0^2+f_{-2}^2)\frac{q^2W}{p}dW; \quad M'_0=\int\frac{d\tau}{R}\Psi_b^*\beta\left(\frac{\alpha_x-i\alpha_y}{\sqrt{2}}\right)\Psi_a. \tag{9a}$$

The quantity R is again the nuclear radius measured in units of $\hbar/mc$. It is somewhat more troublesome to calculate the contribution to the transition probability of the "second"-order terms in A_x, A_y, and A_z since one must take account of several more possible combinations of angular momentum quantum numbers of the electron and neutrino. However, it turns out that the two combinations,

(a′) $j_1=\frac{1}{2}$, $l_1=0$, $m_1=\frac{1}{2}$; $j_2=\frac{1}{2}$, $l_2=0$, $m_2=\frac{1}{2}$,

(b′) $j_1=\frac{1}{2}$, $l_1=1$, $m_1=\frac{1}{2}$; $j_2=\frac{1}{2}$, $l_2=1$, $m_2=\frac{1}{2}$,

give the terms which, having the most sensitive dependence on the nuclear charge, dominate all the others for $2Z/W_0>1$. The major part of the transition probability due to the "second"-order terms in A_x, A_y, A_z is therefore:

$$P_2(W)dW=\frac{G^2}{4\pi^3}|M''_0|^2(f_0^2+g_{-2}^2)\frac{q^2W}{p}dW; \quad M''_0=\int\frac{d\tau}{R}\Psi_b^*\left[\frac{(\sigma\times\mathbf{r})_x-i(\sigma\times\mathbf{r})_y}{\sqrt{2}}\right]\Psi_a. \tag{9b}$$

There are also the cross terms, but these need not be considered since we shall be interested only

[12] This is true in the non-relativistic approximation for the nuclear particles—which is certainly justified; in the same approximation β may be replaced by 1. In the future the Pauli spin-operator $\boldsymbol{\sigma}$ will replace $\beta\boldsymbol{\sigma}$ in all nuclear matrix elements.

in applications for which (9a) is considerably larger than (9b) or conversely; at most, the minimum lifetimes will be too long by a factor of two.

In order to compute minimum lifetimes on the tensor interaction with unfavorable parity change, it is necessary to estimate maximum values of (9a) and (9b). It might be thought that an essential uncertainty is introduced into the lifetimes by the presence of more than one kind of nuclear matrix element. This is certainly true for *actual* lifetimes but is not the case for the *minimum* lifetimes which can be predicted by the theory and which is all that concerns us. An estimate of the maximum value (9a) may be had by treating the $\beta\boldsymbol{\alpha}$ in M'_0 as a velocity vector.[13] We find $M'_0 \leqq W_0$ (cf. reference 7). To get an estimate of (9b) we expand $(f_0^2+g_{-2}^2)$ in powers of (αZ); the most important term in this expansion (for $2Z/W_0>1$) can be written in the form $\frac{1}{4}\alpha^2Z^2(g_0^2+f_{-2}^2)$. Now the matrix element

$$M''_0=\int \frac{d\tau}{R}\Psi_b^*\left[\frac{(\boldsymbol{\sigma}\times\mathbf{r})_x-i(\boldsymbol{\sigma}\times\mathbf{r})_y}{\sqrt{2}}\right]\Psi_a$$

is of order 1; therefore the ratio of (9a) to (9b) is $4W_0^2R^2/\alpha^2Z^2$ if we insert the maximum values of M'_0 and M''_0. Since we are interested only in minimum lifetimes corresponding to a spin change of one unit with parity change we can then use (9a) when $4W_0^2R^2/\alpha^2Z^2\gg 1$. We get:

$$\frac{1}{\tau_{T^{(0)\prime}}}=\frac{1}{\tau_0}R^2|M'_0|^2B_0(Z, W_0). \tag{10a}$$

When $4W_0^2R^2/\alpha^2Z^2\ll 1$, we can neglect (9a) and use (9b), and we obtain:

$$\frac{1}{\tau_{T^{(0)\prime\prime}}}=\frac{1}{\tau_0}\left(\frac{\alpha^2Z^2}{4}\right)|M''_0|^2B_0(Z, W_0). \tag{10b}$$

Equation (10b) holds for $\alpha Z\ll 1$ while (10a) holds for any Z. In both (10a) and (10b) $B_0(Z, W_0)$ is the same function which occurs in (8).

The lifetimes on the tensor interaction—both for favorable and unfavorable parity change—for the various forbidden transitions, may be calculated in a similar fashion, by taking $k=|j_i-j_f|$, $\mu=k$. A first forbidden transition permits a spin change of two units and requires a parity change, a second forbidden transition permits a spin change of three units and requires that the parity remain unchanged, and so on. In general, if n is the order of the forbidden transition and the parity change is favorable—parity change for n odd and no parity change for n even—then the maximum allowable spin change is $(n+1)$ units; if the parity change from initial to final nuclear state is unfavorable, then the spin change $(n+1)\hbar$ will be associated with a forbidden transition of order $(n+1)$. We first calculate the lifetimes corresponding to the case of favorable parity change. For this type of forbidden transition, each additional order involves one more combination of angular momentum quantum numbers of the electron-neutrino pair and therefore two more terms in the double summation (2) since the roles of the electron and neutrino may be interchanged. Table III lists the pairs of quantum number triplets entering into each forbidden transition: each number triplet represents (j, l, m) in the order given. The lifetime $\tau_{T^{(n)}}$ on the tensor interaction for the nth forbidden transition corresponding to a spin change of $(n+1)$ units and favorable parity change is found to be:

$$\frac{1}{\tau_{T^{(n)}}}=\frac{1}{\tau_0}\frac{|M_n|^2}{[1\cdot 3\cdots(2n+1)]^2}R^{2n}B_n(Z, W_0). \tag{11}$$

In (11) R is again the nuclear radius measured in units of $\hbar/mc$; M_n is of order of magnitude unity

[13] This is not quite correct since $\boldsymbol{\alpha}$ not $\beta\boldsymbol{\alpha}$ is the current on the Dirac theory; however, the estimate is close enough for our purposes. In the vector interaction $\boldsymbol{\alpha}$ enters without β so that the estimate given there is more rigorous (cf. 19a).

(cf. Section III below), and is given by:

$$M_n = 4\pi \int d\tau \Psi^*_b \left(\frac{\sigma_x - i\sigma_y}{\sqrt{2}}\right) \Psi_a \left(\frac{r}{R}\right)^n Y^*_{nn} Y_{00}. \tag{11a}$$

It is interesting to note that only one kind of nuclear matrix element arises for each forbidden transition. This follows from the fact that other matrix elements which appear containing combinations of spherical harmonics of the form $Y^*_{mm} \cdot Y^*_{n-m,\, n-m}$ may all be expressed as known constants times $Y^*_{nn} Y_{00}$. The functions $B_n(Z, W_0)$ depend on the nuclear charge Z, the maximum energy of the β-ray W_0, and the order of the transition. The formula (11) holds for arbitrary n but we only give $B_n(Z, W_0)$ for the first three orders:

$$B_1(Z, W_0) = \frac{1}{2} \int_1^{W_0} \frac{W}{p} q^2 dW \left[(g_0^2 + f_{-2}^2) + \frac{9(g_1^2 + f_{-3}^2)}{R^2} \right], \tag{12a}$$

$$= \int_1^{W_0} pWq^2 dW \left[q^2 F_0\left(\frac{1+s_0}{2}\right) + p^2 F_1\left(\frac{2+s_1}{4}\right) \right], \tag{12b}$$

$$B_2(Z, W_0) = \frac{1}{2} \int_1^{W_0} \frac{W}{p} q^2 dW \left[q^4 (g_0^2 + f_{-2}^2) + \frac{30q^2(g_1^2 + f_{-3}^2)}{R^2} + \frac{225(g_2^2 + f_{-4}^2)}{R^4} \right], \tag{13a}$$

$$= \int_1^{W_0} pWq^2 dW \left[q^4 F_0\left(\frac{1+s_0}{2}\right) + \frac{10}{3} q^2 p^2 F_1\left(\frac{2+s_1}{4}\right) + p^4 F_2\left(\frac{3+s_2}{6}\right) \right], \tag{13b}$$

$$B_3(Z, W_0) = \frac{1}{2} \int_1^{W_0} \frac{W}{p} q^2 dW \left[q^6 (g_0^2 + f_{-2}^2) + \frac{63q^4(g_1^2 + f_{-3}^2)}{R^2} + \frac{1575q^2(g_2^2 + f_{-4}^2)}{R^4} + \frac{11025(g_3^2 + f_{-4}^2)}{R^6} \right], \tag{14a}$$

$$= \int_1^{W_0} pWq^2 dW \left[q^6 F_0\left(\frac{1+s_0}{2}\right) + 7q^4 p^2 F_1\left(\frac{2+s_1}{4}\right) + 7q^2 p^4 F_2\left(\frac{3+s_2}{6}\right) + p^6 F_3\left(\frac{4+s_3}{8}\right) \right]. \tag{14b}$$

In (12a), (13a), and (14a) the different f's and g's are exact Coulomb functions of the electron for the continuous spectrum and are explained in reference 11. We have written out (12a)–(14a) because of their usefulness later for the calculation of the probability of orbital electron capture. In deriving (12b), (13b), and (14b) we have made use of the connecting formula which holds for $pR \ll 1$, namely:

$$[g^2_n + f^2_{-(n+2)}] = \frac{2(p^2)^{n+1} R^{2n}}{[1 \cdot 3 \cdots (2n+1)]^2} F_n(Z, W) \left[\frac{(n+1) + s_n}{2(n+1)} \right].$$

The s_n's are functions of Z: $s_n = [(n+1)^2 - \alpha^2 Z^2]^{\frac{1}{2}}$. The F_n's are functions of Z, W and the order of the transition:

$$F_n(Z, W) = \frac{[(2n+2)!]^2}{(n!)^2 \Gamma^2(1+2s_n)} (2pR)^{2(s_n - n) - 2} e^{\pi \alpha ZW/p} \left| \Gamma\left(s_n + \frac{i\alpha ZW}{p}\right) \right|^2. \tag{15}$$

The lifetime given in (11) is strictly correct if the spin of the β-radioactive nucleus is greater than the spin of the final nucleus. If this is not true, then in accordance with the argument given at the beginning of this section, the right-hand side of (11) should be multiplied by $(2j_f+1)/(2j_i+1)$.

It is worth comparing our results with those of Konopinski and Uhlenbeck (cf. reference 7). Since we are interested in the lifetime associated with the maximum possible spin change and favorable parity change, we would use the irreducible tensor of the second rank B_{ij} (cf. reference 7 for notation) for the first forbidden transition, the tensor of the third rank S_{ijk} for the second for-

bidden, and a tensor of the fourth rank S_{ijkl} for the third forbidden transition. The first two have already been worked out and give the lifetimes:

$$\frac{1}{\tau^{(1)}}=\frac{1}{\tau_0}\cdot\frac{1}{2^2\cdot 3}\sum_{ij}|\beta_{ij}|^2B_1(Z, W_0), \tag{16a}$$

$$\frac{1}{\tau^{(2)}}=\frac{1}{\tau_0}\cdot\frac{1}{2^3\cdot 3^3\cdot 5}\sum_{i,j,k}|S_{ijk}|^2B_2(Z, W_0). \tag{16b}$$

The tensor S_{ijkl} leading to a possible spin change of four units can also be worked out[14] and turns out to be

$$S_{ijkl}=\sigma_{(i}x_jx_kx_{l)}-\frac{1}{14}\delta_{(ij}\{3r^2\sigma_kx_{l)}+6(\boldsymbol{\sigma}\cdot\mathbf{r})x_kx_{l)}\}+\frac{3}{35}\delta_{(ij}\delta_{kl)}(\boldsymbol{\sigma}\cdot\mathbf{r})r^2. \tag{16c}$$

A calculation of the lifetime on the lines of the first and second forbidden transitions leads to the expression

$$\frac{1}{\tau^{(3)}}=\frac{1}{\tau^{(0)}}\frac{1}{2^6\cdot 3^5\cdot 5^2}\sum_{ijkl}|S_{ijkl}|^2B_3(Z, W_0). \tag{16d}$$

The B_n's are the same functions of energy and nuclear charge which we found in (11)—as they should be—but the matrix elements and coefficients are considerably different. This is not surprising because the various tensors B_{ij}, S_{ijk}, S_{ijkl} do not give the single selection rules, ± 2, ± 3, ± 4, respectively, but they also lower spin changes. In order to calculate a lifetime which could be compared with experiment it would be necessary to separate each tensor into parts corresponding to the various spin changes (e.g., B_{ij} into parts corresponding to 0, ± 1, ± 2), and then each of these parts into the various "magnetic quantum number" components. It is precisely this separation which the use of wave functions in spherical coordinates for both electron and neutrino accomplishes and we shall therefore compute lifetimes using (11).

If the parity change associated with the nth forbidden transition is incompatible with the actual parity difference between initial and final nuclear states, one must apply the same sort of reasoning which led to (10a) and (10b). One finds from the "small" $\beta\boldsymbol{\alpha}$ in the tensor interaction the following lifetime:

$$\frac{1}{\tau\tau^{(n)\prime}}=\frac{1}{\tau_0}R^{2n+2}\frac{|M'_n|^2}{[1\cdot 3\cdots 2n+1]^2}B_n(Z, W_0), \tag{17a}$$

where

$$M'_n=4\pi\int\frac{d\tau}{R}\Psi^*_b\beta\left(\frac{\alpha_x-i\alpha_y}{\sqrt{2}}\right)\Psi_a\left(\frac{r}{R}\right)^nY^*_{nn}Y_{00}\quad\text{is of order}\,W_0.$$

One gets from the higher order terms in A_x, A_y, and A_z the lifetime:

$$\frac{1}{\tau\tau^{(n)\prime\prime}}=\frac{R^{2n}}{\tau_0}\left(\frac{\alpha^2Z^2}{4}\right)\frac{|M''_n|^2}{[1\cdot 3\cdots(2n+1)]^2}\bar{B}_n(W_0), \tag{17b}$$

where

$$M''_n=4\pi\int\frac{d\tau}{R}\Psi_b^*\left[\frac{(\boldsymbol{\sigma}\cdot\mathbf{r})_x-i(\boldsymbol{\sigma}\cdot\mathbf{r})_y}{\sqrt{2}}\right]\Psi_a\left(\frac{r}{R}\right)^nY^*_{nn}Y_{00}\quad\text{is of order unity.}$$

[14] I am indebted to Professor G. E. Uhlenbeck for advice on the application of the "tensor" method to the third forbidden transition, and for a very interesting conversation on the relative advantages of the "tensor" and "spherical harmonic" methods.

In (17a) the B_n's are the same functions as those which appear in (11). The functions $\bar{B}_n(W_0)$ which enter into (17b) are somewhat different; their definitions for the first three orders ($\alpha Z \ll 1$) are:

$$\bar{B}_1(W_0)=\int_1^{W_0} pWq^2dW\left[q^2+\frac{p^2}{4}\right], \tag{18a}$$

$$\bar{B}_2(W_0)=\int_1^{W_0} pWq^2dW\left[q^4+\frac{5}{6}q^2p^2+\frac{p^4}{9}\right], \tag{18b}$$

$$\bar{B}_3(W_0)=\int_1^{W_0} pWq^2dW\left[q^6+\frac{7q^4p^2}{4}+\frac{7}{9}q^2p^4+\frac{p^6}{16}\right]. \tag{18c}$$

Roughly speaking, one should use (17a) to estimate the minimum lifetime corresponding to an nth forbidden transition with unfavorable parity change when $(W_0^2R^2/4\alpha^2Z^2)[B_n(Z, W_0)/\bar{B}_n(W)]>1$. When the other inequality holds one should use (17b).

According to Konopinski and Uhlenbeck[7] the vector interaction between nuclear particles and the electron-neurino field is also compatible with the accurately known energy spectra of forbidden β-emitters. Since we wish to decide between the vector and tensor theories of β-decay, it is necessary to compute lifetimes for the various forbidden transitions on the basis of the vector interaction. It turns out that as far as lifetimes are concerned, the vector interaction for an nth forbidden transition is essentially equivalent to an $(n-1)$ forbidden transition on the tensor interaction with unfavorable parity change. It must be remembered that an allowed transition on the vector interaction permits no spin change and requires that the parity remain unchanged, a first forbidden transition permits a spin change of one unit and requires parity change, and so on. If we relabel the lifetime to represent the new selection rules so that a maximum spin change of n units is permitted by an nth forbidden transition, we may write for the lifetime $\tau_F^{(n)}$ derived from the "small" α term in the vector interaction:

$$\frac{1}{\tau_F^{(n)\prime}}=\frac{1}{\tau_0}R^{2n}|G'_n|^2D'_n(Z, W_0), \tag{19a}$$

where

$$G_n'=4\pi\int\frac{d\tau}{R}\Psi^*_b\left(\frac{\alpha_x-i\alpha_y}{\sqrt{2}}\right)\Psi_a\left(\frac{r}{R}\right)^{n-1}Y^*_{n-1,\,n-1}Y_{00} \quad \gtrless W_0,$$

$$D'_n\equiv B_{n-1}(Z, W_0). \qquad \text{[cf. Eq. (17a)]}$$

The lifetime $\tau_F^{(n)\prime\prime}$ derived from the fourth component of the vector interaction is:

$$\frac{1}{\tau_F^{(n)\prime\prime}}=\frac{1}{\tau_0}R^{2n-2}\frac{\alpha^2Z^2}{4}|G''_n|^2D''_n(Z, W_0). \tag{19b}$$

The matrix element G'' is not the same as in (17b) but instead is given by:

$$G''_n=4\pi\int\frac{d\tau}{R}\left(\frac{x-iy}{\sqrt{2}}\right)\left(\frac{r}{R}\right)^{n-1}Y^*_{n-1,\,n-1}Y_{00} \quad \gtrless 1,$$

$$D''_n\equiv\bar{B}_{n-1}(W_0). \qquad \text{(cf. (17b))}$$

Again there are cross terms of the form $i(G'_nG''_n+\text{c.c.})$ but it has been checked that these terms are smaller than (19a) when $\alpha^2Z^2/4W^2_0R^2>4/n$ and less than (19b) when $\alpha^2Z^2/4W^2_0R^2<n/4$ so that we need not consider them here. In the case of the tensor interaction with unfavorable parity change a rule was given for finding minimum lifetimes with (17a) or (17b). A similar rule applies

for the vector interaction: when $(W_0^2R^2/4\alpha^2Z^2)(D'_n/D''_n)>1$ one should take (19a), and when the other inequality holds one should use (19b). However approximately $G'_n \approx W_0 G''_n$ (cf. reference 7) so that we may combine (19a) and (19b) to get a "total" lifetime $\tau_F^{(n)}$:

$$\frac{1}{\tau_F^{(n)}}=\frac{|G''_n|^2}{\tau_0}\left[W_0^2R^2B_{n-1}(Z, W_0)+\frac{\alpha^2Z^2}{4}\bar{B}_{n-1}(W_0)\right]. \tag{19c}$$

Equation (19c) can be used without any restriction (except that $\alpha Z \ll 1$) to find a lower limit to the lifetime for a given spin change $n\hbar$ on the vector interaction.

III. COMPARISON WITH EXPERIMENT

In Table I we give the observational data on the five well-known long-lived β-emitters, the spins of the initial and final nuclei where known, the lifetimes, and the measured maximum energies of the β-rays; for the latter two quantities the limits of uncertainty are given wherever they exist. If no such limits are given the figures listed are not in error by more than 20 percent. In Table I the spins of Ca^{40}, B^{10}, and Hf^{176} which are listed have not been measured directly but are inferred with almost complete certainty from nuclei of similar structure whose spins have been measured. This is especially true of Ca^{40} which can be considered to consist of an integral number of α-particles; all similar nuclei—He^4, C^{12}, O^{16}, S^{32}—on which measurements have been made, possess a spin of zero. B^{10} is about equally certain since it fits into the sequence H^2, Li^6, N^{14}, all of which have been found to have a spin of one unit; moreover, its magnetic moment fits into the sequence of decreasing magnetic moments corresponding to the above sequence of nuclei, if its spin is one. Hf^{176} is not so certain, the only evidence being that it is a stable nucleus of even atomic weight and even charge and should possess a spin zero.

To compute numerical values for the theoretical lifetimes it is necessary to know τ_0. The most consistent procedure is to compute τ_0 by applying Eq. (8) to the fast reaction: ${}_2He^6 \rightarrow {}_3Li^6 + e^-$. This must be an allowed transition on the basis of a Gamow-Teller type of interaction which permits a spin change of one unit. If we insert the values for $\tau^{(0)}$ and W_0 which are 1.14 sec. and 7.9, respectively, and evaluate $|M_0|^2$ in accordance with Grönblom's method[15] we find for the maximum value of $\tau_0 = 7\times10^3$ sec. Account has been taken of the factor that the transition probability must be multiplied by $(2j_f+1)/(2j_i+1)$—which is 3 in the present case—since the initial spin is less than the final spin. The value for τ_0—which is a maximum value—is three times as large as Grönblom's value because of a somewhat different definition of τ_0. This maximum value of τ_0 must be close to the correct value since the initial and final wave functions cannot be very different. Even if the value of τ_0 had to be reduced because $|M_0|^2<2$, the arguments of Nordheim and Yost[16] show that the matrix elements for heavier elements and forbidden transitions would have to be reduced even more, thereby effectively increasing τ_0. We can therefore regard τ_0 as really a *minimum*.

TABLE I. Observational data, references given in text.

Reaction	Spin of initial nucleus	Spin of final nucleus	Observed lifetime in years (half-life $\times\log_e 2$)	Maximum energy (in mc^2)
${}_{19}K^{40} \rightarrow {}_{20}Ca^{40}+\epsilon^-$	$4\hbar$	$0\hbar$	2.0×10^9	$W_0=2.4$–3.6
${}_{37}Rb^{87} \rightarrow {}_{38}Sr^{87}+e^-$	$3/2\hbar$	$9/2\hbar$	1–2×10^{11}	$W_0=1.3$–1.5
${}_{71}Lu^{176} \rightarrow {}_{72}Hf^{176}+e^-$	$\geq7\hbar$	$0\hbar$	1.0×10^{10}	$W_0=1.4$
${}_4Be^{10} \rightarrow {}_5B^{10}+e^-$	?	$1\hbar$	0.5×10^3–10^5	$W_0=2.2$
${}_6C^{14} \rightarrow {}_7N^{14}+e^-$	?	$1\hbar$	10^3–10^5	$W_0=1.3$

Table II lists values of the minimum theoretical lifetimes for the various long-lived β-emitters under different assumptions as to the spin and parity changes and in the case of K^{40}, for the upper and lower limits of the maximum energy of the β-ray. Column 2 lists the nuclear radii for the five nuclei; these values were derived using the formula $Rh/mc=1.5\times10^{-13}A^{\frac{1}{3}}$ (cf. Wigner, reference 1). Column 3 lists the

[15] Cf. B. O. Grönblom, Phys. Rev. **56**, 508 (1939): instead of using the operator $(Q_1\sigma x_1+Q_2\sigma x_2)$ as he does, we must use the operator $(Q_1/\sqrt{2})(\sigma x_1-i\sigma y_1)+(Q_2/\sqrt{2})(\sigma x_2-i\sigma y_2)$ which, operating on his wave function ψ, gives $\beta(1)\beta(2)(p(1)n(2)-p(2)n(1))$; it turns out that $|M_0|^2$ is 2 in agreement with his result.

[16] L. W. Nordheim and F. L. Yost, Phys. Rev. **51**, 942 (1937).

spin change, and column 4 lists values of the minimum lifetimes derived on the basis of equation (11)—i.e., the tensor interaction with favorable parity change. The quantity $|M_n|^2$ has in all cases been set equal to unity to get these minimum lifetimes. In principle the maximum value of $|M_n|^2$ is the isotopic number of the β-radioactive nucleus—2 in the case K^{40}, Be^{10}, C^{14}, 13 for Rb^{87}, 34 for Lu^{176}. However, it would be a mere formality to use these larger values and then to state that the matrix elements are actually much smaller because the transitions are not within the same supermultiplet.[17] Moreover, the inclusion of the factor 2 for K^{40} would not alter the fundamental conclusion to which we are led, namely, that the vector interaction predicts too long a lifetime. Column 5 of Table II contains—with one exception—values of the minimum lifetimes based on the tensor interaction with unfavorable parity change; the appropriate equation (17a) or (17b) is used and again the square of the matrix element is taken equal to unity. The exception noted is K^{40} for which the minimum lifetime, $\tau_V^{(4)}$, listed in brackets in column 5 is derived from the vector interaction using (19c) with $|G'_n|^2=1$ and $\tau_0=2.3\times10^3$.[18] In columns 6 and 7 of Table II values of the functions $B_n(Z, W_0)$ and $B_n(0, W_0)$ are given so that the effect of the Coulomb field due to different Z may be seen; also in column 6 the functions $\bar{B}_n(W_0)$ are listed. The $B_n(Z, W_0)$ were computed by numerical integration taking account of the Coulomb correction factors $F_0 \cdots F_3$ *throughout* the specified energy intervals; $B_n(0, W_0)$ and $\bar{B}_n(W_0)$ were also computed by numerical integration.[19] It is worth noting that the influence of the Coulomb field is no greater for the various forbidden transitions on the tensor interaction with favorable parity change than for allowed transitions. We shall discuss the five nuclei separately.

$_{19}K^{40}$

Two theoretical lifetimes are given—corresponding to $W_0=3.6$ (representing a maximum kinetic energy of 1.3 Mev for the emitted electron) and $W_0=2.4$ (representing a maximum kinetic energy of 0.7 Mev). The higher value is more recent and trustworthy having been found by Henderson,[20] using the standard absorption method in conjunction with a thin walled counter in a concentric arrangement. He claims that there are some potassium β-rays which are more energetic than the 1.10 Mev RaE β-rays and that the maximum energy is 1.3 ± 0.1 Mev. The older measurements made by Bocciarelli[21] and by Anderson and Neddermeyer[22] gave the lower value 0.7 Mev but are less reliable. Since Henderson finds only one group of β-rays and no evidence has ever been found for γ-rays in the energy region up to 1.3 Mev,[23] the transition must take place from the ground state of K^{40} with spin $4h$ to the ground state of Ca^{40} with spin zero. With a spin change of four units and with $W_0=3.6$ the tensor (or pseudo-vector) interaction predicts a minimum lifetime of 5.8×10^7 yr. If the parity change was unfavorable, i.e., if the parity of the ground state of K^{40} is the same as Ca^{40}, the minimum lifetime would be 2×10^{10} yr. If the original Fermi theory of β-decay (i.e., vector interaction) were correct, the minimum theoretical lifetime is 7×10^9 yr. This must be a real lower limit since our

[17] Cf. Wigner, reference 1; as Wigner has pointed out, the only transitions within the same supermultiplet occur for positron emitters like C^{11}, N^{13}, etc., and for the light nuclei decaying rapidly with β-emission like He^6, C^{10}, etc. All other transitions are "unfavored" so that the matrix elements must be relatively small compared to the "favored" transitions.

[18] The significance of the smaller τ_0 (by a factor 3) is that τ_0 was evaluated from the reaction $He^6 \rightarrow Li^6+e^-$ assuming that it involved a spin change of one unit and was therefore an allowed transition on the tensor interaction; this brought in a factor 3 in the transition probability. If the vector interaction is, for the moment assumed to be correct, the reaction $He^6 \rightarrow Li^6+e^-$, since it is as fast as reactions which are known to involve no spin change, would still have to be allowed. This would imply a spin zero for He^6 and therefore a $0 \rightarrow 0$ transition. However, there is now only one possible transition, namely $j_i=0$, $m_i=0 \rightarrow j_f=0$, $m_f=0$ and the factor $(2j_f+1)/(2j_i+1)=3$ no longer enters. Since $|G'_0| = |\int d\tau \Psi^*_b(Q_1+Q_2)\Psi_a|^2=2$ (cf. reference 15) and all other terms are identical, the "vector" τ_0 is three times smaller than the "tensor" τ_0.

[19] I am indebted to Messrs. William Pratt and Herbert York of the College of Arts and Sciences, University of Rochester, for these computations.

[20] W. J. Henderson, Phys. Rev. **55**, 238A (1939); I am indebted to Dr. Henderson for correspondence on his measurements.

[21] D. Bocciarelli, Atti accad. Lincei **17**, 830 (1933).

[22] C. D. Anderson and S. H. Neddermeyer, Phys. Rev. **45**, 653L (1934).

[23] A 2-Mev γ-ray emitted by K^{40} has been found by Gray and Tarrant (cf. Proc. Roy. Soc. **143**, 695 (1934)); since there are only 3γ-quanta per 100 β-rays, the γ-ray emission cannot be correlated with the β-emission and is to be associated with orbital electron capture by K^{40} to form A^{40}. Cf. Section IV below.

TABLE II. Minimum theoretical lifetimes in years.

β-emitter	Nuclear radius in units of $\hbar/mc$	Spin change	Lifetimes on tensor interaction; favorable parity change	Lifetimes on tensor interaction; unfavorable parity change	Energy functions $B_n(Z, W_0)$ and $B_n(W_0)$	$B_n(0, W_0)$
$_{19}K^{40}$	1.30×10^{-2}	$4\hbar$	$\tau_T^{(3)}=1.3\times10^{10}(W_0=2.4)$		$B_3(19, 2.4)=4.2\times10^{1}$	$B_3(0, 2.4)=2.3\times10^{1}$
		$4\hbar$	$\tau_T^{(3)}=5.8\times10^{7}(W_0=3.6)$	$[\tau_V^{(4)}=7\times10^{9}(W_0=3.6)]$	$B_3(19, 3.6)=9.6\times10^{3}$	$B_3(0, 3.6)=5.5\times10^{3}$
		$4\hbar$		$\tau_T^{(3)\prime}=2\times10^{10}(W_0=3.6)$	$\bar{B}_3(3.6)=1.2\times10^{3}$	
$_{37}Rb^{87}$	1.69×10^{-2}	$3\hbar$	$\tau_T^{(2)}=3.5\times10^{6}$		$B_2(37, 1.5)=7.2\times10^{-2}$	$B_2(0, 1.5)=1.3\times10^{-2}$
		$3\hbar$		$\tau_T^{(2)\prime\prime}=6\times10^{5}$	$\bar{B}_2(1.5)=2.2\times10^{-3}$	
$_{71}Lu^{176}$	2.13×10^{-2}	$4\hbar$	$\tau_T^{(3)}=2\times10^{11}$		$B_3(71, 1.4)=1.5\times10^{-1}$	$B_3(0, 1.4)=2.5\times10^{-3}$
$_{4}Be^{10}$	0.82×10^{-2}	$1\hbar$		$\tau_T^{(0)\prime}=0.4$	$B_0(2.2)=0.20$	
		$2\hbar$	$\tau_T^{(1)}=2.8\times10^{1}$		$B_1(4, 2.2)=1.1$	$B_1(0, 2.2)=1.0$
		$2\hbar$		$\tau_T^{(1)\prime}=8.7\times10^{4}$	$B_1(2.2)=0.5$	
		$3\hbar$	$\tau_T^{(2)}=4.3\times10^{6}$		$B_2(4, 2.2)=2.7$	$B_2(0, 2.2)=2.6$
$_{6}C^{14}$	0.92×10^{-2}	$1\hbar$		$\tau_T^{(0)\prime}=1.0\times10^{1}$	$B_0(1.3)=3.5\times10^{-3}$	
		$2\hbar$	$[\tau_T^{(1)}=2.2\times10^{4}]$		$B_1(6, 1.3)=1.1\times10^{-3}$	$B_1(0, 1.3)=0.9\times10^{-3}$
		$2\hbar$		$\tau_T^{(1)\prime}=1.7\times10^{8}$	$B_1(1.3)=2.6\times10^{-4}$	

TABLE III. Quantum number triplets.

First forbidden: $n=1$ ($k=2$, $\mu=2$)	3/2, 2, 3/2 1/2, 0, 1/2	3/2, 1, 3/2 1/2, 1, 1/2		
Second forbidden: $n=2$ ($k=3$, $\mu=3$)	5/2, 3, 5/2 1/2, 0, 1/2	5/2, 2, 5/2 1/2, 1, 1/2	3/2, 2, 3/2 3/2, 1, 3/2	
Third forbidden: $n=3$ ($k=4$, $\mu=4$)	7/2, 4, 7/2 1/2, 0, 1/2	7/2, 3, 7/2 1/2, 1, 1/2	5/2, 3, 5/2 3/2, 1, 3/2	5/2, 2, 5/2 3/2, 2, 3/2

calculations are quite exact, and since all theoretical considerations point to a matrix element much smaller than unity with a correspondingly longer lifetime. The scalar and pseudo-scalar theories of β-decay predict even longer minimum lifetimes. These values are to be compared with the observed[24] lifetime, known to 20 percent, of 2.0×10^{9} yr. The vector interaction and *à fortiori* the scalar and pseudo-scalar interactions are therefore excluded, and we must conclude that only the Gamow-Teller type of interaction (tensor or pseudo-vector) is compatible with the observations. This conclusion can be made certain by a very accurate determination of the maximum energy of the β-rays, although Henderson's measurements seem good. When the above result is combined with Konopinski and Uhlenbeck's result (cf. reference 7), that only the tensor and vector interactions can explain the observed energy spectra of Na^{24}, P^{32}, and RaE, we can say that the *tensor theory* of β-decay alone is capable of explaining the lifetimes and energy spectra of forbidden β-emitters. The remainder of our discussion presupposes the correctness of the tensor theory.

If the maximum energy of the potassium β-ray is 1.3 Mev then $|M_3|^2\leqq0.03$; this low value would not be contrary to expectations

[24] Cf. A. Bramley and A. K. Brewer, Phys. Rev. **53**, 502 (1938); the electron intensity is measured as a function of the time so that the lifetime corresponds to the β-emission alone (cf. reference 23).

because of the high order of the transition and the not inappreciable atomic weight of potassium (cf. references 16 and 17). On the other hand, it would follow that a maximum energy of 0.7 Mev is definitely ruled out since the predicted minimum lifetime even on the tensor theory is then considerably larger than the observed value, namely 1.3×10^{10} yr. Hence the theory itself would cast doubt on the correctness of the older energy measurements. The tensor theory also predicts a parity change; since the parity of the ground state of Ca^{40} is presumably even, the ground state of K^{40} has odd parity.[25]

$_{37}Rb^{87}$

The minimum lifetime predicted for rubidium by the tensor theory of β-decay with the most favorable parity change, i.e., no parity change since $n=2$ corresponds to the observed spin change of 3 units (cf. Heyden and Kopfermann, reference 3), is 3.5×10^{6} yr. We have used $W_0=1.5$, since experiments giving higher energy values are usually more reliable.[26] The observed lifetime is $1-2\times10^{11}$ yr.[27] To bring the theoretical and observed lifetimes into agreement, it is necessary to assume that $|M_2|^2\backsimeq2\times10^{-5}$; this value is too small. If the parity of the ground state of Rb^{87} is different from the parity of the ground state of Sr^{87}, a choice of $|M''_2|^2\backsimeq0.04$ will raise the minimum lifetime of 6×10^{9} yr. to the observed value. This seems quite reasonable so that it is likely that the Rb^{87} β-emission involves a parity change.

$_{71}Lu^{176}$

The radioactive isotope of lutecium[28] is interesting because of its very large spin, greater than or equal to $7\hbar$ (cf. Schüler and Gollnow, reference 3). If correct—which is far from certain in view of the complicated pattern and rather small abundance—this is the largest spin which has thus far been measured for any nucleus. Lu^{176} decays to Hf^{176} which is a stable nucleus of even atomic weight and even charge and doubtless has a spin of zero. The maximum energy of the β-ray is 215 ± 15 kilovolts and the observed lifetime is 1×10^{11} yr.[29] The minimum lifetime (on the tensor theory) for a spin change of four units is already as large (cf. Table II) as the observed value. Since it is unlikely that the matrix element $|M_3|^2$ is close to one for this transition, it is probable that only a spin change of three units occurs. Consequently Lu^{176} must decay to an excited state of Hf^{176}, which has a spin of at least $3\hbar$ and probably $4\hbar$. This excited state should emit one or more γ-rays and if it goes to the ground state of Hf^{176}, thereby emitting one γ-ray, should have a rather long life. No one has as yet looked for these γ-rays. If it should turn out that there is no evidence for an excited state of Hf^{176} it may be that the measurement of the spin of Lu^{176}—which was difficult to make—is in error; in this case if the β-decay is to the ground state of Hf^{176}, the tensor theory would predict a spin of $4\hbar$ or possibly $3\hbar$ for Lu^{176}.

$_{4}Be^{10}$

It is hopeless to try to account for the long lifetime (greater than 500 years)[30] of Be^{10} if the ground state is assured to have spin $0\hbar$ and the same parity as the ground state of B^{10}. Even if the parity of the states of the two nuclei is different, the lifetime would be of the order of a year or possibly 10 yr., supposing that $|M'_0|^2\sim0.1$. A spin change of two units leads to a minimum lifetime of about 30 yr. if there is a parity change and to a minimum lifetime of 8.7×10^{4} yr. if there is no parity change. To attain the observed lifetime of at least 500 yr. it would be necessary that $|M_1|^2$ is less than 0.06. This seems somewhat too small for such a light nucleus so that it is probable that the ground state of Be^{10} has a spin of $3\hbar$—since B^{10}

[25] Professor D. Inglis has kindly informed the writer that the application of the harmonic oscillator potential model to K^{40} would lead to odd parity for the ground state; unfortunately this model also predicts a positive magnetic moment for K^{40} in disagreement with Zacharias' measurement (cf. reference 4). However, it is not to be expected that a nucleus as heavy as K^{40} would possess much "shell structure."

[26] Cf. Muhlhoff, Ann. d. Physik **399**, 205 (1930), and reference 6.

[27] A. Hemmendinger and W. R. Smythe, Phys. Rev. **51**, 1052 (1937).

[28] By means of a mass spectrograph, Mattauch and Lichtblau (Zeits. f. Physik 111, 514 (1938)) settled conclusively that the naturally radioactive isotope is Lu^{176} and not Lu^{177} as had previously been thought (cf. Heyden and Wefelmeier, Naturwiss. **26**, 612 (1938)).

[29] W. F. Libby, Phys. Rev. **56**, 21 (1939).

[30] Cf. E. Pollard, Phys. Rev. **57**, 241 (1940); and E. M. McMillan and S. Ruben, unpublished (quoted in S. Ruben and M. D. Kamen, Phys. Rev. **59**, 349 (1941)).

has a spin of one unit[31]—and the same parity as the ground state of B^{10}. A more accurate determination of the lifetime can decide whether there is a parity change or not. The minimum lifetime predicted for a spin change of three units and the most favorable parity change (i.e., no parity change) is 4.3×10^6 yr.; this is incompatible with present observations so that a spin of $4\hbar$ for Be^{10} is ruled out.[32]

${}_6C^{14}$

The maximum energy of the β-ray from C^{14} is considerably less than that from Be^{10}, namely 0.15 Mev[33] instead of 0.60 Mev. The product nucleus N^{14} has a spin of one.[34] If the C^{14} ground state has a spin zero and a parity different from that of the N^{14} ground state, the predicted lifetime would be at least 10 yr. This lifetime would be increased to the lower limit given in Table I provided that $|M_0|^2\sim0.01$—which is rather small. If the spin of C^{14} were $3\hbar$, and a parity change takes place, the minimum theoretical lifetime would be 2.2×10^4 yr.—which falls within the range of values given by Ruben and Kamen. A spin of $4\hbar$ for C^{14} is certainly excluded as is a spin $3\hbar$ with the same parity as N^{14}. Improved experiments on the lifetime can decide between spin $0\hbar$ (or $2\hbar$) and spin $3\hbar$ for C^{14}; e.g., if the lifetime actually turns out to be close to the lower limit of about 10^3 yr. then the spin $3\hbar$ will be excluded and the spin $0\hbar$ (or spin $2\hbar$) will be favored. Of course direct measurements of the spin of C^{14} (and of the other artificially produced long-lived β-emitter Be^{10}) would supply a powerful check on the whole tensor theory of β-decay.

IV. FORBIDDEN ORBITAL ELECTRON CAPTURE

It is only necessary to make several obvious changes in the theory of the tensor interaction as given in Section II to derive a general formula for the lifetimes of nuclei which decay by orbital electron capture with arbitrary spin and parity change. The fundamental difference is, of course, that instead of the emission of an electron-neutrino pair into the continuum, an electron in a definite discrete energy state in the atom is absorbed by the nucleus, and a neutrino is emitted with the available kinetic energy. The original nucleus changes over to a nucleus with a positive charge one unit less and the product nucleus may be left either in an excited or the ground state. In the equations discrete Coulomb wave functions replace the Coulomb wave functions for the continuum which had previously been used for the electron, and the integration over the electron energy spectrum reduces to a single term.

In an allowed transition on the tensor interaction only an s electron[35] ($j=\frac{1}{2}$, $l=0$) will be captured with any appreciable probability. This represents what is usually called K capture[36] although, as it will turn out, $L_{\rm I}$ electrons—which also have $j=\frac{1}{2}$, $l=0$—will under favorable circumstances compete strongly with K-electron capture. In an allowed transition the maximum allowable spin change is $1\hbar$. For a first forbidden transition not only will s electrons be captured but also p electrons: under certain conditions—which will be specified later—p-electron capture becomes more probable than s-electron capture; a nuclear spin change of two units is permitted in a first forbidden transition. In the case of a second forbidden transition d electrons can be

[31] Cf. Millman, Kusch, and Rabi, Phys. Rev. **56**, 165 (1939).

[32] E. P. Cooper and E. C. Nelson, Phys. Rev. **58**, 1117 (1940), have shown that it is impossible to explain a spin of $4\hbar$ for Be^{10} with the Hartree model of the nucleus. It is likely that it is just as impossible to explain a spin of $3\hbar$ for Be^{10} even with tensor forces. The difficulty of reconciling current nuclear theory (proton-neutron symmetry, etc.) with the difference in structure between long-lived Be^{10} and short-lived C^{10} still remains.

[33] S. Ruben and M. D. Kamen, Phys. Rev. **59**, 349 (1941).

[34] Ornstein and Van Wijck, Zeits. f. Physik **49**, 315 (1928).

[35] We are assuming that each individual electron moves in a screened Coulomb field and obeys the Dirac equation corresponding to this field. On this model the K shell contains two s electrons with $j=\frac{1}{2}$, $l=0$, the L shell contains two $L_{\rm I}$ s electrons with $j=\frac{1}{2}$, $l=0$, two $L_{\rm II}$ p electrons with $j=\frac{1}{2}$, $l=1$, four $L_{\rm III}$ p electrons with $j=3/2$, $l=1$, and so on for the higher shells. The energy of the bound states of a Dirac electron depends on the principal quantum number n and $(j+\frac{1}{2})$, where j is the total angular momentum quantum number. However, the $(L_{\rm II}-L_{\rm III})$ splitting is less than the $(L_{\rm I}-L_{\rm II})$ splitting (due to screening) for $Z<60$ (cf. H. E. White, *Introduction to Atomic Spectra*, pp. 314–323). In order to enable the theory to be compared more easily with experiment, we therefore take the $L_{\rm II}$ and $L_{\rm III}$ p electrons together and only give results for $Z<60$. Moreover, we group all the electrons in each shell together as far as the energy is concerned using Slater's screening constants [cf. Phys. Rev. **36**, 51 (1930)], i.e., $W_K=\left[1-\frac{\alpha^2(Z-0.30)^2}{2}\right]mc^2$, $W_L=\left[1-\frac{\alpha^2(Z-4.15)^2}{8}\right]mc^2$, etc.

[36] Cf. C. Möller, Physik. Zeits. Sowjetunion **11**, 9 (1937).

TABLE IV. K and L Dirac wave functions in a Coulomb field.

Z	R	g_K^2	$g_{L_I}^2$	$f_{L_{II}}^2$	$g^2_{L_{III}}/R^2$
10	1.06×10^{-2}	1.6×10^{-3}	4.2×10^{-5}	1.8×10^{-9}	3.6×10^{-6}
20	1.33×10^{-2}	1.4×10^{-2}	8.2×10^{-4}	6.7×10^{-7}	7.2×10^{-5}
30	1.56×10^{-2}	5.6×10^{-2}	4.5×10^{-3}	1.2×10^{-5}	3.2×10^{-4}
40	1.75×10^{-2}	1.6×10^{-1}	1.4×10^{-2}	8.4×10^{-4}	9.7×10^{-3}
60	2.04×10^{-2}	9.5×10^{-1}	1.0×10^{-1}	2.3×10^{-3}	4.7×10^{-3}

captured, the maximum nuclear spin change is three units, and so on. We calculate the lifetimes associated with these different kinds of transitions.

The lifetime $\tau_e^{(n)}$ (the subscript indicates capture) for the nth forbidden transition on the tensor theory with favorable parity change is:

$$\frac{1}{\tau_e^{(n)}}=\frac{1}{\tau_0}\frac{|M_n|^2}{[1\cdot3\cdots(2n+1)]^2}\times R^{2n}B_e^{(n)}(Z_{\text{eff}}, W_0), \quad (20)$$

where τ_0 is the decay-constant as before and equal to 7×10^3 sec., R is the nuclear radius measured in units of $\hbar/mc$, M_n is the nuclear matrix element given by (11a) and $B_e^{(n)}(Z_{\text{eff}}, W_0)$ depends on the order of the transition n, on Z_{eff}, the effective nuclear charge for the captured electron and on W_0, the energy difference (in units of mc^2) between the parent and product nucleus. We have evaluated $B_e^{(n)}$ for an allowed transition and the first three forbidden transitions with the result:

$$B_e^{(0)}=\frac{\pi}{2}\{(W_0+W_K)^2n_Kg_K^2+(W_0+W_L)^2[n_{L_I}g^2_{L_I}+n_{L_{II}}f^2_{L_{II}}]\}, \quad (20a)$$

$$B_e^{(1)}=\frac{\pi}{2}\left\{(W_0+W_K)^4n_Kg_K^2+(W_0+W_L)^4[n_{L_I}g^2_{L_I}+n_{L_{II}}f^2_{L_{II}}]+9(W_0+W_L)^2\frac{n_{L_{III}}g^2_{L_{III}}}{R^2}\right\}, \quad (20b)$$

$$B_e^{(2)}=\frac{\pi}{2}\left\{(W_0+W_K)^6n_Kg_K^2+(W_0+W_L)^6[n_{L_I}g^2_{L_I}+n_{L_{II}}f^2_{L_{II}}]+30(W_0+W_L)^4\frac{n_{L_{III}}g^2_{L_{III}}}{R^2}\right\}, \quad (20c)$$

$$B^{(3)}=\frac{\pi}{2}\left\{(W_0+W_K)^8n_Kg_K^2+(W_0+W_L)^8[n_{L_I}g^2_{L_I}+n_{L_{II}}f^2_{L_{II}}]+63(W_0+W_L)^6\frac{n_{L_{III}}g^2_{L_{III}}}{R^2}\right\} \quad (20d)$$

In (20a) to (20d) $n_K\leq2$ is the number of electrons in the K shell, $n_{L_I}\leq2$ is the number of electrons in the L shell with $(j=\frac{1}{2}, l=0)$, $n_{L_{II}}\leq2$ is the number of electrons in the L shell with $(j=\frac{1}{2}, l=1)$, and $n_{L_{III}}\leq4$ is the number of electrons in the L shell with $(j=\frac{3}{2}, l=1)$. We have only included the terms which involve electrons in the K and L shells since it is very doubtful that capture of electrons in the M or higher shells can ever be detected experimentally. The g_K, g_{L_I}, $g_{L_{III}}$ functions are the "large" radial Dirac wave functions in a Coulomb field corresponding[37] to the quantum number sets $(\bar{n}=1, j=\frac{1}{2}, l=0)$, $(\bar{n}=2, j=\frac{1}{2}, l=0)$, $(\bar{n}=2, j=\frac{3}{2}, l=1)$, respectively. They are given by:

$$g_K^2=\frac{(1+W_K)}{2\Gamma(2s_0+1)}(2\alpha Z_{\text{eff}})^3\exp[-(2\alpha Z_{\text{eff}}R)](2\alpha Z_{\text{eff}}R)^{2s_0-2}, \quad (21a)$$

$$g^2_{L_I}=\frac{(2s_0+1)(2+2s_0)^{\frac{1}{2}}(1+W_L)}{4\Gamma(2s_0+1)((2+2s_0)^{\frac{1}{2}}+1)}\left(\frac{2\alpha Z_{\text{eff}}}{(2+2s_0)^{\frac{1}{2}}}\right)^3\exp\left[-\frac{2\alpha Z_{\text{eff}}R}{(2+2s_0)^{\frac{1}{2}}}\right]\left(\frac{2\alpha Z_{\text{eff}}R}{(2+2s_0)^{\frac{1}{2}}}\right)^{2s_0-2}, \quad (21b)$$

$$g^2_{L_{III}}=\frac{R^2(1+W_L)}{2\Gamma(2s_1+1)}(\alpha Z_{\text{eff}})^3\exp[-\alpha Z_{\text{eff}}R](\alpha Z_{\text{eff}}R)^{2s_1-4}, \quad (21c)$$

[37] Cf. H. A. Bethe, Handbuch der Physik, 24/2, p. 316; $\bar{n}$ is the principal quantum number.

with[38]

$$s_0=(1-\alpha^2Z^2_{eff})^{\frac{1}{2}},\quad W_K=1-\frac{\alpha^2Z^2_{eff}}{2},\quad s_1=(4-\alpha^2Z^2_{eff})^{\frac{1}{2}},\quad W_L=1-\frac{\alpha^2Z^2_{eff}}{8}.$$

In (21a), $Z_{eff}=Z-0.30$ and in (21b) and (21c) $Z_{eff}=(Z-4.15)$. The function $f_{L_{II}}$ which appears in (20a) to (20d) is the "small" component of the Dirac wave function for $(\tilde{n}=2, j=\frac{1}{2}, l=1)$, and is to a good approximation given by:

$$f^2_{L_{II}}=\tfrac{3}{16}\alpha^2Z^2_{eff}g^2_{L_I}. \tag{21d}$$

Values of g_K^2, $g^2_{L_I}$, $f^2_{L_{II}}$, $g^2_{L_{III}/K^2}$ for representative Z's are given in Table IV, with

$$R(\hbar/mc)=1.5\times10^{-13}A^{\frac{1}{3}}.$$

To compute theoretical lifetimes for K or L electron capture on the basis of (20) it is necessary to know M_n and W_0. The value for M_n could be taken from β-emitters in the same region of the periodic table and the same order of transition. When positron emission takes place W_0 can be determined from the maximum energy of the positron. If there is no positron emission only an upper bound of 0.5 Mev can be placed on W_0 since few if any existing measurements of thresholds (for the production of the unstable nuclei decaying by K or L capture) and masses (of the stable product nuclei) are sufficiently accurate to determine W_0. We have, therefore, computed the minimum lifetimes for $W_0=1$ corresponding to absence of positron emission. These lifetimes for different Z are listed in Table V for the allowed, and the first, second, and third forbidden transitions assuming pure K capture. The matrix element M_n in (20) is in each case taken equal to one and, furthermore, it is assumed that the parent nucleus has a larger spin than the product nucleus. If the spin of the parent nucleus is less than the spin of the product nucleus, the right-hand side of (20) should be multiplied by $(2j_f+1)/(2j_i+1)$ where j_i, j_f as before, are the spins of the parent and product nuclei, respectively. Some applications of this table to experiment are given below.

An examination of the allowed transition formula (20a) reveals that for sufficiently negative W_0, L_I capture becomes as probable as K capture. We have listed the values of W_0 for which this occurs, i.e., when $(W_0+W_K)^2g_K^2=(W_0+W_L)^2g_{L_I}^2$, for different Z in column 2 of Table VI and in column 3 the corresponding minimum lifetimes. These lifetimes are to be compared with columns 2 and 3 of Table V; it is seen that they are considerably larger than the lifetimes in column 2 and smaller than the lifetimes in column 3 (when $Z>35$) for a first forbidden transition. For nuclei with exceptionally long lives—which are of the order of the first forbidden values—which decay by orbital electron capture unaccompanied by positron emission, it would be interesting to look for x-rays associated with transitions to the L shell. If the β_4-line (in x-ray terminology) has an intensity comparable with the $K\alpha_1$ line, the transition is allowed; if it is completely absent, the transition is first forbidden. The decay of Fe^{55} with a lifetime 5–10 yr.[39] may be a case in point but no one has looked for the x-rays.

A similar analysis can be made for the first forbidden transition: it is seen from (20b) that again for sufficiently negative W_0 (though

TABLE V. Minimum lifetimes for K capture with $W_0=1$.

Z	$\tau_c^{(0)}$ (sec.)	$\tau_c^{(1)}$ (sec.)	$\tau_c^{(2)}$ (sec.)	$\tau_c^{(3)}$ (sec.)
10	3.4×10^{5}	6.8×10^{8}	3.8×10^{14}	4.3×10^{20}
20	3.8×10^{4}	4.9×10^{8}	1.8×10^{13}	1.2×10^{19}
30	9.8×10^{3}	9.1×10^{7}	2.4×10^{12}	1.2×10^{18}
40	3.4×10^{3}	2.5×10^{7}	5.2×10^{11}	2.1×10^{17}
60	5.8×10^{2}	3.1×10^{6}	4.8×10^{10}	1.4×10^{16}

[38] Cf. end of footnote 35.

TABLE VI. Minimum lifetimes for L capture with $W_0=1$.

Z	$\frac{W_0}{L_I/K}=1$	$\tau_c^{(0)}$ (sec.)	$\frac{W_0}{L_I}=1$	$\tau_c^{(1)}$ (sec.)	W_0 (for $\frac{L_{II,\,III}}{K}=1$)	$\tau_c^{(1)}$ (sec.)
10	−0.99	1.3×10^{10}	−0.99	1.9×10^{18}	−0.79	2.9×10^{12}
20	−0.99	1.1×10^{9}	−0.98	5.1×10^{17}	−0.67	3.8×10^{11}
30	−0.97	5.4×10^{8}	−0.95	1.6×10^{15}	−0.62	4.5×10^{10}
40	−0.93	9.1×10^{6}	−0.91	4.0×10^{13}	−0.58	9.8×10^{9}
50	−0.90	2.5×10^{6}	−0.85	1.4×10^{12}	−0.56	3.4×10^{9}
60	−0.86	6.0×10^{5}	−0.77	7.7×10^{10}	−0.53	1.3×10^{9}

[39] Cf. J. L. Livingood and G. T. Seaborg, Phys. Rev. **55**, 1268 (1939), and S. Van Voorhis, private communication, quoted in Livingood and Seaborg (see reference 42 below).

smaller in absolute magnitude than was true for allowed transitions) $L_{\rm I}$ capture becomes as probable as K capture. The values of W_0 for which this occurs, i.e., when $(W_0+W_K)^4 g_K^2 = (W_0+W_L)^4 g_{L_{\rm I}}^2$ and the corresponding minimum lifetimes are listed in columns 4 and 5 of Table VI. In addition, for values of W_0 even less close to -1, $L_{\rm II,III}$ capture—we consider the capture of $L_{\rm II}$ and $L_{\rm III}$ electrons together because the $L_{\rm II}-L_{\rm III}$ splitting is so small (cf. reference 35)—becomes as probable as K capture. These values of W_0, i.e., when

$$(W_0+W_K)^4 g_K^2 = \left[(W_0+W_L)^4 f_{L_{\rm II}}^2 + 18(W_0+W_L)^2 \frac{g_{L_{\rm III}}^2}{R^2}\right]$$

and the corresponding minimum lifetimes are listed in columns 6 and 7 of Table VII. From purely statistical arguments some nuclei should exist for which the $L_{\rm II,III}$ capture becomes important for a first forbidden transition, but of course the measurement will be difficult to carry out because of the long lifetimes. It is for this reason that we have not given the conditions for appreciable L capture in the case of higher order forbidden transitions; experimental verification is almost out of the question.

Throughout the preceding discussion we have assumed that the transitions take place in accordance with the tensor interaction and with favorable parity change. If the parity change required by the particular allowed or forbidden transition is at variance with the actual parity change which the unstable nucleus must undergo, the lifetime for the same spin change will be considerably increased. A repetition of the arguments which led to (17a, b) and (19a, b) would lead to similar formulae for orbital electron capture. However it does not seem worthwhile to write down these expressions. A rough estimate of the effect on the lifetime of unfavorable parity change in the case of pure K capture can always be obtained by multiplying the value one gets from (20) by $(W_0+W_K)^2R^2$.

The experimental material which could test some of the above conclusions is rather meager. It is necessary to use nuclei for which the lifetimes are long and for which positrons are either completely absent or present as a known fraction of the x-radiation accompanying the orbital

TABLE VII. Data on isobaric pairs.

Isobaric pair	Spins (in units of $\hbar$)	Theoretical lifetime for $W_0=1$ (in yr.)	W_0 for which theoretical lifetime is 10^{12} yr. (in units of mc^2)
$_{27}Co^{57} \rightarrow {}_{26}Fe^{57}$	—	—	—
$_{19}K^{40} \rightarrow {}_{18}A^{40}$	$4 \rightarrow 0$	3×10^{10}*	-0.3*
$_{45}Rh^{101} \rightarrow {}_{44}Rn^{101}$	—	—	—
$_{49}In^{113} \rightarrow {}_{48}Cd^{113}$	$9/2 \rightarrow \frac{1}{2}$	4×10^{11}	$+0.6$
$_{50}Sn^{115} \rightarrow {}_{49}In^{115}$	$? \rightarrow 9/2$	1×10^{10}	$+0.1$
$_{71}Lu^{176} \rightarrow {}_{70}Yb^{176}$	$\geqslant 7 \rightarrow 0$	$>10^{12}$	≤ 1
$_{76}Os^{187} \rightarrow {}_{75}Re^{187}$	$? \rightarrow 5/2$	1	-0.8

* The value given assumes a spin $1\hbar$ and even parity for the excited state (cf. text).

electron capture. One of the best studied reactions which falls into this category is:[40] $_{23}V^{47}+e_K \rightarrow {}_{22}Ti^{47}$ for which no positrons at all are observed; moreover, no γ-rays are observed so that the decay must be to the ground state of Ti^{47}. The observed lifetime is $1.7/\log_e \pm 0.2 = 2.4\pm0.2$ yr. If this decay were an allowed transition with maximum allowable spin change $1\hbar$ and no parity change—the minimum theoretical lifetime according to Table V would be 0.3 days. This value is based on the assumption that $|M_0|^2=1$ and $W_0=1$; if we choose $|M_0|^2 \sim 0.1$, as seems reasonable for an allowed transition in this atomic range, then the theoretical lifetime will be increased to the correct value 2.4 yr. provided that $W_0=-0.88$. This value of W_0 is not close enough to -1 to make $L_{\rm I}$-electron capture comparable to K capture. The vanadium decay might also be explained by assuming that the maximum allowable spin change is $1\hbar$ but that a parity change takes place. The minimum theoretical lifetime with $W_0=1$, $|M_0|^2=1$—using the remark at the end of the last paragraph—would be 1 yr., which is barely reconcilable with experiment. A first forbidden transition with a spin change of $2\hbar$ and parity change seems excluded; as can be seen from Table V, the minimum theoretical lifetime for $W_0=1$, $|M_1|^2=1$ is then 7 yr.

A situation similar to that of vanadium occurs in the case of the reaction[41] $_{25}Mn^{54}+e_K \rightarrow {}_{24}Cr^{54}$. No positrons have been observed although a γ-ray of energy 0.85 Mev has been detected. The lifetime is 1.25 ± 0.05 yr. The excited state of Cr^{54} to which Mn^{54} decays probably has a

[40] Walke, Williams, and Evans, Proc. Roy. Soc. **A171**, 360 (1939).
[41] J. J. Livingood and G. T. Seaborg, Phys. Rev. **54**, 391 (1938).

spin $1\hbar$ since the ground state of Cr^{54}—which is an even-even stable nucleus—must have a spin zero. If Mn^{54} has the same parity and a spin which does not differ by more than $1\hbar$ from the spin of the excited state of Cr^{54}, then with $|M_0|^2 \sim 0.1$ the theoretical lifetime will be brought into agreement with the observed lifetime of 1.25 yr. by choosing $W_0 = -0.85$. If the parity of Mn^{54} is different from the parity of the excited state of Cr^{54}, the minimum theoretical lifetime for $W_0 = 1$, $|M_0|^2 \approx 1$ is 0.9 yr. It is probable that the transition is allowed and that no parity change takes place.

The few other long-lived nuclei which are thought to decay by K-electron capture,[42] such as Fe^{55}; Cl^{36}, etc., are not very well investigated and so will not be considered here. However, it is interesting to apply the theory to some of the known neighboring stable isobars. All the known neighboring stable isobars—taken from Livingood and Seaborg's article[42]—are listed in column 1 of Table VII with the spins where measured, or predicted with reasonable certainty, given in column 2. The pairs (K^{40}, A^{40}) and (Lu^{176}, Yb^{176}), are also listed although one member of each pair, namely K^{40} and Lu^{176}, are electron emitters.

In column 3 are given the theoretical lifetimes for K-electron capture on the assumption that (a) $W_0 = 1$—since positrons are absent, (b) $|M_n|^2 = 0.01$—which is a reasonable guess for highly forbidden transitions, (c) the nuclei decay to the ground state of the parent nuclei, and (d) the parity change is favorable. Values are not given for the pairs (Co^{57}, Fe^{57}), (Rh^{101}, Ru^{101}) since the spins of neither nucleus of the pair is known. A value for the theoretical lifetime is given for the pair (Os^{187}, Re^{187}) under the assumption that Os^{187} has the maximum known spin for an even-odd nucleus, namely, $9/2\hbar$. Similarly a value is given for the pair (Sn^{115}, In^{115}) when we assume that Sn^{115} has a spin of $\frac{1}{2}\hbar$. Since no evidence has been found that the first member of any of the pairs of nuclei listed in Table VII decays by K-electron capture to the second member (with the exception of K^{40} which is discussed in more detail below), we must assume that the lifetimes are greater than say 10^{12} yr. We have therefore tabulated in column 4 the values of W_0 for which the theoretical lifetime attains this value. We see that there is a scattering as would be expected from statistical considerations.

The case of K^{40} is of particular interest as has already been remarked. In Section III (cf. reference 23) it was pointed out that K^{40} emits a homogeneous 2-Mev γ-ray and that about 3 quanta are emitted per 100 disintegration electrons. Furthermore, it followed that this γ-ray could not be correlated with the energy levels of the Ca^{40} nucleus formed in the electron disintegration. It will be shown that the assumption that the γ-ray is associated with K-electron capture to an excited state of A^{40} leads to reasonable results. Suppose the 2-Mev γ-ray is due to a radiative transition from an excited state of A^{40} to its ground state; it follows that there would be sufficient energy available for positron decay of K^{40} to the ground state of A^{40}. Since the spin of the ground state of A^{40} is zero, the positron emission would be third forbidden and formula (11)[43] would predict an observable intensity—about as large as the observed electron intensity of 23 per sec. per gram of potassium—provided the parity of the ground state of A^{40} were even (i.e., different from K^{40} which is taken as odd). Since no positrons are observed the parity of the A^{40} must be odd. The excited state of A^{40} would then presumably be even and have a spin $1\hbar$. The emission of the 2-Mev γ-ray would then be associated with a K-electron capture by K^{40} having a spin $4\hbar$ and odd parity to an excited state of A^{40} with spin $1\hbar$ and even parity. This would be a second forbidden transition with unfavorable parity change. The transition probability would be according to (20):

$$1/\tau_c^{(2)} = 1.3 \times 10^{-16} |M_2|^2 (W_0 + W_K)^8 \text{ sec.}^{-1}$$

to be compared with the observed value 5×10^{-19} sec.$^{-1}$. If we choose $|M_2|^2 \sim 0.01$, then $W_0 \sim -0.3$ which is quite reasonable.

In conclusion, it is a pleasure to thank Professor V. F. Weisskopf for many helpful discussions and advice generously given.

[42] These are listed in J. J. Livingood and G. T. Seaborg, Rev. Mod. Phys. **12**, 30 (1940); a more up-to-date table by Dr. Dessauer of our laboratory has also been very useful.

[43] Equation (11) can be applied to positron emission if $(-Z)$ replaces Z throughout.

The Angular Distribution of Protons Scattered by High Energy Neutrons

HOWARD TATEL*
Harrison M. Randall Laboratory of Physics, University of Michigan, Ann Arbor, Michigan
(Received January 20, 1942)

The scattering of 11-Mev neutrons by protons has been investigated. The neutrons from the disintegration of a beryllium target are collimated by a hole in a protective water wall. They are then scattered in a hydrogen gas cell and the recoil protons are observed at two different angles. The detection system consists of two parallel plate ionization chambers arranged so that protons may pass through both. Only coincidences are recorded thereby diminishing the very large neutron recoil background. The results indicate that the intensity of the protons varies as the cosine of the scattering angle in the laboratory system. Hence the scattering in the center of gravity system is isotropic within the experimental accuracy of ten percent.

INTODUCTION

KNOWLEDGE of the laws of force between the elementary nuclear particles is of fundamental importance. A direct way of studying these forces is to observe the scattering of elementary particles by each other. In this experiment an attempt has been made to study the angular dependence of the scattering of high energy neutrons by protons. The energy of the neutrons is made as high as practical in order to have their wave-lengths as short as possible. As the wave-length gets shorter the scattering should change from simple s scattering as the p scattering begins to show up. As a consequence the exchange properties of the forces begin to affect the scattering, as has been discussed in detail by Rarita and Schwinger.[1] The mean energy of the neutrons used in this experiment is 11 Mev.

EXPERIMENTAL METHOD

The basic experimental set-up is as follows: Neutrons from the cyclotron target are collimated into a beam by means of a hole in a water wall. This beam passes through a cell containing hydrogen gas, and the recoil protons are observed by suitable counters at various angles.

If a neutron of energy E_0 collides with a proton at rest, the energy of the proton E_p after being scattered through an angle θ is

$$E_p = E_0 \cos^2 \theta.$$

In this experiment beryllium is the cyclotron target, and the energy spectrum of the neutrons is continuous. For a given angle the proton energy distribution will also be continuous. In order to interpret the results under these conditions, a very detailed study of the particle spectrum would be necessary. Instead the energy of the protons observed is limited. The highest energy is set by the maximum energy of the emitted neutrons (13 Mev), and the lowest energy is set by the minimum range of the scattered protons after passing through aluminum foils. The mean energy of the neutron group for the forward direction is 11 Mev.

Since in the direct neutron beam the background owing to recoils is too high, it is necessary to make all measurements with the detector off the beam. The two angles chosen for measurement are 16° and 45°. Figure 1 shows the experi-

TABLE I. Energies of protons and neutrons.

Aluminum absorbers	16° Approx. thickness (inches)	16° mg/cm²	45° Approx. thickness (inches)	45° mg/cm²
Scattering cell window	0.006	43.3	0.002	12.7
Collimator window	0.001	6.8	0.001	6.8
Detecting chamber window	0.001	6.8	0.001	6.8
Detector internal foil	0.0007	4.3	0.0007	4.3
Additional absorber	0.006	43.3		
	0.002	12.7		
	0.0005	3.3		
Total		120.5		30.6
Equivalent air-cm (1.52 mg/cm² = 1 air cm)		79.2		20.1
Correction for Al		4.7		0.3
Air distance (collimator to chamber)		2.7		2.7
Equivalent distance in first chamber (8.7 cm × pressure × stopping power of O_2)		16.7		10.1
0.3 cm-range in air to register in counter 2		0.3		0.3
Total range in air centimeters		103.6 cm		33.5 cm
Energy of protons detected (E_θ)		9.44 Mev		4.97 Mev
Energy of neutrons in forward direction (E_0)		10.2 Mev		10.1 Mev

* Now at the Department of Terrestrial Magnetism, Carnegie Institution of Washington.

[1] W. Rarita and J. Schwinger, Phys. Rev. **59**, 556 (1941).

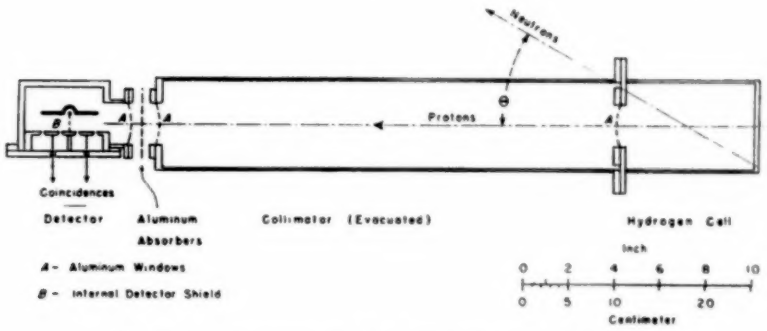

FIG. 1. Arrangement of detecting and scattering system.

mental layout of the scatterer and the detector system. The scatterer is the hydrogen gas in the scattering cell which is 14 cm deep. Its aperture is defined by the port 4.7 cm in diameter. Between this port and the detector is an evacuated collimating tube whose aperture is also 4.7 cm. Between the collimating chamber and the detector is an air gap of 2.7 cm. Here are placed the absorbing aluminum foils. There are aluminum windows on all the ports. Table I shows how the energy of the protons is determined.

THE DETECTING APPARATUS

The apparatus for detection of the recoil protons consists of two parallel plate type ionization chambers each connected to a separate pulse amplifier. The chambers are so arranged that a proton may pass through both. The simultaneous pulses from the amplifiers are recorded by means of a Rossi coincident circuit. Thus, to a large extent the background counting rate in each chamber owing to the recoils of the gas nuclei is eliminated.

In Fig. 2 is shown the plan of the double chamber. The separate chambers are 2.3 cm deep along the proton path, 2 cm wide, and 4 cm high. They are shielded from each other by a thin aluminum foil[2] perpendicular to the plane of their common collection plates.

In Fig. 3 is a block diagram showing the scheme by which coincidences are counted. In the mixing stage the output of the pulse amplifiers is

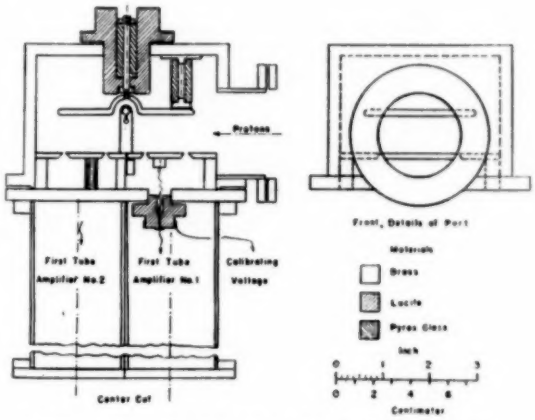

FIG. 2. Double coincident ionization chamber.

fed to two separate gas triodes. The gas triodes have variable bias and act as discriminators. The output of the triodes go to pentodes arranged in a Rossi circuit. The advantage of this arrangement is that the pulses fed to the Rossi circuit are uniform since they are independent of the shape of the pulses at the input of the discriminators.

To see whether or not the apparatus would work as a true coincident circuit, use was made of the following relation:

$$n_c = 2ln_1n_2.$$

Here n_c is the chance coincident counting rate with independent counting rates in chambers 1 and 2 of n_1 and n_2, respectively, with resolving time l of the coincident circuit. Alpha-particle sources of various strengths were placed in chambers 1 and 2. It was found that the above relation was always satisfied independent of the individual counting rates and pulse size for $l = 1.2 \times 10^{-4}$ second.

Since a finely collimated beam of protons was

[2] When the apparatus was first tried out in the cyclotron room the shield foil was 1.5 air-centimeters. However, vibrations induced in the foil by the high noise level in the neighborhood of the cyclotron gave an intolerable voltage noise level to the apparatus. Dr. Geiger suggested that two foils be used instead of one. The two foils damped their individual vibrations so effectively that the foil was no longer a source of trouble.

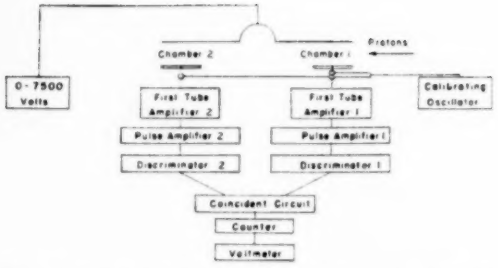

FIG. 3. Scheme for counting coincidences and calibrating the circuits.

not available, polonium alpha-particles are used to standardize the chambers. A thin source of polonium in a collimating tube is placed in the port of the double chamber so that the alpha-particles may pass through the center of both chambers. The pressure in the chamber is reduced until the "noise pulses" in the amplifier begin to mask the pulses from the alpha-particles. This is judged to occur at 7.2 cm of Hg pressure in oxygen. At this pressure the Po alpha-particles have a specific ionization of 95 kev per centimeter in chamber 1. The collecting voltage is 340 volts, which is equivalent to 3600 volts at atmospheric pressure. Since 7200 volts is the maximum available, it is possible to use the chamber up to 2 atmospheres of oxygen. At this pressure a beam of ionizing particles can be detected if it has a mean energy loss of at least 47 kev per air-centimeter. This is approximately the energy loss of 15-Mev protons at the beginning of their range.

The method used for counting the protons is such that the absolute sensitivity of the counters does not affect the final answer, only the relative sensitivity must remain constant. However, to assure reproducibility and uniformity, the manner of operation and efficiency of counting coincidences were investigated as follows. The sensitivity is determined first. The output of a thousand-cycle oscillator is rectified and sent through a milliammeter. The output of the oscillator also appears across a 20,000-ohm resistor. A small part of the output (that across one ohm) is fed onto a ring concentric with the leads from each ion chamber. By varying the oscillator output a series of pulses of any given size may be induced upon the first grids of the amplifiers. Their relative magnitude is read from the milliammeter. Although the induced pulses are all of the same size, they do not appear so at the output of an amplifier. This is because they are mixed with the random "noise pulses" on the first grid of an amplifier. In order to set the sensitivity of an amplifier at a specified value in spite of the distribution of output pulses, the pulses are counted at the output of a discriminator by a vacuum tube voltmeter. The discriminator gives pulses of equal size for each count. The oscillator output is varied until the voltmeter reads one-half what it would read when counting all the pulses (1000 per second). The reading of the oscillator milliammeter at this half value is called the "sensitivity" of the counter. This method of setting the sensitivity proved very useful during the course of making the measurements. It enabled us to check or set the sensitivity of each counter accurately and quickly.

The sensitivity of counter 2 is set, and the coincident counting rate is taken as a function of the sensitivity of counter 1. It was found that the counting rate would change less than 1 percent if counter 1 changed its sensitivity from 0.18 to 0.25, and counter 2 from 0.3 to 0.4 as both counters have a considerable "plateau" in their counting rate *vs.* sensitivity curve.

TEST FOR COLLIMATION

A test for the collimation was made in order to guard against spurious effects caused by scattering. Oxygen recoils in one chamber were counted as the chambers were moved across the beam. The sensitivity was set such that pulses of 2.7 Mev or greater tripped the counter. These recoils were from neutrons of 10 Mev or greater. The observed intensities were: 5 cm east of

TABLE II. Data on scattering. Columns 1 and 4 give the total number of counts observed for a particular day, while columns 2 and 5 give the respective number of millicoulombs of deuterons used. Columns 3 and 6 are, respectively, 1 divided by 2 and 6 by 7. Column 7 gives the hydrogen pressure in lb./sq. in. $P+b$ (protons plus background), b (background), mc (millicoulombs).

1 $P+b$	2 mc	3 $(P+b)$/mc	4 b	5 mc	6 b/mc	7 Press.	8 θ
683	171	3.99 ±0.15	45	83	0.54 ±0.08	29.8	44°
409	122	3.36 ±0.17	43	57	0.76 ±0.11	29.8	44°
778	214	4.12 ±0.15	94	113	0.83 ±0.08	29.8	44°
659	203	3.25 −0.13	71	102	0.70 −0.08	28.5	44°
625	40	15.6 ±0.6	104	32	3.2 ±0.3	92	16°
808	59	13.8 ±0.5	137	41	3.3 ±0.3	94	16°
860	60	14.3 ±0.5	146	39	3.8 ±0.3	94	16°
282	63	4.5 ±0.3	230	66	3.5 ±0.2	0	16°
328	27	1.23 ±0.07	148	27	0.55 ±0.05	0	44°

center, 28.2±0.9; center, 27.4±0.9; 5 cm west of center, 28.1±0.9. Hence, the intensity was uniform over the region of the beam that was used.

CORRECTIONS FOR FINITE SOLID ANGLE

The most important correction that must be made in this experiment arises from the finite solid angle subtended by the detector at the scatter and by the neutron source at the detector. Variation of this solid angle with scattering angle is shown in Fig. 4. The distance between scatter and detector is taken as 62 cm. The diameter of the port is 4.7 cm, and the width of the detector slit is 2 cm. Furthermore, the projected width of the scatterer as seen from the target (4.2 meters away) is taken as 10.6 cm. The size of the correction depends also upon the variation of proton energy with angle and the energy spectrum.

Let $N(E)$ be the number of neutrons with energy greater than E in the forward direction. At 45° the energy for detection is set to have a minimum value E_d. It will be assumed that the variation of scattering cross section with energy is small. If θ is the angle of scattering, then the number of protons scattered between θ, $\theta+d\theta$ is

$$(\sigma_\theta/\sigma_0)N(E_d/\cos^2\theta)w(\theta)d\theta,$$

where σ_θ/σ_0 is the ratio scattering cross section at $\theta=0$ to $\theta=\theta$ and $w(\theta)$ is the relative solid angle (Fig. 4). The total number of particles observed is

$$N_\theta=\int_{\theta_{\min}}^{\theta_{\max}}\sigma_\theta/\sigma_0\,N(E_d/\cos^2{}_0)w(\theta)d\theta\Big/\int_{\theta_{\min}}^{\theta_{\max}}w(\theta)d\theta.$$

σ_θ/σ_0 is assumed to be independent of energy between $\theta_{\max}$ and $\theta_{\min}$ (41°–49°). $N(E)$ is found without serious error at 16°. The three values of $N(E)$ observed at 9.1 Mev, 10.2 Mev, and 11.3 Mev lie on a straight line within the accuracy of the measurement (10 percent). Since $N(E)$ is a straight line function and $w(\theta)$ is symmetrical about the 45° position, the value of $N_{45°}$ observed is the correct one. Hence, a comparison of the number of particles observed at 45° and at 16° may be compared directly to find the ratio of cross sections.

TABLE III. Counts per millicoulombs of deuterons.

	A	B	C	D
16°	14.6 ±0.3	3.5 ±0.17	4.5 ±0.3	3.5 ±0.2
45°	3.72±0.07	0.70±0.05	1.23±0.07	0.55±0.05

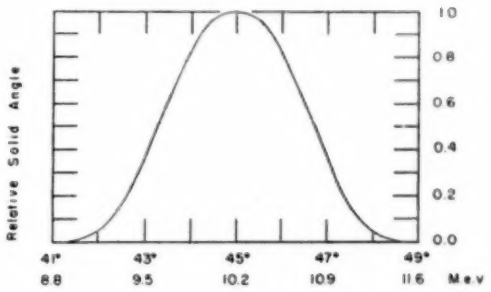

FIG. 4. Relative solid angle *vs.* the angle of scattering θ near 45° and the cut-off energies for θ.

PROCEDURE

First the angle is carefully laid out and the apparatus lined up. Then the proper thickness of aluminum foil is calculated so that the protons will have the correct cut-off energy (Table I). This must be done in conjunction with the oxygen pressure in the detecting chamber so that the energy loss of the most energetic protons will be sufficient for them to be counted. (The electrical sensitivity of the counters is always kept constant.) The field strength in the counters is also adjusted so that the ion collection time is constant. Then coincident counts A are taken at the proton cut-off energy for so many microcoulombs of deuterons. Then enough aluminum is interposed to cut out all protons due to neutrons of energy less than 13 Mev. This latter count B is due to a few proton recoils from neutrons of high energy, chance coincidences, and coincidences from all other causes. These runs are taken alternately—about twenty minutes apiece. After these data are obtained, similar sets of data are taken with no hydrogen in the scattering cell, C, D. The difference in count $(C-D)$ in this case is caused by n, p reactions in the scattering cell. The number of protons is given by $(A-B)-(C-D)$ for a given number of coulombs of deuterons on the beryllium target.

RESULTS

The results are best shown in Tables II and III. The net proton count at 16° is 10.1 ± 0.5 and at 45° is $2.3_4\pm0.1_3$ per millicoulomb of deuterons. The proton ratio is thus 4.3 ± 0.3. The ratio of gas pressures is $94/30=3.13$. Therefore, the ratio of scattered protons at 16° and 45° is $4.3/3.1=1.3_8\pm0.11$. If the scattering were isotropic in the center of gravity system, the proton intensity would vary as the cosine of the angle of scattering for constant solid angle. The ratio of the cosines of the scattering angles used is $0.96/0.70=1.37$. The numerical agreement is probably fortuitous as the statistical fluctuation of the measurements is one of the major difficulties in the experiment. For instance, a typical 14-hour run produces but 700 counts of protons with background, the background being 100 counts. Every precaution has been taken to make instrumental errors small. The amplifier sensitivity was checked at least every half-hour although the sensitivity would rarely change as much as 5 percent. The statistical error ($\sqrt{N}/N$) of a day's run was usually 7 percent. A series of runs separated by two weeks agreed within this fluctuation.

CONCLUSION

The experimental measurement of the scattering of 11-Mev neutrons on protons indicates that the scattering in the center of gravity system is isotropic. The accuracy is ten percent.

It is interesting to compare these results with those of Rarita and Schwinger.[1] They made calculations on high energy n,p scattering for three types of forces between these particles. At the energies used in this experiment, the predicted asymmetry for the forces similar to those predicted by "symmetrical" and "charged" meson theories is very small and well within the experimental error. The third type of force analogous to the "neutral" meson theory predicts about 60 percent more recoils in the forward direction at 11 Mev. Experimentally such asymmetry does not seem to exist. Hence, it would appear that exchange forces similar to the first two agree better with the experiment.

A word about the possibilities of extending the range of the measurement might be of interest at this point. For carrying out this particular experiment, the scattered intensity could be increased considerably by getting closer to the cyclotron and imposing thicker water walls for better collimation. The ion chambers could perhaps be improved so as to increase their effective resolving power. Under such circumstances, it might be possible to extend the measurements into the region of 20 million volts. As a test, a thick (to the proton) paraffin scatterer instead of hydrogen gas was placed before the detector. With lithium as a target it was found the proton owing to neutrons of from 20 to 24 Mev could be detected by the apparatus. A feasible experiment with the present set-up would be to measure the total scattering cross section of hydrogen in the energy region between 5 and 20 Mev.

It was originally intended that this program of research on the properties of high energy neutrons would be carried through as outlined above, and that the present results would be considerably extended in accuracy and reliability. However, because of present conditions, the work must be terminated at this point, and the report is presented not as a final report but as indication of present progress.

ACKNOWLEDGMENT

The author wishes to thank Messrs. Wayne and Ray Middleton and Herman Roemer for their technical assistance. He is also indebted to Professor J. M. Cork for his aid and assistance, and to Professor G. E. Uhlenbeck for his generous counsel throughout the experiment. This investigation was made possible by a grant from the Horace H. Rackham Fund.

The *K*-Absorption Edges of Metal Ions in Aqueous Solution*

W. W. BEEMAN, *Department of Physics, University of Wisconsin, Madison, Wisconsin*
AND
J. A. BEARDEN, *The Johns Hopkins University, Baltimore, Maryland*

(Received January 29, 1942)

The x-ray *K*-absorption edges of Ni^{++}, Cu^{++}, Zn^{++}, $Cu(NH_3)_4^{++}$ and $Cu_2(CN)_4^{--}$ in aqueous solution have been measured with a double crystal spectrometer. Ni^{++}, Cu^{++}, and Zn^{++} have similar edges. Each consists of two absorption maxima which arise from the excitation of *K* electrons into the empty 4*p* and 5*p* levels of the ion. The final levels are broadened by the fields of the coordinated water molecules. Quite different edge structures were found in the complex ions. They probably arise from the scattering of the photoelectron by the other atoms of the ion, the same process which takes place in polyatomic gases.

VERY little has been published on the x-ray absorption edges of dissolved substances. The reason for this fact appears to lie in the complexity and disorder of liquid structure which make impossible any interpretation of the experimental results unless structure very close to the main absorption edge can be resolved. In the latter region, as the present research shows, simple explanations can be given because the absorption structure is determined by final states in which the excited electron remains bound to the parent ion. Most of the earlier work[1] has been done with single crystal spectrometers incapable of resolving the interesting structure close to the absorption edge.

The only previous double crystal measurements are those of Cioffari[2] on the Br *K* edge in bromine water and in a solution of KBr. He was not primarily concerned with solutions, however, and indeed found only slight differences between the above edges and those of liquid bromine and solid KBr, respectively.

EXPERIMENTAL

The double crystal spectrometer used in this research and the technique of taking readings have been completely described in previous publications.[3-5]

In work with solutions some complications are introduced by the absorption of the solvent. In one mm of H_2O at the wave-length of the Cu *K* edge, this amounts to half the incident intensity. Absorption cells are thus limited to a thickness of one or two mm. At the same time there must be enough of the absorbing ion present to give good edge contrast, therefore very dilute solutions may not be used. Most of the present work was done with 1.0 normal solutions and measurements could probably be extended to 0.1 normal without too great difficulty. We made tests with 0.5 and 1.0 normal solutions of $CuSO_4 \cdot 5H_2O$ and found no dependence of the absorption edge on concentration.

The absorption cell was made by drilling a 1-cm diameter hole through the center of a brass plate 1 mm thick and about 4 cm square. Both Cellophane and mica proved satisfactory as entrance and exit windows, the mica rather more so, as it is stiffer and gives a cell of uniform thickness. Cellophane will sometimes bulge out when the cell is filled. The windows were almost as large as the brass plate and were easily attached to its faces with a low melting paraffin. The paraffin also prevented contact between the brass and the solution. Before attaching the windows, the plate was cut with a hacksaw from the outside to the center. The completed cell was filled through this opening with a thin drawn glass tube.

We measured the Cu^{++} edge in each of three solutions, $CuSO_4 \cdot 5H_2O$, $Cu(NO_3)_2 \cdot 6H_2O$, and $CuCl_2 \cdot 2H_2O$ with identical results, indicating that the dissociation was almost complete in each

* This research was supported by a grant made to one of the authors (J. A. B.) by the American Philosophical Society.

[1] B. B. Ray, S. R. Das, and N. Bagchi, Ind. J. Phys. **14**, 37 (1940); N. Bagchi, Ind. J. Phys. **14**, 61 (1940).
[2] B. Cioffari, Phys. Rev. **51**, 630 (1937).
[3] J. A. Bearden and C. H. Shaw, Phys. Rev. **48**, 18 (1935).
[4] W. W. Beeman and H. Friedman, Phys. Rev. **56**, 392 (1939).
[5] C. H. Shaw, Phys. Rev. **57**, 877 (1940).

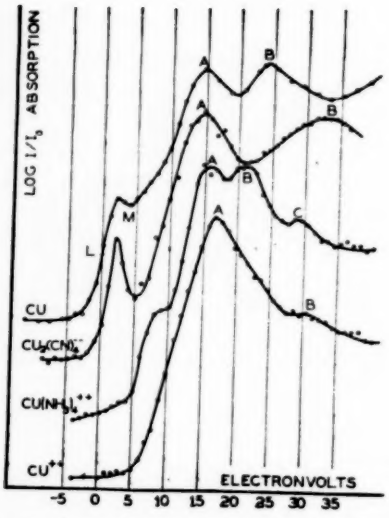

FIG. 1. K-absorption edges of Cu^{++}, $Cu(NH_3)_4^{++}$, $Cu_2(CN)_4^{--}$, and Cu metal, the latter taken from reference 4.

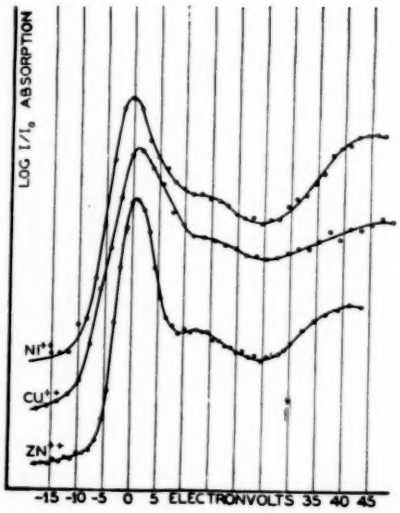

FIG. 2. K-absorption edges of Ni^{++}, Cu^{++}, and Zn^{++}.

solution. $Cu(NH_3)_4^{++}$ was measured in an ammoniacal solution of $CuSO_4 \cdot 5H_2O$ and $Cu_2(CN)_4^{--}$ in a solution of $Cu(CN)_2$ in KCN. Zn^{++} and Ni^{++} were both observed in solutions of the sulphates. All were approximately normal solutions of the absorbing ion. The absorption edges are shown in Figs. 1 and 2. The Cu curve of Fig. 1 is reproduced from reference 4. The four curves of Fig. 1 are on the same frequency scale so that shifts of structure from one curve to the next are accurately portrayed.

DISCUSSION

The K-absorption edges of metallic Ni, Cu, and Zn have been measured[4] and the structure qualitatively explained on the basis of the electron bands to be expected for these solids. Band calculations[6,7] were available only for Cu, and in this case good quantitative agreement was found between the observed maxima and minima of absorption and the calculated density of states curve. In particular, point L on the Cu curve of Fig. 1 gives the energy necessary to excite the K electron into the first empty level at the top of the Fermi distribution, the minimum of absorption at M is due to the small overlap of the $4s$ and $4p$ bands, and the maximum at A to absorption into a high density of states in the $4p$ band.

The absorption edge structure of the ions could also be explained if the energy distribution of final states and the transition probabilities to these states were known. Only for the atomic ions does this appear feasible without detailed calculation. Here the great similarity of the Ni^{++}, Cu^{++}, and Zn^{++} edges and the presence in each of two absorption maxima some 14 to 16 ev apart suggest the hypothesis that the ions are absorbing about as they would in vacuum and that the structure is due to excitation of the K electron into the optical levels of the ion. The transitions allowed by the selection rules are to the various p orbits beginning with $4p$. In Table I we have compared the observed structure and that predicted on the above hypothesis. The optical $4p-5p$ separations in the first column are for the ion of next higher atomic number. The data were taken from Bacher and Goudsmit, *Atomic Energy States*, and a paper by K. C. Mazumder[8] on the Zn III spectrum. The slight uncertainty in the optical separations is due to the splitting of the terms entering into the $4p$ and $5p$ configurations. Not enough of the higher Cu III terms are known to permit any predictions for Ni^{++}.

The observed absorption peak separations are somewhat poorly defined because of the broadness of the second absorption maximum. An attempt has been made to locate its center to within 1 or 2 ev. This is, however, not a matter of great importance, as exact agreement between

[6] H. Krutter, Phys. Rev. **48**, 664 (1935).
[7] E. Rudberg and J. C. Slater, Phys. Rev. **50**, 150 (1936).
[8] K. C. Mazumder, Ind. J. Phys. **10**, 171 (1936).

the observed and predicted separations cannot be expected for the following reason. We have resolved only two absorption maxima. Therefore the second one must contain contributions not only from the $1s-5p$ transition but also from transitions to $6p$, $7p$ and higher levels. The latter will shift the center of the absorption line to higher frequencies, and the observed separation will be greater than the predicted. The magnitude of this shift is hard to estimate, since it depends not only upon the separations of successive absorption lines but also upon their relative intensities. Very rough extrapolations from the spectra of similar but less highly ionized atoms indicate that $6p$ is about 4 ev above $5p$ and $7p$ about 2 ev above $6p$ for Ni^{++}, Cu^{++}, and Zn^{++}. The intensity of absorption falls off rapidly with increasing total quantum number. In argon, intensity ratios of about 4 : 2 : 1 have been found[9] for the $5p$, $6p$, and $7p$ absorption lines. If we take an average of the positions of these three lines weighting them in the above ratios, it is found that the average lies 2.5 ev above the $5p$ position. This agrees nicely with the data of Table I, where the observed $A-B$ separations are 2 or 3 ev greater than the optical $4p-5p$ separations.

Parratt has recently investigated the K-absorption spectrum of argon gas[9] which is of the simple type postulated for the ions. Because of the greater wave-length, he obtained somewhat greater energy resolving power and was able to separate three absorption maxima. They agreed perfectly with the optical terms of potassium.

A second, and quantitatively more satisfactory, comparison can be made between the observed structure and that predicted on the above hypothesis that the ions are absorbing as if they were in a vacuum. From the curves of reference 4 and the present data we can determine the shift from point L of the metal edge (indicating absorption into the first empty level at the top of the Fermi distribution) to point A of the corresponding ion absorption edge. This quantity can also be calculated from optical data with the help of the following cycle, if we assume, of course, that absorption maximum A is caused by a transition to the $4p$ level of the ion. The cycle will be illustrated for copper.

1. Remove a Cu atom from the Cu lattice and use the binding energy S_{Cu}.
2. Remove two outer electrons from the Cu atom and use energy corresponding to the first two ionization potentials of Cu.
3. Excite a $1s$ electron of Cu^{++} to the $4p$ orbit of Zn^{++} by using the energy $h\nu_{ion}$.
4. Return this electron to the $3d$ orbit, and obtain the energy difference $3d^9\,4p-3d^{10}$ of Zn^{++}.
5. Return two electrons to Zn^{++}, and obtain the energy corresponding to the first two ionization potentials of Zn.
6. Place the zinc-like atom at the vacant Cu lattice point and obtain the binding energy S_{Zn}.
7. Allow an electron at the top of the Fermi distribution to return to the K shell of the zinc-like atom and thus obtain the energy $h\nu_{metal}$ and return the system to its original condition.

This cycle gives the energy equation:

$$h\nu_{ion}-h\nu_{metal}=(17.2\pm0.6\text{ ev})+(S_{Zn}-S_{Cu}).$$

All the optical terms involved are summed in the first parenthesis. They were taken from Bacher and Goudsmit. The second parenthesis is the difference between the binding energy of a zinc atom and a copper atom in the copper lattice. It is difficult to estimate accurately the magnitude of this term. However, it can be shown that it is less numerically than the difference between the lattice energy per atom of pure Zn and pure Cu unless the heat of formation of a low zinc brass is negative. Actually the heats of formation of the brasses are positive[10] so we may say that the term in parentheses is numerically less than the approximately 2.0 ev per atom difference in the binding energy of pure Cu and pure Zn. It might, of course, be considerably less depending upon the actual value of the heat of formation. The corresponding term in the cycle for Ni^{++} is probably less than 1.0 ev since Ni and Cu have the same lattice energy to within this amount.

We have evaluated the edge shift for Ni^{++} and Zn^{++} using the same cycle and collected the data

TABLE I.

Edge	$4p-5p$ separation from optical data	Observed $A-B$ separation
Ni^{++}		15–16 ev
Cu^{++}	10.9–12.6 ev	14–16 ev
Zn^{++}	11.8–12.1 ev	13.5–14.5 ev

[9] L. G. Parratt, Phys. Rev. **56**, 295 (1939).

[10] W. Biltz, Zeits. f. Metallkunde **29**, 73 (1937).

TABLE II.

Edges	L to A shift: Calculated from optical data	Observed
Ni-Ni^{++}	17.7–18.2 ev	17.9 ev
Cu-Cu^{++}	16.6–17.9 ev	16.7 ev
Zn-Zn^{++}	7.3– 7.5 ev	8.7 ev

in Table II. In each case the term in the second parenthesis has been omitted from the energy equation, since it is likely that the mistake thus made is less than the experimental accuracy of about 1.0 ev. Some of the terms of Cu^{++} were taken from a paper of L. Bloch and E. Bloch.[11] The numerical agreement between the observed and calculated separations is seen to be quite good, and there can be but little doubt that the correct transitions have been assigned to the two absorption maxima in the ion edges.

The great difference between the optical levels in metals and in solution, then, appears to be that a transition to the *sd* band is allowed in metals, but a transition to the corresponding *s* and *d* states is not allowed in solutions. This is understandable since the exchange of electrons between atoms in metals destroys the meaning of the angular momentum quantum number while the Stark effect and other non-exchange forces exerted on the metal ion by the associated water molecules in solution do not, leaving the *l*-selection rules in force as in free atoms.

Although the positions of the absorption maxima are not affected by the solvent, the absorption lines are broadened considerably. Earlier work with the same instrument indicates that a transition to a sharp optical level should give an absorption line 2 or 3 ev wide at half maximum at these wave-lengths. This width is partly instrumental and partly due to the short lifetime of the excited state. The first absorption maxima of the atomic ions of Fig. 2 are very much broader. It is not possible to define accurately their half maximum width, since the lines are not symmetric, but a minimum value may be found by measuring, at half maximum intensity, the distance from the center of the line to its low frequency side and then doubling the result to get the half maximum width. Calculating in this way, one finds widths of 11.5 ev for Ni^{++}, 13 ev for Cu^{++}, and 8 ev for Zn^{++}. These widths are not caused by any contributions from the tails of the $1s-5p$, or higher absorption lines, since the $4p-5p$ separation is about 11 or 12 ev, three or four times the half maximum width predicted for sharp optical levels. Neglecting the influence of the coordinated water, one might put an upper limit of 4.5 ev on the line width for the $1s-4p$ transition, since in Ni^{++} and Cu^{++} the $4p$ level splits about 1.5 ev because of interaction with the unfilled $3d$ shell. The difference between 4.5 ev and the observed widths must be due to the fields of water molecules. Six molecules are attached permanently[12] to each atomic ion and they subject the ion to a perturbing field of cubic symmetry. This field causes an over-all splitting of the ground states of ions having an unfilled $3d$ shell (amounting to about 2.0 ev).[13] Probably the fact that Zn^{++} has a filled $3d$ shell while Ni^{++} and Cu^{++} do not, explains the narrower $4p$ absorption line of the former, although nothing very quantitative can be said.

The edge structure of $Cu_2(CN)_4^{--}$ seems to be of the same type as that found in polyatomic molecules, the theory of which has been given by R. de L. Kronig.[14] Evidence for this view is furnished by the shape of the initial absorption line (at 2.0 ev in Fig. 1) of the $Cu_2(CN)_4^{--}$ edge. The line fits accurately an inverse square curve, indicating that the absorption is into final states occupying an energy range small compared to the width of the K state plus crystals. Similar initial absorption lines are observed in the edges of most polyatomic molecules. The final states involved are states of positive energy, since the molecule or complex ion is not generally stable after the absorption.

The case for $Cu(NH_3)_4^{++}$ is not so convincing, as there are no sharp absorption lines. This result may be related to the fact that the binding in $Cu_2(CN)_4^{--}$ and in the polyatomic molecules which have been investigated is largely homopolar while the binding of the NH_3 groups to the Cu^{++} is largely ionic.

[11] L. Bloch and E. Bloch, Comptes rendus **200**, 2017 (1935).

[12] J. D. Bernal and R. H. Fowler, J. Chem. Phys. **1**, 515 (1933).

[13] W. G. Penney, Trans. Faraday Soc. **36**, 627 (1940).

[14] For a simplified explanation of the theory and references to the original work, see T. M. Snyder and C. H. Shaw, Phys. Rev. **57**, 881 (1940).

Radiofrequency Spectrum of Indium. Nuclear Spin of In^{113}*

T. C. HARDY, *City College and Columbia University, New York, New York*†

AND

S. MILLMAN, *Queens College, Flushing, New York, and Columbia University, New York, New York*

(Received January 26, 1942)

The atomic beam methods of studying the radiofrequency spectra of atoms in the ground state has been applied to indium. Lines characterized by the transitions $\Delta F=0$, $\Delta m=\pm 1$, were observed, in magnetic fields ranging from 3000 to 7000 gauss, for In^{113} as well as for In^{115}. The experiments give conclusive evidence that the nuclear spin of In^{113} is 9/2 and that its moment is positive, the same as that of In^{115}. The ratio of the hyperfine separation of the ground state of In^{115} to that of In^{113} was found to be 1.00224 ± 0.00010. This is also the ratio of the magnetic moments of the two isotopes. A h.f.s. value of (11413 ± 3) 10^6 cycles/sec. and a nuclear moment of 5.49 ± 0.04 nuclear magnetons were found for In^{115}.

THE existence of two stable isotopes of indium has been established by band spectra measurements as well as by the mass spectrograph. Nevertheless, the less abundant isotope, In^{113}, has not been found in spectra patterns of atomic indium and no positive experimental determination of its nuclear spin and moment has been made. Bacher and Tomboulian[1] were unable to detect any trace of In^{113} in a spectroscopic study of In II although they were certain that this failure was not due to the small abundance (4.5 percent) of In^{113}. These experimenters concluded that the hyperfine structure patterns of the two isotopes overlapped, from which fact they inferred that the spin of In^{113} was 9/2, the same as that of In^{115}, and that the nuclear magnetic moments of the two isotopes were approximately equal. Atomic beam measurements[2] of the nuclear moment of In^{115} also failed to show any indication of the less abundant isotope. This led to the prediction that the nuclear spin of In^{113} was probably 9/2 and if such were the case, the hyperfine structure separation $\Delta\nu$ of the ground state of In^{113} would have to differ from that of the other isotope by less than one percent.

In^{113} forms with Cd^{113} one of the three known stable isobaric pairs in which the elements of a pair differ by one in atomic number. Considerations of beta-processes require one member of such a forbidden pair to be radioactive with the observed stability of the active element interpreted as activity of very long half-life. This in turn is easily understood if the difference in spin between the two nuclei is large. Predictions based on these considerations require a spin of at least 3 units for In^{113}.[3]

In the experiments to be described the radiofrequency spectrum of the ground state of the indium atom was studied with the object of obtaining a positive experimental determination of the nuclear spin of In^{113}. These experiments also yield a determination of the sign of the moment of In^{113}, an improved measurement of the nuclear magnetic moment of In^{115}, as well as a precise determination of the $\Delta\nu$'s of the ground states of these isotopes, and therefore, a precise result for the ratio of the magnetic moments of the two nuclei.

The indium atom in the ground state is a $^2P_{1/2}$ configuration with In^{115} known to have a nuclear spin $i=9/2$. This gives rise to total angular momentum values $(F=i\pm j)$ in units of $h/2\pi$ of 5 and 4 with 20 possible orientations in a magnetic field. These correspond to a like number of hyperfine energy levels in the atom. For the special case of $j=\frac{1}{2}$, the quantum-mechanical

* Preliminary reports of these experiments have been submitted earlier at meetings of the American Physical Society. T. C. Hardy, Phys. Rev. **59**, 686 (1941); T. C. Hardy and S. Millman, Phys. Rev. **60**, 167 (1941).

† Publication Assisted by The Ernest Kempton Adams Fund for Physical Research of Columbia University.

[1] R. F. Bacher and D. H. Tomboulian, Phys. Rev. **52**, 836 (1937).

[2] S. Millman, I. I. Rabi, and J. R. Zacharias, Phys. Rev. **53**, 384 (1938).

[3] H. A. Bethe and R. F. Bacher, Rev. Mod. Phys. **8**, 200 (1936).

theory of the Zeeman effect of hyperfine structure yields the Breit-Rabi formula[2] for the energies of these levels as a function of the applied magnetic field, the magnetic quantum number, the nuclear spin, and the hyperfine separation of the ground state in zero field. In Fig. 1 these energies, E_m, have been plotted, in units of $h\Delta\nu$ as a function of the magnetic field for the case of $i=9/2$. If the spin of In^{113} is also $9/2$, and if in the expression for the energies we neglect the small term involving the nuclear moment, Fig. 1 will apply equally well to either isotope because of the unit chosen for the energy.

Selection rules governing the processes of absorption and emission of radiation permit two types of transitions; $\Delta F=0$, $\Delta m=\pm 1$, and $\Delta F=\pm 1$, $\Delta m=0$, ± 1. Lines arising from the latter type when observed at zero field require a common frequency equal to $\Delta\nu$ and therefore offer a direct way of measuring the difference in the $\Delta\nu$ for the two isotopes. In the case of indium, however, these frequencies (11×10^9 sec.$^{-1}$) are beyond the range of our high frequency equipment. For transitions of the type $\Delta F=0$, $\Delta m=\pm 1$ the frequency f is given by:

$$f=\Delta\nu/2\{[1+0.4(m+1)x+x^2]^{\frac{1}{2}} - [1+0.4mx+x^2]^{\frac{1}{2}}\}\pm g_i\mu_0 H/h \quad (1)$$

with $x=(g_j-g_i)\mu_0 H/(h\Delta\nu)$ and g_j and g_i are the ratios of the electronic and nuclear magnetic moments, expressed in units of the Bohr magneton μ_0 to the respective angular momenta expressed in units of $h/2\pi$. For the ground state of indium, $g_j=\frac{2}{3}$. If g_i is negative (nuclear moment positive) the positive sign is to be taken for the $F=5$ levels and the negative sign for the $F=4$ levels. For small values of the magnetic field the above expression reduces to:

$$f=\frac{g_j-(1\pm 10)g_i}{10}\frac{(\mu_0 H)}{h} - \frac{(2m+1)}{\Delta\nu}\left[\frac{(g_j-g_i)}{10}\frac{\mu_0 H}{h}\right]^2+\cdots,$$

which shows that the frequency of any such line is practically independent of $\Delta\nu$. This unfortunate circumstance makes it necessary to employ intermediate and high fields to secure sufficient resolution to observe the In^{113} line in the neighborhood of the much stronger line from the other isotope.

A full description of the apparatus and technique has been given in earlier papers.[4-6] Essentially, indium atoms issue from the slit of a molybdenum oven maintained at a temperature of about 1100°C and pass in succession between the pole faces of three electromagnets, referred to as A, C, and B, respectively, before arriving at a surface ionization detector. The beam is defined by the oven slit, approximately 0.02 mm wide, and a collimating slit of the same width which is placed between the A and C magnets. The two extreme magnets A and B have curved pole

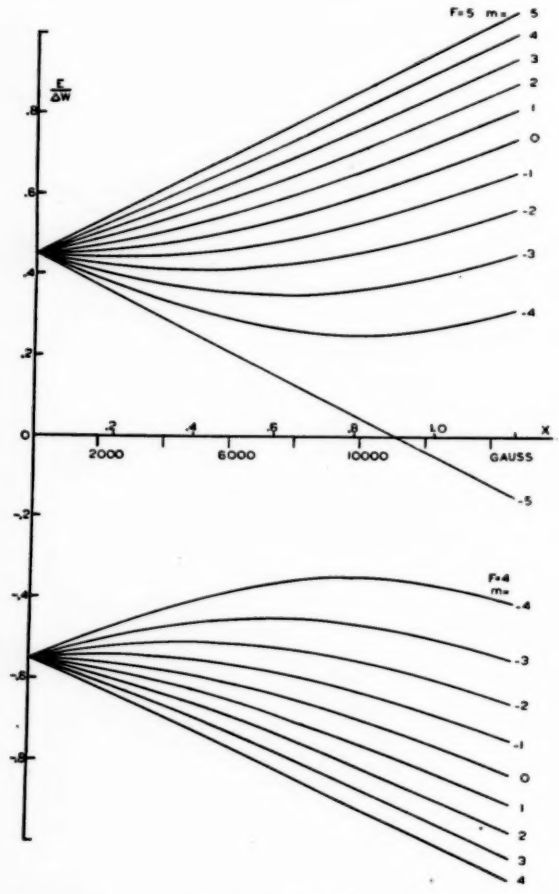

FIG. 1. Computed variation with magnetic field of the energies of magnetic levels arising from a normal h.f.s. doublet corresponding to $j=\frac{1}{2}$, and $i=9/2$.

[4] I. I. Rabi, S. Millman, P. Kusch, and J. R. Zacharias, Phys. Rev. **55**, 526 (1939).
[5] P. Kusch, S. Millman, and I. I. Rabi, Phys. Rev. **57**, 765 (1940).
[6] S. Millman and P. Kusch, Phys. Rev. **60**, 91 (1941).

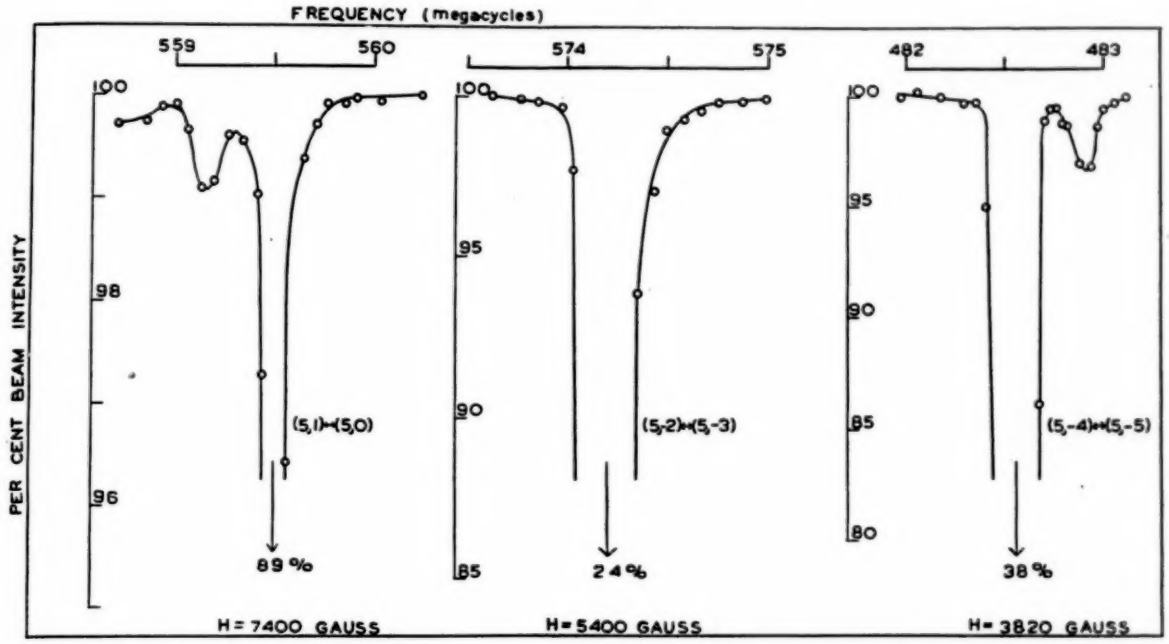

FIG. 2. Resonance curves corresponding to three lines in the radiofrequency spectrum of indium. The principal minima arise from In^{115} and the secondary minima are due to the less abundant isotope. The In^{113} line appears on the low frequency side of the In^{115} line in the case of the $(5, 1) \leftrightarrow (5, 0)$ transition, is not resolved from the principal line in the $(5, -2) \leftrightarrow (5, -3)$ transition, and appears on the high frequency side of the $(5, -4) \leftrightarrow (5, -5)$ line.

faces which produce the inhomogeneous fields necessary to deflect the atoms. The deflection of an atom is determined by its moment and the gradient of the magnetic field. The dependence of the former on the field is determined by the relation, $\mu_m = -dE_m/dH$, whereas the dependence of the latter on field is linear, with the proportionality constant determined by the curvature of the pole surfaces. The arrangement of A and B fields is such that the deflection of an atom by one will be cancelled by an opposite deflection produced by the other provided no change in magnetic moment of the atom occurs as it passes through the region between these two inhomogeneous fields. In this region is the homogeneous field produced by the C magnet, in the gap of which is inserted the "hairpin" shaped copper wires which carry the radiofrequency current. When the frequency of the resulting oscillating field is made equal to $(E_m - E_{m'})/h$, transitions between levels having energies E_m and $E_{m'}$ will be induced in accordance with the selection rules. These transitions usually result in a change in the magnetic moment of the atom and therefore a drop in the beam intensity, since atoms having a magnetic moment in the B field different from that in the A field will not arrive at their original detector positions.

The difficulties encountered in the experiment to be described arose chiefly from the circumstance that the frequencies of the lines of In^{113} differ very little from those of the corresponding lines of In^{115} and that an In^{113} resonance curve could be studied only in the presence of large background beam intensities. The latter difficulty is easily appreciated if one considers the fact that the abundance of the rarer isotope is only 4.5 percent. At the temperature used only 84 percent of these atoms are in the ground state; those remaining are in the metastable $^2P_{3/2}$ state. Since there are twenty states comprising the single electronic $^2P_{1/2}$ level and since a radiofrequency transition involves only two states, with a maximum of about 75 percent[7] of the atoms in these states reorienting, an In^{113} line results in a drop of beam intensity of only, $0.045 \times 0.84 \times 0.1 \times 0.75$, or of 0.28 percent. Changes of this magnitude can be recognized only under unusually steady beam conditions. Such stability is not

[7] H. C. Torrey, Phys. Rev. **59**, 293 (1941).

necessary, however, if the deflecting fields are set at a value for which atoms of some state will have zero magnetic moment and therefore will not be deflected by those fields. The slopes of the energy curves shown in Fig. 1 yield the total magnetic moment of the atom in any state as a function of field. The zero-moment field values are those for which there is either a maximum or a minimum in an energy curve. Atoms in all other states will be deflected and, in fact, can be removed from the beam if the product of moment and gradient is sufficiently large. Since no more than two states can have zero moment for the same field, this scheme reduces the number of states present in the refocused beam from twenty to two. These two states arise from different F levels; one has a minimum in the energy curve and is therefore a focusing state, the other has a maximum in the energy and is a nonfocusing state. When very large field gradients are used the refocused beam consists predominantly of atoms in the focusing state. If the nuclear moment is positive, only states having an F value of $(i+\frac{1}{2})$ and a negative m value can thus be isolated.

INDIUM 113

Figure 2 shows a sample plot of the experimental data for three lines of the In^{115} spectrum. The secondary minima, two examples of which appear in Fig. 2, were observed first in a study of the In^{115} line arising from the transition $(5, -4)\leftrightarrow(5, -5)$. This notation is the same as that used in previous papers; the first number in the parenthesis refers to the F value, the second number to the m value of a state. This particular transition is especially convenient for deciding whether the secondary minima arise from the $^2P_{1/2}$ levels of In^{113} or from any of the 40 possible $^2P_{3/2}$ hyperfine levels of In^{115}. Although abundance considerations alone would indicate a line intensity from the metastable state of In^{115} approximately twice that to be expected from the ground state of In^{113}, the focusing conditions are so different for the two cases that this cannot be used as a criterion. In fact, it is the method of focusing that eliminates the possibility of assigning the line to a transition between $^2P_{3/2}$ levels. The procedure for observing the $(5, -4)\leftrightarrow(5, -5)$ line was to set the focusing fields at a value corresponding to zero moment for the $m=-4$ states of the $^2P_{1/2}$ levels so that only atoms with this m value reached the detector. It is known from the work of Hamilton[8] that the zero-moment field values of the atoms in the $^2P_{3/2}$ state are all in the region 0 to 900 gauss and therefore could not be refocused at the $m=-4$ field value of 9,800 gauss. Moreover, it was found experimentally that owing to the high gradient accompanying the $m=-4$ zero-moment field, only a very small fraction of the atoms in the nonfocusing zero-moment state $(4, -4)$ reached the detector. The refocused beam consisted almost entirely of atoms in the $(5, -4)$ state.

The possibility that the secondary minima exhibited in Fig. 2 were spurious effects, resulting either from stray A and B fields or from inhomogeneity in the C and oscillating fields, was eliminated by the following tests.

(1) The C field was held constant while the $(5, -3)\leftrightarrow(5, -4)$ line was observed with the focusing fields set first at 9,800 gauss, the $m=-4$ zero-moment value, and then at 7,400 gauss, the $m=-3$ value. No change in the separation between the principal and secondary minima was detected. This result is inconsistent with the assumption that the minima arose from stray deflecting fields.

(2) The direction of the magnetizing current in the three magnets was reversed with no effect on the separation. This eliminates the possibility that the secondary minima are produced by the end effects of the oscillating field.[9]

(3) Certain transitions were studied as a function of the C field for fixed values of the deflecting fields. If the secondary minima were the result of inhomogeneity in the C field, the spurious field giving rise to a minimum would be approximately proportional to the main field and the behavior of the separation between principal and secondary minima would be predictable for any transition from the known frequency-field relationship. In particular, the secondary minima would appear on the same side of their respective principal minima for all lines since the frequencies of all transitions studied increase with field. A cursory inspection of the curves exhibited in Fig. 2 shows that the secondary minima cannot be ascribed to the inhomogeneity postulated

[8] D. R. Hamilton, Phys. Rev. **56**, 30 (1939).
[9] S. Millman, Phys. Rev. **55**, 628 (1939).

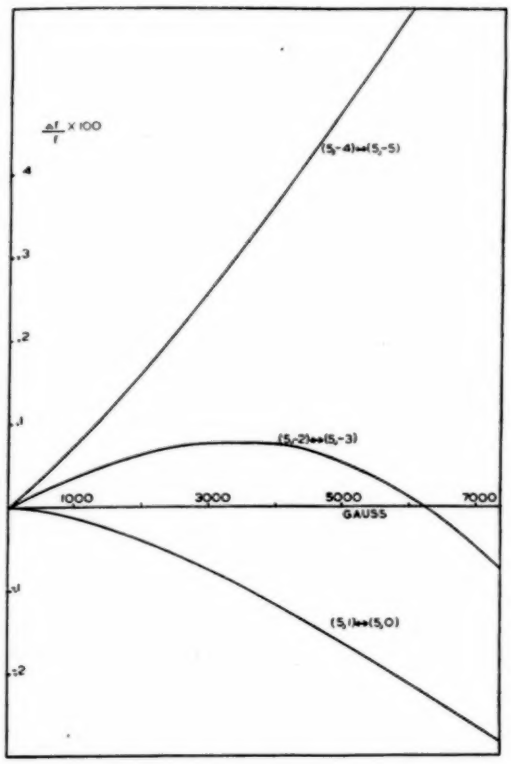

FIG. 3. Variation with magnetic field of the quantity $(f_{113}-f_{115})/f_{115}$ expressed in percent for the three lines shown in Fig. 2. f_{113} and f_{115} refer to the expected frequency positions of the secondary and principal minima, respectively, of a given line. The curves are computed on the assumptions that both the isotopes have a spin of 9/2, and that the $\Delta\nu$ of In^{113} is 1.0 percent less than the $\Delta\nu$ of In^{115}.

above. The sort of inhomogeneity present in the C field apparently serves only to broaden the lines as can be seen in Fig. 2 by comparing the line width with the theoretical value of approximately fifteen kilocycles.

The fact that the ratio of the depth of a secondary minimum to that of the corresponding principal minimum is in agreement with the known abundance ratio of the two isotopes suggests the assignment of the secondary minima to In^{113}. A more direct proof of this assignment is furnished by the certainty with which the relative positions of these minima can be predicted for all fields and for all transitions yet observed by the use of a value for the $\Delta\nu$ of In^{113} computed from any one observed frequency separation. If we assume the nuclear spin of the two isotopes to be the same we can obtain from Eq. (1) an explicit expression for these separations which can be put in the form:

$$\frac{f_{113}-f_{115}}{f_{115}}=\left[1-\frac{x}{\phi}\frac{d\phi}{dx}\right]\left(\frac{\Delta\nu_{113}-\Delta\nu_{115}}{\Delta\nu_{115}}\right),$$

where

$$\phi(x)=(1/2)\{[1+0.4(m+1)x+x^2]^{\frac{1}{2}}-[1+0.4mx+x^2]^{\frac{1}{2}}\}$$

and terms involving g_i have been omitted. Figure 3 shows the computed percentage separations of the secondary minima from the respective principal minima for the three lines shown in Fig. 2 when the $\Delta\nu$ of In^{113} is arbitrarily assumed to be one percent less than that of In^{115}. A change in this percentage value will serve merely to alter the scale of the ordinate and not the shape of the curves.

It is to be noted that in the range of fields used the frequency of the In^{113} $(5, -4)\leftrightarrow(5, -5)$ line is greater than that of the corresponding In^{115} line. The $(5, -2)\leftrightarrow(5, -3)$ lines of the two isotopes interchange positions at about 6,250 gauss and at the field value of 5,400 gauss the frequency separation is still much smaller than that for the other lines shown in Fig. 3. In the case of the $(5, 1)\leftrightarrow(5, 0)$ transition the frequency of the In^{113} line is less than that of the In^{115} line. For any given field the quantity $(f_{113}-f_{115})$ continues to decrease algebraically with increasing m values. The greater separations possible with large values of m, however, were not utilized because states with positive m values could not be isolated, with the result that large background intensities masked the lines of In^{113}. Greater separations resulting from larger fields were not profitable because of the higher frequencies required and because the widths of the resonance curves increase with increasing C field. The latter effect results from the failure to obtain a perfectly homogeneous field and is approximately proportional to the field strength.

It is to be noted that the experimental results shown in Fig. 2 follow closely the behavior of the frequency separations predicted by the curves of Fig. 3 and therefore establish definitely that the spin of In^{113} is 9/2. In order to secure complete quantitative agreement between the theory and the experimental results, a value of 1.00224

± 0.00010 must be chosen for the ratio of $\Delta\nu^{115}/\Delta\nu^{113}$.

The sign of the nuclear magnetic moment may be determined by identifying the F value of a focusing zero-moment state. Rabi has shown[10] that for positive nuclear moment the zero-moment states with minima in the energy curves, namely the focusing states, have the larger F value, whereas for negative moment the focusing states have the smaller F value. The fact that the $(5, -4)\leftrightarrow(5, -5)$ line of In^{113} was observed under the experimental conditions specified above insures a positive sign for its nuclear moment.

$\Delta\nu$ OF In^{115} AND In^{113}

The procedure followed in the measurement of the hyperfine structure separation of the ground state of In^{115} is the same as that described in a preceding paper[6] for Rb^{87} and Cs^{133}. Equation (1) shows that the pair of lines arising from a transition of the type $(F, m+1)\leftrightarrow(F, m)$ for two different F values forms a close doublet with frequency separation given by $(2g_i\mu_0 H)/h$ and that the mean frequency of this doublet will involve only two unknowns, x and $\Delta\nu$. Measurements of the mean frequencies of any two doublets at the same field will then permit the determination of the quantities x and $\Delta\nu$. The value of $\Delta\nu$ was computed from the observed mean frequency of the doublet $(F, -3)\leftrightarrow(F, -4)$ and that of the pair $(F, 4)\leftrightarrow(F, 3)$ because these two show the greatest divergence in their manner of variation in frequency with field and therefore yield a more precise value for $\Delta\nu$. A check on the correctness of our identification of lines was obtained by the experimental observation at the same field of all the eighteen lines of the type, $\Delta F=0$, $\Delta m=\pm 1$, expected in the radiofrequency spectrum. These measurements give a value of 11413 ± 3 megacycles (or 0.3807 cm^{-1}) for the $\Delta\nu$ of In^{115}. The $\Delta\nu$ of In^{113}, obtained from this value by dividing by the ratio 1.00224, is 11387 ± 3 megacycles.

NUCLEAR MOMENT OF In^{115} AND In^{113}

The expression for the separation of any doublet given above can be written as

$$\Delta f=(2g_i\Delta\nu x)/(g_j-g_i).$$

With the value of $\Delta\nu$ known, x is easily determined from the mean frequency of a doublet. Hence the measurement of the frequencies of the two components of any doublet enables one to calculate g_i. The precision of this method is limited by the fact that the small doublet separation is obtained as a difference of two large frequencies. An average of 14 observations yields a value of 1.22 ± 0.01 for the g_i of In^{115}, wherein the nuclear moment is now expressed in units of the nuclear magneton. The value of the moment is therefore $1.22\times 9/2=5.49\pm 0.04$ nuclear magnetons. When this value is divided by 1.00224 we get 5.48 ± 0.04 nuclear magnetons for the nuclear moment of In^{113}. These nuclear moment values do not include a correction arising from the diamagnetism of the atom. Such a correction enters in this determination of the nuclear moment in the same way as in the direct observation of a nuclear resonance curve obtained from molecules.[11,12] This correction, which amounts to approximately 0.6 percent for indium, serves to increase the nuclear magnetic moment.

DISCUSSION

The value of $\Delta\nu$ of the ground state of In^{115} is in excellent agreement with the value of 0.380 cm^{-1} obtained spectroscopically[13] and with that of 0.381 cm^{-1} found by the atomic beam method of zero moments.[2]

A comparison of the value of the nuclear moment of In^{115} here obtained with those values calculated[14] from spectroscopic data with the use of either the formula of Goudsmit or that of Fermi and Segrè gives merely an indication of the reliability of these formulae for calculating nuclear magnetic moments from the observed spectroscopic splitting of various atomic energy states. For example, the splitting of the states: $5s^25p\ ^2P_{1/2}$, $5s^25p\ ^2P_{3/2}$, and $5s^26s\ ^2S_{1/2}$ of In^{115} give moment values of 6.1, 3.8, and 5.0 nuclear magnetons, respectively. There is a real disagreement, however, between the value of the moment obtained in this experiment and the value of 6.4 ± 0.2 nuclear magnetons found by the atomic

[10] I. I Rabi, Phys. Rev. **49**, 324 (1936).

[11] P. Kusch, S. Millman, and I. I. Rabi, Phys. Rev. **55**, 117 (1939).

[12] W. E. Lamb, Jr., Phys. Rev. **60**, 817 (1941).

[13] D. A. Jackson, Zeits. f. Physik **80**, 59 (1933).

[14] H. Schuler and T. Schmidt, Zeits. f. Physik **104**, 468 (1937).

beam method of zero moments.[2] The latter experiment was based upon the measurement of the difference between the field values at which two zero moment peaks, arising from two states with like m and unlike F values, were observed in the beam intensity. In this case the moment is obtained directly from the observed field separation of the peaks without the use of any semi-empirical formula. In the light of the more thorough study of the nature of zero-moment peaks by Hamilton,[8] it appears that the error in the zero-moment experiment resulted from the assumption that a peak in the curve, obtained by plotting beam intensity *versus* field, was actually the position of a zero-moment field. Since the separation between these peaks was small, a slight departure of the position of the maximum from the zero-moment field value resulted in a large error in the nuclear moment.

We wish to thank Professor I. I. Rabi for his interest in this work and Professor J. R. Zacharias for his assistance in the preliminary stages of these experiments. The research has been aided by a grant from the Research Corporation.

APRIL 1 AND 15, 1942 PHYSICAL REVIEW VOLUME 61

Resonance Broadening of Caesium

CHRIS GREGORY*
California Institute of Technology, Pasadena, California
(Received January 19, 1942)

The resonance broadening of homogeneous Cs vapor in absorption was studied by means of the contour method. The intensities were obtained via the method of "astigmatic photometry" by utilizing the astigmatism of the Rowland grating. The pressure of the homogeneous absorbing vapor ranged from 10^{-2} to 17.5 mm Hg. The half breadth (γ) varied rather linearly with the number of atoms per unit volume, with $(\gamma_1/N)\times10^7=1.45$, $(\gamma_2/N)\times10^7=0.84$ for the $^2P_{3/2}$ and $^2P_{1/2}$ components of the resonance lines, respectively. The average value of the ratio of half breadths γ_1/γ_2 was found to be 1.8. The experimental half-width γ is found to be about $1\frac{1}{2}$ times larger than that predicted by W. V. Houston. Below pressures of 10 mm Hg the lines exhibited symmetrical broadening according to the "dispersion" formula. At higher pressures indications of a violet and red asymmetry are present for the $^2P_{3/2}$ and $^2P_{1/2}$ components, respectively. A definite band on the red side of the $^2P_{3/2}$ and one on the violet side of the $^2P_{1/2}$ was observed.

THE present paper is chiefly concerned with shape of the absorption line contours of the resonance lines of homogeneous Cs vapor. In particular, it is wished to ascertain the line contour characteristics as a function of the number of Cs atoms per unit volume N within the absorption cell. The work of Lloyd and Hughes,[1] Watanabe,[2] and Ch'en[3] with K, Na, and Rb, respectively, yielded results which were not in complete accord with various theories on line broadening, not to mention the lack of coherence of their respective data. This lack of coherence, then, can be said to be a secondary incentive for the work on Cs. These difficulties, clearly, can be resolved only by improvements in both theory and experiment. Consequently, an attempt to improve the technique, especially the photographic photometry by the autocalibration or astigmatism method,[4] is made. With regard to the theory, however, it is hoped that this work will prove useful in suggesting the path to be followed in its modification if it is there that the difficulty lies.

---

* Now at the University of Hawaii, Honolulu, T. H.

[1] D. S. Hughes and P. E. Lloyd, Phys. Rev. **52**, 1215 (1937).

[2] K. Watanabe, Phys. Rev. **59**, 151 (1940).

[3] Shang-Yi Ch'en, Phys. Rev. **58**, 884 (1940).

[4] G. H. Dieke, J. Opt. Soc. Am. **23**, 280 (1933); M. I. Bresch, J. Opt. Soc. Am. **28**, 493 (1938).

I. EXPERIMENTAL AND THEORETICAL PARAMETERS

First of all the absorption coefficient which is usually denoted by α_ν is defined to be

$$\alpha_\nu = -(d/dx)\log_e i_\nu, \tag{1}$$

where di_ν is the intensity of radiation of frequency ν withdrawn from the radiation of intensity i_ν when it traverses a path length dx. If α_ν is not a function of path length (1) is equivalent to

$$i_\nu = i_0 \exp(-\alpha_\nu x), \tag{2}$$

where i_0 is the incident intensity of radiation on a slab of thickness x and i_ν the intensity which emerges.

On the other hand the intensity of absorption A_ν at frequency ν is defined as the energy absorbed per unit cross section in unit time by a slab of thickness x:

$$A_\nu = i_0(1-\exp(-\alpha_\nu x)). \tag{3}$$

One concludes, then, that when $\alpha_\nu x \ll 1$, $A_\nu \approx i_0\alpha_\nu x$.

$I(\nu)$, the intensity distribution of a broadened absorption line, is defined to be proportional to α_ν the absorption coefficient

$$I(\nu) \propto \alpha_\nu \tag{4}$$

and its physical significance is apparent from (3), for $\alpha_\nu x \ll 1$. It is found convenient to normalize $I(\nu)$ so that

$$\int_0^\infty I(\nu)d\nu = 1. \tag{5}$$

In case $I(\nu)$ is a function symmetric about $\nu=\nu_0$ at which frequency $I(\nu)$ is a maximum, then a convenient characteristic of the absorption line, $\Delta\nu_{\frac{1}{2}}$, the so-called half breadth is defined by the following equation

$$I(\nu_0 \pm \tfrac{1}{2}\Delta\nu_{\frac{1}{2}}) = \tfrac{1}{2}I(\nu_0). \tag{6}$$

It may so happen that $I(\nu)$ is not symmetrical about $\nu=\nu_0$, say. In this case no satisfactory quantity has been found to characterize the distribution $I(\nu)$. Several suggestions have been set forth[5] but it is doubtful that these are of much use.

It has been shown[6] that the Einstein coefficient of absorption B_{ij} is connected with α_ν in the following manner

$$B_{ij} = \frac{C}{h\nu_{ij}N}\int_{\text{over line}} \alpha_\nu d\Delta\nu, \tag{7}$$

where C is the velocity of light, h Planck's constant, ν_{ij} the frequency, and N the number of atoms per unit volume. Furthermore the so-called f-value is defined[7] as

$$f_{ji} = B_{ij}mh\nu_{ij}/\pi e^2, \tag{8}$$

m being the mass of an electron and e its charge in e.s.u. (7) and (8) enables one to obtain the constant of proportionality in (4).

II. PROCEDURE

Aside from the application of astigmatic photometry the method of procedure is somewhat the same as that used by Hughes and Lloyd[1] and includes the improvement of temperature measurement made by Watanabe.[2] The source consisted of a high intensity tungsten lamp. The concave grating of 21-foot focal length mounted in the Rowland manner had a dispersion of 2.64A/mm. Its resolving power in the first order amounted to approximately 70,000. In the case of the first members of the principal series a red Wratten F No. 49 filter was placed over the slit of the spectrograph to cut off the second-order violet.

The geometry of the Rowland grating is such as to render feasible intensity measurements by utilizing the astigmatic nature of the image on the plate. This astigmatism manifests itself in the following manner. The spectrum produced by the grating has a constant intensity portion near the center, and as one proceeds in a direction transverse to directions of increasing or decreasing λ the intensity falls off in a calculable manner (linearly) if the intensity distribution along the slit length is constant and if the grating is uniformly reflecting. One can, then, for any part of the spectrum obtain calibration marks without any auxiliary apparatus. This method was first suggested by G. H. Dieke[4] and later was subjected to extensive tests by M. I. Bresch[4] who

[5] C. Fuchtbauer and F. Gossler, Zeits. f. Physik **87**, 89 (1933); H. Margenau and W. W. Watson, Phys. Rev. **44**, 92 (1933).

[6] R. C. Tolman, Phys. Rev. **23**, 609 (1924).

[7] R. Ladenburg, Zeits. f. Physik **4**, 451 (1921); R. Ladenburg and F. Reiche, Nature **11**, 596 (1923).

applied the method to the study of line spectra where it was found that the astigmatic method compared favorably with others. It is obvious that errors inherent in the calibration of step weakeners as in the procedure of Lloyd and Hughes, Watanabe, and Ch'en are absent.

The grating used was found to satisfy the conditions whereby the following equations are valid

$$\begin{aligned} L_T &= L \sin\varphi \tan\varphi + s/\cos\varphi, \\ L_C &= L \sin\varphi \tan\varphi - s/\cos\varphi, \end{aligned} \tag{9}$$

where L_T is the total length of the image and L_C is the length of the constant central portion. L is the length of the grating rulings, s the slit length and φ the angle of incidence. In the study of the red Cs lines an aperture for the grating and decker for the slit were designed so as to give as large an image as possible with as small as possible central portion consistent with limitations of measurement and width of usable plate.

For the first members of the principal series $\lambda^2 P_{3/2}=8521.12$, $\lambda^2 P_{1/2}=8943.36$. Eastman IP plates were used.† In the neighborhood of the $^2P_{3/2}$ component the sensitivity of the plate was quite constant and could be considered so for the rather narrow lines. On the other hand in the region of the $^2P_{1/2}$ component the sensitivity varied considerably—because it is impossible to study the broadening at higher pressures ($P>15$ mm Hg). In the case of wide lines astigmatism traces on either side were taken and corresponding corrections for varying sensitivity of the plate were made.

From the known temperature of the absorption cell containing an excess of Cs, the vapor pressure was obtained from the empirical formula[8]

$$\log_{10} p_{mm} = 11.0531 - 1.35 \log_{10} T - 4041/T, \tag{10}$$

where P_{mm} is the pressure in mm of Hg and T the absolute temperature. This enables one to find N, the number of Cs atoms per unit volume.

III. SYNTHESIS. MEASUREMENTS

1. Experimental Evaluation

Two cases are to be distinguished here, namely, the case for narrow lines ($P_{mm}<10^{-2}$) and for wide lines ($P_{mm}>10^{-2}$).

(a) *Narrow Lines*

In this case because of insufficient resolution of the spectrograph and microphotometer due to finite slit width, the contour cannot be adequately compared with a theoretical one without knowing *a priori* the effect of finite slit width. Here, however, resort to the method of total absorption[9] is made. The distribution to be tested is

$$\alpha x = -\log_e \frac{i}{i_0} = \frac{Kx/2\pi}{(\Delta\nu)^2+(\gamma/2)^2}, \tag{11}$$

where use has been made of (2), (7), and (8) with

$$K = \pi e^2 N f / mc \tag{12}$$

and x refers to the tube length in cm. According to Ladenburg and Reiche[9]

$$\int_{-\infty}^{+\infty} \left(1-\frac{i}{i_0}\right) d\Delta\lambda = \text{const.} = A, \tag{13}$$

which assertion had been tested by Minkowski.[10] Putting (11) in (13) and integrating one obtains

$$C = 3.46\times 10^{-18} A^2, \tag{14}$$

where

$$C = \lambda_0^4 e^2 N f x \gamma / 2mc^3 \log_e 10. \tag{15}$$

Knowledge of f and A enables one to obtain γ if the distribution of the form (11) is assumed. This assumption can be readily tested. For the $^2P_{3/2}$ and $^2P_{1/2}$ lines of Cs we have for the f-values, respectively, 0.66 and 0.32,[11] so that (15) yields

$$\begin{aligned} 10^{40} C_1 &= 0.707 N x \gamma_1, \\ 10^{40} C_2 &= 0.416 N x \gamma_2. \end{aligned} \tag{16}$$

We denote the $^2P_{3/2}$ by subscript 1 and $^2P_{1/2}$ by subscript 2.

(b) *Wide Lines*

For pressures greater than 10^{-2} mm Hg resort to the so-called "straight line" method is made. Here again use is made of (11) which is put in

† These plates were hypersensitized in a 4 percent solution of NH_4OH in the usual manner.

[8] J. B. Taylor and I. Langmuir, Phys. Rev. **51**, 753 (1937).

[9] R. Ladenburg and F. Reiche, Ann. d. Physik **42**, 181 (1913).

[10] R. Minkowski, Zeits. f. Physik **36**, 839 (1926).

[11] S. A. Korff and G. Breit, Rev. Mod. Phys. **4**, 471 (1932).

the form

$$(\Delta\lambda)^2 = C[\log_{10}(i_0/i)]^{-1} - \gamma^2\lambda_0^4/4C^2, \quad (17)$$

where C is given by (16) or in general (15). The second term on the right is quite small compared with the first term, so it can be neglected. Examination of (17) discloses, then, that if one plots $(\Delta\lambda)^2$ against $[\log_{10}(i/i_0)]^{-1}$ a straight line results whose slope is C and which passes essentially through the origin. Consequently, the ascertainment of this slope enables us to obtain γ_1 and γ_2 by means of (16).

(c) *Asymmetry and Shift*

For $P_{mm} > 1$ mm Hg asymmetries were evident. Attempts were made to fit the contours to the "$-\frac{3}{2}$" type of curve.[12] This attempt proved futile, so that both wings of the lines were subject to the same tests and considerations as is *b*.

Because of total absorption at the center of the line it is impossible to measure the shift, so that no consideration is given to this phase here. Under ideal conditions the shift, if it existed, could be measured if a short enough workable absorption tube could be constructed.

2. Experimental Results

In all three successful runs were made. However, in run No. 2 the thermocouple was not in its proper position so that temperature determination was not made. Nevertheless, the results are useful in the evaluation of γ_1/γ_2 which presumably is independent of temperature. For lower pressures $\approx 10^{-2}$ mm Hg the γ obtained experimentally is corrected for natural breadth according to the circumstance of the additivity of the breadths due to the two causes.

It was found that for pressures below ~ 1 mm Hg the lines were rather symmetrical in compliance with the theory. For pressures >1 mm Hg (see Table I) the lines exhibited asymmetry and/or irregularities. C_1 and C_2 for both wings of each line were obtained and averaged. At higher pressures band-like structures at the wings of the lines introduced difficulties of measurements.

Averaging the results of the table we obtain, leaving out runs No. 91 and No. 92,

$$10^7\,\gamma_1/N = 1.45\,;\; 10^7\,\gamma_2/N = 0.84\,;\; \gamma_1/\gamma_2 = 1.8. \quad (18)$$

TABLE I. Data on broadening.

Plate	T	P_{mm} Hg	γ_1	γ_2	γ_1/γ_2
		Run No. 1. $x = 7.25$ cm			
54	414.0	5.75×10^{-3}	1.70×10^{7}	1.07×10^{7}	1.60
55	429.9	1.26×10^{-2}	4.60×10^{7}	2.59×10^{7}	1.78
56	460.8	5.01×10^{-2}	1.73×10^{8}	9.11×10^{7}	1.90
57	490.0	1.59×10^{-1}	5.16×10^{8}	3.64×10^{8}	1.42
58	512.4	3.16×10^{-1}	7.56×10^{8}	2.86×10^{8}	2.65
		Run No. 2. $x = 7.00$ cm			
70					1.43
72					1.61
79			(?)		1.74
80					2.17
74					1.92
		Run No. 3. $x = 0.1905$ cm			
87	512.2	0.334	1.07×10^{9}	7.55×10^{8}	1.42
88	532.6	0.640	1.93×10^{9}	7.45×10^{9}	2.58
89	564.8	1.60	4.05×10^{9}	2.51×10^{9}	1.61
90	583.9	2.47	4.31×10^{9}	3.60×10^{9}	1.20
91	609.7	4.71	6.75×10^{9}	5.35×10^{9}	1.26
92	672.7	17.50	1.02×10^{10}	?	?

TABLE II. Comparison of results.

	$10^7\gamma_1/N$	$10^7\gamma_2/N$	γ_1/γ_2
Na	1.10 (0.49)	0.712 (0.49)	1.16 (1.00)
K	3.2 (0.63)	3.2 (0.63)	1.0 (1.00)
Rb	0.96 (0.65)	0.55 (0.65)	1.60 (1.00)
Cs	1.45 (0.71)	0.84 (0.71)	1.80 (1.00)

3. The Line Contours

Examination of the contours indicated that for $P_{mm} < 1$ the broadening was essentially symmetrical and the plots of $(\Delta\lambda)^2$ *vs.* $-[\log(i/i_0)]^{-1}$ were fairly linear. For higher pressures, however, the contours seemed to exhibit irregularities at the wings which may be attributed to several causes. It was concluded that these irregularities are due to Cs_2 bands. In particular, plate No. 92 exhibited a band of width $\sim$16A whose center is $\sim$45A from the center of the $^2P_{3/2}$ component towards the red. Plate No. 91 showed also the corresponding band. A band was also observed on the violet side of the $^2P_{3/2}$ component with width $\sim$20A and $\sim$40A from the center of the doublet. Also the $^2P_{1/2}$ component seems to have a distinct band on the violet side of width $\sim$20A and $\sim$40A away from the line center. Ch'en[3] has observed the corresponding bands for

[12] H. Kuhn, Phil. Mag. **18**, 987 (1934).

Rb. Kuhn[13] has also observed bands on the violet side of the second doublet of the principal series of Cs and some bands for K and Na. In view of these band-like structures and non-uniform plate characteristics the ascertainment of the presence of asymmetry was rather difficult. It is very likely, as the plates showed, that asymmetry sets in at about $p=10$ mm Hg, namely a violet and red asymmetry for the $^2P_{3/2}$ and $^2P_{1/2}$ components, respectively.

4. Theory *vs.* Experiment

According to Weiskopf,[14] Margenau and Watson,[15] Furrsow and Wlassow,[16] and Houston,[17] we have the following theoretical dependence of γ on N for Cs.

W	$10^7\,\gamma_1=0.37N$	$10^7\,\gamma_2=0.20N$
M & W	$=0.79N$	$=0.42N$
F & W	$=1.32N$	$=0.69N$
H	$=0.71N$	$=0.71N$

as compared with the results of measurements $10^7\,\gamma_1=1.45N$, $10^7\,\gamma_2=0.84N$. Thus it appears that the F & W formulae are more consistent with the results than the others.

On the basis of prior work on Na,[2] K,[1] and Rb[3] we can construct Table II in which the values in parentheses are those predicted by Houston.[17] The disagreement seems to be most in the case of K. The majority of results shows that the ratio γ_1/γ_2 is not unity. If we do not include the results for K the table indicates an increase in the ratio γ_1/γ_2 with principle quantum number: 0.2 per quantum number.

I wish to express my gratitude to Professor Bowen for many helpful suggestions and guidance and to Professor Houston for having so kindly discussed the theoretical aspects of the problem.

[13] H. Kuhn, Zeits. f. Physik **76**, 782 (1932).
[14] V. Weiskopf, Zeits. f. Physik **75**, 287 (1932).
[15] H. Margenau and W. W. Watson, Rev. Mod. Phys. **8**, 28 (1936).
[16] Furrsow and Wlassow, Physik. Zeits. d. Sowjetunion **10**, 378 (1936).
[17] W. V. Houston, Phys. Rev. **54**, 888 (1938).

APRIL 1 AND 15, 1942 PHYSICAL REVIEW VOLUME 61

Resonance Absorption of Neutrons in Rhodium, Antimony, and Gold

H. Feeny, C. Lapointe, and F. Rasetti
Department of Physics, Laval University, Quebec, Canada

(Received January 19, 1942)

The following experiments were performed on the resonance neutrons of Rh, Sb^{121}, and Au: absorption in the element itself, absorption in boron, measurement of the total activation in an extended volume of hydrogenous material. The constants evaluated are the resonance energy E_r, the absorption coefficient for self-indication K_r, and the level width Γ. We found: for rhodium, $\Gamma=0.16$ ev; for antimony, $E_r=14$ ev, $K_r=4$ cm²/g, $\Gamma=0.8$ ev; for gold, $E_r=2.6$ ev, $K_r=40$ cm²/g, $\Gamma=0.11$ ev. In antimony and gold, the measurements indicate that a small fraction of the resonance activity induced in thin detectors is due to levels of higher energy. The observed absorption coefficient for thermal neutrons K_{th} in rhodium and gold is found to agree with the one calculated from the Breit and Wigner formula, by taking into account only the resonance level observed. In Sb, the calculated K_{th} is about six times larger than the one observed, which suggests the interference effect of negative levels.

INTRODUCTION

THE resonance absorption of slow neutrons affords the best means of investigating the position and width of nuclear levels. A considerable amount of data are already available for the few elements in which the intensity of the activity produced by slow neutrons and the convenient length of the decay period make the investigation practicable. Among the few suitable activities that have not been thoroughly investigated, there appear to be left the 2.8-day activity due to Sb^{122} and the 2.7-day activity due to Au^{198}. These

are both strong, and the length of the period affords the possibility of accurate measurements. The evaluation of some of the data on antimony and gold required a re-determination of some constants referring to the rhodium 44-second activity.

The sections of this paper describe: (1) absorption measurements for self-indication; (2) measurement of the resonance energy by the boron absorption method; (3) determination of the width of the levels from the total activation; (4) comparison of the observed data with the theoretical one-level formula of Breit and Wigner.

ABSORPTION OF RESONANCE RADIATION

In all of the measurements we employed a neutron source consisting of 250 mg of radium mixed with beryllium powder, contained in a cylinder of 14-mm outside diameter and 25-mm length.

The source was placed at the center of a paraffin cylinder of 8-cm thickness and 20-cm diameter. Care was taken to insure the exact symmetry of the source with respect to the two faces of the cylinder, so that the activities of two identical detectors could be compared by irradiating one on each side of the cylinder. This arrangement was used for the boron absorption measurement.

Absorption curves for self-indication were obtained by irradiating a stack of identical foils simultaneously and then measuring their respective activities. The detectors were placed between two cadmium sheets sufficiently thick to absorb all neutrons of thermal energy. The detectors were sometimes placed in contact with the paraffin and, at other times, at a distance of 6 cm from the surface of the paraffin in order to obtain an approximately parallel beam of neutrons. In this latter arrangement, the effective diameter of the neutron beam was reduced to 3.5 cm by means of heavy boron carbide shields. Further shields limited the angle under which the neutrons could strike the detector to 30 degrees, and hence obliquity corrections were neglected.

All activities were measured by means of a Pyrex glass counter, whose wall thickness was optically measured and found to be 0.14 mm. The cathode consisted of a coil of copper wire in contact with the counter wall. The outside of the counter was silvered and connected to the cathode in order to maintain both at the same potential. Scaling circuits of 2 and 4 were used when required by the strength of the activity.

TABLE I. Self-indication curve for antimony.

Thickness of absorber in mg/cm²	Percentage transmission
0	100
10.6	91.7
21.2	86.8
31.8	80.8
42.4	75.0

The activities obtained by irradiation with the parallel neutron beam were so weak that the detectors had to be placed as close as possible to the counter. To accomplish this, the activated foil was pasted on the inside of a brass tube which could be placed in an exactly reproducible position with respect to the counter. When the irradiation was performed on the surface of the paraffin, the activities were strong enough to make the above procedure unnecessary, and the detectors were held in a rectangular holder fixed close to the counter. The standard procedure of measuring the long-lived activities was to take the number of counts during twenty minutes for each detector. As a rule, 10 such readings were taken for each detector, corrections being made for the decay.

The antimony detectors were made by electrolytic deposition on nickel foil of 0.1 g/cm². The amount of antimony deposited was checked by weighing the foils before and after deposition. The foils contained 10.6 mg/cm² of Sb^{121}, and were cut to a standard size of 3×3 cm². They were identical to within one percent; nevertheless, the self-indication absorption curve was repeated three times, by interchanging the order of the foils. A correction was made for the scattering of the nickel support, by assuming that the scattering cross section of the nickel nucleus[1] is 13×10^{-24} cm², and that only half of the cross section is effective, because the measurements were performed close to the surface of the paraffin.

The percentage activities of the five successive

[1] M. D. Whitaker and W. C. Bright, Phys. Rev. **60**, 155 (1941).

foils used, corrected for the factors previously mentioned, are given in Table I.

The mass absorption coefficient for resonance radiation K_r (which is one-half of the value at exact resonance), was obtained by making the experimental points fit the self-indication curve given by Bethe[2] for the case of Fermi angular distribution of the neutrons. No correction was required for the thickness of the detectors, since each foil absorbed only about 6 percent of the resonance radiation. A good agreement between the experimental points and the theoretical curve was obtained by assuming $K_r=4$, when referred to the isotope Sb^{121}. This agreement, however, does not necessarily imply that only one level is effective.

For the measurements on gold, we used foils 2.5×2.5 cm^2 in size, and 13.5 mg/cm^2 in thickness. An absorption curve for self-indication was first obtained by irradiating the foils on the surface of the paraffin. In order to compare the experimental points with the theoretical curve previously mentioned, a correction had to be applied for the finite thickness of the detectors. This was done by a method similar to the one described by Hornbostel, Goldsmith and Manley.[3] We obtained a good agreement with the theoretical curve, when we assume $K_r=33$. Frisch,[4] who used an approximately parallel beam, found $K_r=40$. This discrepancy induced us to repeat the measurements with our parallel beam arrangement. Under these conditions, we found that the experimental points did not fit the theoretical curve, but instead showed a flattening out with increasing absorption, indicating that the activity is due to more than one level. This observation is interesting, because it shows how easily the inhomogeneity of the activating neutrons can be masked by the effect of obliquity. By subtracting from the activity of each foil a constant amount (about 12 percent of the activity of the first foil), assumed to be due to penetrating neutrons, one can make the experimental points fit the theoretical curve with $K_r=$ of the order of 40. This procedure, however, is somewhat arbitrary. The only permissible conclusion is that detectors of the thickness used are mainly activated through one resonance level, but the effect of other levels is not negligible. This conclusion is confirmed by the boron absorption measurements, to be discussed in the next section.

[2] H. A. Bethe, Rev. Mod. Phys. **9**, 146–147 (1937).
[3] J. Hornbostel, H. H. Goldsmith, and J. A. Manley, Phys. Rev. **58**, 18 (1940).
[4] O. R. Frisch, Danske Vid. Selsk. **14**, 12 (1937).

BORON ABSORPTION MEASUREMENTS

In these measurements we irradiated simultaneously two identical detectors placed in symmetrical positions with respect to the source and the paraffin block. The irradiation with cadmium-filtered neutrons took place at 6 cm from the paraffin, when the arrangement already described was used. The equality of the two beams was checked to within about one percent by using strongly activated detectors.

A boron absorber was placed in front of one of the detectors, and the ratio of the two activities was measured. The boron absorbers were made by allowing a suspension of boron carbide (400-mesh size) in alcohol to settle in an aluminum tray of 5×5 cm^2. The dried powder was then compressed in the form of a package, care being taken to insure uniform thickness.

In order to determine the energy of the resonance neutrons, one has to measure the ratio of the absorption coefficients in boron for these neutrons and for those of thermal energy. Since the boron content of our absorbers may be doubtful, we redetermined the absorption coefficient of boron for thermal neutrons with the same absorbers. This verification was performed with a parallel beam of thermal neutrons produced by a paraffin howitzer and a boron trifluoride ionization chamber connected to a linear amplifier.

If the boron content of the boron carbide is assumed to correspond to the formula B_4C, our measurements gave a mass absorption coefficient of 28 cm^2/g for neutrons of energy kT at room temperature. Measurements made with Pyrex glass plates gave the same result, if we take 20 percent as the B_2O_3 content of Pyrex. It may be noted that there is a certain amount of disagreement in the values of the absorption coefficient given in the literature. Our value agrees with the results of Frisch,[4] Goldsmith and Rasetti,[5] and Fink,[6] whereas somewhat higher values were ob-

[5] H. H. Goldsmith and F. Rasetti, Phys. Rev. **50**, 328 (1936).
[6] G. A. Fink, Phys. Rev. **50**, 738 (1936).

tained by Amaldi and Fermi,[7] and by Weekes, Livingston, and Bethe.[8] In any case, the absolute values of the absorption coefficients are immaterial, since both the coefficients, for resonance and thermal neutrons, were measured with the same absorbers.

In order to test the homogeneity of the activating radiation, sometimes two detectors D_1 and D_2 of the same element were placed one on each side of the paraffin, and two respectively

TABLE II. Activity of a thin rhodium detector in water.

Distance from the source	Thermal + resonance neutrons	Resonance neutrons
7.5 cm	112	67
10. cm	60	31

identical detectors D'_1 and D'_2, on the other side. If B represents the boron absorber, then we have the following arrangement: D_1, D_2 on one side, and B, D'_1, D'_2 on the other. Thus the ratio of the activities of D_1 and D'_1 gives the absorption coefficient in boron for the neutrons that are most strongly absorbed in the detectors, while D_2 and D'_2 give the absorption coefficient in boron for the neutrons that have been filtered by the element itself. If the activation is owing to one narrow level, the two coefficients should be equal. On the other hand, if there exist several levels widely separated in energy, the second absorption coefficient will be considerably smaller than the first.

For antimony, we used detectors D_1 and D'_1 of 67 mg/cm², and D_2 and D'_2 of 112 mg/cm², referred to Sb^{121}. The boron absorber contained 313 mg/cm² of boron. As the average of several measurements, we found the following mass absorption coefficients in boron: unfiltered neutrons, 1.32 cm²/g; filtered neutrons, 1.08 cm²/g.

The values indicate the existence of two or more levels which, however, do not seem to be widely separated in energy.

The effective energy of the neutrons activating a detector of 67 mg/cm², after a small correction for scattering of the neutrons in boron[9] is applied, was found to be 14 ev, while the filtered neutrons activating the thicker detector showed an average energy of 22 ev.

For gold, we used detectors D_1 and D'_1 of 20 mg/cm², and D_2 and D'_2 of 40 mg/cm². The absorption coefficients in boron were: unfiltered neutrons, 2.9 cm²/g; filtered neutrons, 2.3 cm²/g.

These coefficients correspond, respectively, to average energies of 2.6 ev and 4.3 ev. These results confirm the conclusion about the inhomogeneity of the gold resonance neutrons, deduced from the self-indication measurements. This fact seems to have escaped the observation of previous experimenters.

MEASUREMENT OF LEVEL WIDTH BY THE METHOD OF INTEGRATED ACTIVITY

The width Γ of a neutron resonance level can be determined by measuring the activation of a detector under neutron irradiation of known intensity. This can be best accomplished by taking, for a thin detector, the ratio Y of the activities respectively induced by resonance and thermal neutrons, these activities being integrated over an infinite volume of water containing the neutron source. The details of this method are fully explained by Amaldi and Fermi,[7] and Bethe.[10] The width Γ is given by the formula

$$\frac{\Gamma}{E_r} = Y \frac{K_{th}}{K_r} \frac{3^{\frac{1}{2}} L}{\pi l_0},$$

where K_{th} and K_r are, respectively, the absorption coefficients for thermal and resonance neutrons in the detector, $L = 2.4$ cm is the average diffusion length of thermal neutrons in water,[11] $l_0 = 0.65$ cm, the mean free path[12] of resonance neutrons for elastic impacts in water, and E_r is the energy of the resonance neutrons.

This type of measurement has already been performed for rhodium by Amaldi and Fermi.[7] These observers used a thick detector, and therefore we felt it advisable to repeat the measurements with a detector of 2.54 mg/cm², which may be considered as thin both with respect to thermal and resonance neutrons. This detector was made by electrochemical deposition of

[7] E. Amaldi and E. Fermi, Phys. Rev. **50**, 899 (1936).
[8] D. F. Weekes, M. S. Livingston, and H. A. Bethe, Phys. Rev. **49**, 471 (1936).
[9] Bethe, reference 2, p. 136.
[10] Bethe, reference 2, p. 141.
[11] Bethe, reference 2, data corrected according to O. R. Frisch, H. v. Halban, and J. Koch, Danske Vid. Selsk. **15**, 10 (1938); H. B. Hanstein, Phys. Rev. **59**, 489 (1941).
[12] H. B. Hanstein, Phys. Rev. **59**, 489 (1941).

rhodium on copper foil. We found that the 5-minute activity of the copper support was not negligible; so the rhodium deposit was transferred onto an inactive support. The rhodium was cemented to a piece of pure tin sheet by means of a thin layer of Apiezon W wax. The copper was then dissolved in nitric acid, leaving the rhodium free from any activable element. The antimony and gold detectors were also cemented to similar tin sheets, to insure identical conditions.

A cadmium sheet of dimensions large compared to the mean diffusion length of thermal neutrons was placed near the center of a large water tank, and the neutron source was located in the plane of the cadmium sheet. The rhodium detector rested on the cadmium sheet and was irradiated in two positions, at 7.5- and 10-cm average distance from the source. The measurements were repeated with the detector covered with another sheet of cadmium, and hence the effect of thermal and resonance neutrons could be separately evaluated. The activity was measured for one minute, starting 15 seconds after an irradiation of one minute, and each reading was repeated ten times.

The relative activities, corrected for counter background, are the following:

Measurements at larger distances from the source were not performed because of the weakness of the activity. Therefore, the two points obtained were made to fit Amaldi and Fermi's curves for thick detectors. This gave the value $Y=1.22$. If we set[3] $K_{th}=0.80$, and $K_r=11.5$, Γ/E_r becomes 0.16. If we assume[13] $E_r=1.0$ ev, Γ becomes 0.16 ev.

Measurements with thick detectors introduce an error in the ratio of the areas of the two curves, but do not alter their shape; hence our use of Amaldi and Fermi's curves is legitimate.

The same method was used to determine the absolute width of the gold level. We irradiated four gold foils, 20 mg/cm² thick and 2.5×2.5 cm² in area, shielded with cadmium on both sides, in the water tank at average distances of 6, 11, 16, and 21 cm from the source. A fifth identical foil was irradiated at 6 cm from the source, shielded with cadmium on one side only. The relative activities are given in Table III.

For the resonance neutrons, we multiplied the activities by r^2, and plotted these values against the distance r. The curve did not differ to any considerable extent from the ones given by Amaldi and Fermi[7] for neutrons activating silver or rhodium. For thermal neutrons, we determined only one point, because the shape of the curve is accurately known from the work of Frisch, von Halban, and Koch.[14] A graphical evaluation of the areas under these two curves gave the ratio $Y'=1.45$. To deduce the true value of Y, a correction must be applied for the thickness of the detector. It can readily be seen[15] that the measured value Y' must be divided by the expression

$$f=\frac{1}{K_r\delta}\int_0^1 xdx\int_0^{K_r\delta/x} J_0(iy)e^{-y}dy,$$

where J_0 is the Bessel function of order zero.

In our case, $\delta K_r=0.8$, and a numerical integration gave $f=0.52$. Hence $Y=2.8$, and $\Gamma/E_r=0.038$.

Since the use of thick detectors and correction factors might be open to objection, we found it advisable to re-determine this value by using thin detectors of 1.42 mg/cm². Two foils were irradiated at 6 cm from the source, as only the activity close to the source was measurable. The ratio of the activities due to resonance and thermal neutrons was found to be 4.0, which, if the same curves are used as before, gives the same value of Y.

TABLE III. Activity of gold in water as function of distance from the source.

Distance r, cm	Resonance + thermal neutrons	Resonance neutrons
6	231	156
11		38
16		10
21		2.8

These measurements on gold were performed

[13] C. P. Baker and R. F. Bacher, Phys. Rev. **59**, 332 (1941).

[14] O. R. Frisch, H. v. Halban, and J. Koch, Danske Vid. Selsk. **15**, 10 (1938).

[15] See Bethe, reference 2, p. 148, formula (543), integrated by placing $x=\cos\vartheta$ and omitting the second term, since, inside the hydrogenous medium, the neutrons fall on the detector with a cosine distribution.

as a check on the results obtained by another method of measuring the width, to be described in the next section.

MEASUREMENT OF RELATIVE LEVEL WIDTHS

Another procedure for measuring the width of a neutron resonance level consists in taking as standard the level of an element whose width has already been measured. This requires only one measurement of the activity in an arbitrary position with respect to the hydrogenous material, provided that the activation of the standard element be measured in the same position. If A_1 and A_2 represent the activities of the two elements, K_1 and K_2 their respective absorption coefficients for resonance neutrons, δ_1 and δ_2 the respective thicknesses, and E_1 and E_2 the resonance energies, the ratio of the widths Γ_1 and Γ_2 is given by

$$\frac{\Gamma_1}{\Gamma_2}=\frac{E_1}{E_2}\frac{A_1}{A_2}\frac{K_2}{K_1}\frac{\delta_2}{\delta_1}.$$

We therefore measured the activities of thin detectors of rhodium, antimony, and gold, all 5×5 cm^2, irradiated on the surface of the above described paraffin block. Each detector was irradiated both with unfiltered and cadmium-filtered neutrons. The measured activities were corrected for the finite time of irradiation, the decay, and the absorption of the electrons in the counter walls. No corrections were needed for counter sensitivity, since this was found to be constant by checking with a uranium standard. The results are summarized in Table IV.

The activity induced by thermal neutrons in Sb was used by us to determine K_{th} for Sb, by referring it to the activity induced by thermal neutrons in rhodium. We found $K_{th}=0.023$, corresponding to $\sigma=4.7\times10^{-24}$ cm^2, in satisfactory agreement with the data of Rasetti[16] and Goldhaber and O'Neal.[17]

The widths of the Sb and Au levels were calculated by assuming: for antimony, $E_r=14$ ev, $K_r=4.0$; for gold, $E_r=2.6$ ev, and $K_r=40$.

The correction for absorption in the counter walls was deduced directly from the absorption

TABLE IV. Relative activities of Rh, Sb, and Au irradiated on the surface of the paraffin.

Detector	δ mg/cm^2	Initial activity for infinite irradiation. Counts per minute Thermal	Res.	Initial activity corrected for counter absorption Thermal	Res.	Γ/E_r	Γ
Rh	2.54	284	231	344	280	0.16	0.16
Sb	10.7	28	93	39	128	0.057	0.8
Au	1.42	25	63	73	183	0.054	0.14

coefficient of the electrons, for rhodium and antimony. The error committed cannot be large, since the average energies of the electrons emitted by these two elements do not differ considerably, and moreover the correction factor is small. In the case of gold, where the electrons are very soft, we preferred to adopt the following procedure. The activities induced in rhodium and gold by thermal neutrons should be proportional to the respective capture cross sections, since the detectors are thin. We found that the activity of gold had to be multiplied by the factor 2.9, to bring it into agreement with the activity of rhodium, corrected for counter absorption. Consequently we multiplied the activity due to resonance neutrons in gold by the same factor.

The value of K_{th} for rhodium was checked using a parallel neutron beam and a boron trifluoride ionization chamber. We found $K_{th}=0.80$ cm^2/g, in good agreement with the value given by Fink.[6] A reduction of 10 percent was applied to this value, to correct for the partial cross section corresponding to the 4-minute activity. K_{th} for gold was taken from Dunning, Pegram, Fink, and Mitchell.[18]

The measurements on the surface of the paraffin can also be used to calculate the widths by a method which does not require corrections for the electron absorption. For each element, we take the ratio Y' of the activities produced by resonance and thermal neutrons; these ratios are 0.81 for Rh, 3.1 for Sb, and 2.5 for Au. From the water tank experiments, we know that for Rh, $Y=1.22$. We may assume, to a first approximation, that the values of Y are proportional to the values of Y'. This would be exactly true if the resonance energies were the same for all elements, and will still be approximately true if the

[16] F. Rasetti, Phys. Rev. **58**, 869 (1940).
[17] R. D. O'Neal and M. Goldhaber, Phys. Rev. **59**, 102 (1941).
[18] J. R. Dunning, G. B. Pegram, G. A. Fink, and D. P. Mitchell, Phys. Rev. **48**, 265 (1935).

energies are not considerably different. We thus get $Y=4.7$ for Sb, and 3.8 for Au. The corresponding relative widths Γ/E_r are 0.058 for Sb and 0.05 for Au.

It is gratifying that the values of the relative widths calculated by two different methods, for antimony, and by three different methods, for gold, agree as well as can be expected when the experimental errors involved in this type of measurement are considered. We thus feel reasonably certain that our values of the relative widths are essentially correct. As a weighted average of the relative width of the gold level, we take $\Gamma/E_r=0.042$, giving $\Gamma=0.11$ ev.

The level width Γ in every case is sufficiently large compared to the Doppler width Δ for the corresponding resonance energy to justify the neglection of the latter.[19]

For gold, this conclusion is in agreement with the negative result of an attempt to observe the Doppler effect directly through the variation with temperature of the absorption coefficient for resonance neutrons. Two gold foils of 20 mg/cm^2 were irradiated, one on top of the other, inside a Dewar flask imbedded in a paraffin block. The foils could be cooled by contact with a metal plate kept at liquid nitrogen temperature. The irradiation was performed both at room and at liquid nitrogen temperature, and the absorption coefficient in both cases was found to be the same, within the experimental error of one percent. From the curve given by Bethe and Placzek[17] for Γ_{eff}/Γ as a function of Γ/Δ and our value of Γ, it can be seen that no measurable change could be expected.

CHECK OF THE ONE-LEVEL FORMULA

The dispersion formula of Breit and Wigner[20] shows that, when only one resonance level is responsible for the capture of neutrons of thermal energy, the absorption coefficient K_{th} is given by

$$K_{th}=K_r\frac{\pi^{\frac{1}{2}}\Gamma^2}{4E_r^{\frac{1}{2}}(kT)^{\frac{1}{2}}}.$$

Our measurements of Γ enable us to verify the validity of the one level formula by comparing the measured and calculated values of K_{th}. Table V summarizes the results. In the case of rhodium and gold, the agreement is excellent. Our value of Γ for Rh does not considerably differ from the one given by Hornbostel, Goldsmith, and Manley,[3] who deduced it by postulating the validity of the one-level formula. We believe that ours is the first direct determination of the width of the rhodium level with sufficiently thin detectors.

TABLE V. Observed and calculated values of K_{th}

Detector	Γ	K_{th} observed	K_{th} calculated
Rh	0.16	0.80	0.87
Sb^{121}	0.8	0.023	0.134
Au	0.11	0.27	0.32

In the case of antimony, the calculated cross section for thermal neutrons is much larger than the one observed. We must conclude that other levels interfere with the one responsible for the observed resonance activation. It is unlikely that levels at higher energies would have sufficient effect on K_{th} to reduce it to the low observed value, unless they contributed a large fraction of the activation due to nonthermal neutrons. The likeliest assumption is that the small value of K_{th} is due to the interference of a negative level.[21]

[19] H. A. Bethe and G. Placzek, Phys. Rev. **51**, 450 (1937).

[20] See Bethe, reference 2, formula (538).

[21] *Note added in proof.*—According to recent results of J. H. Manley, L. J. Haworth, and E. A. Luebke, Phys. Rev. **61**, 152 (1942), the mean diffusion length in water L would be 2.22 cm instead of 2.4 cm as used in this paper. This would make all the widths smaller by 8 percent.

Potential Energy Curve of the Excited State of KH

G. M. ALMY AND A. C. BEILER*
University of Illinois, Urbana, Illinois

(Received February 9, 1942)

The $^1\Sigma \rightarrow {}^1\Sigma$ spectrum of KH has been photographed at large dispersion and the region from 4150A to 4650A has been analyzed. Previous analyses of the spectrum have on the whole been verified, although certain discrepancies in molecular constants have been removed. For the purpose of testing Mulliken's explanation of the anomalous character of the excited state of an alkali hydride, a potential curve has been constructed for the excited state of KH, by the use of Klein's method. The vibrational energy of the upper state of KH has been followed to about three-fourths of the energy of dissociation, farther than in any other alkali hydride. As in LiH, the curve of the excited state crosses the ionic curve (of K^+ and H^-) and dissociates apparently into $K(^2P)$ and $H(^2S)$. The relative position of the molecular and ionic curves is in reasonable agreement with Mulliken's hypothesis.

INTRODUCTION

THE excited $^1\Sigma$ state of each of the alkali hydrides exhibits an anomalous behavior which appears in the unusual values of the vibrational and rotational constants. The vibrational frequency at small amplitude (ω_e) is surprisingly small for this type of molecule and the vibrational intervals increase to a maximum with increasing amplitude of vibration, instead of decreasing monotonically as in all other known diatomic states. The rotational constant B_v follows a roughly parallel course with increasing v. These unusual constants derive from an anomalous potential energy curve, which is unusually flat at the bottom, rises more steeply than the parabola which fits near r_e, and has less asymmetry than diatomic potential energy curves usually do.

Mulliken[1] has discussed and compared the constants of the alkali hydrides and has proposed that the unusual shape of the upper state potential curve can be understood by assuming that the two low states of an alkali hydride arise from the interaction between two $^1\Sigma^+$ states, one homopolar and derived from unexcited neutral atoms, the other ionic and derived from M^+ and H^-; where M is an alkali atom. Since, however, the excited state dissociates not into the ions, but, in all probability, into M (^2P) and H (^2S), it is also necessary to assume a second similar interaction, between the $^1\Sigma^+$ state derived from M (^2P) and H (^2S) and the $^1\Sigma^+$ state of M^+ and H^-.

The first test of the theory consists in constructing a good potential curve for the upper state of an alkali hydride and comparing its course at $r > r_e$ with that of the nearly coulomb curve of the ionic state. If the second interaction, near dissociation, is neglected the potential curve should go smoothly into the ion-pair curve. Because of the rapid change in vibrational and rotational constants for low v, good values of the equilibrium constants cannot be obtained. Hence the usual empirical methods of choosing parameters in an equation for the potential in such a way that the potential curve will then reproduce the observed vibrational and rotational constants are not trustworthy, especially for the higher vibrational energies.

It is necessary to use a method, such as Rydberg's, in which the curve is built up step by step, so shaped, as the potential energy increases, that (1) the action integral for the linear momentum equals $(v+\frac{1}{2})h$ for the observed energy levels, and (2) the mean value of $1/r^2$ for each vibrational state corresponds to the observed $1/r^2$ obtained from B_v. A convenient method of constructing a curve which satisfies these conditions has been given by O. Klein.[2] It has been applied to LiH by Rosenbaum[3] who made use of the excellent data of Crawford and Jorgensen.[4]

* Now at Westinghouse Electric and Manufacturing Company, Pittsburgh, Pennsylvania.

[1] R. S. Mulliken, Phys. Rev. **50**, 1028 (1936).

[2] O. Klein, Zeits f. Physik **76**, 226 (1932).

[3] E. J. Rosenbaum, J. Chem. Phys. **6**, 16 (1938).

[4] F. H. Crawford and T. Jorgensen, Phys. Rev. **47**, 932 (1935).

The results on the whole supported Mulliken's theory.

In the case of CsH a good potential curve has not been constructed, but it has been shown[5] by means of a power series curve that the upper state has about the predicted relation to the ionic curve.

The spectrum of KH has been analyzed by Almy and Hause,[6] using low dispersion, and by Hori.[7] Hori extended the upper state to $v'=24$, a vibrational energy of 0.84 ev, about three-fourths of the energy of dissociation. The corresponding state in LiH has been followed only about halfway to dissociation. Since the course of the potential curve near dissociation is of special interest in connection with Mulliken's hypothesis it seemed desirable to construct a potential curve for the excited state of KH and to compare it with the ionic curve. That is the principal object of this paper. Certain discrepancies in molecular constants are also discussed and a list of the most likely values of the constants and the energies of dissociation of both states of KH is included.

NEW MEASUREMENTS OF THE SPECTRUM OF KH

Hori obtained the spectrum with an arc source and a spectrograph of medium dispersion (three-meter grating). There were a great many blends of lines, observed lines being assigned frequently to several bands. Since the spectrum is of the many lines type (no band edges) a rotational analysis and location of band origins must precede a vibrational analysis. In bands of high v', however, lines for $K<10$ were apparently not observed by Hori. Lines of low K are best for determining the origin. For these reasons it seemed worthwhile to rephotograph the spectrum and to check the analysis in the region of large v'. It turned out that no important changes were made in values of vibrational energy.

The spectrum was excited in a tube of the design used by Gaydon and Pearse[8] for tne excitation of RbH. This is a much better method than the arc in hydrogen. In our arrangement a tube 3.5 cm by 75 cm carried a waxed-on window at one end, a removable ground joint plug at the other and four side tubes, two for electrodes, two for passing through hydrogen. In the center of the tube was mounted a quartz tube 1 cm by 10 cm, carried in a steel cradle the ends of which were disks fitting loosely into the glass tube and drilled to admit the quartz tube. With a large positive column the potential drop through the quartz tube becomes less than the cathode fall to the steel cradle and an intense constricted discharge runs through the quartz tube. A potential of 3000 volts was supplied from a 5-kva transformer and a current density of 0.12 to 0.19 ampere per sq. cm was obtained in the constriction when tank hydrogen at 3- to 5-mm pressure was flowed through the tube. A little potassium was placed in a bulge on the quartz tube. Refilling was necessary only after several hours of operation.

The KH spectrum was strongly excited and was photographed from 4000A to 6000A in the first order of a 21-foot grating at a dispersion of about 1.3A per mm. The iron arc was photographed for wave-length standards. A spectrum of a hydrogen discharge without potassium, at about the same pressure, was also photographed to enable one to identify the H_2 lines. Only the strongest of these appeared in the KH discharge spectrum. They were also distinguished by being relatively much more diffuse than KH lines.

The positions of about 1200 lines on the best exposure were measured twice, independently, and their wave-lengths computed relative to iron International Secondary Standards. Wave numbers in vacuum were obtained from Kayser's tables. The measurements were made only in the range from 21,634 cm^{-1} to 23,968 cm^{-1}, the latter being near the highest wave number observed in the spectrum of KH. This range covers bands with v' between 9 and 24. The table of wave numbers is too extensive to be included here.

ANALYSIS OF BANDS

In making the analysis, branches were picked out by the criterion of constant second differences along a branch and followed in nearly every case to $K=0$ or 1. Each band analyzed had one vibrational state in common with at least one other band. Combination differences ($\Delta_2 F$) were

[5] G. M. Almy and M. Rassweiler, Phys. Rev. **53**, 890 (1938).
[6] G. M. Almy and C. D. Hause, Phys. Rev. **42**, 242 (1932).
[7] T. Hori, Mem. Ryojun Coll. Eng. **6**, 1 (1933).
[8] A. G. Gaydon and R. W. B. Pearse, Proc. Roy. Soc. **173**, 28 (1939).

TABLE I. Origins and constants of bands reanalyzed. Values by Hori in parentheses.

		B_v''	(3.3730)	(3.2960)	(3.2154)	(3.127)	
		$D_v'' \times 10^5$	(15.5)	(15.9)	(16.0)	(15.8)	
B_v'	$D_v' \times 10^5$	v' \ v''	0	1	2	3	$\Delta G'(v'+\frac{1}{2})$
1.394			21,692.42				
(1.3934)	(9.4)	9	(21,692.4)				
							293.19
							(293.3)
1.383			21,985.61				
(1.3814)	(9.3)	10	(21,985.7)				
							292.83
							(292.8)
1.370			22,278.44				
(1.3679)	(9.2)	11	(22,278.5)				
							291.57
							(291.1)
1.354	12.2		22,570.01				
(1.3528)	(9.0)	12	(22,569.6)				
							289.91
							(289.8)
1.337			22,859.92				
(1.3366)	(8.9)	13	(22,859.4)				
							287.63
							(287.6)
1.319			23,147.55				
(1.3188)	(8.7)	14	(23,147.0)	(22,192.5)			
							285.06
							(285.7)
1.299	8.9		23,432.61				
(1.2984)	(8.5)	15	(23,432.7)	(22,478.2)			
							281.98
							(282.4)
1.278	8.3		23,714.59				
(1.2776)	(8.3)	16	(23,715.1)	(22,760.6)			
							278.51
							(278.6)
1.263	9.6		23,993.10	23,037.48			
(1.2565)	(8.1)	17	(23,993.7)	(23,039.2)			
							274.74
							(274.8)
1.239	8.6			23,312.23			
(1.2353)	(7.8)	18	(24,268.5)	(23,314.0)	(22,388.3)		
							270.69
							(271.6)
1.212	6.7			23,582.92			
(1.2105)	(7.6)	19	(24,540.1)	(23,585.6)	(22,659.9)		
							266.04
							(267.2)
1.190	19.5			23,848.96	22,922.93		
(1.1854)	(7.4)	20	(24,807.3)	(23,852.8)	(22,927.1)		
							261.07
							(261.7)
1.180	10.59				23,184.00		
(1.1600)	(7.1)	21	(25,069.0)	(24,114.5)	(23,188.5)		
							256.19
							(253.8)
1.142	8.0				23,440.19		
(1.1342)	(6.9)	22		(24,368.3)	(23,442.6)		
							249.94
							(250.8)
1.124	10.2				23,690.13		
(1.1102)	(6.7)	23		(24,619.1)	(23,693.4)		
							244.6
							(241.9)
1.082	7.0				23,934.7 (?)	23,034.9 (?)	
(1.0852)	(6.5)	24		(24,861.0)	(23,935.3)	(23,035.4)	
	$\Delta G''(v''+\frac{1}{2})$		955.61	926.21	899.6		
			(954.5)	(925.7)	(899.0)		

computed for all bands analyzed and where these differences were common to two bands, they were found to be equal within errors of measurement.

The rotational constants and band origins were computed by graphical methods. The band origins, rotational constants and vibrational intervals (ΔG) are listed in Table I. Values in parentheses are given by Hori.

For the excited state good values of the vibrational and rotational equilibrium constants are difficult to obtain because of the rapid anomalous changes of $\Delta G'$ and B'_v for v' near zero. Almy and Hause, fitting the values of $\Delta G'$ to a power series in $v'+\frac{1}{2}$ by least squares, with v' running from 0 to 16, found $\omega'_e=254.5$ cm^{-1}, $x'_e\omega'_e=-3.26$ cm^{-1}. Hori gives an expression which represents the band origins in which $\omega'_e=240.18$, $x'_e\omega'_e=-7.015$, values which are certainly in error. Crawford and Jorgensen[4] have shown that the constants obtained by least squares in the similar situation in LiH depend markedly on the number of vibrational levels used.

In view of these discrepancies it appears that the most trustworthy procedure for getting ω'_e and $x'_e\omega'_e$ is a plausible extrapolation of a plot of $\Delta G'=G'(v'+1)-G'(v')$ against $(v'+1)$ to ω'_e, the intercept at $v'+1=0$. Such a plot (data from reference 6), Fig. 1, shows that $\omega_e<254.5$ and that it is 251.0 with an uncertainty of about 1 cm^{-1}. From the slope at the intercept $x_e\omega_e$ is estimated to be -4.5.

A reconsideration of B'_v by similar graphical methods and use of the data of Hori, and Almy and Hause, for bands of low v', leads to an estimate of $B'_e=1.32\pm0.01$ in agreement with Hori's 1.311. α'_e is estimated to be -0.04; Hori gives -0.0527.

TABLE II. Summary of constants of the band spectrum of potassium hydride.

	Ground state	Excited state
T_e (cm^{-1})	0	19,530.2
ω_e (cm^{-1})	985.0	251.0
$x_e\omega_e$ (cm^{-1})	14.65	−4.5
B_e (cm^{-1})	3.415	1.32±0.01
α_e (cm^{-1})	0.083	−0.04
r_e (10^{-8} cm)	2.24	3.60
I_e (10^{-40} g cm^2)	8.20	21.2
a_0 (cm^{-1})	17,027.0	11,932.0
a_1	−2.168	−0.04
a_2	3.015	2.275
D_e (ev)	1.92	1.10±0.15

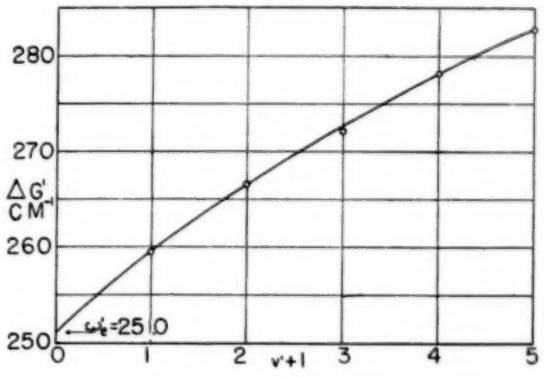

FIG. 1. Large scale plot of $\Delta G'$ *vs.* $v'+1$ at small v' to show intercept, ω_e.

The constants of the ground state of KH are not anomalous. From a consideration of previous and present work the best available values of the constants of the two states are believed to be those included in Table II.

POTENTIAL ENERGY CURVE OF THE EXCITED STATE

For internuclear distances very close to r_e the potential energy curve may be represented by the usual power series.

$$U(r)=a_0\xi^2(1+a_1\xi+a_2\xi^2+\cdots),$$

where

$$a_0=\omega_e^2/4B_e,\quad a_1=-(1+\alpha_e\omega_e/6B_e^2),$$
$$a_2=5/4a_1^2-2x_e\omega_e/3B_e,\quad \xi=(r-r_e)/r_e.$$

The calculated values of the coefficients are given in Table II and $U(r)$ near r_e is plotted in Fig. 2.

Except near r_e Klein's method of constructing a potential energy curve has been used. This method is based on a classical point of view and cannot be used for the lowest values of v. Klein develops a function,

$$S(V,\kappa)=\frac{1}{\pi(2\mu)^{\frac{1}{2}}}\int_0^{I'}[V(r)-E(I,\kappa)]^{\frac{1}{2}}dI,$$

in which $\kappa=P^2/2\mu$, where P is the angular momentum and μ is the reduced mass of the molecule; $V(r)$ is the effective potential energy, $U(r)+\kappa/r^2$; I is the radial action variable, $\oint p_r dr$; and E is the total energy in excess of energy at r_e. I' is the value of I for which $V(r)-E(I,\kappa)=0$. He shows that from partial

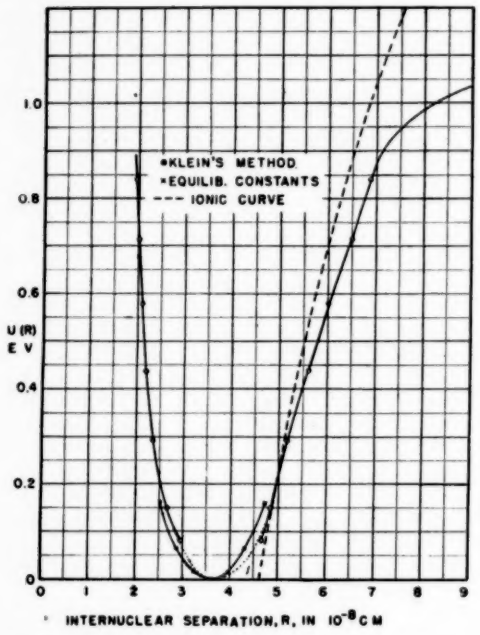

FIG. 2. Results of potential energy calculations.

derivatives of S one can compute $r_{\min}$ and $r_{\max}$ of the potential curve for any selected value of V. Thus, if $f=\partial S/\partial V$ and $g=-(\partial S)/(\partial\kappa)_{\kappa=0}$, then $r_{\max}=(f/g+f^2)^{\frac{1}{2}}+f$, $r_{\min}=(f/g+f^2)^{\frac{1}{2}}-f$. In applying the method to the quantized motion of a molecule one replaces I by $(v+\frac{1}{2})h$ and κ by $(h^2/8\pi^2)K(K+1)$.

The steps followed in obtaining f are as follows. The term values G_v of the vibrational energy states are tabulated, referred to the bottom of the potential curve as zero. One then selects, as a value of $V(r)$, a particular term G_i and subtracts from it each G_v for which $v<i$. Then $(G_i-G_v)^{\frac{1}{2}}$ is plotted against $v+\frac{1}{2}$ and the area under the curve is measured from $v+\frac{1}{2}=0$ to $v+\frac{1}{2}=i+\frac{1}{2}$ (at which point $G_i-G_v=0$, or $V(r)-E(I,\kappa)=0$). The area thus obtained when multiplied by the proper constant is a graphical integration giving a value of Klein's function S. S was thus computed for seven values of V. S was plotted against V and f was found graphically for several values of $V=G_v$, from the slope of the curve.

To obtain g, it is necessary to find the rate of change of S with rotation, or K, at the values of G_v or V for which f was calculated. To this end quantities of the form

$$\{G_i-[G_v+B_vK(K+1)]\}$$

must be plotted against $v+\frac{1}{2}$ and integrated graphically to get $S(I,\kappa)$ for various values of κ, and the derivatives $\partial S/\partial\kappa=-g$ calculated. Since, for small K, $BK(K+1)$ is much less than G_i-G_v the difference

$$\theta_{i,K}=(G_i-G_v)^{\frac{1}{2}}-\{G_i-[G_v+B_vK(K+1)]\}^{\frac{1}{2}}$$

may be expanded as a power series in $B_vK(K+1)/(G_i-G_v)$. $\theta_{i,K}$ was calculated by means of this series, plotted against $(v+\frac{1}{2})$ for $K=2$ and $K=4$ and integrated to get the change in S with K and hence with κ. In making this plot, special care has to be taken in the energy interval nearest G_i, as G_v approaches G_i. The rate of change of S with κ is nearly constant for small κ.

Table III and Fig. 2 contain the results of the potential energy curve calculation by the method described.

ENERGIES OF DISSOCIATION AND RELATION OF POTENTIAL CURVES TO IONIC CURVE

To fix the relative position of the ionic curve and the upper state curve, and thereby to test Mulliken's hypothesis, it is necessary to determine from the spectroscopic data the energy of dissociation of either the upper or lower state.

In the lower state the vibrational intervals decrease linearly in the short range observed, $v''=0$ to $v''=4$. From the constants (Table II), $D''_e=\omega''_e{}^2/4x_e\omega_e=16{,}560\ \text{cm}^{-1}=2.05$ ev. This method usually gives too high a value of D_e.

Figure 3 shows a plot of $\Delta G'$ against $v'+1$. The area under the curve, when extrapolated to $\Delta G'=0$, is D'_e. A linear extrapolation gives $D'_e=1.43$ ev. This is probably too high but certainly shows that the upper state does not dissociate into K^+ and H^-. For, in this case, $D'_e=D''_e+(\text{I.P. of K})-(\text{electron affinity of H})-\nu_e=3.2$ ev. Thus the most likely products of

TABLE III. Calculation of potential curve by Klein's method.

v'	$U(r)$ ev	g 10^8 cm^{-1}	f 10^{-8} cm	$r_{\min}$ Å	$r_{\max}$ Å
2	0.0810	0.0615	0.849	2.962	4.660
4	0.1492	0.0842	1.086	2.666	4.838
8	0.2923	0.1156	1.410	2.346	5.176
12	0.4375	0.1389	1.712	2.194	5.618
16	0.5794	0.1544	1.959	2.106	6.024
20	0.7146	0.1707	2.242	2.019	6.503
24	0.8399	0.1829	2.462	1.956	6.880

dissociation for the excited state are K (^2P) and H (^2S). Combining this assumption with $D''_e = 2.05$ ev, one finds $D'_e = D''_e + \text{K}\ (^2P) - \nu_e = 2.05 + 1.60 - 2.42 = 1.23$ ev, which is 0.2 ev less than obtained by linear extrapolation of the upper state. Since 2.05 ev is an upper limit for D''_e, 1.23 ev is an upper limit for D'_e.

A lower limit of D'_e can also be set. The bands were followed to $v' = 24$, vibrational energy 0.84 ev. This lower limit can be raised somewhat since there is no evidence of rotational dissociation. The bands with $v' = 24$ were weak and not well developed but the band (23, 2) was followed to $K = 30$, which corresponds to a rotational energy of 0.130 ev, or vibrational plus rotational energy of 0.940 ev. Of course a molecule may possess vibrational plus rotational energy in excess of its heat of dissociation since there is a maximum in the effective potential curve when $K > 0$, due to the centrifugal potential $(B_e r_e^2 / r^2 K(K+1))$, which is 0.152 ev at $r_e = 3.6$A, and 0.041 ev at $r = 6.9$A, the greatest r reached in the accurate potential curve. Since the curve is rising steeply at this point the maximum must occur at larger r and it is safe to conclude that the centrifugal potential is not more than 0.02 ev at the maximum of the curve for $K = 30$. Thus a lower limit on D'_e is placed at $0.94 - 0.02$ or 0.92 ev. In this argument it is assumed that the potential curve for $K = 0$ has no maximum.

Thus D'_e is placed between limits of 0.92 ev and 1.23 ev. One can conclude that D'_e is 1.10 ev with an uncertainty of 0.15 ev. From this it follows that $D''_e = \nu_e + D'_e - \text{K}\ (^2P) = 2.42 + 1.10 - 1.60 = 1.92$ ev.

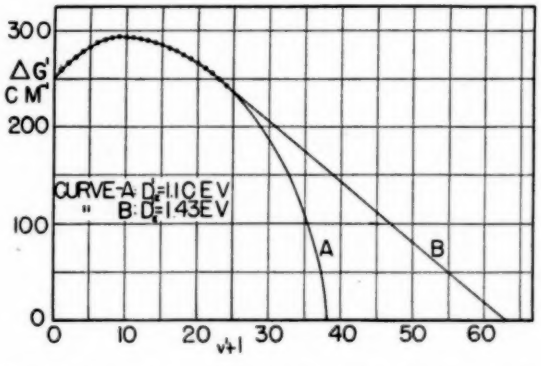

FIG. 3. Plot of $\Delta G'$ against $v'+1$. Area under curve is D'_e, the heat of dissociation of the excited state. Curve B is a linear extrapolation of the plotted data. Curve A is based upon a better method (see text) of estimating D'_e.

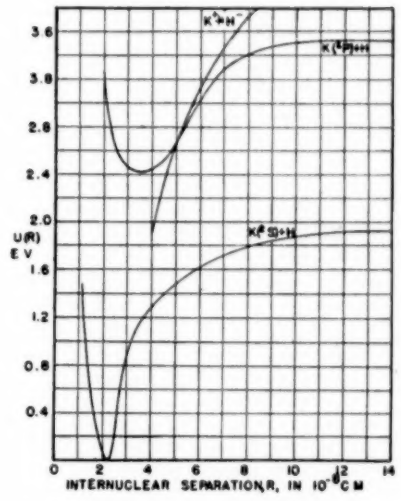

FIG. 4. Potential energy curves of KH molecule.

With D'_e and D''_e fixed the curve for $\text{K}^+ + \text{H}^-$ at large r can be drawn as in Fig. 4. Referred to K (^2S) + H (^2S) as zero energy, its equation is $U(r) = 3.60 - (14.4/r)$, in electron volts, r in A. A repulsion term, β/r^n, which would raise the ionic curve slightly has been neglected. From Mulliken's discussion[1] of such a term in the case of LiH it appears that in KH for r near 5A, where the strong interaction occurs, the correction would raise the ionic curve not more than a few hundredths of an electron volt.

The relation of the actual potential curve and the ion-pair curve in Fig. 4 supports Mulliken's theory as to the anomalous character of the excited state. The test is made less critical by the fact that the excited state does not dissociate into ions but, due presumably to a second interaction, into K (^2P) and H (^2S). Hence the excited state curve must cross the theoretical ionic curve instead of approaching it asymptotically as the theory would require if a single interaction occurred.

We acknowledge with gratitude assistance in the computations by Mr. David Beiler.

Infra-Red Absorption Spectra of the Water Molecule in Crystals

WALDO LYON* AND E. L. KINSEY
University of California at Los Angeles, California

(Received January 12, 1942)

The paper reports the absorption spectra taken under high resolution and dispersion near 3μ which are produced by water in various bound states in certain crystals and indicates the modes of vibration which cause the observed bands. Bands in sodium bromide, $NaBr \cdot 2H_2O$, extending from 3 to 2μ, and bands near 2.5μ in sodium iodide, $NaI \cdot 2H_2O$, and barium chloride, $BaCl_2 \cdot 2H_2O$, are reported and discussed. The absorption of beryl, mica, topaz, and quartz from 2 to 3μ is also studied. It is concluded that bands in beryl, which are strikingly similar to bands of water dissolved in carbon tetrachloride, are caused by monomeric water, or vapor-like molecules, in solid solution in the open crystal lattice of beryl. In mica, it is concluded, only bound hydroxyl groups are present. The evidence indicates that both bound hydroxyl groups and highly perturbed coordinated water exist in topaz. In fused quartz there is evidence for the existence, in some samples, of water in solid solution.

THE purpose of this paper is to report the absorption spectra taken under high resolution and dispersion near 3μ which are produced by water in various bound states in certain crystals, and to indicate the modes of vibration which cause the observed bands.

It is well known that the water bands are quite sensitive to the environment of the water molecule, being modified or perturbed in characteristic fashion by change of state and by solution in various solvents. The relatively inhomogeneous structure of liquid water and ice, however, so broadens the bands and destroys the structure to such an extent that little information regarding the nature of the perturbation is furnished by them. The band structure shown by water in carbon tetrachloride under moderate dispersion in the 1.4μ overtone region,[1] and in the 3μ region[2] under high dispersion and resolution suggested the advisability of examining water bound in crystals as water of crystallization in solid solution, with a grating spectrometer of high resolution. Bound water in crystals absorbs radiation in a far more homogeneous environment than in ice or liquid water, particularly in hydrates of simple structure and with a minimum number of molecules of hydration. Bound water in crystals should be perturbed in a more regular manner, and show a distinct and simple band structure.

In this paper bands in sodium bromide, $NaBr \cdot 2H_2O$, extending from 3 to 2μ, and bands near 2.5μ in sodium iodide, $NaI \cdot 2H_2O$, and barium chloride, $Ba\,Cl_2 \cdot 2H_2O$, are reported and discussed, so far as we know, for the first time. In addition the absorption in the 2 to 3μ region of beryl, mica, topaz, and fused quartz studied previously only under low dispersion is obtained under the high resolution of an echelette grating spectrometer, and is discussed.

THE SPECTROMETER

The instrument used in this study is an echelette grating spectrometer of high resolution and dispersion for the 2–4μ wave-length region with an optical arrangement which is shown in Fig. 1. The echelette grating has 5000 lines to the inch with rulings 11.0 cm long extending over a

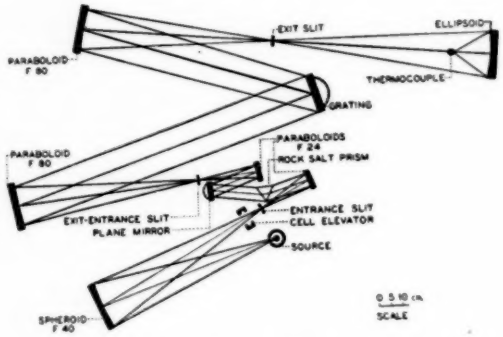

FIG. 1. Infra-red absorption spectra of water molecule in crystals.

* Now at the U. S. Navy Radio and Sound Laboratory, San Diego, California.

[1] E. L. Kinsey and J. W. Ellis, Phys. Rev. **51**, 1074 (1937); **54**, 599 (1938).

[2] J. Fox and A. Martin, Proc. Roy. Soc. **A174**, 234 (1940).

a distance of 16.5 cm and was one of the first aluminum on glass echelettes ruled by R. W. Wood at The Johns Hopkins University. The Pyrex glass blank is 8 inches in diameter. The diamond of the ruling engine was set to give concentration in the first order at 3μ. Two paraboloidal mirrors 8 inches in diameter and of 80-cm focal length collimate the radiation. A 60° rocksalt fore-prism removes the overlapping higher orders and an ellipsoidal mirror concentrates the radiation on the thermocouple. The bismuth-tin, bismuth-antimony thermocouple is connected to a Leeds and Northrup high sensitivity galvanometer which works on an eleven-meter light arm by means of a diffraction edge from a lamp filament reflected in the galvanometer mirror. The entire spectrometer is housed in a metal chamber in which the water vapor content of the enclosed air is maintained below 10^{-3} mg of water per liter.

The Rayleigh resolving power is 0.9A and the practical resolving power is about 5A. In the crystal work described here this resolution was not utilized. Exit and entrance slit widths corresponding to a spectrum spread of 15A were used. Since the angle through which the grating is rotated from a given fiducial position determines the wave-lengths of the radiation falling upon the exit slit, the accuracy of the wave-length measurement is governed by the accuracy with which this angle can be read. For a wave-length accuracy equal to the Rayleigh resolving power (0.9A) the angle reading must be accurate to within 2 sec. The angle is measured by an optical method rather than by means of an accurately divided circle. A small optically flat mirror is mounted on the grating axis so that the plane of the mirror contains the line of centers of the cone axis of the grating mounting. A telescope views the image, formed by the mirror, of a one-meter steel scale mounted on a heavy steel bracket bolted to a concrete wall. Steel clamps conform the steel scale to the arc of a circle (5.3-meter radius) whose center lies on the grating axis. The telescope has an achromatic objective 6 cm in diameter, and is held in a rigid mounting on a large concrete pillar 4 meters distant from the grating. Three alignment errors are present and affect the accuracy of the wave-lengths: (1) error in the position of the center of curvature of the scale; (2) error in the position of the plane mirror on the grating axis; and (3) error in the alignment of the telescope axis through the axis of rotation of the grating. These three errors can be controlled to guarantee an accuracy of 0.9A in wave-length measurements. The fifth and sixth orders of the strong emission lines of a mercury arc were used to calibrate the grating scale.

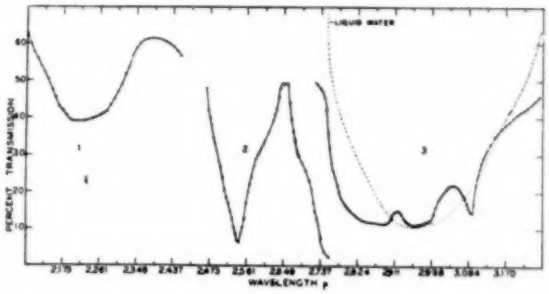

FIG. 2. The absorption of $NaBr \cdot 2H_2O$.

WATER IN SODIUM AND BARIUM HALIDES

The absorption of sodium bromide, $NaBr \cdot 2H_2O$, in the 2.1–3.1μ region is shown in Fig. 2. Since the intensity of absorption varies widely in this range, it was necessary to vary the thickness of the crystal in use to show the bands to advantage. Region 1 near 2.2μ shows the absorption of a crystal 0.011 cm thick, and region 2 near 2.5μ shows the absorption of a crystal 0.0057 cm in thickness. Region 3 near 3.0μ is a region of such very intense absorption that a film remaining on a microscope slide cover-glass which has been dipped into a saturated solution of sodium bromide was used to obtain its spectrum. The film is still too thick to show all the possible structure.

The central component of the 3μ band, region 3 of Fig. 2, lies at approximately 3380 cm^{-1} (2.95μ) and is assumed to be the fundamental symmetric vibration mode ν_r. The other broad band extending from approximately 3453 to 3561 cm^{-1} with center near 3510 cm^{-1} is assigned as the asymmetric vibration mode, ν_a. This assignment causes ν_r to shift by 65 cm^{-1} to a lower frequency from its position in liquid water and ν_a to shift by 70 cm^{-1} in a similar fashion. These shifts are based upon a reasonable assignment of the bands in liquid water discussed in the following para-

graph. Frequency shifts in the liquid water bands in this region caused by cooling and principally by a change of state to ice show that frequencies are lowered as the lattice field becomes more homogeneous, and one would expect to find what this assignment shows, that the frequencies are lowered in the more homogeneous crystal lattice of $NaBr \cdot 2H_2O$.

In liquid water the correlation of absorption maxima with the symmetric (ν_π) and antisymmetric (ν_σ) modes of vibration, which is usually accepted, is very questionable. Fox and Martin,[2] and others, have regarded the maximum near 2.94μ (3403 cm^{-1}), which is observed in the infra-red, as the asymmetric mode ν_σ and have taken the band, which occurs in the Raman effect near 2.90μ (3445 cm^{-1}), as owing to the symmetric ν_π vibration. This assignment requires rather unequal shifts in frequency for ν_σ and ν_π with change of state (liquid to vapor) and with change in environment (solution in carbon tetrachloride), ν_σ shifting by 353 cm^{-1} from liquid water to vapor, and ν_π by 209 cm^{-1}. ν_σ shifts by 302 cm^{-1} and ν_π by 169 cm^{-1} in passing from the spectrum of water in carbon tetrachloride to the spectrum of liquid water. In fact, ν_π lies on the short wave-length side of ν_σ in liquid water and on the long wave-length side of it in water vapor and in water in carbon tetrachloride. Since both ν_σ and ν_π are valence vibration frequencies and are mainly determined by the O—H bond force constant, these changes of environment ought to produce shifts in ν_π and ν_σ which are not very different. If, however, we identify the Raman band in liquid water at 3580 cm^{-1} as ν_σ, as Ellis[3] did in 1931, and regard the Raman band at 3445 cm^{-1} as ν_π, the frequency shifts of the two fundamental modes are more nearly the same. Table I, giving the difference $\nu_\sigma - \nu_\pi$ for water in various states, shows that the variations for different environments including water in sodium bromide are not large. If the assignment of Fox and Martin is used, one of the sodium bromide bands (3510 cm^{-1}) would have a higher frequency than in liquid water, a circumstance which is not likely (the water being more highly coordinated in the crystal), and the difference $\nu_\sigma - \nu_\pi$ would be 42 cm^{-1} for liquid water as compared with 130 cm^{-1} for $NaBr \cdot 2H_2O$. The infra-red band at 2.94μ in liquid water is a composite being a superposition of ν_π, ν_σ, and a frequency ν_h which appears only in ice, crystals, and as a Raman band (3219 cm^{-1}) in liquid water. The large frequency shifts observed in the 2.94μ band with temperature change, which have in the past been attributed to frequency changes in ν_σ are more likely caused by changes in the relative intensity of its com-

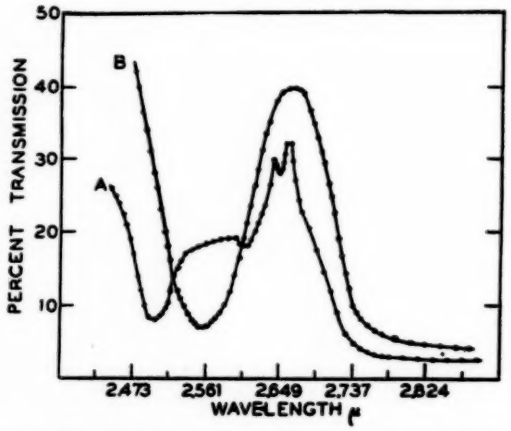

FIG. 3. Absorption of: *A*, $BaCl_2 \cdot 2H_2O$; *B*, $NaI \cdot 2H_2O$.

TABLE I. Frequency differences for water in various states.

Frequency difference	Water vapor	Water in CCl_4	Liquid water	$NaBr \cdot 2H_2O$
$\nu_\sigma - \nu_\pi$	102 cm^{-1}	91 cm^{-1}	135 cm^{-1}	130 cm^{-1}
$\nu_{\pi R} - \nu_\pi$				445
$\nu_{\sigma R} - \nu_\sigma$			396	424
$\nu_{hR} - \nu_h$				496

TABLE II. Comparison of assignments.

Assignment	Water in CCl_4	Liquid Water	$NaBr \cdot 2H_2O$	Ice
ν_R		440[a]–500[b] cm^{-1}		601[a] cm^{-1}
"Dihydrol" ν_h		3219[a] (3.106μ)	3229 cm^{-1} (3.093μ)	3136[a] (3.19μ)
ν_π	3614 cm^{-1} (2.767μ)	3445[a] (2.90)	3380 (2.959)	3330[a] (3.003)
ν_σ	3705 (2.699)	3580[c] (2.79)	3510 (2.849)	
$\nu_{hR} = \nu_h + \nu_R$			3725±20 (2.670–2.699)	
$\nu_{\pi R} = \nu_\pi + \nu_R$			3825±20 (2.631–2.605)	
$\nu_{\sigma R} = \nu_\sigma + \nu_R$		3976[d] (2.515)	3934 (2.542)	
$\nu_\pi + 2\nu_R$ $\nu_\sigma + 2\nu_R$			4350–4610 (2.30–2.19)	

[a] See reference 6.
[b] See reference 8.
[c] See reference 3.
[d] See reference 1.

[3] J. W. Ellis, Phys. Rev. **38**, 693 (1931).

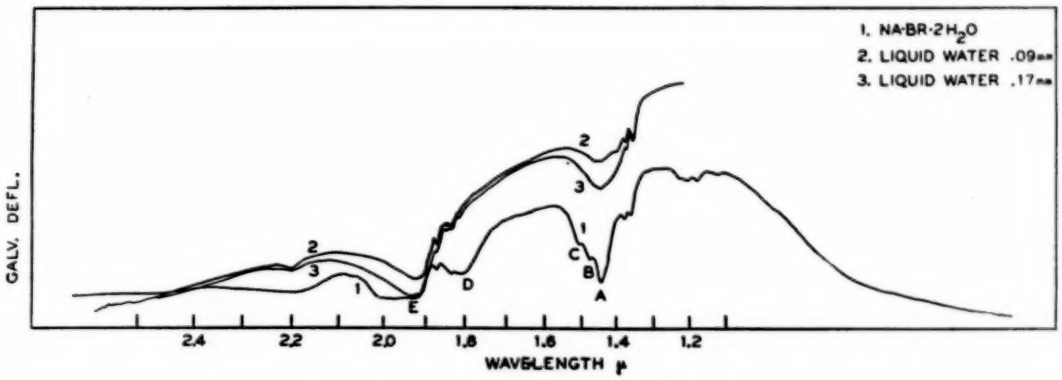

FIG. 4. Spectrum of $NaBr_2 \cdot 2H_2O$ and liquid water.

ponents (cf. Cross, Burnham, and Leighton's[4] work on the Raman effect). Where there is little or no overlapping, as in the Raman band ν_h at 3.14μ (3221 cm^{-1}), temperature has little effect upon the frequency. This latter band, which is weakened by a rise in temperature and by dilution of the water with nitric acid, is caused undoubtedly by polymerization, due as Bernal and Fowler[5] have suggested to the persistence of tridymite-ice-like water. Because it appears in $NaBr \cdot 2H_2O$ we will speak of it as the "dihydrol" band. In water vapor ν_σ is predominantly strong and the "dihydrol" band is missing. For water in carbon tetrachloride ν_π and ν_σ are both strong; ν_h is still missing. In liquid water ν_σ, ν_π, and ν_h are all present with ν_h and ν_π strong. In ice ν_π and ν_h are strong and ν_σ is weak or missing. ν_σ is not found in the Raman spectrum of ice.

TABLE III. Interpretation of bands near 2.52μ.

Assignment	$BaCl_2 \cdot 2H_2O$	$\Delta\nu$	$NaBr \cdot 2H_2O$	$\Delta\nu$
"Dihydrol"	3280 cm^{-1} R^a	546	3229 cm^{-1}	496
"Dihydrol"$+\nu_R$	3775		3725	
ν_π	3340 R^a	519	3380	445
$\nu_\pi+\nu_R$	3839		3825±20	
ν_σ	3450 R^a	552	3510	424
$\nu_\sigma+\nu_R$	4002		3934	

R: Raman band.
[a] See reference 7.

TABLE IV. $NaBr \cdot 2H_2O$ bands.

Bands in Fig. 4	Assignment	Computed value
A. 6896 cm^{-1}	$\nu_\pi+\nu_\sigma$	6890 cm^{-1}
B. 6748	ν_σ+Dihydrol	6739
C. 6631	ν_π+Dihydrol	6609

The third and long wave-length component of the 3μ band of sodium bromide is of less intensity than the other two but quite sharp. It lies in the region of the first overtone of the deformation vibration ν_δ (1645 cm^{-1}). Since no pure harmonic bands have been observed for ice or liquid water, it is more likely to be the dihydrol frequency which falls in liquid water at 3219 cm^{-1}, and in the sodium bromide at 3229 cm^{-1}. Table II compares the assignments for water in sodium bromide with the assignments for liquid water, water in carbon tetrachloride and ice. The frequencies in this region decrease in the order: vapor (with bands at $\nu_\sigma = 3656$[2] and $\nu_\pi = 3654$),[6] water in carbon tetrachloride, water in sodium bromide, ice.

Two Raman bands observed by Nayar[7] for sodium bromide indicate the existence of two frequencies in the 3μ region, but they are not likely to be the ν_π and the ν_σ bands reported here in the infra-red. They fall at 3430 cm^{-1} (2.915μ) and 3570 cm^{-1} (2.801μ) on either side of the broad band at 3510 cm^{-1}. They are apparently components of ν_σ.

The 2.52μ (3934 cm^{-1}) band in $NaBr \cdot 2H_2O$ given in Fig. 2 shows the sharpening and the intensity increase characteristic of the behavior of water bands under crystal lattice or solution perturbation. The molecular extinction coef-

[4] Cross, Burnham, and Leighton, J. Am. Chem. Soc. **59**, 1134 (1937).
[5] J. D. Bernal and R. H. Fowler, J. Chem. Phys. **1**, 515 (1933).
[6] J. H. Hibben, J. Chem. Phys. **5**, 166 (1937).
[7] P. G. N. Nayar, Proc. Ind. Acad. Sci. **A8**, 479 (1938).

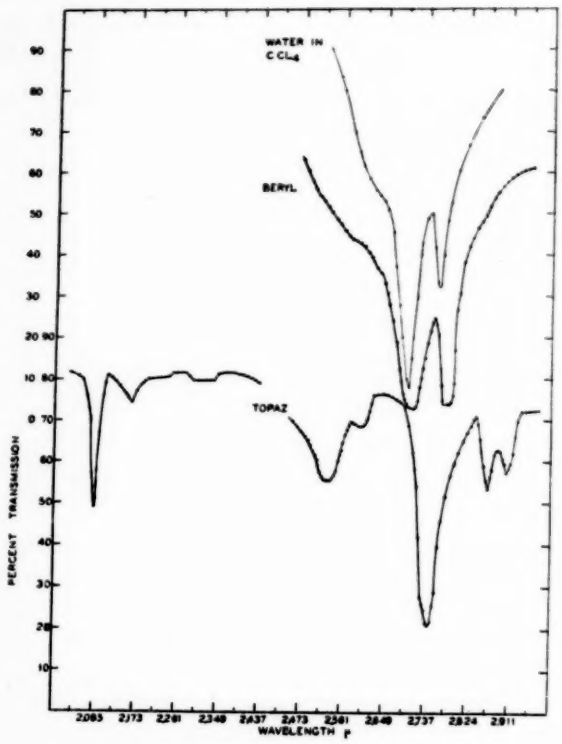

FIG. 5. Band of water in silicates and in CCl_4.

ficient at maximum absorption increases from 0.46 (Fox and Martin[2]) to about 2.0. In liquid water the band falls at 3976 cm^{-1} as measured by Fox and Martin. It is interpreted as the combination of the asymmetric vibration ν_σ and a frequency of hindered rotation, ν_R.[8] There are evidences of two other bands which appear as shoulders, one at 3820 cm^{-1}, approximately, and the other approximately at 3713 cm^{-1}. The three bands—the deep band, and these two shoulders—are separated from the three frequencies ν_σ, ν_π, and ν_h by 424, 450, and 490 cm^{-1}, respectively, indicating that the three bands may be combinations of the fundamental frequencies with a frequency of hindered rotation around 450 cm^{-1}.

It is of interest to compare the $NaBr \cdot 2H_2O$ bands in this region with those of a barium chloride ($BaCl_2 \cdot 2H_2O$) and a sodium iodide ($NaI \cdot 2H_2O$) crystal. In the 2.52μ region, shown in Fig. 3, structure appears for barium chloride consisting of one fairly strong band at 4002 cm^{-1} (2.499μ) and two weaker bands at 3839 cm^{-1} (2.605μ), and 3775 cm^{-1} (2.649μ). Table III gives an interpretation for these bands. The sodium iodide band falls at 3918 cm^{-1} (2.552μ) quite close to the bromide band at 3934 cm^{-1} (2.542μ), but no structure appears because of the excessive thickness of the crystal sample (0.02 cm).

Sodium bromide has a broad band at 2.271μ (4510 cm^{-1}). There is no counterpart to this band in liquid water. It falls in the region of a combination of the valence vibrations and the first overtone of a hindered rotation in the neighborhood of 450 to 500 cm^{-1} ($\nu_\sigma + 2\nu_R = 3510 + 1000$).

The authors are indebted to Professor Joseph W. Ellis for data on the combination bands of $NaBr \cdot 2H_2O$ in the 1 to 2.3μ region. Professor Ellis took the spectrum of $NaBr_2 \cdot 2H_2O$ on his quartz-prism, self-recording spectrometer, and obtained the spectrum shown in Fig. 4. The 1.44μ ($\nu_\sigma + \nu_\pi$) band of liquid water is shifted to a longer wave-length for the coordinated water in the crystal, where it has developed three components. Table IV lists the three components of the 1.44μ band, and suggests an interpretation. The relative intensities of the three components support the assignment chosen. The 1.79μ ($\nu_\sigma + \nu_\delta + \nu_R$) band ($D$ in Fig. 4) is much more intense for coordinated water than for liquid water. This increase is in agreement with the increase found for the hindered rotation band at 2.52μ. Figure 4 shows the broad absorption region at 2.2μ, which was also obtained on the grating spectrometer. The band marked E in Fig. 4 is the $\nu_\sigma + \nu_\delta$ band at 1.93μ.

WATER IN SILICATES

The 3μ infra-red absorption spectra of silicates offer interesting information on the behavior of water in the silicate crystal structure. The O—H bands are apparently produced in various ways, e.g., by water in solid solution, by an hydroxyl group in the silicate structure, and by coordinated water of crystallization. Matossi and Bronder[9] have analyzed the many absorption and reflection bands of beryl (aquamarine) from 1.3μ to 10μ with an instrument of low resolving power, and have accounted for the fundamental and

[8] C. H. Cartwright, Phys. Rev. **49**, 470 (1936).

[9] F. Matossi and O. Bronder, Zeits. f. Physik **111**, 1 (1938).

combination frequencies of the silicate radical. A band near 2.7μ, however, is questionable. Matossi and Bronder tentatively assign it to an hydroxyl group. They point out that water can be present in this silicate to the extent of 1 percent, whereas the intensity of the band indicates an impurity of 5 to 10 percent. We obtained the band under the high resolution of the grating instrument and present it in Fig. 5. The band is strikingly similar in structure and position to the band obtained for water in carbon tetrachloride, a fact which suggests an interesting and curious cause for it. The centers of the two bands in beryl fall at 2.710μ (3690 cm^{-1}) and 2.780μ (3598 cm^{-1}) as compared to 3705 cm^{-1} and 3614 cm^{-1} for water in carbon tetrachloride. In the beryl band a shoulder appears on the short wavelength side similar to that for water in carbon tetrachloride. This correlation suggests that the 3690 cm^{-1} band is the envelope of the enhanced Q lines of ν_σ for the water molecule; the 3597 cm^{-1} band is ν_π, and the shoulder is the envelope of the R lines of ν_σ. Beryl is a silicate with rings of linked tetrahedra ($Be_3Al_2Si_6O_{18}$), and is an elegant structure composed of hexagonal rings made of six silicon-oxygen tetrahedra (W. L. Bragg).[10] The aluminum and beryllium atoms bind these rings into a coordinated structure, such that each aluminum atom lies in a sixfold group. The structure does not offer a place for a bound hydroxyl group as does the structure of topaz or mica, but the hexagonal rings produce large open channels, 4.2A across in the beryl structure. The existence of water monomers in this open structure seems possible and would account for the spectrum obtained. An hydroxyl group bound to aluminum gives a single band near 3640 cm^{-1}, e.g., in mica. Beryl does not show this band. It seems, therefore, that monomeric, i.e., vapor-like water exists in solid solution in beryl with beryl acting as an "inactive" solvent like carbon tetrachloride.

Matossi and Bronder[9] find an intense absorption band for muscovite (common mica) near 2.75μ, and assign this band to the hydroxyl group in the mica structure, $K\,Al_2(Al\,Si_3\,O_{10})\,(OH)_2$. Figure 6 shows this band under high resolution (thickness of mica sample 0.0075 mm). The band center lies at 2.747μ (3641 cm^{-1}). The weak uniform bands appearing at regular intervals are probably caused by interference in the mica film, since these small bands vary with the thickness of different mica samples. The strong hydroxyl band lies at a frequency common to other compounds containing an O−H group, e.g., ethyl alcohol in carbon tetrachloride. In muscovite the O−H group is linked to the aluminum atom with no links between O−H groups. Each O−H, therefore, is a monomer acting as an O−H oscillator located in the open mica structure (cf. Bragg and Pauling).[10, 11]

Matossi and Bronder[9] find evidence for water in topaz, $(AlF)_2SiO_4$, but find the complex spectrum in the 2 to 3μ region unintelligible. They explain the many bands as due to O−H groups under various types of binding in the topaz structure. The 2–3μ spectrum under high resolution (Fig. 5) suggests a more explicit assignment than that of these authors. The sample used was not sufficiently large to cover the entire entrance slit of the spectrometer; the

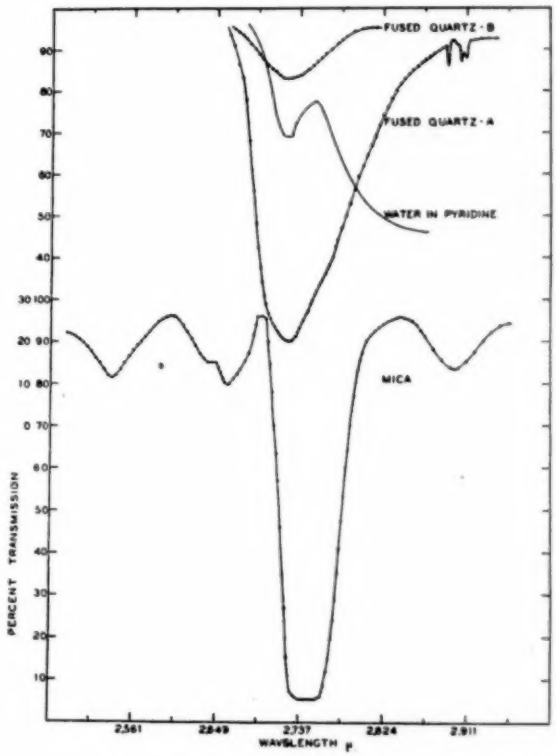

FIG. 6. Absorption in mica and quartz.

[10] W. L. Bragg, *Atomic Structure of Minerals* (1937).

[11] L. Pauling, *Nature of the Chemical Bond* (1940).

absorption bands should, therefore, be much deeper than indicated (thickness of sample 0.05 cm). An intense band is found at 2.745μ (3643 cm^{-1}), which undoubtedly must be caused by a bound O−H group as in mica (mica 3641 cm^{-1}). Topaz is an aluminosilicate, and a bound hydroxyl is possible, even probable, in its structure. The fluorine atoms of the conventional topaz structure may be partly replaced by O−H groups (cf. Bragg).[10] When an O−H group replaces a fluorine atom it is bound to an aluminum atom in a manner similar to the linkage in mica. The remaining, less intense, absorption bands of topaz occur near the positions of bands in liquid water and in sodium bromide, and suggest the possibility of structural or coordinated water in the open topaz lattice under considerable perturbation. It is attractive, for example, to interpret the doublet at 2.906μ (3441 cm^{-1}) and 2.867μ (3488 cm^{-1}) on the long wave-length side of the O−H band as ν_π and ν_σ. But the difference in wave numbers is only 47 cm^{-1} as compared with 102 cm^{-1} for water vapor, 135 cm^{-1} for liquid water, and 130 cm^{-1} for water in sodium bromide. It may be, on the other hand, that the ν_σ mode splits into a doublet under the perturbing crystal field. ν_π would then lie toward longer wave-lengths in a region not yet investigated (under high resolution) for topaz. Table V gives the suggested, but questionable, assignments. A narrow band at 2.086μ (4793 cm^{-1}) may be a combination band of the O−H fundamental and that of a SiO_4 group; e.g., Matossi and Bronder[9] suggest the combination of the O−H vibration (3643 cm^{-1}) and the first overtone of a fundamental frequency of the SiO_4 group at 600 cm^{-1}. It is suggested that in addition to a bound O−H group, coordinated water is present in topaz, but not monomeric water as in beryl. The 2.53μ band ($\nu_\sigma+\nu_R$) and the 2.60μ band ($\nu_\pi+\nu_R$) indicate a hindered rotation for these proposed water groups in the topaz structure.

WATER IN FUSED QUARTZ

The absorption spectrum of fused quartz has been studied for many years, and a band at 2.72μ is of particular interest. In 1929 Parlin[12] studied its absorption as a function of temperature, and attributed the band at 2.72μ to a combination of two frequencies of the SiO_2 molecule. In the same year Plyler[13] studied the absorption of crystalline quartz and reported a band of very low intensity at 2.72μ, which he regarded as the second overtone of a fundamental frequency at 9μ. Drummond[14] in 1934 found that the 2.7μ band is absent in some specimens of fused quartz and of varying intensity for other specimens. This wide variance of intensity suggested to Drummond that the 2.72μ band is caused not by SiO_2, but by an impurity, namely, dissolved CO_2. He made a study of the spectrum of fused and crystalline quartz from 1μ to 8μ in 1936.[15] Ellis and Lyon[16] attributed the 2.72μ band to water vapor as the impurity.

The process of manufacture of fused quartz has apparently changed during the past three decades, inasmuch as older specimens exhibit the 2.72μ band, whereas later specimens do not, as illustrated in Fig. 6. The older specimen *A* is 2 mm thick, and the newer specimen *B*, is 4 mm thick. The center of the band lies at 2.723μ (3672 cm^{-1}). Figure 6 compares the absorption by fused quartz with that by 0.5 percent water dissolved in pyridine (data from Errera, *et al.*).[17] Pyridine is an active solvent perturbing the water molecule by a linkage between the

TABLE V. Water bands in topaz.

Assignment	Liquid water	Topaz	$\Delta\nu$
ν_π	3445 cm^{-1} 2.90μ	3441 cm^{-1} 2.906μ	
			404 cm^{-1}
$\nu_\pi+\nu_R$		3845 2.601	
ν_σ?	3580 2.79	3488 2.867	
			464
$\nu_\sigma+\nu_R$	3976 2.515	3952 2.530	
Bound OH		3643 2.745	

[12] W. A. Parlin, Phys. Rev. **34**, 81 (1929).

[13] E. K. Plyler, Phys. Rev. **33**, 48 (1929).

[14] D. G. Drummond, Nature **134**, 739 (1934).

[15] D. G. Drummond, Proc. Roy. Soc. **153**, 318 (1936); Nature **138**, 248 (1936); and **139**, 70 (1937).

[16] J. W. Ellis and W. Lyon, Nature **137**, 1031 (1936), and **139**, 70 (1937).

[17] Errera, Gaspart, and Sack, J. Chem. Phys. **8**, 63 (1940).

nitrogen of the pyridine and the hydrogen of water. The band for water in pyridine lies at 2.719μ (3678 cm^{-1}). For water in carbon tetrachloride (an inactive solvent) a double band, (ν_σ, 3705 cm^{-1} and ν_π, 3614 cm^{-1}) is found, but for water in pyridine ν_π is not found. The band in fused quartz is at a somewhat higher frequency than is found for hydroxyl groups bound to an atomic structure, namely, 3600 to 3400 cm^{-1} (cf. Pauling[11] or, for example, the 3643 cm^{-1} O–H band in mica). It is suggested that the 2.72μ band in fused quartz is due to water in a solid, closely-packed solution perturbed by the oxygens of the SiO_2 group. Water appears to be more probable than carbon dioxide as an impurity in view of the studies on silicates, and since the 2.72μ band does not show the double structure characteristic of CO_2 in this region.

APRIL 1 AND 15, 1942 PHYSICAL REVIEW VOLUME 61

On the Large Scale Distribution of Matter in the Universe

F. ZWICKY
Norman Bridge Laboratory of Physics, California Institute of Technology, Pasadena, California

(Received August 2, 1941)

The following considerations represent an attempt to analyze those effects which govern the large scale distribution of matter in the universe. It is proposed to discuss the problems of: (a) the frequency of occurrence of *clusters of nebulae* which contain different numbers of nebulae, (b) the relative numbers of *nebulae* in dependence of their intrinsic luminosity and mass, and (c) the frequency distribution of various types of *stars* in dependence of their mass and intrinsic luminosity. It is found observationally that clusters of nebulae become the more frequent the fewer nebulae they contain. On the other hand the data so far available indicate that the luminosity function for nebulae exhibits a frequency maximum at the absolute magnitude $M_0 = -14.2$. Reasons are advanced which suggest that this result which was obtained from the purely observational approach to the problem of the general distribution of matter cannot be final. The theoretical analysis of the frequency distribution of various types of stars is largely complicated because of the interference of effects due to light pressure and the generation of energy through subatomic processes and cannot at the present be carried through. The analogous problems for the nebulae and the clusters of nebulae, however, lend themselves to a simple qualitative analysis which, starting from the assumption of a stationary universe, makes use of the principle of the conservation of energy, the virial theorem and the application of statistical considerations to distributions of the Boltzmann and the Smoluchowski types. The results obtained are in good agreement with the observed distribution of the clusters of nebulae. In addition an understanding is arrived at of the important fact that the velocities of field nebulae on the average are only about half as large as those of cluster nebulae. The theoretical considerations given, however, are in *complete contradiction with the luminosity function now generally adopted for the nebulae inasmuch as the existence of a large number of intrinsically faint nebulae* representing more than half of all of the matter in the visible universe *is predicted* which to date must have been overlooked. On the basis of this prediction various criteria are developed to facilitate the discovery of intrinsically faint stellar systems and a systematic search for such systems utilizing the 18-inch Schmidt telescope on Palomar Mountain is described. On the basis of the results achieved so far it is shown that the new distribution function of nebulae in the so-called local group of nebulae deviates markedly in the direction of the theoretical expectations from the luminosity function derived by previous observers. Practical methods are discussed, the application of which should make possible the construction of a more representative distribution function for nebulae over a large range of luminosities. In the final section some of the known observational facts are briefly reviewed which favor the assumption of a stationary rather than an expanding universe.

A. STATEMENT OF THE PROBLEM

ONE of the most conspicuous aspects of the distribution of matter in space lies in the existence of a great variety of types of condensations. Starting from the elementary particles, conglomerations of ever increasing dimensions and material content may be found until we arrive by the way of the stars and the stellar systems (or the nebulae) at the clusters and clouds of nebulae which at the present time are the largest known aggregations of matter which possess individual characteristic structures.

We shall here be concerned with the analysis of the *frequency distribution of various types of large scale condensations of matter*. So far the so-called purely *observational approach* has been made use

of exclusively to determine the relative numbers of various types of stars, of nebulae and of clusters of nebulae. Through this approach the accumulation of important data during the recent decades has been rapid and frequency distributions for stars and for nebulae were arrived at which at first sight seem trustworthy. A closer scrutiny of the problem however reveals that the purely observational approach has, of necessity, become the victim of some rather serious oversights. This is nothing new or surprising since the purely observational approach, because of the interference of the ever present demon of selectivity, has often been restricted to the discovery of partial truths only, just as the pure theory has often become sterile because of lack of recognition of the simple and perhaps best established fact that the totality of all natural phenomena is beyond the imagination of any theory starting from *a priori* premises. It is the purpose of this investigation to show through the analysis of concrete examples that even the "geographical" aspects in astronomy are as yet by no means satisfactorily established. New discoveries promise to be abundant if the purely observational approach is supplemented by constructive theory which does not stop with the analysis of already known phenomena but which insists upon checking its conclusions through new types of observations.

The particular problems with which we shall deal here are:

(a) The frequency distribution of *clusters of nebulae* of varying mass and luminosity.

(b) The frequency distribution of *nebulae* or of stellar systems of varying mass and luminosity.

(c) The frequency distribution of *stars* of varying mass and luminosity.

Although the problems of the frequency distribution of nebulae and of clusters of nebulae will be particularly favored, problem (c) is at least of equal importance, but its solution has not yet been pushed sufficiently far to be discussed in greater detail at the present time.

B. SOME OF THE RESULTS OF THE PURELY OBSERVATIONAL APPROACH

(α) The Clusters of Nebulae

Nebulae appear either as isolated objects (field nebulae) or in groups whose membership runs from as few as two to as many as several thousand presumably physically related nebulae. The largest of these groups are called *clusters* if they show relatively high central condensations and *clouds* of nebulae if the accumulation resembles a swarm of objects without any particularly marked central condensation. The formation of groups of nebulae may be partly due to chance but in most cases it will be caused by the mutual attraction of the nebulae. The radial distribution of nebulae in large spherically symmetrical clusters is such that it is in agreement with conclusions drawn from statistical mechanics based on the assumption that between the nebulae the ordinary Newton inverse square law of attraction is operative.[1]

Few systematic investigations are as yet available about the frequency of groups containing different numbers of nebulae.[2] From the material on hand, however, the important fact is fairly apparent that isolated nebulae are the most numerous and that in a given large volume of space the frequency ν of the groups steadily decreases as the number N of nebulae in the groups increases. The frequency function $\nu(N)$ may therefore be assumed to be monotonously decreasing with increasing N. The morphology of the clusters of nebulae and the frequency function $\nu(N)$ present problems which can adequately be solved with large Schmidt telescopes but the quantitative discussion of these problems must be postponed until more data are available.

(β) The Nebulae

The investigations on the frequency distribution of nebulae of various types are first of all concerned with the number $n(M)$ of nebulae in a given volume of a given absolute magnitude M expressing the absolute luminosity L. From the standpoint of statistical mechanics the frequency function $n'(\mu)$ would be more interesting where μ is the mass of a nebula. Although these masses are not yet adequately known we may assume that the functions $n'(\mu)$ and $n(M)$ or rather $n(L)$ are similar in character.

Through extensive investigations by Hubble[3]

[1] F. Zwicky, Astrophys. J. **86**, 217 (1937).
[2] E. Holmberg, Astrophys. J. **92**, 200 (1940).
[3] E. Hubble, Astrophys. J. **84**, 158 (1936).

and others a frequency distribution $n(M)$ for extragalactic nebulae was established which is of the type of a Gaussian error curve with the frequency maximum located at the absolute photographic magnitude* $M_o = -14.2$. The dispersion in magnitude was found to be about $\sigma = 0.85$. With the customary normalization

$$\int_{-\infty}^{+\infty} n(M)dM = 1, \qquad (1)$$

the distribution function now generally adopted is

$$n(M) = \exp\left[-(M-M)^2/2\sigma^2\right]/(2\pi)^{\frac{1}{2}}\sigma$$
$$= 0.469 \exp\left[-(M-M_o)^2/1.445\right]. \qquad (2)$$

The continuous curve in Fig. 3 represents this function which is based on the statistical evaluation of a large number of nebulae both in the general field and in clusters of nebulae. The distribution in the local group of nebulae according to Hubble[4] slightly favors the fainter nebulae. It should here be mentioned that until recently the local group was known to include the large and small Magellanic clouds, the Andromeda nebula (Messier 31) and its two companions (M_{32}, NGC 205), the spiral nebula M_{33} and the two irregular systems NGC 6822 and IC 1613. If we properly include our own galactic system the mean luminosity for the local group is about $M_o = -14.0$, a value which agrees very closely with the value $M_o = -14.2$ furnished by field nebulae and clusters. How secure the observational basis for the distribution function (2) seemed until recently is well illustrated by Hubble's discussion of the slight discrepancy between the luminosity function of the local group and that of the larger sample collection of nebulae respectively, when he states that "the slight discrepancies are largely accounted for by the presence of three very faint dwarfs in the local group—IC 1613, and NGC 6822 and 205. The results suggest that there might be, in the general field, many similar dwarfs so faint that they would be overlooked in general surveys. A careful reexamination of the surveys demonstrates that such nebulae would be detected if they existed in considerable numbers, and, therefore they must be regarded as relatively rare objects.* Their presence in the local group appears to be a unique feature of the group, and they detract from its significance as a fair sample of nebulae in general."

In spite of the strong observational support of the distribution function (2) certain facts, *both observational and theoretical* have recently come to light which indicate that the *distribution function (2) is really quite incorrect* inasmuch as it is based on a particular *observational selection* and does not embrace the totality of all nebulae. The principal reasons which suggest that the true function $n(M)$ must be very different from the function (2) are as follows.

One objection against the luminosity function of the type (2) for nebulae derives from the fact that this function possesses a maximum for a luminosity roughly equivalent to the absolute magnitude $M_o = -14.2$ while for the frequency distribution of clusters of nebulae no such maximum exists. It is very difficult to see why the results should be so radically different in the two cases of the grouping of nebulae into clusters and the grouping of stars into nebulae. If both of these groupings are due either to random accumulation or to Newton's law of attraction and if the dissolution of these groups is the result of close encounters with other groups, the frequency distributions $\nu(N)$ and $n(M)$ or rather $\bar{n}(L)$ should be similar in character unless some additional effect is operative which suppresses the existence of small nebulae while no such effect hinders the formation of small clusters of nebulae. It will be shown in the following that probably no such effect exists and that therefore the luminosity function $n(M)$ for nebulae derived at the present from the purely observational approach is incorrect. In support of this contention the following qualitative considerations may be advanced.

(1) During the past few years further *faint*

* If L_1 and L_2 are the energies radiated per second by two bodies 1 and 2, the difference in their absolute magnitudes is given by $M_1 - M_2 = 2.5 \log_{10} L_2/L_1$. The absolute photographic magnitude of the sun is $M(\odot p) = +5.3$. Therefore the luminosity L_{0p} (in the photographic range) of an average nebula of the photographic absolute magnitude $M_{0p} = -14.2$ is $L_{0p} = 65 \times 10^6\, L(\odot p)$.

[4] E. Hubble, *The Realm of the Nebulae* (Yale University Press, 1936), p. 149.

* Baade in Astrophys. J. **88**, 112 (1938) also states that the luminosity function (2) may be considered as "well established."

members were added to the local group. These are the *Sculptor* and *Fornax* systems[5] discovered by the staff of the Harvard College Observatory. Also, according to Baade,[6] the *Wolf-Lundmark nebula* which is not contained in Hubble's original list must be added to the local group.*

(2) Nebulae can reach statistically stationary states characterized by a Boltzmann distribution of coordinates and of velocities only so long as the mean free paths Λ of the constituent particles (stars) are smaller than the linear dimensions D of the system. With decreasing mass the ratio Λ/D for some nebulae may become so great that these nebulae never can reach a Boltzmann steady state but remain indefinitely of an irregular extended (Smoluchowski) type.[7] For low masses we therefore expect a great variety of types of nebulae ranging from the relatively extended Smoluchowski type (S) of low surface brightness to the compact type of high surface brightness represented by a globular star cluster (G). In nebulae of very great mass the characteristics of the types S and G co-exist in the same individual nebulae, applying to the center disk and to the peripheral parts, respectively. The identification and determination of the properties of individual nebulae of small mass, because of the small surface brightness of the type S and the compactness of type G will be more difficult than the analysis of the larger nebulae. There are therefore good reasons to believe that the frequency function (2) is based on the selection of material which favors the brighter nebulae of larger surface brightness.

(3) Investigations on the morphology of nebulae and of clusters of nebulae rather strongly support the contention that these objects form a statistically stationary ensemble.[8] In such an ensemble one must expect the heavier and presumably more luminous nebulae to show a higher tendency[1] toward clustering than the fainter nebulae. The faintest nebulae will be distributed most uniformly throughout space. If, as might be expected in a statistically stationary ensemble the less massive nebulae tend less toward clustering than the more massive nebulae the necessity of covering large fields in order to locate the least massive nebulae and to analyze their properties adds to the difficulty of establishing equally representative collections of nebulae of small and of large masses respectively.

From the preceding considerations the case against the luminosity function (2) for nebulae seems strong enough to justify (1) an attempt on the basis of a simple theory of the large scale distribution of matter to estimate the approximate number of faint nebulae actually existing but not represented by the function (2), and (2) a determined search for such faint nebulae. In Section C we shall therefore discuss some of the theoretical aspects of the luminosity function of nebulae while in Section D we present some preliminary results of the search for very faint nebulae obtained through the utilization of the 18-inch Schmidt telescope on Palomar Mountain and the large reflectors of the Mount Wilson Observatory.

(γ) The Stars

The frequency distribution of stars in dependence of their absolute brightness and their mass has long occupied the attention of astronomers. From the observational standpoint the problem is obviously one of great difficulty, because the fainter stars become, intrinsically, the more difficult it is to secure representative collections of such stars. It is interesting to note that about seventeen years ago a change of outlook took place regarding the luminosity function of stars which is very similar to the change of outlook which we may expect to take place in the near future regarding the luminosity func-

[5] W. Baade and E. Hubble, Pub. Astr. Soc. Pac. **51**, 40 (1939).

[6] Private communication by Dr. Baade.

* After it was found that these three systems belong to the local group of nebulae and that they are intrinsically faint Hubble and Baade stated in the Pub. Astr. Soc. Pac. **51**, 44 (1939) that "Hitherto it has been assumed that the two branches (of the luminosity function) are symmetrical, although the brighter branch alone has been reliably determined. Although the information now available suggests that the local group is not a fair sample of nebulae in general the new data emphasize the importance of a thorough reexamination of the luminosity function." However according to the considerations given in the following it cannot be expected that the local group contains a larger percentage of faint nebulae than the general field and neither is it likely that the correctly formulated luminosity function exhibit any maximum at all.

[7] F. Zwicky, Phys. Rev. **58**, 478 (1940); Astrophys. J. **93**, 411 (1941).

[8] F. Zwicky, *Th. von Karman Anniversary Volume* (1941), pp. 137–153.

tion of nebulae. Some twenty years ago, from the data then available astronomers concluded that in a large region of our galaxy centered around our sun the absolute number of stars rapidly increases as the brightness declines from stars of the absolute magnitude $M=-5$ (stars which are about 10,000 as bright as the sun whose absolute magnitude is approximately $M(\odot)\leqq+5$) to stars of $M=+7$. For such stars which are about ten times fainter than the sun the luminosity function seemed to exhibit a maximum. In 1924 however Seares[9] showed that intrinsically faint stars are far more numerous than had been previously supposed and that if the luminosity function has any maximum at all it must lie at stars $M>+13$ which are at least one thousand times fainter than the sun.

Unfortunately no satisfactory theory of the frequency distribution of stars of different luminosity and mass is available. While the theory of the frequency distribution of clusters of nebulae and of nebulae is simplified by the fact that no good reason is known at the present why the clusters of nebulae and the nebulae should not exist as aggregations of matter of continuously increasing mass up to a certain point, the problem presented by the stars is entirely different, since because of the interference of the energy generation through subatomic processes and the action of the light pressure certain types of stars whose existence in any statistically stationary ensemble might otherwise be expected do not occur because they do not satisfy the laws of dynamic stability.

At the present the frequency distribution of various types of stars can only be approached through a more systematic search. This search is essentially confined to the neighborhood of the sun but has at its disposal some powerful means such as the search for large proper motion stars and the spectroscopic method of determining parallaxes as well as a number of additional criteria which it is not necessary to discuss here in detail. For the nebulae all of these criteria are not available and new criteria therefore had to be found, some of which will be discussed in Section D.

[9] F. H. Seares, Astrophys. J. **59**, 310 (1924).

C. SOME STATISTICAL MECHANICAL CONSIDERATIONS ON THE LARGE SCALE DISTRIBUTION OF MATTER

(α) On the Clustering of Nebulae

We shall first apply a few simple theorems to the problem of the clustering of nebulae. As a first approximation we assume that the universe is in a stationary state of statistical equilibrium* and that the nebulae are more or less permanent objects whose identity or whose number can be materially changed only through rare and most violent processes such as direct collisions, the effects of which we shall touch upon later.

The Principle of Conservation of Energy

Suppose we start from a uniform distribution of nebulae for which the average potential energy $\bar{E}_{p0}$ may arbitrarily be set equal to zero. The average kinetic energy per unit mass in this distribution we denote with $\bar{E}_{k0}$. For $\bar{E}_{k0}=0$ any static distribution of nebulae is unstable according to Earnshaw's theorem. Clustering with subsequent aquisition of kinetic energy by the nebulae will therefore result from this instability. For $\bar{E}_{k0}\neq 0$ a uniform distribution of nebulae results if

$$\bar{E}_{k0}\gg -\bar{E}_p, \tag{3}$$

where $\bar{E}_p$ is the average potential energy per unit mass in any possible state of clustering. In actuality condition (3) is not fulfilled since clustering obviously exists and we therefore shall have to replace the inequality (3) by a more accurate relation which we may obtain from the energy principle. For simplicity we shall bunch together on the one hand all nebulae and groups of nebulae for which $\bar{E}_p$ is negligible and on the other hand the larger clusters of nebulae for which $\bar{E}_p$ is appreciable. The nebulae in the first group we shall denote with the index e (external with respect to the clusters) and the nebulae in the second group with the index i (internal). The total mass of the external field nebulae in a given large volume is M_e while the total mass of the nebulae in larger clusters is M_i. If the average kinetic and potential energies per unit mass of

* In the final section E, at the suggestion of the editors some of the evidence now available is briefly reviewed, which favors the assumption of a stationary rather than an expanding universe.

the cluster nebulae are $\bar{E}_{ki}$ and $\bar{E}_{pi}$ and the average kinetic energy per unit mass of the field nebulae is $\bar{E}_{ke}$ we have under the assumptions stated*

$$M_e\bar{E}_{ke}+M_i(\bar{E}_{ki}+\bar{E}_{pi})=(M_i+M_e)\bar{E}_{ko}\geqslant 0. \quad (4)$$

Co-existence of Smoluchowski Distributions and Boltzmann Distributions in the Realm of Nebulae

When in a physical system, such as the co-existence of a liquid (i) and its vapor (e) in a closed vessel the number of impacts between the elementary particles is very great, equipartition of energy (constancy of temperature) is ultimately established and we have $\bar{E}_{ke}=\bar{E}_{ki}$. However the manifold of the field nebulae and the cluster nebulae in some fundamental aspects differs from the physical system just described because of the length of some of the mean free paths involved.

Terrestrial systems in which some of the mean free paths are so long that deviations from the Boltzmann Gibbs distribution law result were considered by Maxwell[10] and later on particularly by Smoluchowski[11] and Knudsen.[12] In the theory of the large scale distribution of matter considerations of the types described by these authors play a decisive role. They explain, as we shall see, some of the important characteristics of nebulae and of clusters of nebulae. They also make it clear that the lack of equipartition of energy (constancy of temperature) among the large scale condensations of matter does not necessarily indicate that the universe is not in a thermodynamically stable state.

In the realm of the nebulae we deal with mean free paths in the large clusters which are comparable with the diameters of the clusters while for the field nebulae the mean free paths are much larger. This means that in the central parts of stationary large clusters we may expect a Boltzmann distribution of matter and of its kinetic energy, while in "extra cluster" space Smoluchowski distributions will have to be introduced. This suggests that a "cosmic temperature jump" exists between the inside and the outside of clusters. Strictly speaking all nebulae, the field nebulae included, are more or less closely associated with one cluster of nebulae or another.[13] The existence of a region around a cluster in which a relatively sharp transition from a higher average kinetic energy to a lower average kinetic energy takes place justifies the introduction of intracluster nebulae and extra-cluster nebulae and lends a precise meaning to the long used distinction between field nebulae and cluster nebulae.

In Fig. 1 the distribution[3] of the average kinetic energy per unit mass is shown as a function of the distance r from the center of a large cluster.

The distance $r=r_c$ from the center at which the "cosmic temperature jump" occurs is given roughly by the relation

$$\bar{E}_{ki}-\bar{E}_{ke}\backeq\Phi(r_c+\lambda(r_c))-\Phi(r_c), \quad (5)$$

which expresses the fact that for $r=r_c$ the mean free path of the nebulae becomes so large that running from r_c to $r_c+\lambda$ the nebula may transform a considerable fraction of its excess kinetic energy into potential energy.

For $r_c>0$ the cluster is of the Boltzmann compact type while for $r_c=0$ the cluster is of the Smoluchowski open type. In passing we mention that the Coma cluster of nebulae is of the first type showing a distribution of mass and of kinetic energies which would be expected from Boltzmann's principle,[1] while the system of the field nebulae including many open groups represent a distribution of the Smoluchowski type. The two masses M_i and M_e previously introduced correspond roughly to the total masses of the two types of groupings in a given very large volume.

An estimate of these total masses M_i and M_e as well as of the kinetic energies $\bar{E}_{ki}$ and $\bar{E}_{ke}$ may

* The possibility that the expression (4) is negative cannot be dismissed *a priori*. If negative, it would mean that the total kinetic energy of all the nebulae is not sufficient to disrupt all of the clusters. This, however, would make necessary values for the masses of nebulae much larger than we can tolerate at the present time without running into contradiction with a number of other phenomena previously discussed (see reference 1), such as the characteristics of the velocity dispersion in clusters and the fact that no gravitational lens effects among the nebulae have as yet been found.

[10] C. Maxwell, *Scientific Papers* (Cambridge Univeristy Press, 1890), Vol. II, p. 703.

[11] M. v. Smoluchowski, Wied. Ann. **64**, 101 (1898).

[12] M. Knudsen, Ann. d. Physik **34**, 593 (1911).

[13] F. Zwicky, Pub. Astr. Soc. Pac. **50**, 218 (1938).

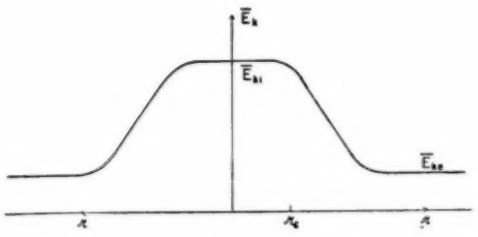

FIG. 1. Average kinetic energy of nebulae per unit mass as a function of the distance from the center of a large cluster of nebulae.

be obtained from an application of the virial theorem and the Boltzmann principle.

The Virial Theorem

Large clusters of nebulae represent stationary assemblies in the sense that the number of nebulae which in a given time escape from a cluster through its boundary ($r=r_c$) on the average is equal to the number of nebulae captured by the cluster. The virial theorem states[1] that for any mechanical system whose particles interact according to the inverse square law of attraction

$$\tfrac{1}{2}\langle d^2\theta/dt^2\rangle_{Av}=(2\bar{E}_{ki}+\bar{E}_{pi})M_i, \qquad (6)$$

where M_i and θ are the total mass and the polar moment of inertia of the system. For a stationary cluster the left side of (6) is zero and therefore

$$\bar{E}_{pi}=-2\bar{E}_{ki}. \qquad (7)$$

Substituting (7) in (4) we obtain

$$M_e\bar{E}_{ke}-M_i\bar{E}_{ki}=(M_i+M_e)\bar{E}_{ko}\gtrsim 0. \qquad (8)$$

From this and the fact that certainly $\bar{E}_{ki}$ is greater than $\bar{E}_{ke}$ we conclude that

$$M_e/M_i\gtrsim\bar{E}_{ki}/\bar{E}_{ke}\gtrsim 1. \qquad (9)$$

This relation expresses the important fact that clustering among nebulae as such has its natural limit. At the same time as clusters grow more numerous and become more compact $\bar{E}_{ki}$, which is equal to $-\bar{E}_{pi}/2$, increases correspondingly. The resulting increase of M_e therefore automatically depletes the population of the clusters in favor of the field nebulae. We have here an excellent illustration of the universal principle that *every process which, generally speaking, involves a contraction automatically is associated with another process which involves expansion,* and vice versa. The contraction of the stellar cores in novae and in supernovae with the subsequent expulsion of the outer layers of the stars involved provides another illustration while the examples of *explosions* caused by molecular and nuclear *contractions* are too numerous to be mentioned specifically.

Although more observations are badly needed, relation (9) can be subjected to a qualitative test with the data on hand. While the average velocity for cluster nebulae[3] is of the order of $v_i=500$ km/sec. the average velocity of the field nebulae is of the order $v_e=250$ km/sec.[1,3] and consequently

$$\bar{E}_{ki}\leqq 4\bar{E}_{ke}, \qquad (10)$$

from which it follows that

$$M_e\gtrsim 4M_i, \qquad (11)$$

a relation which is in accordance with the approximately known relative abundance of field nebulae and of cluster nebulae.

While from the considerations given so far the relation (11) can be only derived if (10) is taken as an observational fact we may drive the theory one step further which leads to another justification of (11). This additional step is furnished through an application of Boltzmann's principle and in turn justifies our initial assumption of the stationary character of the distribution of the nebulae and of their kinetic energies.

The Boltzmann Principle

For a gravitational isothermal gas sphere which has reached a statistically stable state and in which the mean free paths are small compared with the total dimensions of the sphere the radial distribution of matter was determined by Emden.[14] We shall call this the Emden distribution. Vice versa if we know from observation that a spherically symmetrical cluster of objects satisfies the Emden distribution we may conclude that this distribution is in accordance with Boltzmann's principle and that between the objects the ordinary Newton inverse square law of attraction is operative. From an analysis of the distribution of nebulae in the Coma cluster it was shown previously[1] that the conditions just mentioned are satisfied and that therefore

[14] R. Emden, *Gaskugelm* (Teubner, Leipzig, 1907).

the interaction between the nebulae is governed by Newton's law. The application of the Boltzmann principle to the whole realm of nebulae on the other hand is not quite correct since in a great part of this realm the mean free paths are too long and the number of encounters too small, a fact which leads us to the recognition of a cosmic "temperature jump" between the cluster nebulae and the field nebulae. We may, however, still assume that the Boltzmann principle leads to qualitatively correct results for the relative population of the clusters and of the general field of nebulae because of the fact that the relative abundance of the field nebulae and of the cluster nebulae is determined by the relative volumes V_e and V_i occupied by the two types of nebulae and by their average kinetic energies. Qualitatively we may therefore write*

$$M_i/M_e = \exp\left[-\bar{E}_{pi}/kT\right] V_i/V_e, \tag{12}$$

where

$$kT \leqq 2\bar{E}_{ke}/3, \tag{13}$$

since for $\bar{E}_{ke}=0$ the clusters cannot be disrupted by any encounters with field nebulae, which in this case would disappear entirely. Furthermore from (7) and (9)

$$\bar{E}_{pi} = -2\bar{E}_{ki} = -2\gamma \bar{E}_{ke} M_e/M_i, \tag{14}$$

where $0 \leq \gamma \leq 1$ and therefore

$$M_i/M_e = \left[\exp\left(3\gamma M_e/M_i\right)\right] V_i/V_e \tag{15}$$

or

$$\left[\exp\left(-3M_e/M_i\right)\right] V_e/V_i \leq M_e/M_i \leq V_e/V_i. \tag{16}$$

While the upper limit for M_e/M_i corresponds to the case that $\bar{E}_{ko}$ is very large and practically no clustering takes place, the lower limit represents the maximum possible clustering ($\bar{E}_{ko}=0$) and the smallest ratio M_e/M_i.

From the fact that matter is not uniformly smeared out over space but exhibits a great tendency to agglomeration we conclude that $\bar{E}_{ko}$ is small compared with $\bar{E}_{ki}$ or even $\bar{E}_{ke}$. For purposes of discussion we shall set $\bar{E}_{ko}=0$ although the exact value of $\bar{E}_{ko}$ can probably be deduced only when more is known about the nature of the redshift on the one hand and perhaps the problem of relativistic cosmology on the other. With $\bar{E}_{ko}=0$ we have

$$V_e/V_i = xe^{3x},$$

where

$$x = M_e/M_i. \tag{17}$$

Strictly speaking this is an equation for x since $\bar{E}_{pi}$ can be expressed in terms of M_i and V_i which in turn leads to a relation between V_e/V_i and M_e/M_i. This relation, however, is so complicated that for purposes of a clear illustration of the physical principles discussed it will be more advantageous to compare (17) directly with the observational data. In this comparison we are also interested in the values of $\bar{\rho}_i/\bar{\rho}_e$ where $\bar{\rho}_i$ and $\bar{\rho}_e$ are the average density of matter inside and outside of the large clusters. It is

$$\bar{\rho}_i/\bar{\rho}_e = M_i V_e/M_e V_i = e^{3x}. \tag{18}$$

Table I gives some of the values of x, V_e/V_i and $\bar{\rho}_i/\bar{\rho}_e$ in the range in which we shall be interested.

Observationally the field nebulae are several times as numerous as the cluster nebulae, so that, in order of magnitude $x=3$ and consequently $V_e/V_i \sim 20000$ which also is in approximate agreement with the observations. It will be of great interest to determine accurate values of V_e/V_i through a more general survey of clusters of nebulae and to compare the values of M_e/M_i and $\bar{\rho}_i/\bar{\rho}_e$ resulting from Table I with other independent determinations of these quantities. At the present not enough observations are available to make an accurate comparison although we can state that qualitatively the data on hand check the validity of our considerations.

It may be asked why, instead of analyzing step by step the distribution in space of nebulae and of their velocities through the application of various fundamental theorems we have not approached the problem in the stereotype manner of statistical mechanics, which is to determine directly the most probable distribution in phase space of our assembly of nebulae. Such an approach which would be the only rigorous one, however, meets with two difficulties which have not yet been overcome. These difficulties are

(a) The number of encounters among nebulae in a great part of the universe known to us is not

* A strict application of Boltzmann's principle involves the introduction of partition sums with the potential energies of the individual nebulae entering the exponentials so that a segregation of nebulae of different mass will result.

large enough to make the distribution of nebulae random in a statistical sense. The problem of the coexistence of Boltzmann and *Smoluchkowski distributions* therefore remains to be investigated in more detail.

(b) The assembly of nebulae is a *cooperative assembly* in the sense that the potential energy is represented through *conditionally convergent sums*, the values of which depend on the shapes of the configurations (clusters and clouds) involved. This fact leads to peculiar deviations from the laws of thermodynamics as formulated for non-cooperative assemblies for which ordinary equations of state exist. For cooperative assemblies the laws of thermodynamics need reformulation.

(β) On the Theory of the Frequency Distribution of Nebulae

The distribution function $n(M)$ for nebulae of different absolute magnitudes M now generally adopted is explicitly given by (2). In Section B_β we advanced some reasons which suggest that this distribution function cannot be correct. With the help of the physical principles which we discussed in the previous section C_α and which enabled us to derive some of the major characteristics of the clustering of nebulae we now can proceed to derive a more quantitative estimate on just how far the function (2) is in error.

We first list some of the reasons why the intergalactic space between the nebulae incorporated in the distribution function (2) must be populated by very considerable amounts of matter in the form of intergalactic gases and dust, individual stars and groups of stars or nebulae which are fainter and smaller than those which obey the distribution function (2).

TABLE I.

$x=M_e/M_i$	$V_e/V_i=xe^{3x}$	$\bar{\rho}_i/\rho_e=e^{3x}$
1	20	20
1.5	135	90
2	807	403
2.5	4520	1808
3	2.43×10^4	8103
3.5	1.27×10^5	3.63×10^4
4	6.52×10^5	1.63×10^5
4.5	3.28×10^6	7.29×10^5
5	1.64×10^7	3.27×10^6
5.5	8.03×10^7	1.46×10^7
6	3.94×10^8	6.56×10^7
6.5	1.91×10^9	2.94×10^8

(1) The kinetic energy of translation of the field nebulae per unit mass is

$$\bar{E}_{ke}=\langle v_e^2\rangle_{\text{Av}}/2. \tag{19}$$

The available observational data indicate that[3]

$$(\langle v_e^2\rangle_{\text{Av}})^{\frac{1}{2}}\leqq 250 \text{ km/sec.}, \tag{20}$$

while for the nebulae in large clusters

$$\bar{E}_{ki}=\langle v_i^2\rangle_{\text{Av}}/2, \tag{21}$$

where

$$(\langle v_i^2\rangle_{\text{Av}})^{\frac{1}{2}}\leqq 500 \text{ km/sec.} \tag{22}$$

The average potential energy $\bar{\epsilon}_{pi}$ per unit mass of the stars in the nebulae themselves, by the virial theorem is

$$\bar{\epsilon}_{pi}=-2\bar{\epsilon}_{ki}, \tag{23}$$

where

$$\bar{\epsilon}_{ki}=\langle w_i^2\rangle_{\text{Av}}/2 \tag{24}$$

and w_i rarely exceed 100 km/sec. Therefore

$$|\bar{\epsilon}_{pi}|<\bar{E}_{ke}. \tag{25}$$

Encounters between nebulae consequently are quite capable of *disrupting* nebulae to a large degree and producing fragments or stellar systems which are smaller than the original objects involved in the encounters. Because of the occurrence of encounters the frequency distribution of small and of large nebulae must be similar to the frequency distribution of atoms and smaller and larger molecules in a gas for which the average translational energy $3kT/2$ is larger than the dissociation energy of the molecules. Because of collisions which frequently result in dissociation the smaller units must exist in preponderant numbers. This effect is enhanced because of the much greater *a priori* probability (larger volume available) of the smaller units.

(2) In the nebulae themselves, as contraction proceeds, $\bar{\epsilon}_{ki}$ increases at the same time with $|\bar{\epsilon}_{pi}|$. During this process a certain amount of kinetic energy is liberated from the system in order to maintain internal equilibrium in accordance with the virial theorem (24). This kinetic energy will be liberated through the expulsion of stars or groups of stars into intergalactic space and we again have a phenomenon which illustrates the principle that contraction on the one hand and expansion on the other are necessarily related effects. The net result is that intergalactic

space will be populated by stars and groups of stars.

(3) In passing we mention further phenomena which involve contractions such as the collapse of stars in novae and in supernovae during which processes gas clouds are ejected into interstellar and intergalactic space.[7] Light pressure on the interstellar gas and dust clouds acts to populate intergalactic space with the same objects.

In order to obtain a *minimum estimate* of the stellar population of intergalactic space we disregard the effects (1) and (3). To the effect (2) a similar analysis then applies which we have given for the relation between cluster nebulae and field nebulae. We can thus again use a relation analogous to (15) to estimate the ratio between the total mass m_i of the large nebulae incorporated in the distribution function (2) and the mass m_e of the intergalactic objects not represented by this function. We have

$$m_e/m_i \leqq [\exp(-3m_e/m_i)]\Omega_e/\Omega_i, \qquad (26)$$

where Ω_e and Ω_i are the partial volumes occupied, respectively, by the nebulae incorporated in the distribution function (2) and by the "intergalactic" space between these nebulae. Since approximately

$$\Omega_e/\Omega_i = 10^6, \qquad (27)$$

we read from Table I that

$$m_e/m_i \leqq 4. \qquad (28)$$

Because of the neglect of the effects (1) and (3) the ratio m_e/m_i will be greater than estimated by (28). The fact, for instance, that the nebulae possess already very considerable kinetic energies which are a result of the clustering of nebulae rather than due to the release of potential energy in the formation of the nebulae themselves will make the effective kT in the Boltzmann factor of relation (12) greater than indicated by the formulae of the type (13) and (14), with the result that m_e/m_i becomes greater than given by these formulae.

Since no good reason seems to exist why any particular agglomeration of stars in interstellar space should be excluded, we conclude that *individual stars, multiple stars, open and compact star clusters and stellar systems of increasing population will be found in numbers presumably decreasing in frequency as the stellar content of the systems in question increases.* This important conclusion from our theoretical considerations is so radically at variance with the now generally adopted luminosity function (2) that a serious effort seems justified to decide between the two alternatives through further systematic observations. Some suggestions regarding such observations will be discussed in Section *D*.

D. THE SEARCH FOR INTRINSICALLY FAINT NEBULAE

(α) Discovery of New Faint Stellar Systems in the Local Group

The reasons given in the preceding for the probability of the existence of a far greater number of faint nebulae than was hitherto suspected seemed powerful enough to warrant a new search for such nebulae. Because of its great speed and large field the 18-inch Schmidt telescope on Palomar Mountain is well suited for this task. During the extensive search for supernovae in the period from September, 1936, until date quite a number of faint and relatively extended objects was noted. Without the possession of some distance criterion however, it would have been necessary to photograph these nebulae indiscriminately with one of the large reflectors under good seeing conditions in order to ascertain their distance and intrinsic nature. Such a procedure obviously would have been tedious and inefficient. The problem therefore was to develop, if possible, some criteria which would enable us to search for nearby nebulae with some greater chance of success. Although we cannot hope with the Schmidt telescope to resolve in faint nebulae, even if in the local group, a sufficient number of stars to determine their character, the three following qualitative criteria may sometime be of considerable help.

(1) Nebulae of small stellar content N which are of the extended "Smoluchowski" type may often be expected not to possess any kind of central condensation and to show relatively great *irregularities in surface brightness* ($\sim N^{\frac{1}{2}}$) giving them a patchy granulated appearance. Repeated long exposures of the same fields were therefore taken in order to see whether in some of the faint nebulae any such intrinsic granulation could be

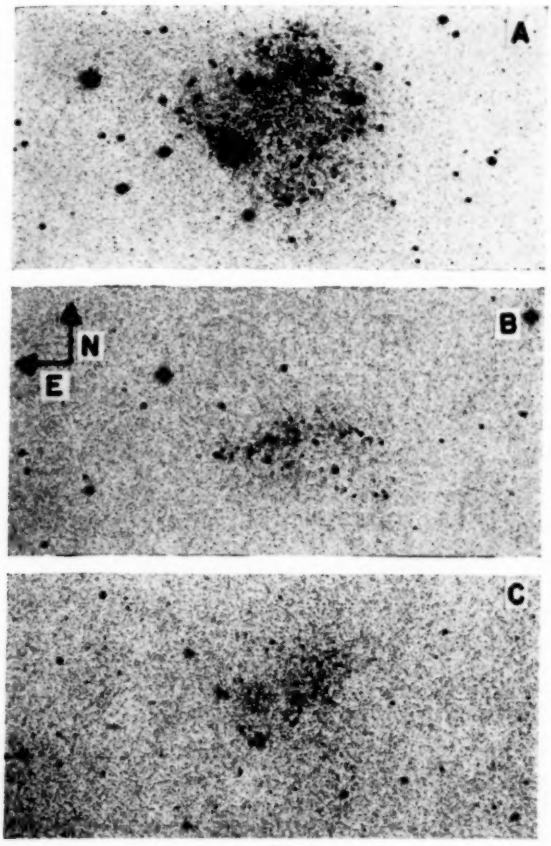

FIG. 2. (B) This nebula (1940: R.A. 9^h 55.9^m, Decl. $+31°$ 2′) which is located in the constellation of Leo at a distance of about 1.3 million light years is the faintest stellar system now known. Its absolute brightness, according to Baade is about 600,000 times that of the sun. (A) This nebula (1940: R.A. 10^h 8.1^m; Decl. $-4°$ 24′) in the constellation of Sextans is about one million light years distant and is probably the second faintest system known at the present time. Its brightness is about 1.5 million times that of the sun. The irregularities in surface brightness in both the Sextans system and the Leo system appear much less pronounced when photographs are made in red light only. Both stellar systems belong to the so-called local group of nebulae. (C) This nebula (1941: R.A. 9^h 36^m, Decl. $+71°$ 27′) is located in Ursa Major. Its average surface brightness which is exceedingly low and its structure suggest that it is a system similar to IC 1613 which nebula is a member of the local group. If we put the Ursa Major system tentatively at a distance of about one million parsecs (=3.26 million light years) and incorporate it in the group of nebulae associated with the bright systems Messier 81 and Messier 82, its diameter becomes about 4000 light years and its brightness about four million times that of the sun making it very similar to IC 1613. All of the three systems shown were discovered with the 18-inch Schmidt telescope on Palomar Mountain. The fact that even with this unusually fast telescope it is difficult to make such nebulae as the Ursa Major system stand out clearly against the various lights of the night sky indicates that a considerable number of quite nearby dwarf nebulae may thus far have escaped discovery. In the reproductions shown the contrasts have been very strongly enhanced in order to make the nebulae stand out clearly.

found which is coarse enough to be distinguished from the accidental granulation of the photographic grain.

(2) For faint nebulae which show bright stars in numbers increasing with decreasing brightness in about the same way as IC 1613 or Messier 33 the granulation effect may be expected to be more pronounced on "blue" films than on panchromatic films shielded by a red filter.

(3) In cases like the Fornax system[5] where neither one of the criteria (1) or (2) is of any help, the system may happen to be near enough to be conspicuous through its relatively large angular diameter.

With the help of the principles just mentioned six objects were singled out for further investigation with the 100-inch telescope. Among these six objects two nebulae located in Leo and in Sextans, respectively, turned out to be new extremely faint nebulae in the local group. Reproductions of 100-inch photographs of these two nebulae may be found in the article by E. Hubble in the *Scientific Monthly** of November, 1940. These show clearly the absence of a central condensation and the existence of great irregularities in surface brightness. Since the search for dwarf nebulae of the type described is most effectively conducted with medium size telescopes we here reproduce in Fig. 2 photographs of three of these nebulae which were obtained by Dr. N. U. Mayall with the 36-inch Crossley reflector at the Lick Observatory. For permission to publish these photographs thanks are due to Dr. W. H. Wright, director of the Lick Observatory, and to Dr. Mayall.

In addition to the fact that the Leo system and the Sextans system are the faintest extragalactic systems known so far, their location in the sky is such as to be of value for the investigation of the relative motion of the Milky Way, an investigation which in the past was hampered by the fact that the members of the local group of nebulae known previously show a lopsided distribution favoring a cap around the south galactic pole.

It should be emphasized that the criteria (1), (2), and (3) often may help in detecting nearby

* Some inaccuracies in this article regarding the discovery of the new systems in Leo and Sextans were corrected by Hubble in a note to Sci. Monthly **52**, 486 (1941).

nebulae of the Smoluchowski type, but that they are still considerably selective and that, worst of all, they do not in any way facilitate the establishing of a representative collection of intrinsically small nebulae of the elliptical and globular types.

(β) The Luminosity Function of the Local Group

If we limit the local group to nebulae of distance moduli $\mu = m - M \leqslant 23$ (distance 1.3×10^6 L.Y.) the fourteen objects now known in this group may be arranged in the following ranges of absolute luminosity M.

The rectangles in Fig. 3 with a total area equal to unity graphically represent the frequency distribution of absolute luminosities in the local group.

It is seen that the faint nebulae are much more prominent than would be expected from the luminosity function $n(M)$ given by (2). While for the unobscured areas in the sky presumably no more nebulae brighter than about $M = -14$ and of distance modulus $\mu \leqslant 23$ exist than are listed in Table I it is very unlikely that we now know all of the nebulae fainter than say $M = -13$. Extrapolating from the progress which has been made during the past few years in shifting the mean value M_0 towards smaller luminosities it is very probable that this trend will continue through further discoveries.

It should here be mentioned that the globular cluster NGC 2419, the absolute magnitude of which is $M = -8.3$, lies at a distance of 200,000 light years from the center of the Milky Way.[15]

TABLE II.*

Range in Absolute magnitude	Systems of the local group of nebulae
−8.25 to −9.10	Leo system
−9.10 to −9.95	None
−9.95 to −10.80	Wolf-Lundmark nebula, Sextans and Sculptor systems
−10.80 to −11.65	NGC 205, NGC 6822, IC 1613
−11.65 to −12.50	Fornax system
−12.50 to −13.35	Messier 32
−13.35 to −14.20	None
−14.20 to −15.05	Messier 33
−15.05 to −15.90	Small Magellanic cloud
−15.90 to −16.75	Large Magellanic cloud
−16.75 to −17.60	Messier 31, galaxy

* I am indebted to Dr. W. Baade of the Mt. Wilson Observatory for some of the data given in this table.

[15] W. Baade, Astrophys. J. **82**, 396 (1935).

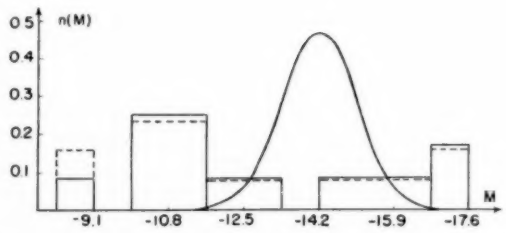

FIG. 3. Luminosity function of the local group of nebulae. The curve represents the luminosity function (2) of the text. The drawn out rectangles represent the frequency distribution in absolute magnitudes of the "local" nebulae listed in Table II. If the globular cluster NGC 2419 is admitted as an independent system a frequency distribution results which is indicated by the broken lines. It is probable that many more "local" nebulae will be found which fall into the range $M > -14.2$.

Although its radial velocity of +9 km/sec. is not in itself larger than the velocity of escape from the Milky Way its total velocity might well be larger. But even if this is not the case it may be justified to consider it as a companion of the Milky Way which must independently be incorporated in the luminosity function of the nebulae.*

It must also be remembered that the systematic search for faint nebulae has only just begun and that the results achieved so far justify the expectation that many additional faint nebulae will be found. It will, however, be very difficult to establish the complete luminosity function by an investigation of the local group alone, although such telescopes as the 48-inch Schmidt telescope now in construction will no doubt be of great help in achieving a solution of this problem.

In regard to the question whether or not the local group is a representative sample collection of nebulae it follows from our previous considerations that this group as well as any other group or cluster rather favors the massive and more luminous nebulae because of the segregation resulting from Boltzmann's principle. *In a large sample collection of nebulae including both clusters and field nebulae the number of faint nebulae should be relatively larger than that found in the local*

* A more exact theory will have to take into account the fact that the stellar systems themselves are not rigid units but are made up of various types of subsystems, the frequency distribution of which is in some definite way related to the luminosity function of nebulae. In such a theory it may appear convenient and justified to consider as statistically independent systems all of the globular clusters of the Milky Way system, of the Andromeda nebula and of other stellar systems.

group. The ultimate result may therefore well be in accord with the predictions of our theory. That is, it may be found that in contradistinction with the luminosity function (2) the relative number of nebulae increases as their intrinsic brightness decreases. Some additional attempts which are now being made to establish the correctness of this expectation may be briefly sketched.

(γ) The Luminosity Function in the Virgo Cluster of Nebulae and its Surrounding Regions

The Virgo cluster lies at a distance of about seven million light years. Its six hundred known constituent nebulae have a mean apparent magnitude $+12.7$ which is equivalent to a mean absolute magnitude of about $M=-14.2$ and seem to be adequately represented by the luminosity function (2). Because of the segregation effect which results from Boltzmann's principle it must be suspected that the more luminous nebulae are represented in unduly large numbers if only the cluster itself is investigated. The following procedure therefore suggests itself. Determine the radial distribution in nebular density to a distance of say three times the apparent diameter of the Virgo cluster of nebulae in the range of apparent magnitude $+9$ to $+10$, $+10$ to $+11$, etc. With the 18-inch Schmidt telescope it will be possible to explore these ranges to a limit of about $+15$ to $+16$. It should then be expected that distribution curves of the type shown in Fig. 4 will be found.

If these expectations can be verified through the observations which are now being conducted at Palomar it should be possible to establish a fairly complete luminosity function in the range from the brightest nebulae ($M=-18$) to those of intrinsic brightness $M=-10.5$ (luminosity equal to about one million suns). In addition curves of the type shown in Fig. 4 should enable us to determine the relative masses of nebulae.

(δ) The Luminosity Function in Distant Clusters of Nebulae

In the case of a distant cluster the following method suggests itself in order to obtain a third independent check of our theory. First, count the individual nebulae discernible with a large telescope, determine their luminosities and calculate the total integrated brightness of these nebulae. Then run microphotometer tracings well across the cluster and determine the total brightness of the cluster. The difference between the two luminosities represents the contribution of the faint not individually discernible nebulae in the cluster, which, compared to the integrated brightness of the discernible nebulae should give an estimate of the relative importance of the fainter branch of the luminosity function to the brighter branch. In order for this procedure to be successful the cluster in question should lie in a region of the sky in which the intervening number of bright stars is small. Such clusters are rare but a new cluster in Pisces (Right ascension $23^h\ 7.5^m$, Decl. $+7°\ 13'$ (1940)) which promises to meet all of the necessary requirements has recently been found with the 18-inch Schmidt telescope on Palomar Mountain.

Finally it should be mentioned that the search for supernovae conducted during the past few years has led to some interesting results concerning the stellar population of intergalactic

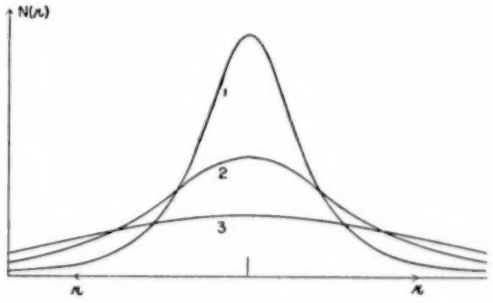

FIG. 4. Radial distribution of nebulae of different mass to be expected in a stationary cluster of nebulae. The curves 1, 2 and 3 qualitatively represent the numbers $N(r)$ per unit volume of nebulae of different mass $\mathfrak{M}_1>\mathfrak{M}_2>\mathfrak{M}_3$.

space. It was found that supernovae occur far outside the nebulae suggesting that stars are present in these regions although they cannot be detected under normal circumstances. Further refinements of the observational technique will no doubt enable us in the future to detect objects of fainter surface brightness than was hitherto possible and to obtain in this way additional information about the amount of matter dispersed throughout intergalactic space.

E. BRIEF REVIEW OF SOME OF THE EVIDENCE NOW AVAILABLE WHICH FAVORS THE ASSUMPTION OF A STATIONARY RATHER THAN AN EXPANDING UNIVERSE

In the preceding discussion it is shown that on the assumption of a stationary universe the luminosity function (2) for nebulae cannot be correct and that the jump in the velocity dispersion from cluster nebulae to field nebulae can quantitatively be accounted for on the basis of the coexistence of a Boltzmann distribution for the cluster nebulae and a Smoluchowski distribution for the field nebulae. On the assumption of an expanding universe our general conclusions concerning the luminosity function of nebulae still remain qualitatively valid although the necessary proof has not here been given. On the other hand it was shown previously[16] that the magnitude and even the sign for the jump in the velocity dispersion from the clusters to the general field is in contradiction with the hypothesis of an expanding universe. It is therefore of interest to mention briefly some additional evidence which favors the hypothesis of a stationary universe.

(a) The observed large scale distribution of matter in space and in velocities exhibits the degree of uniformity which permits the assumption of a stationary universe. The uniformity in the morphological types of nebulae throughout the observable regions of space also is in accord with this assumption.[8] These aspects of uniformity have been discussed at length by Hubble.[4] On the quantitative characteristics of the large scale distribution of matter the following evidence is available.

(b) As is to be expected in a stationary universe a large proportion of the clusters of nebulae exhibit quantitatively correct characteristics of stationary assemblies. It was shown for the first time with the help of the 18-inch Schmidt telescope that the clusters of nebulae are far more extended than was previously thought[1,17] and that many of the clusters possess spherical symmetry. Among the clusters of this type, arranged in order of decreasing membership are the clusters in Coma[1] (at least 2000 nebulae), Perseus, Hydra,[17] Cancer, Pegasus[17] and Fornax (R. A. $3^h\ 34^m$, Decl. $-36°\ 0'$, about 100 nebulae) as well as a number of small condensations in the Pisces cloud.[18]

(c) The observed radial distributions of the numbers of nebulae in clusters are such that with the help of two reduction factors affecting the density and the distances from the center of the clusters all of the known distribution curves of globular clusters can quantitatively be reduced to *one standard curve* as will be shown in another place. This curve is practically identical[1] with the distribution curve of surface brightness observed in globular nebulae and both curves are represented quantitatively by the density curve derived theoretically for a bounded isothermal gravitational (Emden) gas sphere. Incidentally, these results furnish the first proof that Newton's law is valid as a first approximation in describing the interactions among objects separated by distances of the order of one million light years. Previously, from observations on double stars, the validity of Newton's law had been established only for the interactions of objects separated by distances of less than one light year.

The observed radial distribution in clusters of nebulae has not been accounted for on the hypothesis of an expanding universe. If in an originally contracted universe all of the present clusters had existed in a much more condensed state their present radial distribution curves should be determined by the original velocity distribution of the nebulae which would result in radial distributions in clusters quite different from the actually observed Boltzmann-Emden distributions.

From the remarkable fact that even clusters which contain only about one hundred nebulae exhibit the Emden distribution we may conclude that the exchange of momentum and energy among the nebulae of such a cluster has been effective and the time available long enough to establish a statistically stationary assembly and that we are therefore justified, as was done in this paper, to analyze the problem of the luminosity function of nebulae on the assumption of a stationary universe.

[16] F. Zwicky, Proc. Nat. Acad. Sci. **25**, 604 (1939).

[17] F. Zwicky, Proc. Nat. Acad. Sci. **27**, 264 (1941) and J. B. Edson and F. Zwicky, Proc. Nat. Acad. Sci. **27**, 366 (1941).

[18] F. Zwicky, Proc. Nat. Acad. Sci. **23**, 251 (1937); and Clyde W. Tombaugh, Pub. Astr. Soc. Pac. **49**, 259 (1937).

(d) The velocity distribution in clusters of nebulae such as the Virgo cluster for which enough observations are available is independent of the distance from the center.[19] (For information on a great number of unpublished observations I am indebted to Mr. Humason and to Dr. Hubble.) Equipartition of energy among nebulae of presumably about the same mass, in order of magnitude, is therefore established to distances from the center of a cluster where the effects of encounters become too weak and the characteristics of the velocity distribution go over into those of Smoluchowski distributions. As was shown in this paper the average jump in velocity dispersion from the interior of the large clusters to the general field can be quantitatively related to the ratio of the total mass of all cluster nebulae and of all field nebulae in a very large volume of space [Eqs. (10) and (11)]. Furthermore, according to data kindly supplied me by Dr. Hubble the velocity dispersion in clusters depends on the central density of the cluster. These observations check a theoretical correlation between the total radius, the velocity dispersion and the average central density (or the total mass) of a cluster which may be derived on the assumption that a globular cluster is a statistically stationary assembly.

(e) The time of formation of a stationary cluster of nebulae according to an estimate previously made[16] is of the order of 10^{18} years. Since clusters of nebulae in their present extents could not have existed in a greatly contracted universe[16] we are here confronted with a contradiction to the hypothesis of an expanding universe which allows only a few billion years for the clusters to be formed.

(f) In a stationary universe the formation of clusters of nebulae should, according to Boltzmann's principle be accompanied by a segregation of nebulae of different mass. Evidence for this effect has now also been secured and will be presented in a forthcoming publication.

[19] S. Smith, Astrophys. J. **83**, 23 (1936).

(g) A number of the structural and kinematic features of nebulae such as the density and velocity distributions in globular and elliptical nebulae furnish most convincing evidence[8] that these nebulae have reached statistically stationary states and that the procedure employed in the derivation of the fundamental relations (26) and (28) concerning the luminosity function of nebulae can thus be directly justified. For the quantitative discussion of the morphology of nebulae and the relaxation times involved we refer to previous publications.[8]

(h) The observed second-order effects in the redshift of light from nebulae so far favor the assumption of a stationary universe. Hubble[4] states as the conclusion of his investigation on the number of nebulae depending on apparent magnitude, that "Careful examination of possible sources of uncertainties suggests that the observations can probably be accounted for if redshifts are not velocity shifts. If redshifts are velocity shifts, then some vital factor must have been neglected in the investigation." The second-order effects involved must however be rediscussed once a better luminosity function is established and also more information is available on the effects of "nebulae as gravitational lenses."

In conclusion this relative appraisal may be made. The hypothesis of the expanding universe compensates for the instability of a uniform distribution of matter through an all over expansion and explains the redshift as due to real velocities. On the other hand this hypothesis is in contradiction with several features of the large scale distribution of matter which can satisfactorily be accounted for on the hypothesis of a stationary universe. Expansion on this theory is assumed to be unnecessary because of dynamic stabilization of the universe through the formation of large scale condensations. The redshift in this case must find an independent explanation, for instance as a gravitational drag of lights as I have proposed it some time ago.[20]

[20] F. Zwicky, Proc. Nat. Acad. Sci. **15**, 773 (1929) and Phys. Rev. **34**, 1623 (1929).

Proportional Counter Amplification at Low Voltages*

M. E. Rose and W. E. Ramsey†
Bartol Research Foundation of the Franklin Institute, Swarthmore, Pennsylvania

(Received February 13, 1942)

The investigation of gas amplification in proportional counters has been extended to low voltages where the transition to ionization chamber behavior is observed. In order to avoid field distortion due to positive ion space charge, it is necessary to use a source of radiation which is not too strong. This, in turn, necessitates the measurement of very small ionization currents (of order 10^{-14} ampere) at low gas amplification. A counter has been designed which is cabable of measuring the small ionization current without amplification and by a comparison with the observed amplified current at higher voltages, the amplification factor is directly obtained. In accordance with previous results, the low voltage gas amplification in polyatomic and simpler gas mixtures is qualitatively the same. From a comparison of the experimental results with the theoretical expression previously derived for the amplification factor it is concluded that at low voltages where amplification sets in the fluctuations in energy loss of the electrons initiating avalanches plays an important role. These fluctuations correspond to a distribution in starting positions of the avalanches with the result that the amplification sets in gradually and at considerably lower voltages than would be expected on the basis of the observations at high voltages.

I. INTRODUCTION

THE development and application of proportional counters are to a very large degree dependent upon information concerning the gas amplification to be expected under given conditions of counter voltage, counter geometry, nature of the gas filler, and gas pressure. While the criteria as to desirable counter characteristics are determined by the type of experiment and the purpose for which the counter is to be used, it is in general advantageous to choose operating conditions which permit one to obtain large and stable amplification. That is, it is essential that the counter not only amplify the charge (formed by the primary radiation) by a large factor, but the gas amplification should not change too sensitively with voltage. In order to define the circumstances under which such amplification may be obtained, a preliminary investigation[1] was undertaken, the results of which may be summarized as follows.

According to the work reported in I, gas mixtures can be roughly classified into two categories based on the voltage dependence of the amplification factor.[2] Mixtures rich in a polyatomic constituent (ethyl alcohol, ethyl ether, commercial methane, and boron trifluoride were investigated) exhibit comparatively stable gas amplification with an amplification factor increasing essentially exponentially with voltage across the counter up to the high voltage limit of the proportional region. Mixtures in which the dominant constituents are simple gases of the monatomic or diatomic type (argon, neon, oxygen, hydrogen, etc.) are characterized by an amplification factor which at high voltages increases extremely rapidly (much faster than exponentially) with counter voltage. At lower voltages, however, the amplification in counters filled with these gases is again less sensitive and comparable with that obtained with polyatomic gas mixtures. From the experience with counters filled with methane and argon it appears that the amplification factor at a given voltage increases with added amounts of the simpler gas without any noticeable loss of stability until a critical argon concentration is reached. Thus one may expect the optimum mixture to be one containing both polyatomic and simple constituents with the concentration of the latter as great as is consistent with voltage "insensitivity." It may also be added that whether or not a mixture gives stable amplification depends on the pressure, with the critical concentration also varying with

* A brief account of the following work appeared in Phys. Rev. **61**, 198 (1942).

† The design of the apparatus was carried out by the second-named author (W.E.R.), while the measurements and the interpretation of the data were obtained by the first author (M.E.R.).

[1] M. E. Rose and S. A. Korff, Phys. Rev. **59**, 850 (1941), referred to in the following as I.

[2] The amplification factor is defined as the ratio of the amount of charge collected by the central wire (anode) to the amount of charge originally formed by the primary radiation. In the proportional region of counter voltage the amplification factor is independent of the amount of primary ionization.

change of pressure (cf. Fig. 3 of I). Too low a pressure promotes instability.

Finally, a theoretical analysis based on a simple avalanche model, providing a mechanism for the amplification process, gave a result for the amplification factor which was in substantial agreement with the observations in the case of the stable type mixtures. Arguments were advanced which make it plausible that the radically different behavior of unstable type mixtures is caused by the release of secondary electrons by photoelectric effect at the outer cylinder (cathode). This effect is neglected in the theory and would not be expected to play a role for the polyatomic gases.

II. THE PRESENT INVESTIGATION

Because of instrumental limitations the measurements in I were confined to high voltages and large amplification factors. These measurements have now been extended by the present investigation into the region of low gas amplification where the transition to ionization chamber behavior is observed. In addition to the interest attached to a study of this transition region the present method also permits a more direct determination of the amplification factor than was hitherto possible.

The principle of the method used here is based on the following facts: At very low counter voltages, but sufficiently high to avoid ion recombination (a few volts at the gas pressures, of the order 10 cm Hg, ordinarily used), all the charge formed by the primary rays is collected *without amplification*. The counter, when designed to measure such charge or the current due to it, then functions as an ionization chamber. That this is the case may be recognized from the measurements of the current to the central system as a function of voltage on the cylindrical cathode. Up to a certain limiting voltage this current is found to be constant. At the limiting voltage, threshold voltage for proportional counter behavior, amplification sets in and the measured ionization current begins to increase with counter voltage. The amplification factor at any particular voltage is then obtained directly from the ratio of the corresponding ionization current to the constant current measured below the threshold voltage.[3] For this reason it is essential that the ionization current below the threshold voltage be measured with care. Since this current must be quite small (of order 10^{-14} ampere in the present experiment, cf. Section III), it is important that the counter be so designed as to incorporate all the constructional refinements of an ionization chamber. This problem of design is considered in the next section.

III. APPARATUS AND PROCEDURE

The design of the apparatus and the experimental procedure to be followed are entirely determined by the size of the minimum current to be measured. This minimum current, or ionization current without any gas amplification, cannot, as one might at first suppose, be made arbitrarily large by using a very strong source of radiation. While using such an intense source would obviate the necessity for sensitive measuring apparatus, and general care in eliminating leakage, it would result in the wire being constantly surrounded by a dense cloud of positive ions for high gas amplifications. This positive ion sheath effectively reduces the electric field about the wire and distorts the phenomena to be observed.[4] In order to avoid such a limitation the ionization chamber and the measuring circuit were designed with sufficient care to permit the use of a weaker source and a corresponding minimum current of 10^{-14} ampere. That with this arrangement any positive ion sheath which may exist introduces no field distortion is evidenced by the fact that a lead absorber placed between the radium source and the chamber *reduces the measured current by the same relative amount for all cylinder voltages*. Furthermore, measurements taken with the radium entirely removed demonstrates that, over the same range of potentials, there is a complete absence of leakage phenomena.

In the tube *A*, Fig. 1, the usual Geiger-Mueller counter geometry was preserved, and the tube and wire were submitted to the cleaning and

[3] With the method employed in I, it is necessary to know the specific ionization of the primary rays and their energy and path length in the counter. The chief difficulty lies in determining the specific ionization since this has been measured in comparatively few gases.

[4] See C. G. Montgomery and D. D. Montgomery, Rev. Sci. Inst. 11, 237 (1940).

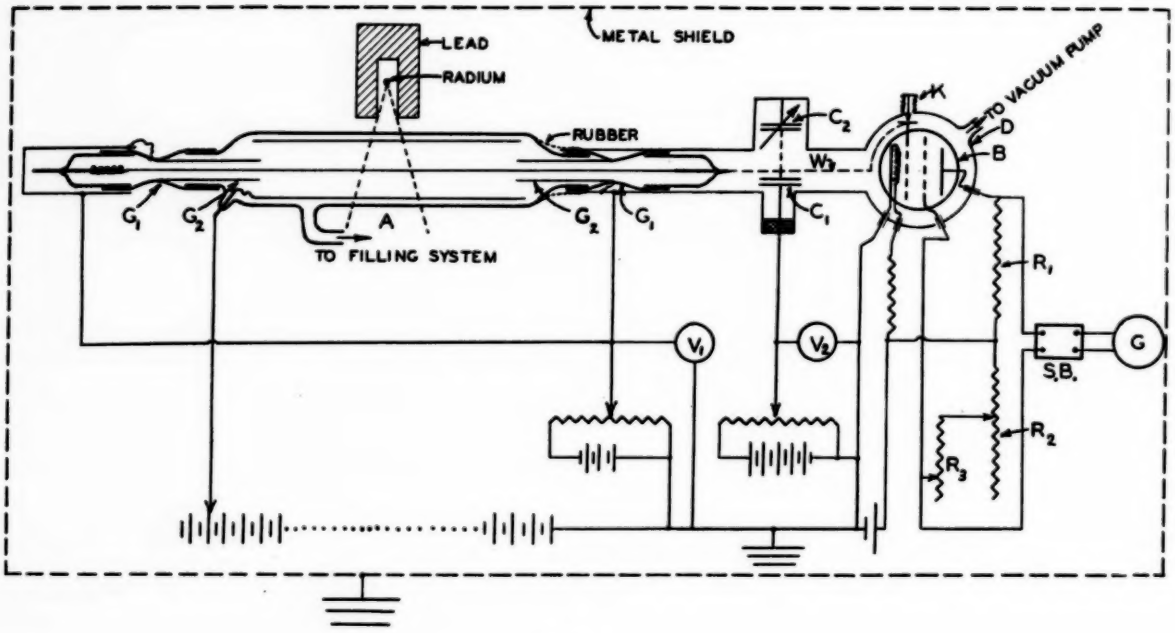

FIG. 1.

baking processes employed in preparing fine counters. The ends of the tube were, however, specially constructed to eliminate all leakage from the cylinder to the wire. One end of each of the guard rings G_1 is fastened by a copper to glass seal to the body of the counter and at the other end by a similar seal to a glass tube which carries the counter wire. The guard rings G_1 prevent direct leakage from cylinder to wire while the shields G_2, supported by G_1, prevent charge moving on the glass surfaces from inductively affecting the potential of the wire.

As shown in Fig. 1 the collecting wire of the counter-ionization chamber is connected directly to the grid of an FP-54 pliotron (electrometer tube). Closing the key K momentarily assigns to this grid and wire system (W) a potential V_1 which is altered only by the ionization current to be measured and the grid current of the vacuum tube. Since the pliotron is operated at or very near the floating potential, the grid current referred to is always less than 5 percent of the smallest current measured. A standard balanced circuit with a fairly sensitive galvanometer G provides the means for measuring variations in the potential of the wire system. With the key K closed the galvanometer spot is brought to zero deflection by adjusting R_2 and R_3. After K is released the ionization current alters the potential of this system and produces a drift of the spot. This drift, however, is continuously checked by alterations of V_2 and a zero deflection is maintained. This means, of course, that while charge is being collected by W the potential of W is kept constantly at V_1. This null procedure eliminates the leakage between guard ring and wire which would appear if the voltage of the central system were allowed to change to values differing from the guard ring potential V_1. After a minute or two has elapsed since the release of K, the total change in V_2 is recorded. With the previously determined[5] change in the potential of W associated with a given change of V_2 (for a given capacity of W), the total change of V_2 provides us with the total charge collected during the interval involved. Spurious ionization currents are eliminated by evacuating the metal chamber containing the electrometer tube and the associated connecting cylinders. Since the system is thus sealed the key K is fastened to the inner side of a small copper

[5] With K closed, alterations of V_1 result in a deflection of the galvanometer spot. Such deflections vary linearly with ΔV_1 over a wide range. Now with K open alterations ΔV_2 result in deflections of G which may, from the first calibration, be identified with known changes in the potential of W.

syphon which permits of operation from the outside. Provision is made for increasing the capacity of the wire system from twenty to several thousand centimeters by adding a series of capacitors. Control is achieved through a ground metal joint not indicated in the diagram. This entire unit is represented in Fig. 1 by the variable capacitor C_2. Thus by varying C_2 it is possible to measure currents varying by factors of ten thousand or more and to maintain at the same time small potential variations of the central system. The null procedure involving a variable V_2 can be used over a wide range of currents if desired by causing V_2 to vary over a wide range. Actually for the larger currents, where all leakages are unimportant, the rate of drift method was utilized. Passing from one procedure to the other during a run presents no difficulties whatever.

It should be pointed out that although the absolute values of the capacity of W for different settings of C_2 were fairly well known, only the ratios of these values are required for a determination of the amplification factor, which is itself a ratio of currents. These ratios of capacity were determined experimentally by measuring the rate of change of potential of the central system with the different values of C_2 for a series of fixed ionization currents. It should be further pointed out that the number of particles which pass through the counter is sufficiently large to eliminate the appearance of any measurable statistical fluctuations in the ionization current.

IV. RESULTS AND DISCUSSION

As typical curves the amplification factor is given in Fig. 2 as a function of cylinder voltage for an argon-oxygen mixture (94 percent argon) and for commercial methane at pressures of 9 and 32 cm Hg. It will be noted that the low voltage behavior of gas amplification for both the polyatomic and simpler gases is qualitatively the same, in contrast to the high voltage dependence.[1] The larger amplification factor with argon and the fairly rapid decrease of amplification factor with increasing pressure is in accord with the results of the previous investigation. Moreover, the theoretical formula there derived for the amplification factor [cf. Eq. (1) below] is in conformity with the observed pressure dependence since the threshold voltage should increase with pressure (cf. also Table II of reference 1).

The most interesting feature of the present results is the transition from the ionization chamber to the proportional counter region. It may be seen from Fig. 2 that the sub-threshold ionization current upon which the quantitative results depend (represented by the horizontal portion of the curves), is well defined, especially in the case of the higher methane pressure, where the current measured at seven different voltages showed an extreme variation of one percent. In the case of the other curves shown, for which gas amplification begins at a lower voltage, the sub-threshold current was fixed by fewer points, but in any case at least four points with a variation of less than 3 percent were obtained.

The measurements were extended to voltages sufficiently above the threshold to allow a comparison with the previous results. In such cases as are comparable approximate agreement is found.[6] Another basis of comparison consists in

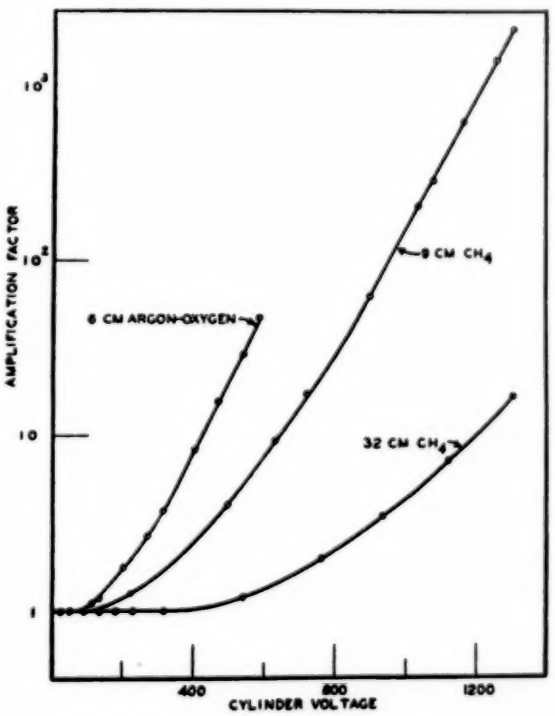

FIG. 2.

[6] Exact agreement could not be expected because of the effect of the difference of cathode sizes in the counters previously used (1-cm diameter in most cases) and that used here—2.7-cm diameter.

the attempt to fit the observed results by a theoretical curve obtained from the aforementioned formula for the amplification factor A [cf. Eq. (14) of I]:

$$A = \exp k V^{\frac{1}{2}}[(V/V_t)^{\frac{1}{2}} - 1], \qquad (1)$$

where V is the cylinder voltage and V_t is the threshold voltage which, for reasons given below, is to be regarded as an adjustable parameter. In Eq. (1) k is a constant dependent on the nature of the gas, gas pressure, and wire and cylinder radii.[7] This formula was successful in accounting for the results obtained in the previous work (in the case of stable amplification) and by means of the comparison between theory and experiment the table of threshold voltages given in I was obtained.

When a comparison between the present results and the theoretical formula is made, two points of disagreement are noted:

(a) On a logarithmic or linear scale Eq. (1) predicts a sharp cut-off of the amplification, that is, a finite slope ($d \log A/dV$) at amplification unity, in contrast to the gradual increase observed; (b) The threshold voltages predicted by (1) are much larger than those observed (Fig. 2). The observed threshold (120 volts) in the case of 9-cm methane may be compared with the value of about 400 volts to be expected from the results of I.

This disagreement is, however, apparent only when one takes into consideration the assumptions on which the derivation of (1) is based. The assumption of interest in the present connection involves the neglect of fluctuations in energy loss. Thus, it is assumed that at a given cylinder voltage there exists a point at a distance r_0 from the wire axis at which the avalanches start and that *this distance is the same for all electrons initiating such avalanches*. The value of r_0 which was used in obtaining (1) was, in fact, the average starting point for sustained ionization. While this assumption would be expected to be valid for large voltages, for which the mean r_0 is considerably greater than the wire radius r_1, it should also be expected that it will break down at low voltages, particularly at the threshold voltage. This is immediately evident when one considers the effect of a distribution in starting points r_0 which would naturally enter as an essential component of the avalanche model when fluctuations are taken into account. At low voltages, the gas amplification is at first caused by those few electrons which have large r_0 (the "tail" of the r_0 distribution). As the voltage is increased the r_0 distribution function shifts outwards from the wire until it is virtually entirely outside the point r_1 so that practically all the electrons contribute to the amplification. Therefore, the amount of charge collected when gas amplification sets in, and hence the amplification factor itself, would increase more slowly than if all avalanches started at the same point and a curve of the sort obtained ($d \log A/dV$ or $dA/dV = 0$, for $A = 1$) would be expected. One may say that the form of the amplification curve near the threshold is to a certain extent a picture of the r_0 distribution function for larger r_0 than the average value.

It is also clear that the effect of a distribution in starting points implies the onset of gas amplification at a considerably lower voltage than would otherwise be expected. Roughly speaking, the difference between the threshold voltage obtained from Eq. (1) and that observed would be directly correlated with the difference between the average r_0 and the largest value of r_0 for which the number of electrons initiating avalanches is appreciable.

At higher voltages when all but the small r_0 tail of the distribution function lies outside r_1, so that almost all the primary electrons are effective in initiating avalanches,, the assumption of a fixed r_0 previously made, while not yet rigorously fulfilled, would be more satisfactory than at the threshold where only the most energetic electrons are effective. Thus, Eq. (1) may be regarded as an asymptotic formula valid for very large voltages. From the agreement between theory and observations found in I, it follows that the approach to the asymptotic formula is sufficiently rapid as to justify its use for amplication factors greater than about 10. From the picture presented here it would appear that the constant

[7] The constant k also depends on the form of the energy distribution of secondary electrons arising in the avalanche process. In the approximation made in deriving (1) the relative number of slowest electrons enters and, as is shown in I, a plausible assumption can be made for this quantity. Otherwise, in the absence of information as to the detailed form of the energy distribution, k would have to be regarded as a second adjustable parameter. The first procedure was adopted in I.

V_i in the formula should be interpreted as an "extrapolated" threshold voltage. With these restrictions as to the realm of validity of the formula, the essentially linear portions of the curves in Fig. 2 may be fitted by a function of the voltage of the form (1).

Finally, it may be added that other effects may contribute in determining the shape of the amplification curve at the true threshold voltage. Thus, "end-effect," (that is, decrease of the field near the ends of the cylindrical cathode) would have the effect of suppressing a sharp rise of gas amplification but would not affect the magnitude of the threshold voltage. It is probable that the proposed explanation of the results constitutes the most important factor operative in determining the low voltage dependence of the amplification factor.

APRIL 1 AND 15, 1942 PHYSICAL REVIEW VOLUME 61

Thermionic Properties of the Iron Group

H. B. WAHLIN
Department of Physics, University of Wisconsin, Madison, Wisconsin

(Received February 3, 1942)

As a preliminary to the main problem, the temperature scales for Fe, Ni, and Co have been determined for vacuum heat treated specimens of the metals. The thermionic work functions found differ from those reported by other investigators and are as follows: β-Fe 4.48 ev, γ-Fe 4.23 ev, Ni 4.61 ev, and Co 4.40 ev. The probable cause for the difference between these results and those of others is discussed and the effect of minute quantities of certain impurities is described.

INTRODUCTION

THE thermionic and photoelectric properties of the members of the iron group have been investigated carefully by Glasoe,[1] Cardwell,[2,3] Fox and Bowie,[4] and others. However, recent ideas on heat treatment, as well as on the effect of small amounts of impurities, have changed the procedure sufficiently so as to justify a repetition of their work. Impurities become particularly important in studying metals with as low melting points as have the members of the iron group, since these impurities may, under prolonged heat treatment, diffuse to the boundary and thus give a highly impure surface. Obviously, since thermionic emission is to a major extent dependent on the surface conditions, the work function and the constant factor in Richardson's equation will be appreciably affected.

In order to obtain reliable results it is necessary to determine the temperature scales of the metals under conditions of heat treatment as nearly identical as possible with those used in the thermionic studies. This determination has been carried out and the results have been published elsewhere.[5]

EXPERIMENTAL PROCEDURE

In making thermionic measurements it is in general more desirable to use a flat strip filament rather than a round one. The reason for this is that when a disappearing filament optical pyrometer is used in measuring the temperatures the deviation from Lambert's law is likely to give a non-uniform field if a round filament is used and a good match cannot be observed, thus increasing the error in the temperature measurement. In all the work described below flat strips of about 0.07 mm thickness and 2 to 3 mm width were used.

These filaments after being rolled to uniform thickness were cleaned carefully by dipping in chromic acid cleaning solution to remove greases

[1] G. N. Glasoe, Phys. Rev. **38**, 1490 (1931).
[2] A. B. Cardwell, Proc. Nat. Acad. Sci. **14**, 439 (1928).
[3] A. B. Cardwell, Proc. Nat. Acad. Sci. **15**, 544 (1929).
[4] G. W. Fox and R. M. Bowie, Phys. Rev. **44**, 345 (1933).
[5] H. B. Wahlin and R. Wright, J. App. Phys. **13**, 40 (1942).

and other organic impurities from the surface. This procedure was followed by a careful washing and a slight etching of the surface with dilute hydrochloric acid. A final rinsing with hot distilled water followed. This method of cleaning gave results identical with those obtained when hot KOH was substituted for the chromic acid so that apparently the acid introduced no measurable impurities. After the cleaning, the filaments were not touched with bare hands.

The experimental tubes were the conventional single guard ring type with the filaments mounted in a U shape. The collector and guard ring were of molybdenum. These were given a prolonged intermittent induction heating in a Pyrex tube connected to one auxiliary vacuum system, after which they were assembled to form the main thermionic tube.

The assembled tubes, connected to a vacuum system, were baked for periods ranging from 100 hours to 500 hours at temperatures ranging from 450° to 300°C. The reason for this range in baking temperatures was so that a test could be made on the influence of high temperature baking on the work function. It has been suggested that if these high temperatures are maintained while the filament is being heated, the volatile constituents of the glass will react with the filament and will change the work function. An increase in the work function was observed when the filaments were heated during baking at 450°. This increase, however, was too small to ascribe it definitely to the procedure in heating.

The technique finally adopted was to bake the tube for 24 hours at 450°C. The furnace was then removed and the collector and guard ring given an induction heating to such a temperature that they appeared a very dull red in a darkened room. The furnace was then replaced and the baking continued at 300°C. After twelve to twenty-four hours of this treatment, the filament heating was begun below red heat and the temperature gradually raised to about 1250°K. It was found that if the temperature was raised gradually so as to allow sufficient time for the small crystal units to grow into larger ones, prolonged heating at 1250°K could be carried out without undue evaporation. The low temperature induction heating apparently did not throw any non-volatile impurities onto the filament because the same results were obtained when no induction heating was used as when it was used. However, the degassing time was materially reduced when induction treatment was combined with baking.

The experimental tubes were kept on the vacuum system continuously and the final vacuum reached with the filaments heated was 3×10^{-8} mm.

RESULTS

Iron

First sample: This was a specimen prepared electrolytically from a ferrous sulphate solution and an iron anode. The results were unreliable and a steady state could not be reached. A strip of this specimen annealed in hydrogen gave a distinct trace of hydrogen sulphide, showing an inclusion of sulphur in the electrolytic deposits. The liberation of the sulphur in the experimental tube contaminated it in such a way that subsequent backing failed to remove the contamination. The tube was therefore destroyed to prevent its future use. Probably a prolonged heating in hydrogen of iron prepared from a sulphate solution would remove the impurity.

Second sample: The second group of specimens was prepared electrolytically from a ferrous chloride solution and an armco iron anode. These specimens gave satisfactory results with prolonged vacuum heat treatment.

The procedure in preparing a specimen for the final data was to raise the temperature of the filament slowly to a final degassing value of 1250°K. Several days were generally taken to get it to this temperature. Care was then taken that the temperature did not at any time fall below the A_3 point ($\beta-\gamma$ transition). After a stable condition had been reached and the thermionic data for γ-iron were taken, the temperature was lowered into the β-range and the heating continued. Care was now taken to keep the filament temperature below the transition point. When a steady state had again been reached and the data were obtained, the temperature was again raised (with two of the specimens) into the γ-region and further thermionic results recorded. These were found to be in agreement with the first ones.

The average of the results for 4 filaments,

which showed no appreciable temperature gradient, is:

Below $\beta-\gamma$ transition,

$$\varphi=4.48\pm0.06 \text{ ev}, \quad A=26 \text{ amp/cm}^2/T^2.$$

Above $\beta-\gamma$ transition,

$$\varphi=4.21\pm0.06 \text{ ev}, \quad A=1.5 \text{ amp/cm}^2/T^2.$$

Probably the most reliable value for the work function published is that which Glasoe[1] obtained photoelectrically. He reported a value of 4.77 ev. Glasoe heated his specimen to a relatively high temperature and then cooled it to room temperature before measurements were made. This procedure may account for the difference between his results and those reported here. For, when the iron passes from the γ to the β form, the equilibrium distribution of crystal planes on the surface of the specimen is disturbed and heating time in the β state must be allowed in order to reestablish this equilibrium—partly by thermal etching and partly by migration of atoms along the surface. The author attempted to check this hypothesis by making a set of determinations of the work function, immediately after the filament had been changed from the β to the γ and from the γ to the β. Because of a rapid initial change in the surface, reliable results could not be obtained. All that can be said is that the work function calculated was definitely higher than the equilibrium value. This would indicate that an appreciable part of the change in the work function with degassing reported by observers is not a degassing effect, but is due to the gradual establishment of the equilibrium distribution of crystal planes exposed to the surface.

Two qualitative observations on iron should be noted here. It was found that while the filaments showed no crystal structure visible with the naked eye initially, with continued heating, crystal growth took place, and single crystals extending the full width of the filament (about 2.5 mm) were sometimes observed. In general, the filaments had a "galvanized" appearance after heating. This effect was not noted with nickel and cobalt. It was also found that each time the filament passed through the A_3 point, it warped and with repeated transitions twisted sufficiently to short circuit portions of the specimen.

Nickel

First sample: This was a specimen of cobalt free nickel prepared at the Research laboratory of the International Nickel Company by the electrolysis of a chloride solution and a platinum-iridium anode.

Filaments of this material gave initial work functions of about 4.8 ev. Continued heating increased the φ to values ranging from 5.0 to 5.2 ev with A ranging from 800 to 3000 amp/cm^2/T^2. Flashing to temperatures close to the melting point increased the work function if it produced any change at all. Eight filaments from this sample were used and various changes in heating were tried. The results for all were in the range listed above. These values are in the range reported by Glasoe[1] and Fox and Bowie.[4]

Second sample: This consisted of a sintered strip made from cobalt-free powder by the International Nickel Laboratory. The initial φ ranged from 4.8 to 5.0 ev with a high value for Richardson's A. Continued heating and flashing brought the value down until a final stable value was reached. The average for three specimens is

$$\varphi=4.61\pm0.06 \text{ ev}, \quad A=30 \text{ amp/cm}^2/T^2.$$

Third sample: In order to test whether or not the difference between the two samples discussed above might be due to a platinum contamination from the anode, a sample was prepared in this laboratory. A nickel chloride solution containing 0.1 percent cobalt was used with low cobalt nickel shot as the anode material. The deposits were made on stainless steel from which they could be removed with ease. The first deposit was discarded in order that an equilibrium might be established between the composition of the electrolyte and that of the anode. This was felt to be essential so that the successive deposits would have the same composition.

Two filaments of this material gave identical results *viz.*,

$$\varphi=4.61 \text{ ev}, \quad A=70 \text{ amp/cm}^2/T^2.$$

Thus, the φ agrees with the value obtained for the sintered sample, but the A has more than

twice the value. This may be due to the small amount of cobalt in the latter sample, and if so, may be of considerable interest and importance. However, before any conclusions are drawn further studies must be made with samples of varying cobalt content.

Fourth sample: A new deposit was made from the same electrolyte as was used in preparing sample 3. In this case platinum was used as the anode material.

This sample gave a work function which increased with continued heating and flashing to a final value in the same region as that obtained with sample 1. The behavior of this sample throughout the heating was similar to that of sample 1. The A in this case was abnormally high.

Fifth sample: This was a strip of high purity nickel which had been melted in a vacuum. The method of preparation is unknown. This failed to give good voltage saturation and as the results would be meaningless, no data were taken.

It would seem from a comparison of the results of the first four samples that platinum when used as an anode material has a marked effect on the thermionic properties. The amount of platinum contamination may not be enough to influence the volume properties markedly, but as pointed out earlier, a prolonged heat treatment may cause it to diffuse to the surface and thus create a highly impure surface condition. The thermal etching of the surface may also uncover more platinum and increase the surface concentration. The fact that with samples 1 and 4 continued heating increased the work function might be taken as evidence of either or both of these processes. In the case of samples 2 and 3, where possible platinum contamination was absent, continued heat treatment decreased φ.

Cobalt

The results on cobalt are not as satisfactory as those on iron and nickel, in that the spread between runs was greater. All the thermionic data were taken above 1120°K, in the region where the metal has a face-centered cubic structure.

First sample: This specimen was made electrolytically from a reagent quality cobaltous chloride solution with cobalt cubes as anode material. The metal was again deposited on stainless steel. The results of studies with eight filaments gave

$$\varphi = 4.41 \pm 0.10 \text{ ev}, \quad A = 41.$$

Second sample: The electrolyte used in this case was from the same supply as above, but an anode of spectroscopic graphite was used. The behavior of these filaments was so nearly the same as that of specimen 1, that one can conclude that no serious contamination is introduced when graphite is used.

The work function given above is higher than the value (4.12 ev) listed by Cardwell[3] for the face-centered cubic form of cobalt. The author is at a loss to explain the difference.

From the observations listed above, one must conclude that the problems encountered in the preparation and treatment of metals increase as the temperature to which the metal can be heated is lowered. Whereas in the case of a high melting point, low vapor pressure metal such as tungsten or molybdenum, a large part of metallic impurities may be removed by high temperature heating, this is not always possible in the case of low and intermediate melting point ones. Great care must therefore be taken so as to eliminate, during the preparation of the metal, non-volatile impurities even though they are present in minute quantities. This is borne out by the results on nickel described above.

It is the author's belief that as a result of the evidence presented above, the work functions of the members of the iron group can be fixed as

β-Fe	4.48 ± 0.06 ev,	$A = 26$
γ-Fe	4.21 ± 0.05 ev,	$A = 1.5$
Ni	4.61 ± 0.05 ev,	$A = 30$
Co	4.41 ± 0.10 ev,	$A = 41$.

In conclusion, the author wishes to acknowledge the financial support given by the Wisconsin Alumni Research Foundation through the University Research Committee and also the assistance given by the Research Laboratory of the International Nickel Company in furnishing samples of pure electrolytic and sintered nickel. Mr. E. M. Wise of that laboratory has made many helpful suggestions. Dr. Rufus Wright, Mr. George Jarvis, and Mr. George Olmsted have rendered valuable service in helping to obtain the data.

The Temperature Scale, Thermionics, and Thermatomics of Tantalum

MILAN D. FISKE
Department of Physics, University of Wisconsin, Madison, Wisconsin
(Received January 17, 1942)

The energy cycle $\varphi_0^- + \varphi_0^+ = \varphi_0^0 + V$ has been followed experimentally for tantalum. This involved a redetermination of the temperature scale with emissivity varying linearly from $\epsilon_{\lambda T} = 0.439$ at $T = 1200°K$ to $\epsilon_{\lambda T} = 0.384$ at $T = 2400°K$ for $\lambda = 0.669\mu$. Thermionic measurements of the electron work function and of the positive ion work function yielded, respectively, $\varphi_0^- = 4.19$ ev and $\varphi_0^+ = 10.0$ ev, with an electron emission constant $A^* = 55$ amp. cm^{-2} deg^{-2}. By a gain of weight method the work function of the neutral tantalum atom was found to be $\varphi_0^0 = 7.97$ ev. The ionization potential of tantalum is not known but may be estimated to be about $V = 7.3$ ev. These values fail to close the energy cycle by 1.1 ev which is believed to be outside the experimental uncertainty of the measurements.

INTRODUCTION

IT may be shown that for a given metal the electron work function φ^-, the positive ion work function φ^+, the ionization potential V, and the work function of the neutral atom φ^0 at any temperature are related by the equation

$$\varphi^- + \varphi^+ = \varphi^0 + V. \qquad \text{(A)}$$

This cycle has been followed experimentally for but a few metals (W, Mo, Cb), and the agreement of the measured values with the prediction of (A) is satisfactory except for the case of columbium. At the time this present program was initiated (1937) no data for tantalum on the temperature scale or on φ^-, φ^+, or φ^0 had appeared in the literature since the technique of high vacuum had been advanced to its present stage. Data on φ^+, φ^0, and V were entirely lacking.

The purpose of this work has been to determine if the cycle closes for tantalum. To that end the temperature scale was redetermined, a new measure of the electron work function made, the positive ion work function obtained, and the thermatomic work function calculated from a "gain of weight" method.

TEMPERATURE SCALE AND EMISSIVITY

The temperature scale for tantalum was determined by using the methods described by Wahlin.[1] A strip of the metal of 0.055-mm thickness was wrapped about a 3-mm diameter mandrel and welded to form a tube of 85-mm length. A 0.55-mm hole drilled into the center of the tube wall served as a blackbody of the same temperature as the tube itself. Stock tantalum[2] from the Fansteel Company was used for the emissivity cylinder, and in all the subsequent phases of this work. This tube filament was mounted in a glass envelope and evacuated. The envelope was baked at 400°C for 200 hours, and the filament outgassed at 2000°K for 1000 hours, with occasional 30-second flashings to 2350°K, until a final vacuum of 4×10^{-8} mm was obtained for temperatures below 1800°K.

The true temperature T of the tube was measured by sighting on the hole a disappearing filament optical pyrometer calibrated directly from gold-point melts in this laboratory, supplemented by the conventional rotating sector method for other temperatures. The brightness temperature T_B was found by sighting the pyrometer either side of the hole. The average spread of readings at any one temperature was less than 0.5°. Data were taken on two different specimens. The average deviation of an experimental point from the resulting T_B *vs.* T plot was less than 1°.[3]

[1] H. B. Wahlin and L. O. Sordahl, Phys. Rev. **45**, 886 (1934).

[2] Of typical analysis Ta 99.9 percent, Fe 0.01 percent (max), C 0.003 percent (max).

[3] In connection with this work it was found the writer had an eye defect which caused his pyrometer readings to be at variance with those of several other observers, far outside the spread of the settings. Agreement was good with sources of large size such as the outside of the filament, but poor for sources of small size, such as the blackbody hole. Thus, in one typical instance Dr. R. W. Wright obtained 1545.7°K for the surface, and 1650.7°K for the hole, while the writer obtained 1545.2°K for the surface and 1643.7°K for the hole. This gave values for the emissivity of 0.415 and

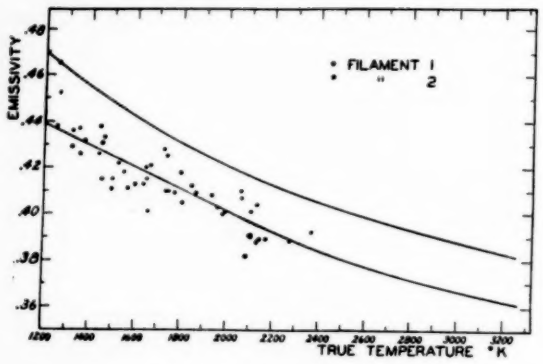

FIG. 1. The emissivity of tantalum at $\lambda=0.669\mu$. Upper plot is from data of Malter and Langmuir.

The emissivity $\epsilon_{\lambda T}$, of tantalum, was calculated from

$$\ln \epsilon_{\lambda T}=C_2/\lambda[(1/T)-(1/T_B)],$$

where $C_2=1.4362$ cm deg. is the second radiation constant, and $\lambda=0.669\mu$ is the effective wavelength at which measurements of T and T_B were made. $\epsilon_{\lambda T}$ was plotted as a function of T (see Fig. 1) and a straight line drawn through the mean of the experimental points. This plot was extrapolated beyond $T=2368°$K parallel to the emissivity data given by Malter and Langmuir.[4] The highest temperature at which the blackbody could be operated was 2368°K, and for higher temperatures T_B as a function of T was calculated from the emissivity curve.

Values of $\epsilon_{\lambda T}$ and T_B as function of T as taken from their graphs are given in Table I. Included are values listed by Malter and Langmuir,[4] by Utterbach and Sandermann,[5] and by Worthing.[6] It is seen that the various temperature scales are in fair agreement except at very high temperatures, and all show the same decrease in $\epsilon_{\lambda T}$ with increasing T, in marked contrast with the temperature independent emissivities of other metals as found in this laboratory.[7]

ELECTRON WORK FUNCTION

The experimental set-up and heat treatment schedule for measurement of the electron work function was that previously reported by Wahlin and co-workers.[1] A tantalum wire filament 0.070 cm in diameter was slightly flattened by rolling, bent into a hair pin shape, and mounted inside a collector plate equipped with a single guard ring. The slight flattening of the filament largely eliminated objectionable deviations from Lambert's law, so that the filament when heated appeared of uniform brightness across its entire width.

A careful schedule of baking, induction heating of collector plates, and heat treatment of the filament was followed for each specimen. At the end of a typical schedule of 300 hours with the filament at 2600°K a final vacuum of less than

TABLE I. Temperature scale and emissivity data for tantalum. W—Worthing; L-M—Langmuir-Malter; U-S—Utterbach-Sandermann.

T °K	T_B MDF-RWW	T_B L-M	T_B W	T_B U-S	$\epsilon_{0.669}$ MDF-RWW	$\epsilon_{0.665}$ L-M	$\epsilon_{0.665}$ W
1250	1193				0.437	0.469	
1300	1238				.435		
1400	1327	1332	1329	1337	.430	.455	0.442
1500	1415				.425		
1600	1502	1508	1506	1508	.421	.442	.434
1700	1589				.416		
1800	1675	1682	1680	1678	.411	.431	.426
1900	1760				.406		
2000	1844	1851	1851	1843	.401	.421	.418
2100	1925			1926	.397		
2200	2007	2018	2018		.392	.413	.411
2300	2089				.388		
2400	2169	2181	2180		.384	.405	.404
2500	2249				.381		
2600	2329	2341	2339		.378	.399	.397
2700	2410				.375		
2800	2488	2499	2495		.372	.393	.390
2900	2561				.370		
3000	2634	2652	2647		.367	.388	.384
3100	2707				.365		
3200	2781	2803			.363	.384	
3300	2855		2870		.360	.381	.375

0.438, respectively. Since the defect was the writer's all emissivity data were taken by R. W. W., and on all subsequent work care was taken that the image in the pyrometer was of sufficient size that the defect did not introduce an error in temperature measurements.

The defect may be explained if one postulates that the minimum retinal area required by the eye for intensity matches is greater for the writer than is normal. It is well known that brightness matches cannot be made accurately between point sources, but rather that the eye requires a certain image area as a minimum for significant comparison. This "minimum area" may well vary from one eye to the next. If that area should be larger than the size of the image of the pyrometer-filament and blackbody hole the eye might attribute the lower brightness of the region around the hole to the hole itself. Thus the hole brightness would be taken as an average of the brightness of the hole plus a small region about the hole. This would result in the measurement of the hole temperature being fictitiously lower than should be. Clearly this effect would disappear for a source of uniform brightness over a large area.

It might appear from this that measurement of temperatures of small filaments, etc., with an optical pyrometer would have some uncertainty unless the observer by comparison with several other observers or by other tests knows himself to be free of this defect.

[4] L. Malter and D. B. Langmuir, Phys. Rev. **55**, 743 (1939).

[5] C. L. Utterback and L. A. Sandermann, Phys. Rev. **39**, 1008 (1932).

[6] A. G. Worthing, Phys. Rev. **28**, 190 (1926).

[7] These include W, Mo, Fe, Ni, Co, Rh, Th, Pt, Cb.

3×10^{-8} mm of mercury was obtained for the entire temperature range employed.

Data were taken on three filaments on each of which an average of seven runs was made scattered over 200 hours. A Richardson plot for three runs scattered over 100 hours is shown in Fig. 2. The average deviation of experimental points from any of these linear plots covering a 300° range was less than 0.5°.

The Schottky correction to the work function owing to the field applied to insure absence of space-charge saturation was in each case less than 0.02 ev. This correction used with the value calculated from the Richardson plots leads to a work function of tantalum $\varphi_0^-=4.19$ ev with an average deviation of 0.02 ev, and an emission constant $A^*=55$ amp. cm^{-2} deg.$^{-2}$ with an average deviation of 5 amp. cm^{-2} deg.$^{-2}$.

If one accepts with Riemann[8] a temperature dependence of the work function owing to thermal expansion of the lattice, one may readily show that the Richardson plot will yield the emission constant A as

$$A=A_1\exp\left[(h^2\alpha/4mk)(3n/\pi)^{\frac{2}{3}}\right],$$

where h, m, k have their usual significance, n is the number density of free electrons, α is the coefficient of linear expansion, and $A_1=120$ amp. cm^{-2} deg.$^{-2}$. Employing Worthing's[6] value for α one obtains for tantalum the theoretical emission constant $A=55.8$ amp. cm^{-2} deg.$^{-2}$. If the agreement of this with the experimental value is more than "purely accidental" as Wigner[9] would suggest, one would conclude that for tantalum as for most other pure metals the reflection coefficient is negligible, and moreover, that the roughness factor is unity. The latter conclusion is supported by the fact that filaments removed after use in the measurements exhibited specular reflection, had a very high polish, and felt slippery—characteristics of a microscopically smooth surface.

Table II presents a summary of the data on emission constants of tantalum. Cardwell's photoelectric determination of the work function is probably the best of the previous measures, for the others were obtained before the importance of vacuum conditions was understood.

[8] A. L. Riemann, Nature **133**, 833 (1934).
[9] E. Wigner, Phys. Rev. **49**, 696 (1936).

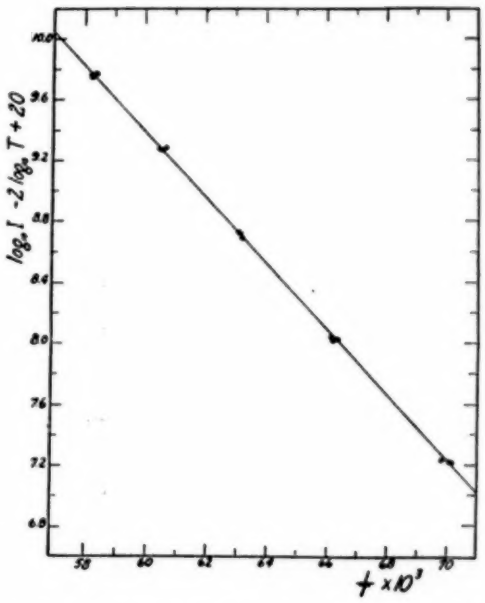

FIG. 2. Richardson electron plots for three different runs spread over 100 hours: $\varphi_0^-=4.19$ ev. $A^*=52$ amp. cm^{-2} deg.$^{-2}$.

Dushman used Worthing's temperature scale to obtain his thermionic values. His data plotted on the temperature scale of this work yield $\varphi_0^-=4.17$ ev, $A^*=85$ amp. cm^{-2} deg.$^{-2}$ in good agreement with the values obtained here.

POSITIVE ION WORK FUNCTION

That metals raised to sufficiently high temperatures emit singly charged positive ions of the parent metal itself was first shown conclusively by Wahlin[10] and shortly after by Smith.[11] These emission currents in general were smaller than the electron emission currents at the same temperature by a factor of 10^6 or so and were appreciable only when there was considerable vaporization of the filament material.

Smith[12] applied Bridgman's[13] thermodynamic treatment of electron emission to this thermal emission of positive ions and obtained the equation

$$\ln I=-(\varphi_0^+e/kT)+2\ln T+ln\ 2\pi k^2eM/h^3 +\ln(1-r)-(H/k)+S. \quad (1)$$

Here φ_0^+ is the positive ion work function, M

[10] H. B. Wahlin, Phys. Rev. **34**, 164 (1929).
[11] L. P. Smith, Phys. Rev. **34**, 1496 (1929).
[12] L. P. Smith, Phys. Rev. **35**, 381 (1930).
[13] P. W. Bridgman, Phys. Rev. **27**, 173 (1926).

the atomic mass; e, k, h, and T have the usual meaning;

$$H=\int_0^T \frac{dT}{T^2}\int_0^T C_{pm}dT, \qquad (2)$$

in which C_{pm} is the specific heat at constant pressure of the ion in the metallic phase, and

$$S=\frac{S_\rho}{k}+\frac{1}{k}\int_0^T \frac{dT}{T^2}\int_0^T C_{p\rho}dT. \qquad (3)$$

$C_{p\rho}$ is the specific heat at constant pressure associated with surface charging, and S_ρ is the entropy at $T=0$ associated with the heat of surface charge.

H may be evaluated by using the scheme of Jones, Langmuir, and Mackay.[14] For C_{pm} one uses C_{vm}, the specific heat at constant volume, in the temperature range 0°K to T_0°K corrected with the semi-empirical equation of Lindemann and Magnus[15] $C_{pm}=C_{vm}+aT^3$. a is a constant calculated from a similar thermodynamic relation

$$C_{pm}=C_{vm}+(9\alpha^2V/\beta T^3)T^3,$$

where V is the atomic volume, and α is the coefficient of linear expansion and β the compressibility both for the metal at the temperature T. C_{vm} is obtained directly from the Debye theory of specific heats in terms of θ, the characteristic temperature of the metal.

This value of C_{pm} is plotted from 0°K to a temperature T_0 where the plot intersects a straight line drawn through the experimental high-temperature values of C_{pm}, which may be represented by $C_{pm}=N+ZT$.

One then obtains for H

$$H=N\ln T+\frac{Z}{2}T+\frac{1}{T}\left(NT_0+\frac{ZT_0^2}{2}-E(T_0)-\frac{2}{5}aT_0^{5/2}\right)-N\ln T_0-ZT_0+F(T_0)+\frac{4}{15}aT_0^{3/2}+\frac{1}{T_0}E(T_0)+\frac{2}{5}aT_0^{3/2}. \qquad (4)$$

Here

$$E(T_0)=\int_0^{T_0} C_{vm}dT$$

and

$$F(T_0)=\int_0^{T_0}\frac{dT}{T^2}\int_0^T C_{vm}dT$$

are given in *Handbuch der Physik*[16] as E/T and F/T, functions of θ/T.

The only data on the specific heat of tantalum are those of Pirani[17] obtained in 1912. His data show such a spread for the few points taken that the uncertainty in N and Z is very great. Further, the purity of the tantalum prepared at this early date is rather questionable. The best values for the data seem to be $N=5.35$ cal. g-atom^{-1} deg.$^{-1}$ and $Z=15\times10^{-4}$ cal. g-atom^{-1} deg.$^{-2}$.

Seitz[18] lists θ for tantalum as 245°K. a may be computed to be $a=1.18\times10^{-5}$ cals. g-atom^{-1} deg.$^{-5/2}$, whence

$$H=-32.0+12.32\log_{10}T+7.5\times10^{-4}T+2530/T. \qquad (5)$$

Then the positive ion equation becomes

$$\log_{10}I+0.688\log_{10}T+1.64\times10^{-4}T+554/T=-5032\varphi_0^+/T+F, \qquad (6)$$

where

$$F=S/2.303+\log_{10}(1-r)+14.29. \qquad (7)$$

The experimental arrangement and procedure for measurement of the positive ion emission

TABLE II. Emission constants for tantalum.

Observer	Date	A^* amp cm^{-2} deg.$^{-2}$	φ_0^- ev
I. Langmuir[1]	1913	30	4.0
I. Langmuir[2]	1916	28	4.05
H. Lester[3]	1916		4.44†
H. J. Spanner[4]	1924		4.2
S. Dushman[5]	1925	60	4.12
Cardwell[6]	1931		4.12–4.19*
Rentschler[7]	1932		4.12*
Fiske	1941	55	4.19

* Photoelectric.
† Calorimetric.
Unmarked are thermionic.
[1] Phys. Rev. **2**, 450 (1913).
[2] Trans. Am. Electrochem. Soc. **29**, 125 (1916).
[3] Phil. Mag. **31**, 197 (1916).
[4] Ann. d. Physik **75**, 609 (1924).
[5] Phys. Rev. **25**, 338 (1925).
[6] Phys. Rev. **38**, 2041 (1931).
[7] Rev. Sci. Inst. **3**, 794 (1932).

[14] Jones, Langmuir, and Mackay, Phys. Rev. **30**, 201 (1927).
[15] F. A. Lindemann and A. Magnus, Zeits. f. Electrochem. **16**, 269 (1910).
[16] *Handbuch der Physik* (Julius Springer, Berlin, 1910), Vol. 10, p. 368.
[17] M. Pirani, Verh. d. Phys. Ges. **14**, 1037 (1912).
[18] F. Seitz, *Modern Theory of Solids* (McGraw-Hill, 1940), Chapter 3.

from tantalum were the same as for electron emission, except that the collecting potential was reversed. Positive ion runs were usually taken immediately preceding or following an electron run. The emission current was measured as a function of T and the left side of (6) plotted as a function of $1/T$. The slope of this line had the value 5032 φ_0^+ ev and the intercept had the value F^*. Figure 3 shows such a plot.

Some 22 different runs were taken on the three filaments. The data obtained showed a much lower reproducibility and greater day-to-day variation than did the electron data. Consecutive runs occasionally differed by half a volt or so in φ_0^+ while F^* shifted 1.0 to 1.5 or so, although φ_0^- would be constant to 0.01 ev and A^* be virtually unchanged. No consistent variation of φ_0^+ and F^* could be found with varying conditions. Previous filament temperature history, vacuum conditions, procedures in a run, etc., were all changed, but no significant drift of the positive ion emission followed them. Average deviation of points from the linear plot was 2°, four times that for the electron plots. Thus it is felt that this work cannot assign φ_0^+ closer than 0.3 ev to the average $\varphi_0^+ = 10.0$ ev. F^* is uncertain to 1.0 about 13.0.

From (7) and F^* the measured value of F we must have

$$13.0 = 14.29 + \log_{10}(1-r) + (S/2.303).$$

If we tentatively disregard S we see that $\log_{10}(1-r) = -1.29$, or $r = 0.94$, and all but 6 percent of the ions approaching the surface are reflected. This is greatly in contrast with the case for electrons or neutral atoms for which r is about zero. On the other hand if we disregard r, then S is not negligible, and there is an appreciable contribution to F from the heat of surface charge. One notes that this would demand that any temperature variation of the second term of (3) be assigned to other terms in the positive ion equation, and this must eventually be borne by φ_0^+.

THERMATOMIC WORK FUNCTION

A metal heated to temperatures approaching its melting point vaporizes at such an appreciable rate that its rate of mass loss per unit area m, may be measured as a function of temperature.

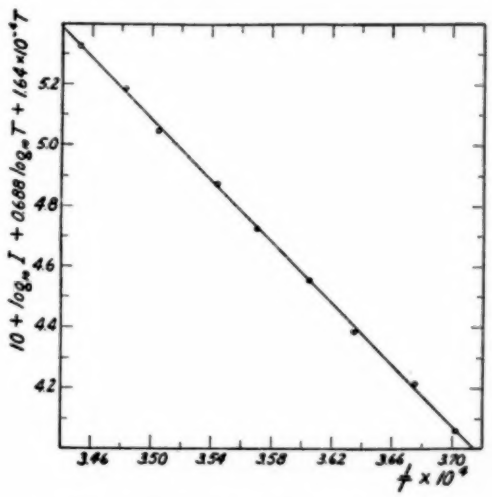

FIG. 3. Richardson positive ion plot $\varphi_0^+ = 10.10$ ev. $F^* = 13.05$.

The metallic vapor obeys ideal gas laws and hence the equilibrium state between the metal and its vapor may be treated in a simple thermodynamical way to obtain the vapor pressure p as a function of temperature. Kinetic theory reasoning serves to connect m with p.

Jones, Langmuir, and Mackay[14] employed this line of reasoning to obtain a measure of L_0, the latent heat of vaporization at the absolute zero:

$$L_0/T = 4.577(2\log_{10} M + 2\log_{10} T + 0.058 - \log_{10} m) - H.$$

If one uses for H the expression (5) he obtains for tantalum

$$(5032/T)\varphi_0^0 = 53.0 - 3.17\log_{10} T - 4.577\log_{10} m - 7.5\times10^{-4} T - 2530/T.$$

Here the writer has used φ_0^0, the thermatomic work function,[19] as a terminology more consistent with "positive ion work function" and "electron work function" than is the more cumbersome "latent heat of vaporization."

m is usually measured by one of two methods. The first is to follow the change in radius of a cylindrical filament in vacuum by following its change in resistance which varies inversely as the square root of the radius providing the resistivity remains constant. This method is subject to a

[19] This phrase was suggested to the writer by Professor H. B. Wahlin.

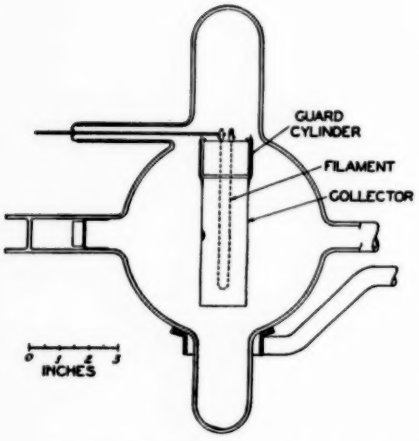

FIG. 4. Tube for evaporation data.

systematic error due to a change in resistivity caused by outgassing and recrystallization. Malter and Langmuir[20] found an apparent change in resistivity of 0.2 percent for a tantalum wire during an evaporation run. This corresponded roughly to a 2.5 percent error in mass loss determination.

The other method consists of actually weighing the filament to determine its mass loss. The procedure usually is to operate two identical filaments under identical preliminary outgassing and heat-treatment conditions. Then one alone is raised to an elevated temperature for a definite time. The mass difference between equal lengths from the two filaments will then give the desired mass loss. This procedure is also subject to serious errors. In order to avoid development of "hot spots" it is necessary to evaporate as little as can be accurately weighed. Yet in cutting and handling the filament and measuring its length it is difficult to eliminate errors which are an appreciable fraction of the mass loss itself.

In view of these difficulties a different method for measuring was tried. The filament was entirely surrounded by a 0.001-inch thick tantalum collector cylinder so that upon this cylinder would deposit all the metal evaporated from the filament within. This collector was hooked over a guard cylinder provided above (see Fig. 4) to make the filament within the collector all at the same temperature. The filament was pyrometered through a small hole in the side of the collector.

[20] D. B. Langmuir and L. Malter, Phys. Rev. **55**, 748 (1939).

The technique of measuring m was to operate the filament during preliminary baking and outgassing at a temperature where evaporation was inappreciable (1600°K), then to raise it to the evaporation temperature for a definite time—20 minutes to several hours—and then to remove the collector cylinder and measure on a microbalance its gain in mass. The collector was handled entirely by tools and carefully protected from dust.[21]

The results of seven runs are shown in Table III. Also included in this table are the data of Langmuir and Malter after conversion to the temperature scale used in this work. The data are insufficient to permit use of a Richardson type plot for an experimentally more significant evaluation of φ_0^0. The mean deviation from the average value of 7.97 ev is 0.03 ev, certainly less than the probable error of the determination.

Examination of the method indicates that the only serious source of error lies in run-to-run variation of air contamination of the collector when it is removed from the vacuum system. This is rather difficult to evaluate. Humidity variation is the most serious contributor to this error. However, simple tests indicated that the error is under 5 percent, and prompt weighing of the collector after removal reduces this to the order of 1 percent.

Air contamination may be eliminated entirely by use of a magnetically operated balance enclosed within the vacuum system, as described by Blewett.[22] This device was tried, but the desired sensitivity and reproducibility could not be obtained and use of such a balance was discarded.

IONIZATION POTENTIAL

There appears nowhere in the literature a value of the ionization potential of tantalum and apparently there are no sufficiently high term values to permit a spectroscopic estimation of it. In a private communication Dr. C. C. Kiess of the National Bureau of Standards estimated that for tantalum $V=7.3$ ev. He based his estimate on an interpolation from neighboring elements in the periodic table.

[21] Changes in mass of the 10-gram collector of the order of 5 milligrams could be reproducibly measured to 20 micrograms.

[22] J. P. Blewett, Rev. Sci. Inst. **10**, 231 (1939).

The writer estimates from an interpolation in group V of the periodic table that $V=7.4$ ev while an interpolation of Series 10 leads to $V=7.3$ ev. The uncertainty in such interpolation must be at least 0.3 ev.

THE ENERGY CYCLE

Collecting the foregoing determined values of the terms involved in the energy cycle we find $\varphi_0^-=4.19\pm0.02$ ev; $\varphi_0^+=10.0\pm0.3$ ev; $\varphi_0^0=7.97\pm0.05$ ev; and $V=7.3\pm0.3$ ev. Then $\varphi_0^-+\varphi_0^+=14.2\pm0.3$ ev and $\varphi_0^0+V=15.3\pm0.4$ ev. The probable values fail to close the cycle by 1.1 ev, and even for the limit values there is still lacking 0.4 ev.

Several possibilities present themselves as reasons for the energy cycle not closing. The evaporation of a neutral atom from a lattice is not a simple process. One may visualize it as concurrent evaporation of an electron and a positive ion with recombination in close proximity of the surface. It seems not unlikely that in the recombination lattice vibrations are set up which introduce into the cycle an irreversible term of magnitude difficult to estimate.

The fact that the electron work function is measured at temperatures 1200° below those at which the positive ion work function is determined suggests that the emitting surface itself may be different. If there exists a high-temperature Curie point so that the body-centered lattice shifts to, for instance, a face-centered lattice the cycle certainly would fail to close by the difference of the work functions from these different structures.

The factors determining the statistical distribution of exposed crystal faces in the thermionic surface are not as yet understood, and one cannot overlook the possibility that this distribution is temperature dependent. This most certainly would introduce a temperature-dependent measured work function. Such a variation even if small in the ordinary range of thermionic measures would become appreciable over the temperature interval separating measurement ranges of the two work functions. Hence again the energy cycle even if exact at any single temperature would seem not to be closed when applied to widely different surface conditions at greatly separated temperatures.

TABLE III. Evaporation data of tantalum.

T°K	m g cm^{-2} sec.$^{-1}$	m Langmuir-Malter g cm^{-2} sec.$^{-1}$	φ_0^0 ev
2633	2.88×10^{-7}	0.693×10^{-7}	7.90
2649	2.80	0.867	7.95
2700	4.38	1.66	7.98
2737	6.59	2.61	7.99
2804	16.0	5.80	7.96
2807	12.4	6.04	8.04
2850	23.0	9.87	8.02

The writer wishes to express his appreciation of the encouragement and advice of Professor H. B. Wahlin, who suggested this problem, and to acknowledge the assistance of Dr. R. W. Wright in determining the temperature scale.

The V^3I Relation for Vaporizing Molybdenum†

FRANCIS T. WORRELL*
University of Pittsburgh, Pittsburgh, Pennsylvania
(Received February 2, 1942)

If a cylindrical filament of circular cross section, whose radiancy and resistivity are functions of temperature only, be maintained at a constant and uniform temperature in vacuum by electrical heating alone, and it vaporizes uniformly, the product of the current by the cube of the voltage drop across the filament will be a constant. In order to test this for filaments under ordinary experimental conditions, voltage and current measurements have been made on well-aged Mo filaments which have been maintained in vacuum of the order of 2 to 5×10^{-8} mm Hg at a constant brightness temperature till they burned out. It was found that V^3I decreased rather uniformly with time of operation for each of the four filaments tested. For 500 minutes of operation at 2250°K the percentage decreases found for V^3I ranged from 0.49 percent to 0.85 percent, corresponding to temperature changes ranging from 7.5°K to 13°K. Possible changes in electrical and radiation properties of the filaments, and their effect on V^3I, are discussed.

INTRODUCTION

THE V^3I relation may be stated as follows: If a uniform cylindrical wire in vacuum be maintained at a constant and uniform temperature by electrical heating alone, then, regardless of changes in the diameter of the wire owing to uniform vaporization, the product V^3I remains constant, where I is the current in the wire and V is the voltage drop along this wire. It is assumed here that the electrical and radiation properties of the wire do not change with time. This relation has been used by Langmuir,[1] who first derived it, Langmuir and Mackay,[2] Langmuir and Malter,[3] and probably others, as a means of maintaining the temperature of a filament at a constant value.

Some data obtained by Worthing (unpublished) and by Norris[4] indicate that this relation does not hold. Norris, using molybdenum in sealed-off lamps, found that for filaments electrically heated in vacuum the temperature did not stay constant when V^3I was held constant. He found instead that roughly a constant temperature-constant current relation held.

The V^3I relation can be derived rather simply. Consider a solid filament of circular cross section of diameter $2r$, length L, and resistivity ρ. Let this filament be electrically heated in vacuum to a constant and uniform temperature. If the potential difference between the ends of the filament be V, and the current through the filament I, then

$$V/I=R=\rho L/\pi r^2. \quad (1)$$

Under the conditions specified, since there are no

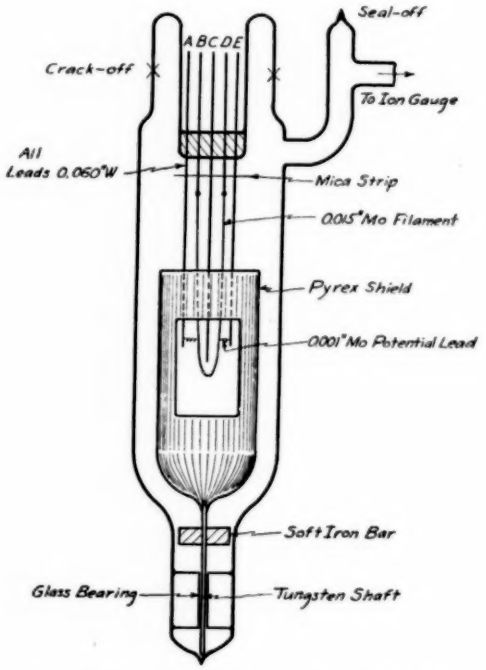

FIG. 1. Diagram of the experimental tube.

† Submitted to the Graduate School of the University of Pittsburgh in partial fulfillment of the requirements for the degree of Doctor of Philosophy.

* Now at the Department of Physics, University of Tennessee, Knoxville, Tennessee.

[1] I. Langmuir, Phys. Rev. **2**, 329 (1913).

[2] I. Langmuir and G. M. J. Mackay, Phys. Rev. **4**, 379 (1913).

[3] D. B. Langmuir and L. Malter, Phys. Rev. **55**, 748 (1939).

[4] L. H. Norris, M. S. Thesis, University of Pittsburgh, 1933.

conduction or convection losses, all the energy supplied electrically is given off as radiation. Thus we may also say

$$VI = \mathfrak{R} 2\pi r L, \tag{2}$$

$\mathfrak{R}$ being the radiancy of the wire, expressible, for instance, in watts/cm². To be strictly correct one should add to the right side of (2) a term which represents the energy per unit time required to vaporize the molybdenum. However, at the temperature at which measurements were taken this can be neglected. If we square (2) and multiply by (1) we get

$$V^3I = 4\pi L^3 \rho \mathfrak{R}^2. \tag{3}$$

If we assume that the radiancy and resistivity are functions of the temperature alone, then, at constant temperature, the right side of (3) is constant, and, therefore V^3I is constant. Note that r does not appear in the equation. This relation, therefore, is independent of the filament diameter, and can be used as a criterion of temperature constancy for a vaporizing filament, under the above conditions.

APPARATUS

The experimental tube is shown in Fig. 1. There were five leads through the top. Leads B and D supported the filament. The lower ends of leads A and E were connected to the filament by fine wire potential leads. In operation lead C was at about -200 volts with respect to the filament. This served to stop electron emission from the filament.

The mica strip, which was anchored to leads B and C, prevented the deposition of vaporized molybdenum on the support for the leads, thus avoiding trouble from leakage currents between the various leads.

The glass shield inside the tube could be rotated by placing a U-magnet outside the tube close to the soft iron bar, and rotating it. This shield had two holes oppositely placed through which the pyrometer could be sighted on the filament in the tube. When measurements were not being taken, and the filament was at a higher temperature, the portion of the tube wall through which readings were taken was protected from vaporizing molybdenum by having the shield rotated to a position 90° away from the former one.

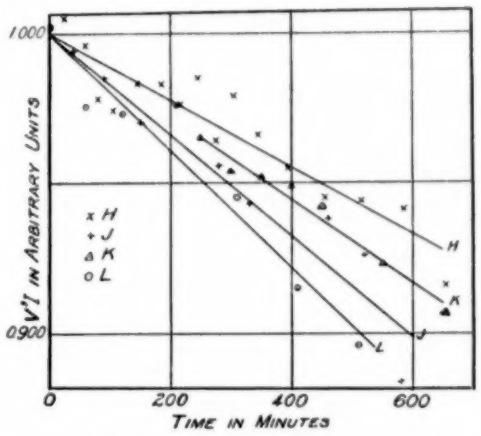

FIG. 2. Variation of V^3I with time of operation at 2250°K for four filaments. All values of V^3I are expressed as percentages of an early value.

Temperature measurements were made with a laboratory-built, disappearing-filament optical pyrometer.[5] The calibration of Stephens[6] was used.

Current and voltage measurements were made with a type K potentiometer modified[7] to a limited double potentiometer with one branch a deflection instrument. This feature allowed the rapid measurement of two quantities in succession without changing the position of the drum.

PROCEDURE

Preparation of the Tube

The 0.015″ molybdenum filament, which had previously been polished, was arc-welded to leads B and D, as shown in Fig. 1. Potential leads of 0.001″ molybdenum were tied to the lower ends of leads A and E and to selected points on the filament. The contacts where the leads were tied were improved by discharging through the potential leads a 0.02-μf condenser charged to 110 volts. Since the potential leads were small in diameter compared with the filament, the temperature drop because of conduction losses was negligible; so the section of the filament between them was essentially at a uniform temperature.

After mounting the internal structure the tube was sealed along the line marked X–X (Fig. 1), and sealed to the pump. The tube was then

[5] 1919 Report of Standards Committee on Pyrometry, J. Opt. Soc. Am. **4**, 305 (1920).
[6] R. E. Stephens, J. Opt. Soc. Am. **29**, 158 (1939).
[7] A. G. Worthing, J. Opt. Soc. Am. **10**, 599 (1925).

baked at 500°C for about 50 hours, and the filament outgassed by passing an electric current through it. No attempt was made to outgas the other metal parts. After the pressure had gone below 5×10^{-8} mm Hg the filament was aged for 5 minutes at 2450°K. Then, with the filament at a lower incandescent temperature, and after a preliminary warming of the pumping line, the tube was sealed off. The pressure in any one tube remained constant after sealing, and varied among the different tubes from 2×10^{-8} mm Hg to 5×10^{-8} mm Hg, as measured by an ion gauge.

Taking the Readings

The filament was heated to 1500°K. Readings were taken of the current I, voltage drop between the potential leads V, and voltage drop across the entire filament V', measured between two points immediately outside the tube. The temperature of the filament was then raised to a value determined by the heating current, $I'=2.20I$, where I is the previously determined current. This corresponded to a temperature of 2250°K. After the filament had been at the higher temperature for a period ranging from 60 to 100 minutes the temperature was again lowered to 1500°K, and readings were taken. This procedure was continued till the filament burned out.

A.c. was used to heat the filament to the higher temperature, since d.c. heating results in a wavy filament surface.[8]

At the beginning and ending of the run on each filament the transmission of the tube wall was measured to find what blackening may have occurred. This was done by forming inside the tube an image of the filament of an auxiliary lamp, and measuring the brightness of this image with and without the tube in position. The ratio of the first brightness to the second is the square of the transmission. If any change in the transmission of the wall occurred it was assumed to be linear with time, and a corresponding correction was applied to the values of V^3I.

RESULTS

The variation of V^3I with time of operation at 2250°K for four filaments, H, J, L, and K, is shown in Fig. 2. For comparison purposes the values of V^3I for each filament are expressed as percentages of that for an early reading. It is seen that in the first 500 minutes of operation the decrease in V^3I is 5.6 percent for filament H, 8.4 percent for J, 9.8 percent for L, and 6.9 percent for K. From some data by Worthing[9] on molybdenum we may show that, at 1500°K,

$$d(V^3I)/V^3I=11.5dT/T. \qquad (4)$$

This means that the above-mentioned changes in V^3I correspond to changes in temperature of about 0.49 percent, 0.73 percent, 0.85 percent, and 0.60 percent, respectively, or about 7.5°K, 11.0°K, 13°K, and 9.0°K, respectively, at 1500°K.

It can be seen that the data for filament K are the best; individual readings deviate on the average about 0.4°K from the curve. For filament H the deviation is about 0.6°K. The values for filament L are moderately consistent; those for J are so scattered as to be not very reliable, though they show the same trend as the others.

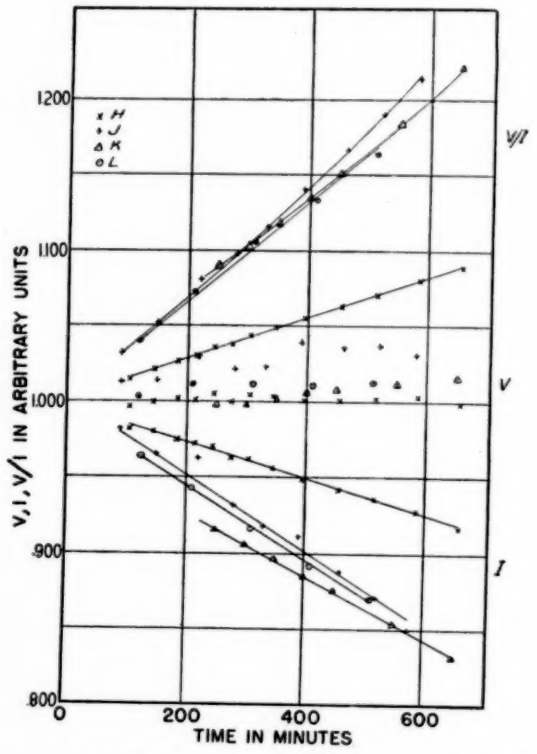

FIG. 3. Variation of V, I, and V/I with time of operation for the four filaments. V, I, and V/I are expressed as percentages of an early value.

[8] R. P. Johnson, Phys. Rev. **54**, 459 (1938).

[9] A. G. Worthing, Phys. Rev. **28**, 190 (1926).

The relative variations of V, I, and V/I with time for the same filaments are shown in Fig. 3. The curves for filaments J, K, and L appear to agree well with one another, but not with those for H. The values of V scatter more for J and L than for H and K.

A limit is imposed on the certainty of the values of V^3I by the fluctuations in V, for which possibly unsatisfactory potential lead contacts are to blame.

DISCUSSION

The data show definitely that V^3I does not remain constant, but decreases with time. The theoretically necessary conditions for constancy of V^3I are constancy of temperature with time, uniformity of temperature along the wire, good vacuum conditions, a wire of circular cross section, and dependence of resistivity and radiancy on temperature only. With the possible exception of the dependence of resistivity and radiancy on temperature only, these conditions were apparently satisfied. Within the range of pressures used in the tube for various filaments the change in V^3I did not appear to depend on vacuum conditions.

It is seen from Eq. (1) that a decrease in V^3I could be caused by a decrease in resistivity, a decrease in radiancy, or both. If there were a decrease in resistivity it might result from some change in the internal structure of the material. Such a decrease is known to take place during aging.[10] The initial effect of aging is to remove strains and change the wire structure from a fibrous one to a granular one. Later, the effect is probably to cause grain growth and changes in the surface. The later aging takes a much longer time than the initial aging, and during this period the resistivity decreases. After aging is completed no change in resistivity is to be expected.

The resistivity of the wire would decrease if some impurity originally present in the wire were removed by vaporization as time went on. The principal impurity in the wire was iron, amounting to 0.005 percent. It does not seem likely that 0.005 percent of iron dissolved in molybdenum would cause the resistivity change of the order of 10 percent needed to cause a 10 percent change in V^3I. The slopes at zero composition of resistivity-composition curves seem to be an order of magnitude less than this.

Radiancy is also affected by changes in internal structure,[10] and, in addition, by surface changes. All that can be said about the surface conditions is this: Each filament was polished before using, till its surface, when examined under a microscope, appeared smooth, except for a few residual die marks. The surfaces were still smooth after the filaments had burned out. It is still possible, however, for sufficient surface changes to have taken place to cause variations in radiancy large enough to account for the observed changes in V^3I.

An inspection of Figs. 2 and 3 will show that the filaments do not agree with one another. From Figs. 2 and 3 we see that, compared with J, K, and L, V^3I and I in filament H decreased less rapidly, and V and V/I increased less rapidly. Filament H was possibly operated at a lower temperature than the others, though a consideration of the operating conditions does not make this seem plausible. Since the higher temperature of operation of each filament was determined by the current, which was a constant multiple of the current corresponding to a temperature of 1500°K, and since the latter temperature was determined by a pyrometer, it would appear that filament H could have been at a lower temperature than the others only if it had a higher emissivity. It is not obvious why this should happen.

Filament H was apparently not aged to the extent that the others were. This appears to be the reason for an initial rapid decrease in V^3I with a sudden leveling off afterwards to a straight-line variation of smaller slope. This initial rapid decrease in V^3I does not appear on the graph in Fig. 2, because in plotting the data for H the time axis was moved so that time started after the change in slope of the curve. Because the higher operating temperature was determined by the current, and the aging temperature was taken too low to produce sufficient aging, it happened that the chosen operating temperature was higher than the aging temperature. Whitney,[11] while measuring the emissivity

[10] I. Langmuir and J. B. Taylor, Phys. Rev. **50**, 78 (1936), footnote.

[11] L. V. Whitney, Phys. Rev. **48**, 458 (1935).

of molybdenum, found that when molybdenum which had been heated to a certain temperature was raised to a higher temperature its emissivity immediately dropped, then gradually rose to its original value. If the emissivity of filament H were rising during this early period, and, therefore, its temperature at constant brightness were dropping, one would indeed have a rather rapid decrease in V^3I until the emissivity reached its final value. This does not explain, however, why the various curves for H should differ from the corresponding curves for the other filaments.

In conclusion, the data show that there is a definite decrease in V^3I with time, though quantitatively the results obtained from the various filaments do not agree. No explanation has been found for the differences between the various filaments on the basis of the available data. It would seem necessary, in view of the results, to reconsider previous work in which constancy of V^3I was assumed.

The writer wishes to express his indebtedness to Dr. A. G. Worthing, who suggested this problem, for his help and encouragement during the course of the work. He also wishes to thank his colleagues for the help they have rendered at various times. Special thanks are due Dr. David Halliday and Dr. Charles S. Smith, for helpful discussions. The analysis of the wire used in the filaments was supplied by Mr. A. Poritsky, of the Cleveland Wire Works of the General Electric Company.

APRIL 1 AND 15, 1942 PHYSICAL REVIEW VOLUME 61

On the Calculation of the Distribution Function

C. W. UFFORD, *Allegheny College, Meadville, Pennsylvania*

AND

E. P. WIGNER, *Princeton University, Princeton, New Jersey*

(Received January 22, 1942)

The distribution function for particles confined to a large circle is found for a repulsive potential of long range. The distribution function is calculated exactly from the Boltzmann-Gibbs equation, and compared with the solution of an implicit equation of the type used by Debye and Hückel in the theory of electrolytes. The solution of the Debye-Hückel equation agrees, for our particular potential, only fairly well with the exact distribution function.

I.

ALTHOUGH the problem of classical statistical mechanics is, in principle, solved by the Boltzman-Gibbs equation

$$P(x_1, y_1, z_1, \cdots x_n, y_n, z_n)dx_1\cdots dz_n = \exp(-\beta V)dx_1\cdots dz_n \quad (1)$$

for the probability of the configuration characterized by the rectangular coordinates x_1, y_1, z_1, $\cdots$, x_n, y_n, z_n, the answering of questions of immediate physical interest meets, in most cases, serious mathematical difficulties. In (1), $\beta=1/kT$ and V is the potential energy

$$V=\sum_{i<k} v(|r_i-r_k|), \quad (1a)$$

which we shall assume to be the sum of interactions between pairs.

Many of the quantities of immediate physical importance depend on the distribution function $g(r)$, i.e., on the probability of a distance r between, say, the particles 1 and 2. This is given by

$$g(|r_1-r_2|)=\text{const.}\int\cdots\int \exp(-\beta V) \times dx_3dy_3dz_3\cdots dx_ndy_ndz_n. \quad (2)$$

However, one can evaluate (2) easily only in the case of dilute matter, i.e., gases. For condensed material, the integrations in (2) are so difficult that indirect methods had to be devised for the

evaluation of the distribution function. These methods have two features in common: (a) they do not give g directly but only as the solution of an implicit equation the solving of which, though in most cases not very easy, is still less difficult than the integrations of (2); and (b) the implicit equation for g is not exact, i.e., its solution is only an approximation to the rigorous expression (2). The first implicit equation was given by Debye and Hückel[1] in their theory of electrolytes. More rigorous equations are due to Kirkwood[2] and Mayer.[3]

The present authors became interested in these methods because integrals of the type (2) occur in the theory of the so-called correlation energy. The present note deals with a special problem in which all particles are confined to a large circle of length L; and in which the potential between a pair of particles is given by

$$\beta v(x) = -\ln \sin^2 \pi x/L, \tag{3}$$

where x is the distance between the particles, measured along the circle. We found that for this interaction the distribution function can be evaluated exactly by (2), and that the implicit equation corresponding to Debye and Hückel's theory also can be solved. The comparison of the two results gives an indication of the accuracy of the Debye-Hückel equation (5) for the case of a repulsive potential of long range. In the case of long range forces the Debye-Hückel equation can be expected to give good results.

In the Debye-Hückel theory the distribution function is given, apart from a constant, by an average potential U

$$\ln g(x) = -\beta U(x) + C. \tag{4}$$

The average potential contains the potential $v(x)$ of the original particle around which we investigate the distribution of the others, and the average field of the other particles. There are $g(x')dx'$ particles at a distance x' from the original particle; and their potential, at x, is given by $g(x')dx'v(x-x')$. Hence

$$U(x) = v(x) + \int g(x')v(x-x')dx' \tag{4a}$$

and the implicit equation becomes

$$\ln g(x) = -\beta v(x) - \beta \int g(x')v(x-x')dx' + C. \tag{5}$$

The constant C is determined by the condition that the integral of g must be $n-1$,

$$\int g(x)dx = n-1. \tag{5a}$$

In most cases g is a constant if x is large compared to the average distance between neighboring particles. One can, therefore, substitute

$$g(x) = g_0(1+h(x)), \tag{6}$$

in which $h(x)$ vanishes for large x. Substitution of (6) into (5) gives a somewhat different form to the implicit equation

$$\ln (1+h(x)) = -\beta v(x) - g_0\beta \int h(x')v(x-x')dx' + C', \tag{6a}$$

since the integral of $g_0 v(x-x')$ is independent of x.

II.

The calculations remain to be done. For evaluating (2) we can write

$$\exp(-\beta V) = \prod_{i<k} \sin^2 \pi(x_i - x_k)/L$$
$$= 2^{-n(n-1)} \left| \prod_{i<k} (\exp 2\pi i x_i/L - \exp 2\pi i x_k/L) \times \exp(-\pi i(x_i+x_k)/L) \right|^2. \tag{7}$$

The factor $\exp(-\pi i(x_i+x_k)/L)$ may be omitted since its absolute value is 1. If we write

$$\omega_i = \exp 2\pi i x_i/L, \tag{7a}$$

we get

$$\exp(-\beta V) = 2^{-n(n-1)} \left| \prod_{i<k} (\omega_i - \omega_k) \right|^2, \tag{7b}$$

the product on the right can be written as a determinant $\Delta = |\Delta_{il}|$ where

$$\Delta_{il} = \omega_i{}^l = \exp 2\pi i l x_i/L \quad (l = 0, 1, 2, \cdots n-1). \tag{8}$$

[1] P. Debye and E. Hückel, Physik. Zeits. **24**, 185, 305 (1923); P. Debye, Physik. Zeits. **25**, 97 (1924).

[2] J. G. Kirkwood and Elizabeth Monroe, J. Chem. Phys. **9**, 514 (1941); J. G. Kirkwood, J. Chem. Phys. **3**, 300 (1935).

[3] J. E. Mayer and E. Montroll, J. Chem. Phys. **9**, 2 (1941); J. E. Mayer and S. F. Harrison, J. Chem. Phys. **6**, 87 (1938).

This gives

$$\exp(-\beta V)=2^{-n(n-1)}\Delta\Delta^*. \quad (9)$$

The determinant $|\Delta_{il}|$ is, in case of odd n, apart from a factor $\exp -\pi i(n-1)(x_1+\cdots+x_n)/L$, the wave function of a one-dimensional degenerate Fermi gas.

One can integrate (9) immediately by developing both Δ and Δ^* with respect to the two rowed minors of the first two rows. The minor of the l_1l_2 columns in Δ is

$$\exp 2\pi i(l_1x_1+l_2x_2)/L - \exp 2\pi i(l_2x_1+l_1x_2)/L. \quad (10)$$

Its cofactor is orthogonal to the cofactor of every two rowed minor of Δ^*, excepting the cofactor of the minor of the l_1l_2 columns. The product of the cofactors of the l_1l_2 minors of Δ and Δ^* gives $(n-2)!$ if integrated over $x_3, \cdots, x_n$. Thus

$$\int\cdots\int \exp(-\beta V)dx_3\cdots dx_n = \sum_{l_1<l_2} 2^{-n(n-1)}(n-2)!\,|\exp 2\pi i(l_1x_1+l_2x_2)/L - \exp 2\pi i(l_2x_1+l_1x_2)/L|^2. \quad (10a)$$

This is, according to (2), proportional to $g(x_1-x_2)$. The sum in (10a) can be readily evaluated and gives, with (5a),

$$g(x)=\frac{n}{L}\left(1-\frac{\sin^2\pi nx/L}{n^2\sin^2\pi x/L}\right) \approx\frac{n}{L}\left(1-\frac{\sin^2\pi nx/L}{\pi^2n^2x^2/L^2}\right). \quad (11)$$

The last expression is valid if x remains of the order of magnitude of the average distance of two particles, i.e., is not very much larger than L/n. Equation (11) gives the rigorous expression for g; it is the lowest curve in Fig. 1. The abscissae in this figure are $n\pi x/L$ so that the average distance of two particles corresponds to the abscissa π in the graph. The ordinates are multiplied by L/n.

That the solution of the Debye-Hückel Eq. (5) is different from (11), can be seen by inserting (11) and (3) into the right side of (5). If $g'(x)$ is the value of $g(x)$ obtained by these substitutions,

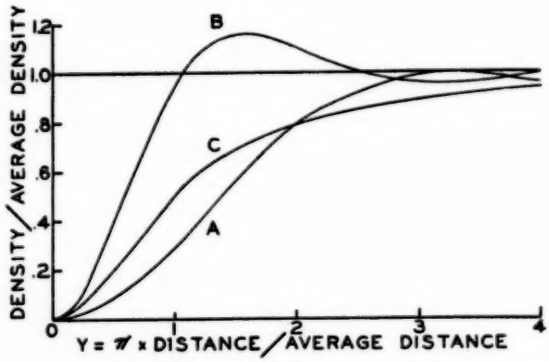

FIG. 1. Distribution functions. The ordinates are the distribution function $g(x)/(n/L)$ representing the density of particles divided by the average density. The abscissae are $y=\pi nx/L$, π times the distance divided by the average distance of nearest neighbors. The distance is equal to the average distance for the abscissa $y=\pi$. Curve A represents the rigorous value of the distribution function $g(x)/(n/L)$ given by (11) from the Boltzmann-Gibbs equation. Curve B represents the distribution function, $g'(x)$ of (12a), obtained by inserting the rigorous value (11) in the right-hand side of the Debye-Hückel Eq. (5). Curve C represents the distribution function (13) obtained by solving the Debye-Hückel equation.

this gives

$$\ln g'(x)=-\frac{\sin 2\pi nx/L}{\pi nx/L}+2Ci(2\pi nx/L) \quad (12)$$

or

$$g'(x)=\exp\left[-\frac{\sin 2\pi nx/L}{\pi nx/L}+2Ci(2\pi nx/L)\right]. \quad (12a)$$

$g'(x)$ is the uppermost curve in Fig. 1. If (11) were a solution of (5), the value of $g'(x)$ in (12a) would be equal to the rigorous value of $g(x)$ given by (11); and the uppermost curve of Fig. 1 would coincide with the lowest curve. One sees that this is far from being true. The evaluation of the integral obtained by inserting (11) and (3) into (5), i.e., the derivation of (12), requires a somewhat lengthy calculation and will not be given in detail. Ci in (12) is the cosine integral as defined in Jahnke-Emde.[4]

One would expect, on the basis of the lowest and highest curves in Fig. 1, that the solution of (5) would be represented by a curve similar to the middle one of the figure. This corresponds to

$$g(x)=\frac{n}{L}\left(1-\frac{1}{1+n^2\sin^2\pi x/L}\right) \quad (13)$$

[4] E. Jahnke and F. Emde, *Tables of Functions* (B. G. Teubner, 1933), second edition.

and the following calculation shows that (13) is indeed the solution of (5) for the potential (3). In order to show this, one can first verify (5a), using the assumption $n \gg 1$, and then calculate

$$I = -\beta \int g(x')v(x-x')dx'$$

$$= \frac{n}{L}\int_0^L \left(1 - \frac{1}{1+n^2\sin^2 \pi x'/L}\right) \cdot \times \ln \sin^2 \pi(x-x')/L dx'. \quad (13a)$$

The first term is a well known definite integral; its value is $-2n \ln 2$. In order to integrate the second term, one can change the limits of integration and integrate from $-\frac{1}{2}L$ to $\frac{1}{2}L$. Then the first factor will be very small, except for very small x' for which the sine can be replaced by its argument. Thus (13a) becomes

$$I = -2n \ln 2 - \frac{n}{L}\int_{-\frac{1}{2}L}^{\frac{1}{2}L} \frac{\ln \sin^2 \pi(x-x')/L}{1+\pi^2 n^2 x'^2/L^2} dx'. \quad (13b)$$

If x is of the order of L, the remaining integral will have two maxima: at $x'=0$ and at $x'=x$. However, the integral over the second maximum is inversely proportional to n and can be neglected. The integral over the first maximum becomes, if one replaces $x-x'$ by x in the numerator

$$I = -2n \ln 2 - \ln \sin^2 \pi x/L \quad \text{for } x \gg L/n. \quad (13c)$$

If x is not large as compared with L/n, the sine can be replaced by its argument in (13b) since the denominator becomes very large for $x' \gg L/n$. This gives, with $y' = \pi n x'/L$ and $y = \pi n x/L$,

$$I = -2n \ln 2 - \frac{1}{\pi}\int_{-\infty}^{\infty} \frac{\ln (y-y')^2/n^2}{1+y'^2} dy'$$

$$= -2n \ln 2 + \ln n^2 - \frac{1}{\pi}\int_{-\infty}^{\infty} \frac{\ln (y-y')^2}{1+y'^2} dy' \quad (13d)$$

and

$$\frac{\partial I}{\partial y} = -\frac{2}{\pi}\int_{-\infty}^{\infty} \frac{dy'}{(1+y'^2)(y-y')} = -\frac{2y}{1+y^2}, \quad (13e)$$

since the main value of the integral has to be taken in (13e). We now have

$$I = -2n \ln 2 + \ln n^2 - \ln (1+y^2) - \frac{1}{\pi}\int_{-\infty}^{\infty} \frac{\ln y'^2}{1+y'^2} dy'. \quad (13f)$$

In the last integral the lower limit can be replaced by 0 if a factor 2 is inserted. Substitution then of z for $\ln y$ shows that the integral in (13f) vanishes and we have

$$I = -2n \ln 2 + \ln n^2 - \ln (1+\pi^2 n^2 x^2/L^2) \quad \text{for } x \ll L. \quad (13g)$$

Since $n \gg 1$,

$$I = -\beta \int g(x')v(x-x')dx' = -2n \ln 2 + \ln n^2 - \ln (1+n^2 \sin^2 \pi x/L) \quad (14)$$

holds for both regions (13c) and (13g). Insertion of (13), (14), and (3) into (5) shows that (5) is indeed satisfied by (13). C in (5) has the value $\ln 2^{2n} n/L$. The solution (13) of (5) is shown in Fig. 1 lying for small abscissae between the other two curves.

III.

One sees that the solution of the Debye-Hückel equation agrees fairly well with the correct distribution function if the potential is given by (3). In particular, the total volume of the "hole" in the distribution function is 1 in both cases. Nevertheless, (5) gives too high a probability of a close approach of two particles since (13) is too high for small abscissae. The failure of (5) in this respect could have been foreseen and depends only on the repulsive character of our potential (3). What is essentially neglected in (5) is that the particle under consideration, particle 2 in our notation, has an effect on the rest of the particles. In our case, it pushes them away from itself so that the distribution of the particles 3, 4, $\cdots$, n will, in reality, show a hole around the point where particle 2 is. Thus particle 2 will be under a lower potential than the average potential U given by (4a). However, the difference between the actual and the average potential is smallest for small x because, where the second particle is close to the first, there are very few particles to be shoved away from its neighborhood.

Evaluation of Functions Related to Tait's Mean Free Path*

PAUL ROSENBERG†
Department of Physics, Columbia University, New York, New York
(Received January 24, 1942)

A new and extended table of values is given for the functions,

$$\Psi(x)=x\exp(-x^2)+(2x^2+1)\int_0^x \exp(-y^2)dy, \quad \text{and} \quad x^5/\Psi(x),$$

which occur frequently in kinetic theory. The integrals

$$\Theta_n=\int_0^\infty \frac{4x^n\exp(-x^2)}{\Psi(x)}dx$$

$n=3, 4, 5$, are evaluated by numerical quadrature. The new values disagree with the values found by Tait, but agree with the values found by Boltzmann. The value of Θ_4, which determines Tait's mean free path for a single system, is 0.6774560. A table is given for the function

$$\Phi(\alpha)=\alpha^2\int_0^\infty \frac{x^5\exp(-\alpha x^2)}{\Psi(x)}dx,$$

which is useful in scattering experiments. $\Phi(\alpha)$ is evaluated by numerical quadrature for 27 selected values of α.

THE function,

$$\Psi(x)=x\exp(-x^2)+(2x^2+1)\int_0^x \exp(-y^2)dy,$$

occurs frequently in kinetic theory, particularly in expressions for mean free paths, and in discussions of viscosity, diffusion, and thermal conduction.

Tait[1,2] published a table of $\Psi(x)$ which was limited to values of x from 0.1 to 3.0 in intervals of 0.1. A table which is more extended than that of Tait has now been computed and is given in Table I.[3] The range of the argument x is extended from 3.0 to 20.4, and the interval is reduced to 0.5 for values of x below 1.5.

Table I gives also the values of $x^5/\Psi(x)$ which are necessary for computing functions such as Θ_n and $\Phi(\alpha)$, defined further below.

Three important expressions involving $\Psi(x)$ are the integrals

$$\Theta_n=\int_0^\infty \frac{4x^n\exp(-x^2)}{\Psi(x)}dx,$$

where $n=3, 4, 5$. Θ_4 determines Tait's mean free path for a molecule in its own gas. These three integrals were evaluated numerically by Tait[1,4] and by Boltzmann,[5] but their results disagree after the third figure as shown in Table II.

In view of this discrepancy between the findings of Tait and of Boltzmann, it was desirable to perform new and independent numerical quadratures of Θ_n. The results are given in the last line of Table II. In each case the new values of Θ_n disagree with the values of Tait, but agree rather well with the values of Boltzmann.

* Publication assisted by the Ernest Kempton Adams Fund for Physical Research of Columbia University.

† Now at the Radiation Laboratory, Massachusetts Institute of Technology, Cambridge, Massachusetts.

[1] P. G. Tait, Trans. Roy. Soc. Edinburgh **33**, 65 (1886); Tait, *Scientific Papers* (Cambridge University Press, 1900), Vol. 2, paper 77, p. 124.

[2] The values of $\Psi(x)$ in the references under footnote 1 are correct; but in all other published tables of $\Psi(x)$ two typographical errors appear repeatedly for $x=1.1$ and for $x=2.7$. The tables in which these errors appear are the following. J. H. Jeans, *The Dynamical Theory of Gases* (Cambridge University Press, 1904), first edition, p. 347; (1916), second edition, p. 430; (1921), third edition, p. 436; (1925), fourth edition, p. 438: J. H. Jeans, *An Introduction to the Kinetic Theory of Gases* (Cambridge University Press, 1940), p. 305: L. B. Loeb, *The Kinetic Theory of Gases* (McGraw-Hill Book Company, 1927), first edition, p. 531; (1934), second edition, p. 653. Tait's original table gave $\Psi(x)$ to 6 places past the decimal point; the tables in Jeans and in Loeb reproduced Tait's table to 5 places past the decimal point.

[3] Table I includes Tait's original values of $\Psi(x)$ except for $x=0.1, 0.2, 0.3, 0.4$, in which cases $\Psi(x)$ is recomputed in order to extend Tait's values to seven figures.

[4] P. G. Tait, Trans. Roy. Soc. Edinburgh **33**, 251 (1887); Tait, *Scientific Papers* (Cambridge University Press, 1900), Vol. 2, paper 78, p. 153.

[5] L. Boltzmann, Akad. d. Wissenschaften Wien Sitz. **96**, 891 (1887).

TABLE I. Values of $\Psi(x)$ and $x^5/\Psi(x)$.

x	$\Psi(x)$	$x^5/\Psi(x)$	x	$\Psi(x)$	$x^5/\Psi(x)$	x	$\Psi(x)$	$x^5/\Psi(x)$
0.05	0.1000833	0.000003122399	4.1	30.68118	37.76133	9.7	167.6564	512.1988
.1	.2006660	.00004983405	4.2	32.15231	40.64754	9.8	171.1127	528.2605
.15	.3022450	.0002512449	4.3	33.65890	43.67595	9.9	174.6044	544.6541
.2	.4053121	.0007895150	4.4	35.20093	46.84996	10.0	178.1316	561.3827
.25	.5103522	.001913507	4.5	36.77842	50.17294	10.2	185.2923	595.8591
.3	.6178401	.003933057	4.6	38.39135	53.64828	10.4	192.5948	631.7164
.35	.7282393	.007212173	4.7	40.03973	57.27936	10.6	200.0391	668.9822
.4	.8419993	.01216153	4.8	41.72356	61.06956	10.8	207.6252	707.6829
.45	.9595544	.01923060	4.9	43.44284	65.02228	11.0	215.3531	747.8462
.5	1.081321	.02889984	5.0	45.19757	69.14088	11.2	223.2228	789.4991
.55	1.207701	.04167293	5.1	46.98775	73.42877	11.4	231.2343	832.6684
.6	1.339068	.05807024	5.2	48.81338	77.88931	11.6	239.3876	877.3813
.65	1.475789	.07862174	5.3	50.67445	82.52590	11.8	247.6827	923.6648
.7	1.618194	.1038627	5.4	52.57098	87.34192	12.0	256.1196	971.5461
.75	1.766608	.1343279	5.5	54.50295	92.34075	12.2	264.6983	1021.052
.8	1.921318	.1705496	5.6	56.47038	97.52578	12.4	273.4187	1072.211
.85	2.082609	.2130526	5.7	58.47325	102.9004	12.6	282.2810	1125.048
.9	2.250723	.2623557	5.8	60.51157	108.4680	12.8	291.2851	1179.591
.95	2.425902	.3189663	5.9	62.58534	114.2319	13.0	300.4309	1235.868
1.0	2.608351	.3833840	6.0	64.69456	120.1956	13.2	309.7186	1293.905
1.05	2.798269	.4560970	6.1	66.83923	126.3624	13.4	319.1480	1353.729
1.1	2.995825	.5375848	6.2	69.01935	132.7356	13.6	328.7193	1415.368
1.15	3.201185	.6283164	6.3	71.23492	139.3188	13.8	338.4323	1478.848
1.2	3.414479	.7287554	6.4	73.48593	146.1153	14.0	348.2872	1544.197
1.25	3.635847	.8393527	6.5	75.77240	153.1284	14.2	358.2838	1611.443
1.3	3.865384	.9605592	6.6	78.09431	160.3616	14.4	368.4222	1680.609
1.35	4.103208	1.092812	6.7	80.45168	167.8181	14.6	378.7025	1751.726
1.4	4.349386	1.236552	6.8	82.84449	175.5016	14.8	389.1245	1824.820
1.45	4.604011	1.392207	6.9	85.27275	183.4151	15.0	399.6883	1899.918
1.5	4.867132	1.560210	7.0	87.73646	191.5623	15.2	410.3940	1977.047
1.6	5.419114	1.934958	7.1	90.23562	199.9464	15.4	421.2414	2056.234
1.7	6.005696	2.364184	7.2	92.77023	208.5710	15.6	432.2306	2137.507
1.8	6.627149	2.851253	7.3	95.34029	217.4392	15.8	443.3616	2220.891
1.9	7.283658	3.399527	7.4	97.94580	226.5546	16.0	454.6344	2306.416
2.0	7.975359	4.012359	7.5	100.5868	235.9203	16.2	466.0490	2394.107
2.1	8.702340	4.693107	7.6	103.2632	245.5400	16.4	477.6054	2483.990
2.2	9.464667	5.445128	7.7	105.9750	255.4172	16.6	489.3036	2576.096
2.3	10.26236	6.271796	7.8	108.7223	265.5549	16.8	501.1436	2670.448
2.4	11.09547	7.176461	7.9	111.5051	275.9565	17.0	513.1254	2767.076
2.5	11.96402	8.162497	8.0	114.3233	286.6257	17.2	525.2490	2866.005
2.6	12.86798	9.233288	8.1	117.1769	297.5658	17.4	537.5143	2967.264
2.7	13.80739	10.39220	8.2	120.0660	308.7800	17.6	549.9215	3070.878
2.8	14.78225	11.64259	8.3	122.9906	320.2717	17.8	562.4705	3176.876
2.9	15.79255	12.98786	8.4	125.9506	332.0444	18.0	575.1613	3285.284
3.0	16.83830	14.43138	8.5	128.9460	344.1016	18.2	587.9938	3396.129
3.1	17.91951	15.97653	8.6	131.9769	356.4465	18.4	600.9682	3509.439
3.2	19.03615	17.62669	8.7	135.0433	369.0823	18.6	614.0843	3625.240
3.3	20.18825	19.38523	8.8	138.1450	382.0130	18.8	627.3423	3743.559
3.4	21.37579	21.25555	8.9	141.2823	395.2412	19.0	640.7420	3864.424
3.5	22.59879	23.24101	9.0	144.4550	408.7709	19.2	654.2836	3987.862
3.6	23.85723	25.34502	9.1	147.6631	422.6053	19.4	667.9669	4113.900
3.7	25.15112	27.57092	9.2	150.9067	436.7477	19.6	681.7921	4242.565
3.8	26.48046	29.92213	9.3	154.1858	451.2013	19.8	695.7590	4373.882
3.9	27.84525	32.40201	9.4	157.5002	465.9702	20.0	709.8677	4507.882
4.0	29.24549	35.01395	9.5	160.8502	481.0568	20.2	724.0828	4644.817
			9.6	164.2356	496.4653	20.4	738.5106	4784.033

Recent experiments[6-8] on the scattering of molecular beams have involved a modification of Θ_5, namely, the function

$$\Phi(\alpha)=\alpha^2\int_0^\infty \frac{x^5\exp(-\alpha x^2)}{\Psi(x)}dx.$$

[6] W. H. Mais, Phys. Rev. **45**, 773 (1934).

[7] S. Rosin and I. I. Rabi, Phys. Rev. **48**, 373 (1935). Rosin and Rabi give values of $\Psi(x)$ to three significant figures which disagree with the results of the present calculations in the second and third significant figures. Rosin and Rabi's value of Θ_5 is 0.844 which disagrees with the results of Tait, of Boltzmann, and of Rosenberg, in the second significant figure (cf. Table II). (In the notation used by Rosin and Rabi $\Theta_5=4I(\alpha)$ for $\alpha=1$.)

[8] P. Rosenberg, Phys. Rev. **55**, 1267 (1939); **57**, 561 (1940).

$\Phi(\alpha)$ is used to determine the average mean free path of a molecular beam particle traversing a scattering gas. α is the square of the ratio of the most probable speed of the particles of the scattering gas to the most probable speed of the particles of gas in the source of the beam.

$\Phi(\alpha)$ is now evaluated by numerical quadrature for 27 selected values of α. The results are given in Table III.

The following convergence test is used to determine the upper limits in the numerical quadratures of $\Phi(\alpha)$. If the quadrature is carried out from $x=0$ to a value $x=L$, the remainder R is given by

$$R=\alpha^2\int_L^\infty \frac{x^5\exp(-\alpha x^2)}{\Psi(x)}dx$$

$$<\alpha^2\int_L^\infty \frac{x^3\exp(-\alpha x^2)}{2P}dx=S,$$

where $$P=\int_0^L \exp(-y^2)dy.$$

S can be evaluated analytically, yielding

$$S=[(\alpha L^2+1)/4P]\exp(-\alpha L^2).$$

In each quadrature of $\Phi(\alpha)$, L is chosen large enough so that S is negligibly small compared to the eighth significant figure in the value of $\Phi(\alpha)$.

TABLE II. Values of Θ_n.

	Θ_3	Θ_4	Θ_5
Tait	0.650404	0.677072	0.838098
Boltzmann	0.650511	0.677464	0.838264
This paper	0.6505144	0.6774560	0.8382656

TABLE III. Values of $\Phi(\alpha)$.

α	$\Phi(\alpha)$	α	$\Phi(\alpha)$
0.	0.2820948 ($=1/2\pi^{\frac{1}{2}}$)	8.	0.1071319
.05	.2756271	9.	.1019461
.1	.2698879	10.	.09744985
.5	.2364264	11.	.09350219
.6	.2301268	12.	.08999987
.8	.2190537	15.	.08146816
1.	.2095664	17.	.07696826
1.2	.2012941	20.	.07143003
2.	.1762257	21.	.06983411
3.	.1553010	22.	.06834015
4.	.1405107	25.	.06437612
5.	.1293167	30.	.05907038
6.	.1204532	35.	.05489229
7.	.1132050	40.	.05149165

A similar convergence test is used in the quadratures of Θ_n.

The quadratures of Θ_n and $\Phi(\alpha)$ are performed by Simpson's $\frac{1}{3}$ rule. In all but a few of the quadratures, the interval in x is so small that the sum of the odd terms is equal to the sum of the even terms to the first six or more figures. The equality of these two sums is regarded as an internal check on the accuracy of the numerical computations.

The values of $\Psi(x)$ and $x^5/\Psi(x)$ are exact to only six of the seven figures given in Table I. The values of Θ_n and $\Phi(\alpha)$ are computed to eight figures and are given correct to seven figures in Table II and Table III.

Values of the probability integral are taken from the table of Burgess.[9] Values of the descending exponential are obtained from the table of Newman.[10]

Mr. David S. Cohen assisted in the numerical computations.

[9] J. Burgess, Trans. Roy. Soc. Edinburgh **39**, 257 (1898).
[10] F. W. Newman, Trans. Camb. Phil. Soc. **13**, 145 (1883).

Supersonic Absorption and Stokes' Viscosity Relation

L. TISZA
George Eastman Research Laboratory of Physics, Massachusetts Institute of Technology, Cambridge, Massachusetts

(Received December 4, 1941)

It is pointed out that the reduction of the *two* viscosity coefficients to *one* according to the Stokes' relation $2\mu+3\lambda=0$ is not justified except in the special case of a monatomic gas. The generalization of this relation by the re-introduction of the second independent viscosity coefficient $\kappa=\frac{2}{3}\mu+\lambda$ makes it possible to develop the phenomenological theory of the absorption and dispersion of sound, in agreement with experiment in complete analogy to the corresponding optical phenomena. The connection of the well-known relaxation theory with classical hydrodynamics can be established and in the case of polyatomic gases κ is expressed by the characteristic constants of this theory. The case of liquids is discussed. In polyatomic gases and liquids one has generally $\kappa\gg\mu$. Other hydrodynamical consequences of the introduction of κ are discussed.

I. INTRODUCTION

IT is a well-known fact that the supersonic absorption in polyatomic gases and in liquids exceeds by far the absorption predicted by the classical theory based on viscosity. For the very extended literature we refer to the detailed bibliography contained in the recent review of Richards.[1] The effect of heat conductivity on absorption is in general still smaller; we shall not discuss it in the following.

The "anomalous" absorption in gases is accompanied by a dispersion of sound velocity. Both absorption and dispersion were interpreted with success by the relaxation theory first proposed by Herzfeld and Rice[2] and developed by many others.[1]

This theory is based on the hypothesis that the molecular vibration requires a much larger number of collisions for reaching the state of thermal equilibrium than the translation and rotation. In other words, the relaxation time τ for the vibrational degrees of freedom is much greater than the relaxation time for the Maxwell distribution for the translational degrees of freedom. The latter is under ordinary conditions of the order of 10^{-9} sec. This hypothesis leads in a straight-forward way to a complex and frequency dependent specific heat making it possible to account for the absorption and dispersion of sound.

The persistence of the excited vibrational states over a period covering many thousand collisions has been proved through direct spectroscopic evidence by R. J. Dwyer.[3] On the other hand, τ could be calculated theoretically from molecular data by Landau and Teller.[4]

We therefore may consider it an unquestioned fact that there is a time lag in the establishment of equilibrium for the internal degrees of freedom and consequently a dissipation of energy. The purpose of the present paper is to show that the classical hydrodynamical equations can be easily generalized so as to include this phenomenon. One has merely to re-introduce the second viscosity coefficient which appeared automatically in the hydrodynamical equations but which was eliminated by the well-known relation of Stokes.

For perfect polyatomic gases the relaxation theory may be considered as a kinetic calculation of this viscosity coefficient. Our phenomenological scheme remains of course valid for liquids, too, while the relaxation theory encounters in this case the characteristic difficulties of the kinetic theory.

II. THE STOKES' RELATION

The so-called second approximation of the hydrodynamical equations is based on the hypothesis of Newton according to which the stress tensor p_{ik} is a linear function of

$$u_{ik}=\tfrac{1}{2}(\partial u_i/\partial x_k+\partial u_k/\partial x_i),$$

[1] W. T. Richards, Rev. Mod. Phys. **11**, 36 (1939).
[2] K. F. Herzfeld and F. O. Rice, Phys. Rev. **31**, 691 (1929).
[3] R. J. Dwyer, J. Chem. Phys. **7**, 40 (1939).
[4] L. Landau and E. Teller, Physik. Zeits. Sowjetunion **10**, 34 (1936).

the time derivative of the deformation tensor (u_i is the ith component of the flow velocity). The most general relation of this kind is[5]

$$p_{ik}=p_0\delta_{ik}-2\mu u_{ik}-\lambda\delta_{ik}\sum_\alpha u_{\alpha\alpha}, \qquad (1)$$

where δ_{ik} is the Kronecker symbol, p_0 the pressure in the first approximation (the hydrostatic pressure), and μ, λ are the viscosity coefficients. The first one is the ordinary shearing viscosity, the second is sometimes called compression coefficient. Defining in the usual manner the scalar pressure p as the mean value of the diagonal elements of the stress tensor, we obtain

$$p=\tfrac{1}{3}\sum_\alpha p_{\alpha\alpha}=p_0-(\tfrac{2}{3}\mu+\lambda)\sum_\alpha u_{\alpha\alpha}. \qquad (2)$$

Introducing the notation

$$\tfrac{2}{3}\mu+\lambda=\kappa \qquad (3)$$

and making use of the continuity equation, we have

$$p=p_0+\kappa(1/\rho)d\rho/dt. \qquad (2a)$$

That is, the constant κ—which we shall prefer to use instead of λ—has a simple meaning: It gives the second-order correction to the hydrostatic pressure, arising as a consequence of a compression or dilatation.[6]

A difficulty arises, however, in the determination of κ, because the pressure of the first approximation p_0 is properly defined for the hydrostatic case only. We may extend the definition to our non-static case by the following convention:

We define $p_0(\rho)$ as the pressure which would result from an *adiabatic compression* starting from the equilibrium state $p_0(\rho_0)$. Obviously p_0 is a function of *one* independent variable, of the density. Therefore, there exists a function $\mathbf{P}=\int 1/\rho dp_0$, such that $d\mathbf{P}/dx_i=1/\rho dp_0/dx_i$.

The second approximation of the hydrodynamical equations may then be written in our notation:

$$du_i/dt=-\partial/\partial x_i(\mathbf{P}+U)+\mu\nabla^2u_i$$
$$+(\mu/3+\kappa)\partial/\partial x_i\sum_\alpha \partial u_\alpha/\partial x_\alpha \qquad (4)$$

where U is the potential of the external mass forces. We see that our decomposition (2a) of the pressure into two terms is reasonable, because the first term gives rise to forces of *conservative* and the second term to forces of *dissipative* character.

It has to be noted that (2a) and (4) are not the most general formulae, because non-adiabatic processes as heat conduction and radiative transfer of heat also give rise to additional terms to the hydrostatic pressure. Consequently, heat conduction gives dissipative effects as sound absorption. The non-adiabatic radiative heat transfer is particularly important in meteorology, where we have to add to the hydrostatic pressure $p_0(\rho)$ a term which is a function of two variables ρ, T. This case has been thoroughly discussed by V. Bjerknes.[7] In the present paper we are concerned only with the viscous effects.

In general it is usual to specialize (2a) and (4) by the relation

$$3\kappa=2\mu+3\lambda=0. \qquad (5)$$

This relation has been the object of much controversy. Most of the hydrodynamical textbooks introduce it by referring simply to Stokes.[8] It is sometimes maintained that (5) is only an arbitrary convention for the definition of the scalar pressure.[9] In other textbooks the inadequacy of this relation has been pointed out,[10] but so far as we know, its generalization has never been thoroughly discussed.

For monatomic gases, (5) can be rigorously derived from the kinetic theory. But, as we saw in the introduction, for polyatomic gases there is a time lag for the establishment of equilibrium of the internal degrees of freedom, and similar conditions may be expected in general for any system where the energy is distributed over different kinds of degrees of freedom, i.e., for any system except a monatomic gas. In the case of the existence of such a relaxation time τ, the pressure of the fluid will depend not only on the instantaneous value of the density, but also on

[5] E.g., H. Lamb, *Hydrodynamics* (1932), sixth edition, p. 574.

[6] We would prefer to call this term a "first-order correction," but this would be in contradiction with the usual expression of "hydrodynamical equations of the first approximation," for the equations without any viscosity term.

[7] Reference 5, p. 247.

[8] E.g., "It has been argued with great force by Professor Stokes . . ." Lord Rayleigh, *The Theory of Sound*, second edition, Vol. 2, p. 315.

[9] E.g. Enc. Math., third edition, Vol. 4, p. 69.

[10] E.g., M. Brillouin, *Leçons sur la Viscosité* (Paris, 1907). Report of the Committee on Hydrodynamics. Bull. Nat. Research Comm. No. 84 (1932).

the "history" of the system. The Newton hypothesis (1) or (2a), claiming proportionality of the pressure with the first time derivative of the density, means that only the dependence on the *near past* is considered. This is justified if the times involved in the phenomenon are small compared to the relaxation time, or if one has $\omega \ll \tau^{-1}$ where ω is the sound frequency.

If the last condition is not satisfied, we may proceed as in the similar case in optics and consider the "constant" κ as a complex function of frequency.

Finally, we must discuss the view according to which the relation (5) is merely a convention. Indeed, it is possible to introduce (5) as a definition of $p_0(\rho)$, instead of defining it by our above-mentioned convention. According to (2a) one has then $p=p_0$: first- and second-order pressures are identical, i.e., one cannot introduce the concept of the "pressure in first approximation" and has to allow the pressure to depend on other variables than the density alone. Though this procedure is not less justified than that proposed by us, the introduction of the constant κ and the clean separation of conservative and dissipative forces seem to be useful for many hydrodynamical problems.

Before going over to the discussion of the consequences of the introduction of κ, we will quote two passages of the papers of Stokes. These will make it evident that Stokes himself did not consider the relation (5) as a definition, but foresaw the possibility of the present generalization in case experiment would demand it.

". . . Of course we may at once put $\kappa=0$ if we assume that in the case of a uniform motion of dilatation the pressure at any instant depends only on the actual density and temperature at that instant and not on the rate at which the former changes with the time. In most cases to which it would be interesting to apply the theory of the friction of fluids, the density of the fluid is either constant or may without sensible error be regarded as constant, or else changes slowly with the time. In the first two cases the results would be the same and in the third nearly the same whether κ were equal to zero or not. Consequently, if theory and experiments should in such cases agree, the experiments must not be regarded as confirming that part of the theory which relates to supposing κ to be equal to zero."[11]

". . . I have always felt that the correctness of the value $\frac{1}{3}\mu$ for the coefficient of the last term of (4) does not rest on as firm a basis as the correctness of the equation of motion of an incompressible fluid, for which the last term does not come in at all. If the supposition made above be not admitted, we must replace the coefficient $\frac{1}{3}\mu$ by a different coefficient which has to be written $\frac{1}{3}\mu+\kappa$ and κ must be positive as otherwise the more alternate expansion and compression, alike in all directions, of a fluid, instead of demanding the exertion of work upon it, would cause it to give out work. . . ."[12]

III. ABSORPTION AND DISPERSION OF SOUND

The additional term in the equation of motion will give rise to a new term in the dissipation function

$$\kappa \int\int\int \left(\sum_\alpha \frac{\partial u_\alpha}{\partial x_\alpha} \right)^2 dxdydz. \tag{6}$$

In particular it will give rise to an additional absorption of sound which we are going to consider.

We shall restrict ourselves to small amplitudes and derive from (4) and the equation of continuity in the usual approximation the wave equation of sound

$$\ddot{\rho} - V_0^2 \nabla^2 \rho - (4\mu/3+\kappa) 1/\rho \nabla^2 \dot{\rho} = 0, \tag{7}$$

where $V_0=(\partial p/\partial \rho)^{\frac{1}{2}}$ is the sound velocity in the absence of viscosity. In the plane wave solution

$$\rho = \rho_0 + \rho_1 e^{i(\omega t - kx)} \tag{8}$$

k is complex, with the real and imaginary parts giving the sound velocity V and the absorption coefficient per unit length for the amplitude α. In other words we have

$$\text{real part } (k) = \omega/V, \text{ imaginary part } (k) = -\alpha. \tag{9}$$

Neglecting the quadratic term in the viscosity we have

$$k = \omega/V_0[1-(4\mu/3+\kappa)i\omega/2\rho V_0^2], \tag{10}$$

i.e.,

$$V = V_0, \quad \alpha = (4\mu/3+\kappa)\omega^2/2\rho_0 V_0^3. \tag{11}$$

[11] G. G. Stokes, Math. Phys. Papers **1**, p. 88.
[12] G. G. Stokes, Math. and Phys. Papers **3**, p. 136. We have slightly changed the notation.

The κ viscosity gives an absorption coefficient proportional to ω^2 and no dispersion, just as the μ viscosity does.

In the case of a perfect polyatomic gas the fraction of the absorption proportional to κ must be identical with the value given by the relaxation theory in the limit of low frequencies. The result of this theory can be expressed in the following form:[1]

$$\omega^2/k^2=p/\rho_0\left[1+(\gamma-1)\left(1-\eta+\frac{\eta}{1+i\omega\tau}\right)^{-1}\right], \quad (12)$$

where $\gamma=c_p/c_v$ is the ratio of the (static) specific heats at constant pressure and volume and $\eta=c_i/c_v$ is the fraction of the specific heat at constant volume corresponding to the internal degrees of freedom for which the equilibrium is established with the relaxation time τ. (More generally one would have to consider different η and τ values for every normal vibration.)

We obtain from (12) on neglecting the square of the second term,

$$k=\frac{\omega}{V_0}\left[1-\frac{1}{2}\cdot\frac{i\omega\tau(\gamma-1)}{(1+i\omega\tau(1-\eta))\gamma}\right]. \quad (13)$$

In the limit of small frequencies $\omega\tau\ll1$ we have

$$k=\omega/V_0[1-\tfrac{1}{2}i\omega\tau\eta(\gamma-1)/\gamma]. \quad (14)$$

The comparison (14) with the last term of (10) yields

$$\kappa=\rho_0V_0^2\tau\eta(\gamma-1)/\gamma. \quad (15)$$

We obtain a very simple form for κ if we remember that $V_0^2=\frac{1}{8}\pi\gamma\bar{v}^2$ where $\bar{v}$ is the mean thermal velocity and if we define the mean free path l' relative to the excitation of the vibration in question by the relation $l'=\tau\bar{v}$ we have thus

$$\kappa=\tfrac{1}{8}\pi\rho_0\bar{v}(\gamma-1)l'\eta. \quad (16)$$

More generally one has

$$\kappa=\tfrac{1}{8}\pi\rho_0\bar{v}(\gamma-1)\sum_i l'_i\eta_i, \quad (16a)$$

where the sum is taken over the different internal degrees of freedom, e.g., the different normal vibrations.

Equations (16) or (16a) can be easily compared to the ordinary viscosity, given by the well-known elementary formula

$$\mu=\tfrac{1}{3}\rho_0\bar{v}l, \quad (17)$$

where l is the mean free path in the ordinary sense.

These results cease to be valid for $\omega\geq\tau^{-1}$. In this frequency region the pressure will depend not only on the density and the rate of compression, as claimed by the relation of Newton, but on the whole history of the system. (A "non-Newtonian" behavior occurs also with respect to the shearing viscosity μ.) One can proceed, however, as in the analogous case in optics and introduce formally a coefficient $\kappa(\omega)$ depending on frequency. Comparing now (10) with (13) rather than with (14), we get

$$\kappa(\omega)=\rho_0V_0^2(\gamma-1)\eta\gamma[1+i\omega\tau(1-\eta)]^{-1}. \quad (18)$$

Separating real and imaginary parts:

$$\kappa=\kappa_1-i\kappa_2$$

we have according to (9) (10)

$$\alpha=\kappa_1\omega^2/2\rho_0V_0^3, \quad V=V_0(1+\kappa_2\omega/2\rho_0V_0^2). \quad (19)$$

Using (18) we get

$$\alpha=\frac{(\gamma-1)\eta\omega^2\tau}{2V_0\gamma[1+(1-\eta)^2\omega^2\tau^2]} \quad (20)$$

and

$$V=V_0\left[1+\frac{(\gamma-1)\eta(1-\eta)\omega^2\tau^2}{2\gamma[1+(1-\eta)^2\omega^2\tau^2]}\right]. \quad (21)$$

Equations (20) and (21), though somewhat different in notation, are of course identical with the corresponding formulae of the relaxation theory and are in general agreement with experiment. It should be possible to determine from the measurements the numerical values of the constants τ, η and so of κ. Unfortunately, there is a considerable deviation between the measurements of different laboratories, and keeping in mind the criticisms of W. T. Richards,[1] we would not attempt to fix the numerical values of these constants. We remark merely for orientation that on the basis of the experimental results obtained and compiled by Kneser[13] one has for CO_2 and N_2O $\kappa/\mu\sim2\times10^3$. For air κ and μ seem to be of the same order of magnitude.

[13] H. O. Kneser, Ann. d. Physik 16, 337 (1933).

The "anomalous" absorption of supersonics in liquids has been first observed by Biquard,[14] and has been corroborated since by many workers.[1] According to more recent results, V and α/ω^2 are for most liquids constant over wide ranges of frequencies,[15,16] i.e., we find very often a "Newtonian" behavior and can operate with a constant, real κ.

Kneser[17] proposed to interpret the absorption in liquids exactly as in the case of gases by the relaxation time connected with the internal molecular vibration. Herzfeld has shown recently[18] that, at least for water, the vibrational energy is insufficient to account for the effect. Herzfeld mentions the possibility that the relaxation time connected with the configurational energy might be of importance, as it was previously suggested by Debye. He proposes tentatively an equation which is equivalent to our Eq. (3).

The question may be put somewhat more generally. Roughly speaking, the energy of a liquid can be considered as consisting of molecular and intermolecular vibrations, of Debye quanta and of configurational energy (quasi-crystalline structure). This does not mean, of course, that we assume any strict additivity between these types of energies. In any case these types of energies will be distinct from the translational energy of the sound wave, and one will have to attribute different relaxation times to them. Therefore, practically the whole thermal energy of the liquid will contribute to the absorption ($\eta\sim 1$), whereas under ordinary conditions for gases ($\eta\ll 1$). On the other hand, because of the strong interaction in the liquid the relaxation time will be smaller than in the case of the gases. Although we cannot assume the formula (16a) to hold quantitatively for liquids, the experimental evidence of values of κ varying widely from one liquid to the other is not too surprising.

As concerns the determination of the numerical value of κ for the different liquids from experiment, we are faced with still greater difficulties than in the case of gases. Should we assume that the observed loss in the propagation of supersonics is owing entirely to the *true absorption* given by our formula (11) then we could determine κ out of the relation

$$L=\mu+\tfrac{3}{4}\kappa, \tag{22}$$

where L is the experimental "loss factor" defined and tabulated for the different liquids by Willard.[15] We would thus get values up to 2000 for κ/μ. It has to be kept in mind, however, that losses are not always caused by true absorption (energy converted into heat) but also to the scattering of the supersonic wave by density fluctuations.[19] As we do not see the possibility of an independent measurement of κ, the absorption measurements ought to be carefully analyzed as to the possibility of an evaluation of κ.

In the cases where α/ω^2 and V vary with the frequency, κ has to be chosen again as a function of ω. It is, however, not surprising that the formula (16a) derived for gases cannot quantitatively account for the experiments.

It is obvious that the knowledge of κ could prove useful in the investigation of liquid structure. The molecular interpretation of the experimental results would, however, be difficult in view of the different mechanisms contributing to κ. The situation is not very much different, though still more complicated, than in the case of the ordinary μ viscosity. The monatomic liquids would, therefore, be of special interest. The only monatomic liquid studied is mercury with an absorption which does not exceed considerably the classical value[20] ($\kappa/\mu\sim 1.5$). It is not quite certain, however, that mercury is a typical case.

IV. HYDRODYNAMICAL CONSEQUENCES OF THE INTRODUCTION OF κ

We have seen that the experiments on supersonic absorption lead for many liquids and gases to the result that the newly introduced viscosity coefficient exceeds by far the ordinary viscosity

[14] P. Biquard, Comptes rendus **193**, 226 (1931); Ann. d. Physik **6**, 195 (1936); Biquard indicated that the anomalous absorption might be due to the breakdown of Stokes' relation for high frequencies.
[15] G. W. Willard, J. Acous. Soc. Am. **12**, 438 (1941).
[16] F. E. Fox and G. D. Rock, J. Acous. Soc. Am. **12**, 505 (1941).
[17] H. O. Kneser, Ann. d. Physik **32**, 277 (1938).
[18] K. F. Hezfeld, J. Acous. Soc. Am. **13**, 33 (1941).
[19] R. Lucas, J. de Phys. **8**, 41 (1937). For a discussion of other sources of error cf. reference 15.
[20] R. Bär, Helv. Phys. Acta **10**, 332 (1937).

$\kappa \gg \mu$. The question arises, naturally, what are the other hydrodynamical consequences of the introduction of κ and why the usual method of ignoring it did not lead to more difficulties.

It can be seen from (6) and (8) and the continuity relation that the energy dissipation due to the κ viscosity for a periodic process of the frequency ω is of the order of

$$\kappa\omega^2(\rho_1/\rho_0)^2. \tag{22}$$

Hydrodynamics usually deals with problems where compressibility can be neglected, i.e., $\rho_1/\rho_0 \ll 1$. In fact, this was the chief reason why Stokes thought the value of κ was of secondary importance.[11] This circumstance can be, however, compensated if $\omega \gg 1$. This is the case of acoustical waves and still more of supersonics which have been amply discussed.

On the other hand, there are problems for which the compressibility cannot be neglected, when the flow velocities reach and exceed the sound velocity. These problems are treated by the so-called *gas dynamics*. In this case ρ_1/ρ_0 is of the order of unity and (22) can no more be neglected even if $\omega \sim 1$.

Not only the viscous, but also the turbulent dissipation has to be revised in the case of gas dynamics. The origin of turbulence has been studied chiefly for incompressible liquids. In this case a change in circulation may arise only as a consequence of the shearing viscosity near solid walls (Grenzschichttheorie of Prandtl). Computing the time derivative of circulation around a contour moving with the liquid on the basis of Eq. (4) one gets an additional term proportional to κ, which we shall consider now:

$$(d/dt) \oint \mathbf{u} \cdot d\mathbf{r} = \kappa \oint \frac{1}{\rho} \operatorname{grad} \operatorname{div} \mathbf{u} \cdot d\mathbf{r}. \tag{23}$$

This can be written in a more convenient form by using Stokes' theorem and the continuity equation:

$$\frac{d}{dt} \oint \mathbf{u} \cdot d\mathbf{r} = \kappa \iint \operatorname{grad} \frac{1}{\rho} \times \operatorname{grad} \frac{d \ln \rho}{dt} dF, \tag{24}$$

where dF is the surface element of a surface F spanned by the contour.

Let us consider two series of surfaces with $1/\rho = \text{constant}$ and $(d/dt) \ln \rho = \text{constant}$, respectively. We choose the distances of the neighboring surfaces to be $1/h_1 = |\operatorname{grad} 1/\rho|$ and $1/h_2 = |\operatorname{grad} d/dt \ln \rho|$. These surfaces form tubes which cut elementary surfaces f out of the surface F. It follows readily that

$$\frac{d}{dt} \oint \mathbf{u} \cdot d\mathbf{r} = \kappa \iint \frac{dF}{f}, \tag{25}$$

i.e., the rate of change of the circulation around a contour is equal to the number of tubes cutting the surface F.

Equation (25) is in formal analogy to a formula of Bjerkness concerning the rate of change of circulation in a fluid where the pressure is not entirely determined by the density, which is important in meteorology.[7]

It is a pleasure for us to thank Professor K. F. Herzfeld for his critical remarks and Dr. Biquard for discussing the experiments on supersonic absorption.

Letters to the Editor

PROMPT publication of brief reports of important discoveries in physics may be secured by addressing them to this department. The closing date for this department is the third of the month. Because of the late closing date for the section no proof can be shown to authors. The Board of Editors does not hold itself responsible for the opinions expressed by the correspondents. Communications should not in general exceed 600 words in length.

On a New Type of Vector Coupling in Complex Spectra

GIULIO RACAH
The Hebrew University, Jerusalem, Palestine
March 2, 1942

TWO types of vector coupling are generally considered by the spectroscopists, the (LS) and the (jj) coupling; the first takes place when the spin-orbit interaction is weak compared to the electrostatic, the second when the electrostatic interaction is the weaker. We wish to point out that a third type of definite vector coupling is possible, the (jl) coupling, which takes place when the electrostatic interaction is weak compared to the spin-orbit interaction of the parent ion, but is strong compared to the spin coupling of the external electron. In this case the total angular moment **j** of the parent ion and the orbital moment **l** of the external electron are coupled together and have a resultant **K**; then **K** is coupled with the spin of this electron, and their resultant is **J**.

Since the exchange forces act on the spins, it is not sufficient for the extreme (jl) coupling that the spin-orbit interaction of the external electron is weak, but also the exchange integrals G_k must be small compared to F_2; this condition has however a minor importance in the two-electron-like configurations with almost closed shells, since in this case most of the coefficients of G_k vanish.

The general structure of a configuration in (jl) coupling is a pair structure; these pairs have all the characteristic properties of doublets (line strengths, Zeeman and Paschen-Back effect, etc.) with the only difference that they may have a half-integral K and an integral J instead of an integral L and a half-integral J, and that $g(K)$ differs generally from unity.

Although this coupling was not yet explicitly used by the spectroscopists, it occurs actually in a number of known spectra: The most striking example is given by the $3d^95g$ configuration of Cu II, in which Shenstone[1] was unable to resolve the pairs; but also in other configurations of Cu II and of the rare gases the levels tend to occur in pairs. A calculation of the "purity" of the (jl) coupling in the $2p^5(^2P_{1\frac{1}{2}})nd$ configurations of Ne I (as made by Shortley[2] for the (jj) coupling) gives, for instance, a purity of 99–100 percent for the levels with $J=2$ and $J=3$, and of 90–96 percent for those with $J=1$; the latter deviation is easy to understand, since in this case the effect of G_1 tends to break the (jl) coupling.

Four notations at least were proposed for the levels of this and of similar configurations, but no one was generally accepted, because two are empirical and two, the (LS) and the (jj) notations, do not give a satisfactory picture of the actual vector coupling; we propose, therefore, that the levels of these configurations should be denoted by the K value of their pair: For instance, a suitable form for the notation of the level 12229.82 of Ne I (which was denoted as $3d''_1$ or $3d7_2$ or $3d2a'$) would be $(^2P_{1\frac{1}{2}})3d[2\frac{1}{2}]_2$; the K value is written in square brackets, the round brackets being as usual reserved for the term of the parent ion.

The doubling of the levels in the spectra of the rare gases was already pointed out by Shortley and Fried,[3] who also calculated the electrostatic interaction in an approximation which corresponds to the above-mentioned conditions for extreme (jl) coupling and obtained that in this approximation all levels should be double. Their numerical calculations of the coefficients of Slaters F^2 may be resumed by the formula

$$f_2(jlK)=-\frac{6h^2+3h-2j(j+1)l(l+1)}{4j(j+1)(2l-1)(2l+3)},$$

where

$$h=(\mathbf{j}\cdot\mathbf{l})=\frac{K(K+1)-j(j+1)-l(l+1)}{2};$$

this formula is very similar to the corresponding one for the (LS) coupling,[4] and will be demonstrated shortly in another paper.

The g values in (jl) coupling may be calculated with the ordinary methods of vector coupling; the result is

$$g=\frac{2J+1}{2K+1}+2\frac{K(K+1)+j(j+1)-l(l+1)}{(2K+1)(2J+1)}(g_j-1),$$

where g_j is the g factor of the parent ion.

The agreement with the experimental values is, of course, not so good as that of the g values calculated with the actual eigenfunctions;[5] nevertheless, owing to its simplicity and to its independence from the coupling parameters, this formula may be helpful to the spectroscopists for the classification of new spectra.

[1] Shenstone, Trans. Roy. Soc. **A235**, 195 (1936).
[2] G. H. Shortley, Phys. Rev. **44**, 666 (1933).
[3] G. H. Shortley and B. Fried, Phys. Rev. **54**, 749 (1938).
[4] G. Racah, Phys. Rev. **61**, 537 (1942).
[5] J. B. Green and J. A. Peoples, Jr., Phys. Rev. **54**, 602 (1938); J. B. Green and B. Fried, Phys. Rev. **54**, 876 (1938).

On the Deep Configuration of Cobalt

GIULIO RACAH
The Hebrew University, Jerusalem, Palestine
March 2, 1942

A RECENT paper of Russell, King, and Moore[1] (RKM) gives a very extensive classification of the spectrum of Co I; some assignments of terms to high configurations are given as tentative, but the assignments to the deep configurations are given as definitive, because the *theoretical* paper of Marvin[2] is considered as conclusive. We wish to point out that Marvin's results do not seem

conclusive to us, and to suggest an exchange in the assignments of the quartets P, i.e., that a^4P should be assigned to $3d^74s^2$ and b^4P to $3d^84s$.

Marvin assumed the assignments of the quartets to be *experimentally* assured, and based his calculations on this assumption: In order to explain the inverted position of the quartets P (which according to the theory should be in the same order and at the same distance as the quartets F) he was compelled to assume that the interaction parameters F_2 differ by 20 percent in the two configurations; but it is difficult to admit such a difference.

We fitted the experimental values of RKM (with exclusion of b^2D and c^2D) to the theoretical formulas by means of the least squares, and calculated the mean deviation Δ and the mean error μ, which are defined by

$$\Delta^2=\Sigma\Delta_i^2/n \quad \text{and} \quad \mu^2=\Sigma\Delta_i^2/(n-m),$$

where Δ_i is the deviation of each term, n the number of terms, and m the number of free parameters; the results are

with the old assignments $\Delta=\pm482$, $\mu=\pm799$,
with the proposed assignments $\Delta=\pm423$, $\mu=\pm702$.

We made also the same calculation with the assumption that F_2 and F_4 should have the same values in the two configurations, and obtained

with the old assignments $\Delta=\pm919$, $\mu=\pm1245$,
with the proposed assignments $\Delta=\pm562$, $\mu=\pm762$.

We see from these results that the proposed assignments agree better with the theory, and that, if these assignments are right, it has very little sense to assume, in this approximation, different parameters for the two configurations, since the better agreement is chiefly due to the greater number of parameters, and μ does hardly change. This last conclusion strengthens the assumption of Ufford[3] that the radial integrals containing electrons of identical n and l are to be taken as equal, regardless of the fact that these electrons belong to different configurations; the use of this rule may be of some aid in the classification of new spectra. The results of the calculation with unified parameters are shown in Table I.

But the most conclusive proof that the proposed assignments are right is given by the consideration of the

TABLE I. Observed and calculated low terms in Co I.
($F_2=1393$, $F_4=119.1$, $G_2=1128$)

Config.	Term	Obs.	Calc.
d^7s^2	a^4F	793	1477
d^8s	b^4F	4158	3794
d^8s	a^2F	7879	7177
d^7s^2	a^4P	13976	13444
d^8s	b^4P	15549	15761
d^8s	a^2D	16655	17246
d^7s^2	a^2G	16808	17171
d^8s	a^2P	18518	19144
d^7s^2	b^2P	20739	21160
d^7s^2	a^2H	22096	21160
d^7s^2	b^2D	22413	23475 (23286)*
d^8s	b^2G	23195	22831
d^9	c^2D	27886	27886
d^7s^2	^2F		33127
d^8s	^2S		51648
d^7s^2	^2D		53067 (53235)*

* With configuration interaction between d^7s^2 and d^9.

TABLE II. The g sums for the deep configurations of Co I.

Config.		d^7s^2	d^8s	d^9	All
$J=1/2$	N	2 =2	2 =3		4 =5
	O	3.34	3.37		6.71
	T	3.33	3.33		6.67
3/2	N	4 =5	4 =4	1 =1	9 =10
	O	4.22 (3.97)*	4.29 (4.54)*	0.82	9.33
	T	4.27	4.27	0.80	9.33
5/2	N	3 =5	4 =4	1 =1	8 =10
	O	3.93 (3.79)*	4.68 (4.82)*	1.20	9.81
	T	3.83	4.68	1.20	9.71
7/2	N	2 =3	3 =3		5 =6
	O	2.17	3.28		5.45
	T	2.13	3.27		5.40
9/2	N	3 =3	2 =2		5 =5
	O	3.37	2.45		5.82
	T	3.35	2.45		5.80
11/2	N	1 =1			1 =1
	O	1.09			1.09
	T	1.09			1.09
All	N	15 =19	15 =16	2 =2	32 =37
	O	18.12	18.07	2.02	38.21
	T	18.00	18.00	2.00	38.00

* g sums with the old assignments.

TABLE III. Calculated and observed g factors of the terms b^4P and a^2D.

Level	LS	Marvin	Author	Obs.
$b^4P_{2\frac{1}{2}}$	1.60	1.597	1.50	1.50
$a^2D_{2\frac{1}{2}}$	1.20	1.219	1.30	1.28
$b^4P_{1\frac{1}{2}}$	1.73	1.720	1.54	1.47
$a^2D_{1\frac{1}{2}}$	0.80	0.879	0.99	1.09

g factors. RKM have shown that the g-sum rule holds very good for the three deep configurations together; since the g-sum rule must hold for each configuration separately,[4] we calculated the partial g sums: As it is shown in Table II, the agreement is also very good with the proposed assignments, but it is squarely bad with the old.

Since three terms of the deep configurations are still unknown, the number of expected levels is given together with the number of known levels, and we see also that the little deviations from the g-sum rule observed by RKM may easily be ascribed to the deviations of the unknown levels from the theoretical g values.

Marvin could not explain the conspicuous g sharing between a^2D and b^4P, since no g sharing takes place between terms of different configurations; with the proposed assignments both terms belong to $3d^84s$, and a rough evaluation of the sharing may be made even neglecting the action of the other terms of the configuration. In this approximation the sharing depends only on the ratio between the spin-orbit interaction coefficient a and the difference Δ between the baricenters of the unperturbed terms; from the separations of the two couples of levels with the same J we obtained $a=474$ and $\Delta=570$, and used these values for calculating the g factors: The results are given in Table III and confirm the proposed assignments.

The assignments of the terms of the higher configurations must also be revised, since they are chiefly based on the assignments of the low quartets; a theoretical discussion

is, however, premature, since the formulas for the d^7sp configuration are not yet calculated;[5] we wish only to point out the valuable aid that the consideration of the g sharing may give to this revision.

[1] Russell, King, and Moore, Phys. Rev. **58**, 407 (1940).
[2] H. H. Marvin, Phys. Rev. **47**, 521 (1935).
[3] C. W. Ufford, Phys. Rev. **44**, 732 (1933).
[4] E. U. Condon and G. H. Shortley, *Theory of Atomic Spectra*, p. 386.
[5] We obtained recently the formulas for d^6p, which are in good agreement with the observations made with Ni II and will be published shortly.

Thick-Target Yield of Na^{24} under Deuteron Bombardment

CARL L. BAILEY AND JOHN H. WILLIAMS
University of Minnesota, Minneapolis, Minnesota
March 7, 1942

THE yield of Na^{24} from the reaction

$$Na^{23}+H^2 \rightarrow Na^{24}+H^1$$

has been studied in the range 1.5 to 3.0 Mev, with deuterons furnished by the pressure electrostatic generator[1] at the University of Minnesota.

Thick targets, made of NaOH fused on brass plugs, were used. Yields were measured by detection of the activity of Na^{24}, by use of a Barth type[2] linear amplifier and a pressure ionization chamber, and were referred to unit quantity of bombarding ions. The thick-target yield as a function of energy E_L measured in the laboratory system is given in Fig. 1.

The Gamow (thin-target) formula[3]

$$y=(\kappa/E)e^{-2\eta\gamma}, \qquad (1)$$

where E is measured in the center of mass system, was found adequate to interpret the results. In applying (1) the observed yields (Y) were reduced to thin-target yields

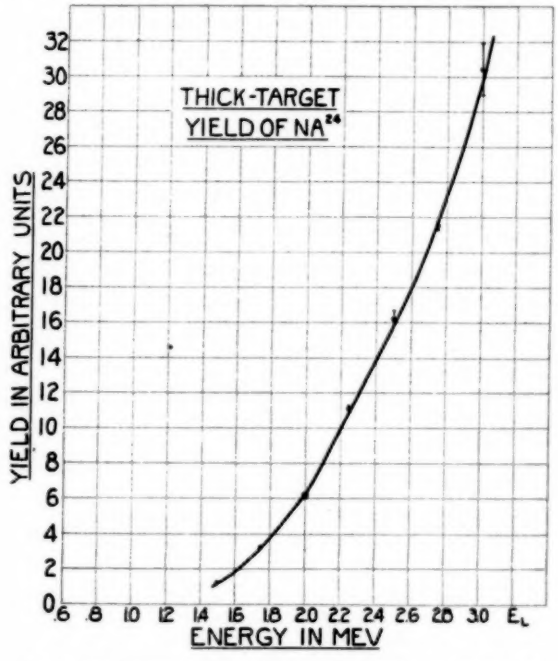

FIG. 1. Thick-target yield for the reaction $Na^{23}+H^2 \rightarrow Na^{24}+H^1$.

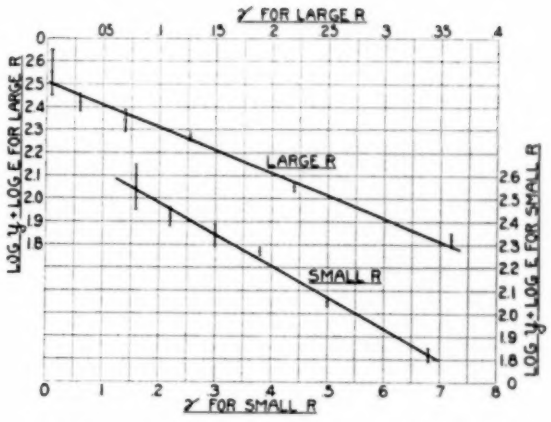

FIG. 2. Gamow-type plots of derived thin-target data for two choices of nuclear radius.

(y) by assuming the range of H^2 in the target proportional to E^1:

$$y=dY/d(E^1). \qquad (2)$$

γ is a function[3] of the barrier height of the struck nucleus and hence of the nuclear radius. Calculations were made for two radii: the first (large) was derived from the many-body theory[3] of alpha-decay, and the second (small) from the work of White *et al.*[4] on the positron decay of light nuclei and that of Wigner[5,6] on nuclear Coulomb energy. The two radii are

(large) $r_0=2.05\times10^{-13}$ cm,
(small) $r_0=1.45\times10^{-13}$ cm.

Logarithmic plots of (1) for each of the two radii are given in Fig. 2. While the fit may be somewhat better for the large radius, a choice of r_0 is hardly possible from these data. However, it is uncertain whether the radius as derived from the positron decay experiments is applicable to disintegrations produced by charged particle bombardment.

It is thus clear that experiments of the above type, where the bombarding energy is less than the barrier height calculated from a reasonable radius, do not serve to distinguish between possible choices of radii. The experiments do impose an upper limit to the choice of radius, since the excitation function shows no abrupt change up to the highest available bombarding energy.

Furthermore, the results show that the excitation function is amply represented by a Gamow function. Bethe's calculations[3] on the data of Lawrence, McMillan, and Thornton[7] agree with this conclusion. The Oppenheimer-Phillips[8] treatment would fit the data equally well, since the O-P and Gamow theories are indistinguishable in this region of atomic numbers. However, Bethe has shown[9] that the O-P process is less likely for light nuclei.

We are indebted to Dr. M. Phillips for stimulating discussions on the interpretation of these experiments.

[1] Williams, Rumbaugh, and Tate (to be published soon).
[2] D. B. Penick, Rev. Sci. Inst. **6**, 115 (1935).
[3] H. A. Bethe, Rev. Mod. Phys. **9**, 69 (1937).
[4] White, Creutz, Delsasso, and Wilson, Phys. Rev. **59**, 63 (1941).
[5] E. Wigner, Phys. Rev. **51**, 952 (1937).
[6] E. Wigner, Phys. Rev. **56**, 519 (1939).
[7] Lawrence, McMillan, and Thornton, Phys. Rev. **48**, 493 (1935).
[8] J. R. Oppenheimer and M. Phillips, Phys. Rev. **48**, 500 (1935).
[9] H. A. Bethe, Phys. Rev. **53**, 39 (1938).

Errata: The Vibration-Rotation Energies of Polyatomic Molecules

(Phys. Rev. **60**, 794 (1941))

HARALD H. NIELSEN
Mendenhall Laboratory of Physics, Ohio State University, Columbus, Ohio
February 27, 1942

IN the recent paper by the above title a few errors which are essentially of a typographical nature have occurred. While none of these affects the final results in any manner, it has seemed desirable to call attention to them for the benefit of anyone wishing to work through the problem from the beginning. The changes are as follows:

1. From the foregoing definitions it is obvious that what in Eq. (15) has been termed I_{xz} should have been I_{yz} and similarly that I_{yz} should be I_{xz}. This error is purely typographical.

2. In the second-order Hamiltonian H_2 there is an error in the coefficient of $q_{s\sigma}p_{s'\sigma'}$. It should read:

$$(-ih/2)\sum_{s\sigma}\sum_{s'\sigma'}(\lambda_{s'}/\lambda_s)^{\frac{1}{2}}[(A_{s\sigma s'\sigma'}/I_{xx}^{(e)})+(B_{s\sigma s'\sigma'}/I_{yy}^{(e)})$$
$$+(C_{s\sigma s'\sigma'}/I_{zz}^{(e)})-(a_{s\sigma}a_{s'\sigma'}/2(I_{xx}^{(e)})^2)-(b_{s\sigma}b_{s'\sigma'}/2(I_{yy}^{(e)})^2)$$
$$-(c_{s\sigma}c_{s'\sigma'}/2(I_{zz}^{(e)})^2)-(d_{s\sigma}d_{s'\sigma'}/(I_{xx}^{(e)})(I_{yy}^{(e)}))$$
$$-(e_{s\sigma}e_{s'\sigma'}/(I_{yy}^{(e)})(I_{zz}^{(e)}))-(f_{s\sigma s'\sigma'}/(I_{zz}^{(e)})(I_{xx}^{(e)}))].$$

This term contributes to the energy only in E_0/hc which, as we have pointed out, is of no physical interest and its value was not calculated in this paper.

3. In the coefficient of $(P_xP_y+P_yP_x)$ and $(P_xP_z+P_zP_x)$ in the second-order Hamiltonian H_2 the algebraic sign preceding the terms $(e_{s\sigma}f_{s''\sigma''}/I_{zz}^{(e)})$ and $(d_{s\sigma}e_{s''\sigma''}/I_{yy}^{(e)})$ should be $+$. Moreover, the third term in the coefficient of $(P_xP_z+P_zP_x)$ and the second term in the coefficient of $(P_yP_z+P_zP_y)$ should be, respectively, $-(c_{s\sigma}f_{s''\sigma''}/I_{zz}^{(e)})$ and $-(e_{s\sigma}b_{s''\sigma''}/I_{yy}^{(e)})$. These errors also are purely typographical and what is more, terms of the above type cannot contribute to the energy in second order of approximation.

4. In the second-order transformed Hamiltonian H_2' an error in copying from the author's original manuscript has occurred. In the coefficients of the terms $(P_\alpha^2P_\beta^2+P_\beta^2P_\alpha^2)$ the quantities $d_{s\sigma}^2$, $e_{s\sigma}^2$ and $f_{s\sigma}^2$ should be deleted so as to read:

$$[a_{s\sigma}b_{s\sigma}/(I_{xx}^{(e)})^2(I_{yy}^{(e)})^2](P_x^2P_y^2+P_y^2P_x^2)$$
$$+[a_{s\sigma}c_{s\sigma}/(I_{xx}^{(e)})^2(I_{zz}^{(e)})^2](P_x^2P_z^2+P_z^2P_x^2)$$
$$+[b_{s\sigma}c_{s\sigma}/(I_{yy}^{(e)})^2(I_{zz}^{(e)})^2](P_y^2P_z^2+P_z^2P_y^2).$$

The quantities $[d_{s\sigma}^2/(I_{xx}^{(e)})^2(I_{yy}^{(e)})^2]$, $[e_{s\sigma}^2/(I_{yy}^{(e)})^2(I_{zz}^{(e)})^2]$ and $[f_{s\sigma}^2/(I_{xx}^{(e)})^2(I_{zz}^{(e)})^2]$ are the coefficients of the terms $(P_\alpha P_\beta+P_\beta P_\alpha)^2$, respectively. The transformed Hamiltonian H_2' should therefore include also the following terms:

$$+[d_{s\sigma}^2/(I_{xx}^{(e)})^2(I_{yy}^{(e)})^2](P_xP_y+P_yP_x)^2$$
$$+[e_{s\sigma}^2/(I_{yy}^{(e)})^2(I_{zz}^{(e)})^2](P_yP_z+P_zP_y)^2$$
$$+[f_{s\sigma}^2/(I_{zz}^{(e)})^2(I_{xx}^{(e)})^2](P_zP_x+P_xP_z)^2.$$

The actual energy relations stated in Eqs. (26) to (30) and in Section IV are believed to be correct as they stand except that the algebraic sign within the parentheses of the numerators of the last two terms in (27) should be $+$ and that the definitions of x_0 and y_0[1] in (28) should be interchanged.

I am indebted to Dr. Samuel Silver of the University of Oklahoma who has verified the calculations reported in the earlier paper and who has called my attention to some of the errors corrected herein.

[1] The terms x_0, y_0, and z_0 are of the order of magnitude of the coefficients of centrifugal distortion; D_J, D_{JK}, and D_K. These latter terms become important only for larger values of J, say $J>6$, and then only because they are multiplied by quantities quartic in J and K. The terms x_0, y_0, and z_0, on the other hand are multiplied by terms only quadratic in J and K and will contribute amounts to the energy small even as compared to the centrifugal distortion. The terms x_0, y_0, and z_0 may, therefore, actually be omitted from the effective reciprocals of inertia.

Proceedings of the American Physical Society

MICHIGAN MEETING, DETROIT AND ANN ARBOR, FEBRUARY 20–21, 1942

THE 247th meeting of the American Physical Society and the Midwinter Meeting of the Ohio Section were jointly held on February 20 and 21, 1942. They began in Detroit on Friday in the Rackham Educational Memorial. Contributed papers were presented in the morning and a symposium on topics of applied physics was offered in the afternoon. The gratitude of the Society was amply earned by the Local Committees, headed by G. P. Brewington at Detroit and E. F. Barker at Ann Arbor. At Ann Arbor on Saturday, the Society convened in the Rackham Building of the University of Michigan to hear contributed papers in the morning and a symposium on the infra-red and ultraviolet in the afternoon. The dinner was held on the evening of the 20th at Huyler's Restaurant, Detroit, President Bridgman presiding. The principal after-dinner address was delivered by T. A. Boyd on the "Origin and Early History of Most of the Important Features of the Automobile." There were ninety-five who registered at Detroit on the first day of the meeting.

The symposia consisted of the following invited papers:

Symposium on Topics of Applied Physics

I. Ceramic Insulators for Spark Plugs. FRANK RIDDLE, *Ceramic Division, Champion Spark Plug Company, Detroit.*

II. The Fatigue Characteristics of Rubber. F. F. YOST, *U. S. Rubber Company, Detroit.*

III. Static Electric Effects on Rubber Tired Vehicles. NIEL HANDLE, *U. S. Rubber Company, Detroit.*

IV. Some Applications of X-Ray Inspection to Defense Problems. DON M. MCCUTCHEON, *Metallurgical Engineer, Ford Motor Company, Dearborn.*

Symposium on the Infra-Red and Ultraviolet

I. Precision Measurements with the Infra-Red Recording Prism Spectrometer. H. M. RANDALL, *University of Michigan.*

II. The Application of a Lithium Fluoride Prism in Infra-Red Spectroscopy. NORMAN WRIGHT, *The Dow Chemical Company, Midland.*

III. Coriolis Interaction and the Infra-Red Spectra of Certain Polyatomic Molecules. HARALD H. NIELSEN, *Ohio State University.*

IV. Some High Dispersion Grating Spectra in the Ultraviolet. ROBERT S. MULLIKEN, *University of Chicago.*

Meeting of the Council. The Council met on Friday afternoon, February 20th, and made forty-eight elections to Membership, one reinstatement to Membership, and five elevations from Membership to Fellowship. These names are appended. The resignations of four Members were reported. Karl K. Darrow and A. L. Hughes were appointed representatives of the Physical Society on the Council of the American Association for the Advancement of Science for 1942.

Transferred from Membership to Fellowship: Léon Brillouin, L. Marton, W. G. Pollard, Nathan Rosen, and Philip Rudnick. *Reinstated to Membership:* R. Robert Brattain. *Elected to Membership:* William B. Agocs, Clayton H. Allen, George E. Beggs, Jr., Ely E. Bell, Richard Blythe, Arthur A. Brown, Arthur A. Burr, Sabinus H. Christensen, Emory Cook, Virgil A. Counter, Paul C. Cross, R. Hobart Ellis, Jr., John Ellis Evans, Henry A. Fairbank, Milton Greene, John A. Habrle, Samuel W. Harding, Milton D. Hare, G. Truman Hunter, Robert M. Kalb, Wilfred Kaplan, An-Tsai Kiang, M. C. Leverett, Kurt S. Lion, Elwood Maple, Arnold C. McLean, Katherine E. Mounce, Max Muller, Welville B. Nowak, Wesley L. Nyborg, Evert M. Ostlund, Turner E. Pardue, Charles D. Prater, Walter P. Reid, Joshua H. Rosenbloom, Herbert C. Rothenberg, Kurt Rothschild, Gertrud Schwarzmann, Armand Siegel, Harry Soodak, Robert S. Spencer, William P. Staker, Charles Stevens, Alexander Strasser, Robert I. Strough, Walter E. Tolles, Rohn Truell, and Nelson L. Walbridge.

The abstracts of the twenty-eight contributed papers are reproduced below, three of these papers (Nos. 7, 11, and 28) having been read by title.

KARL K. DARROW, *Secretary*
American Physical Society,
Columbia University,
New York, New York.

ABSTRACTS TO CONTRIBUTED PAPERS

1. Rubber in Vibration. S. D. GEHMAN, *The Goodyear Tire & Rubber Co.*—A machine is described which has been used for determining the vibration properties of various types of rubber mountings used for the isolation of mechanical vibrations. The vibrations are excited by oppositely rotating eccentric weights and are recorded on a tape. It was found that resonance curves for various types of rubber vibrations such as shear, torsion, and compression are, except for some minor deviations, adequately accounted for by the equation which contains a damping term proportional to the velocity and inversely proportional to the frequency. The apparent static modulus of rubber in compression depends upon the shape of the piece, more explicitly, on the ratio of load area to the free area. The same is true for the dynamic modulus. It was found that pieces of similar shape have identical values for the dynamic modulus and also for the internal friction. Some curves are given showing the dependence of dynamic modulus and internal friction on the shape factor. The dynamic stiffness shows the largest deviation from the static values at high shape factors. The internal friction has a linear relationship to the dynamic modulus when the shape factor is varied. This results in damping which is practically independent of the shape.

2. Equations of State for Stressed Rubber. R. H. CASTON, R. L. ANTHONY AND E. GUTH, *University of Notre Dame.*—A simple technique was developed to obtain the equations of state of typical unaccelerated and accelerated pure gum compounds which do not show crystallization in the range of extensions investigated. The samples were relaxed at constant length until the change in force with time was negligibly small. This technique yielded for both types of compounds: (1) Linear dependency of stress upon absolute temperature, (2) S-shaped stress-strain curves, (3) a thermoelastic inversion point. This inversion point occurs at 10 percent extension for the unaccelerated compound and at 15 percent for the accelerated compound. Below these critical extensions the stress decreases with rising temperature as in the case of a normal solid; above these critical extensions the stress increases with rising temperature. Using thermodynamics only, the stress-strain curves were decomposed into their additive parts due to internal energy and entropy, the entropy stress being S-shaped. The decomposed parts were compared with the theory of James and Guth.[1] This theory explains that the thermoelastic inversion point is due to ordinary thermal expansion, accounts quantitatively for the dependency of the entropy stress on extension and for the linearity of the stress-temperature curves.

[1] H. M. James and E. Guth, Phys. Rev. **59**, 111 (1941); E. Guth and H. M. James, Ind. Eng. Chem. **33**, 624 (1941).

3. The Transition from Thermionic to Cold Emission. CHARLES J. MULLIN, *Saint Louis University*, AND EUGENE GUTH, *University of Notre Dame.*—The theory of Schottky emission is extended to include in the current those electrons which tunnel through the top of the potential barrier at the metal surface when rather strong electric fields are used. It is found that these tunnelling electrons contribute to the periodic deviations from the Schottky line, increasing the amplitude of the deviations; this increase leads to a better agreement with experiment, especially for large fields. This agreement requires that the Nottingham[1] reflection coefficient be very small for fields greater than 10^4 volts per cm. Expressions are developed for the electron current emitted by a metal for various field intensities ranging from the small fields of thermionic work to the large fields used in cold emission. Results are obtained to indicate the temperature and field dependence of the electron current for all fields and temperatures of interest. Of particular interest is the expression developed for the current in the "transition region," i.e., $T\sim 500$–$1200°K$ and $F\sim 10^7$–10^8 volts per cm. The modifications which must be made in the theory to take account of the polycrystalline nature of the emitting surface have no effect on the periodic deviations from the Schottky line, and very little effect on the fluctuations observed in field photo-currents.

[1] W. B. Nottingham, Phys. Rev. **49**, 78 (1936).

4. Electronic Energy Bands in Face-Centered Iron. J. B. GREENE, *University of Illinois*, AND MILLARD F. MANNING, *University of Pittsburgh.*—Energy bands for the face-centered form of metallic iron have been calculated, by using relations given previously by Krutter[1] and by Shockley.[2] E *vs.* k curves for a number of directions in k space have been calculated. From these, energy contours in k space have been drawn and the number of energy levels per unit energy range obtained. In general, the energy bands resemble those obtained for copper by Krutter, but the concentration of energy levels near the top of the "d" band is less than Slater[3] obtained for copper. From the $n(E)$ curves interpretations of a number of properties of gamma-iron can be given.

[1] H. M. Krutter, Phys. Rev. **48**, 664 (1935).
[2] W. Shockley, Phys. Rev. **51**, 128 (1936).
[3] J. C. Slater, Phys. Rev. **49**, 537 (1936).

5. Electronic Energy Band in Body-Centered Iron. MILLARD F. MANNING, *University of Pittsburgh.*—Energy bands for the body-centered form of iron have been calculated by the Wigner-Seitz-Slater method by using relations given previously by Chodorow and Manning.[1] The structure of the energy bands is different from that obtained for metallic tungsten, which is the only other body-centered transition metal for which calculations have been made. There is one narrow band which begins at the energy for which $3s_1'g_2'+2s_2'g_1'=0$, three bands beginning at the energy for which $d_1'=0$, and two beginning at the energy for which $d_2'=0$. The band which begins at $3s_1'g_2'+2s_2'g_1'=0$ accounts for most of the binding energy and is probably related to the 2.56 electrons per atom which Pauling has suggested form homopolar bonds in iron group elements.

The $n(E)$ curves for the body-centered structure show interesting differences from the $n(E)$ curves for the face-centered structure. From the $n(E)$ curves interpretations of various properties of metallic iron can be given.

[1] M. Chodorow and M. F. Manning, Phys. Rev. **52**, 731 (1937).
[2] L. Pauling, Phys. Rev. **54**, 899 (1938).

6. Thermal Expansion, Compressibility, and Electronic Polarizability of Ionic Crystals. KASIMIR FAJANS, *University of Michigan.*—Deviations from additivity of the Lorentz-Lorenz refraction and other properties of ionic substances have demonstrated[1] the tightening (decrease of refraction, polarizability, size) of electronic shells of anions in the field of cations and loosening (increase of refraction, etc.) of the shells of cations in the field of anions. The expansion coefficients of alkali halides increase, contrary to the expectations of the electrostatic lattice theory of rigid ions, from lithium to rubidium salts.[2] This can be explained if one takes into account that the increase of interionic distance with temperature causes a diminution of the tightening of the anion, i.e., an increase of its size. Since the tightening effect is stronger in the cesium chloride than in the sodium chloride structure, one can also understand why the expansion coefficients of cesium halides are larger than those of other alkali halides. The compressibility of analogous ionic crystals increases parallel to their electronic polarizability.[3] There is, however, a marked deviation from proportionality which shows that the tightening of the electronic shells due to interionic forces diminishes the compressibility. In accord with this, the compressibility is smaller for the cesium chloride than for the sodium chloride structure.

[1] K. Fajans and G. Joos, Zeits. f. Physik **23**, 1 (1924). K. Fajans, J. Chem. Phys. **9**, 281, 378 (1941).
[2] K. Fajans and H. G. Grimm, Zeits. f. Physik **2**, 308 (1920).
[3] W. A. Wooster, *Text-Book on Crystal Physics* (Cambridge, 1938).

7. On the Proof of the Maxwell-Boltzmann Distribution Law. MING-CHEN WANG, *University of Michigan.*—Part of the purpose of the H theorem of Boltzmann is to prove that the Maxwell-Boltzmann distribution law is the *only* stationary solution of the Boltzmann equation. Recently Halpern and Doermann[1] have tried to prove the same fact without introducing the H function. In this proof they made use of the principle of microscopic reversibility, which in the classical theory is only valid for spherical molecules. It will be shown that this restriction is not necessary. By making use of Boltzmann's concept of cycles of critical constellations, the proof can be simplified and extended to the general case of non-spherical molecules.

[1] Halpern and Doermann, Phys. Rev. **55**, 1077 (1939).

8. Finite Self-Energies in Radiation Theory. ALFRED LANDÉ AND L. H. THOMAS, *Ohio State University.*—The Maxwell-Yukawa field theory of the point electron[1] can be derived from a Lagrangian function, according to F. Bopp, with linear field equations for the Maxwell field D, H and the Mie field E, B. Although the energy density is not positive definite there is no conflict with general principles in this unitary theory since force and work along the path of the electron vanish identically. So there is no accumulation of energy on the electron, even if the latter vibrates with frequency $\nu > c/r_0$ (r_0 = electronic radius) in spite of negative energy carried by the Yukawa waves. Moreover one can devise a scheme of transitions with positive probabilities so that the energy of the pure radiation field becomes positive, and yet correspondence with the classical Maxwell-Yukawa emission process is maintained. This scheme of transitions leads to a positive Yukawa radiation density for $\nu > c/r_0$ in addition to Planck's density of the Maxwell radiation.

[1] Developed in Phys. Rev. **60**, 514 (1941).

9. The Self-Energy of the Electron. L. H. THOMAS AND ALFRED LANDÉ, *Ohio State University.*—The theory of the interaction of electrons with the electromagnetic field may be modified by introducing an additional field of Yukawa type carrying negative energy.[1] The electrons may be supposed to satisfy Dirac's equation, initially for zero rest mass; and the fields may be supposed quantized, with longitudinal as well as with transverse waves. If a positron-electron theory is built up by second quantization, the longitudinal waves may be separated, leaving a rest mass, finite by cancellation of infinite terms between the electromagnetic and Yukawa quanta. Second-order perturbation theory (following Weisskopf) then gives zero contribution to the self-energy and momentum of the electron from the transverse waves.

[1] See Alfred Landé and L. H. Thomas, "Finite self-energies in radiation theory," preceding abstract.

10. The Internal Temperature-Density Distribution of Sirius A. G. BLANCH AND A. N. LOWAN, *New York City*, R. E. MARSHAK, *University of Rochester* AND H. A. BETHE, *Cornell University.*—Following the procedure adopted for the sun[1] the Mathematical Tables Project, W. P. A., New York City, has integrated the star equations for Sirius A, another well-known star of the main sequence. Expressed in solar units, the mass, luminosity, radius of Sirius A are 2.34, 38.9, 1.78, respectively. The point-convective model is used as before, but Morse's[2] improved tables of the opacity coefficient replaces Strömgren's. Account is taken of the scattering opacity which becomes as much as 17 percent of the absorption opacity at the boundary of the convective core. A hydrogen content of 35 percent by weight gives fairly close fitting of the radiative envelope to the convective core, and leads to a central temperature of $29.5 \cdot 10^6$ degrees C and a central density of 37 g/cm^3. In agreement with the solar calculation, the hydrogen content does not differ from the value found with the Eddington standard model whereas the central temperature and density are considerably higher than the corresponding Eddington values. This agreement between the calculations for the sun and Sirius A is especially striking since Morse's values of the opacity are uniformly lower than Strömgren's—sometimes as much as 50 percent.

[1] Blanch, Lowan, Marshak and Bethe, Astrophys. J. **94**, 37 (1941).
[2] P. M. Morse, Astrophys. J. **92**, 27 (1940).

11. The Theory of Hydrogen Three. H. FESHBACH, *Massachusetts Institute of Technology.*—The effect of including tensor forces in the theory of H^3 has been considered. As is known, beside the $^2S_{\frac{1}{2}}$ state, the ground state also contains $^4D_{\frac{1}{2}}$, $^2P_{\frac{1}{2}}$, $^4P_{\frac{1}{2}}$ terms. There are two S states and three D states. Representations of all these have been found in Eulerian coordinates.[1] With a technique similar to Rarita and Schwinger,[2] representations have now been found in terms of operators acting on the most important $^2S_{\frac{1}{2}}$ state. The problem has been reduced to that of three coordinates in the plane of the three particles by integrating over the Eulerian angles, making use of these representations. This has been done for both exchange and non-exchange forces. The most important states turn out to be the S and D states which are anti-symmetric with respect to the exchange of two like particles, as far as their dependence on both spin and Eulerian angle is concerned. This work opens the way for an application of the James-Coolidge method to the problem.

[1] G. Breit, Phys. Rev. **35**, 569 (1930).
[2] W. Rarita and J. Schwinger, Phys. Rev. **59**, 436 (1941).

12. The Application of the W.K.B. Approximation to the Radial Dirac Equations for the Hydrogen Atom. G. E. UHLENBECK AND R. J. BESSEY, *University of Michigan.*—Following the method of Pauli, we have applied the W.K.B. approximation to the radial Dirac equations for the hydrogen atom. For the discrete spectrum this leads exactly to the Sommerfeld fine structure formula. In contrast to the unrelativistic case, the whole integer total quantum numbers and the behavior of the wave functions near the origin are given automatically right. For the continuous spectrum, the W.K.B. solutions yield, besides the correct behavior at the origin, the correct phases for $r \to \infty$.

13. On the Theory of the Internal Conversion of Gamma-Radiation. R. J. BESSEY, *University of Michigan.*—One easily derives from the Dirac equations an expression for the internal conversion coefficient of gamma-radiation in terms of a number of radial integrals. This can be done for both the K and L shells, and for arbitrary order of either electric or magnetic multipole radiation. By approximating the radial integrals one can obtain expressions in closed form, most of which have been derived in the literature by independent methods. A comparison of the numerical results for the K and L conversion coefficients and their ratio, which are given by these approximations, will be presented for the case of indium ($Z=49$, gamma-ray energy $=336$ kv). This shows that in this region, especially for the conversion coefficients themselves, more exact calculations are needed.

14. Radioactive Isotopes of Praeseodymium. J. W. DEWIRE, M. L. POOL AND J. D. KURBATOV, *Ohio State University.*—The 3.5-minute and 19-hour periods previously obtained by neutron bombardment of praeseodymium and assigned to Pr^{140} and Pr^{142}, respectively,[1,2] have been further studied. The 19-hour period has been formed by the action of alpha-particles on lanthanum, protons on cerium, and deuterons on praeseodymium. From the deuteron bombardment, a half-life of 19.3 ± 0.1 hours was obtained from observations extending over 16 half-lives. Determinations of the half-life from the other bombardments were in good agreement with this value. When studied with a magnetic spectrometer of the 180° focusing type, the Pr^{142} electron spectrum was found to be simple and had an endpoint of 2.14 ± 0.02 Mev. This is in fair agreement with the 2-Mev endpoint recently reported by Wu and Segrè at the Stanford meeting. A weak gamma-ray of about 1.9 Mev was found to be associated with this period. The ratio of the number of beta-rays to gamma-rays emitted was about 25. Praeseodymium bombarded with fast neutrons gave a 3.4 ± 0.1-minute positron period. The beta-ray spectrum from cloud chamber measurements will be shown.

[1] M. L. Pool and L. L. Quill, Phys. Rev. **53**, 437 (1938).
[2] J. K. Marsh and S. Sugden, Nature **136**, 102 (1935).

15. A Voltage Stabilizer for a D.C. Generator. W. M. SCHWARZ, *The Ohio State University.*—A very simple voltage stabilizer has been developed for use on the generator supplying the magnetic field of the Ohio State University cyclotron. It consists essentially of a power tube used as a variable shunt resistor across the generator field coils. The current in this power tube is determined by the generator output voltage, the variations of which are amplified by a direct coupled amplifier. Thus the control unit is of comparatively low power, since it is required to handle a current that is only a small fraction of the size of the total generator field current. The control obtained has been found to be quite adequate, and is of the order of one part in 2000. Except for a short warming up period, no difficulty with drift has been observed. Probably because of exceedingly stable thermal conditions in the magnet coils of the cyclotron, auxiliary current stabilization has not been found necessary.

16. A.C. Resonant Pendulum Without Iron. DAVID K. WEIMER AND HAROLD P. KNAUSS, *Ohio State University.*—An iron pendulum bob has its motion maintained if it swings toward and away from a solenoid which is part of a circuit tuned to resonance at power line frequency, the tuning being adjusted when the bob is away from the solenoid. That the maintenance of this motion does not depend on non-linear magnetic properties of iron is shown by substituting for the bob a second coil suspended coaxially with the first so that it can swing toward or away from it. The two coils are connected in series so that they attract each other, and in series with them is connected a condenser chosen to produce resonance at power-line frequency with the coils separated. The maintenance of motion is ascribed to the time lag in reaching the steady-state current corresponding to the instantaneous self-inductance at any phase of the motion. Thus the current and the attractive force are larger[1] when the coils approach than when they recede.

[1] Weimer, Phys. Rev. **60**, 65A (1941).

17. Solar Influence on Cosmic-Ray Intensity. JAMES W. BROXON, *University of Colorado.*—As reported,[1] an inverse relation between cosmic-ray intensity and international magnetic character was established by Chree's method. Similar procedure has been followed, with total sunspot area replacing magnetic character, selected days still being determined by cosmic-ray intensity. In general agreement with Graziadei and Kolhörster, an essentially inverse relation was found. For instance, a negative sunspot pulse was associated with the cosmic-ray positive primary pulse. The sunspot pulse peaks preceded the cosmic-ray primary peaks by three or four days, however. It is noted that a serious objection by Forbush to Vallarta and Godart's[2] explanation of 27-day cosmic-ray fluctuations in terms of direct influence of heliomagnetism would be removed if sunspot magnetic moments were sufficiently great. Simple estimates of magnitudes in conjunction with their computations indicate these moments are somewhat too small. The phase lead of sunspot relative to cosmic-ray pulses might be associated with the supposed solar emission of charged particles contributing to terrestrial ring currents.

[1] J. W. Broxon, Phys. Rev. **59**, 678 (1941).
[2] M. S. Vallarta and O. Godart, Rev. Mod. Phys. **11**, 180 (1939).

18. A New Cosmic-Ray Geomagnetic Relation. FOSTER EVANS, *University of Colorado.*—Previously it has been shown that if the primary cosmic radiation consists of charged particles predominantly of one sign, there is set up in the vicinity of the earth a radial current caused by the motion of slow interstellar electrons. By including the effect of the earth's magnetic field it is found that in addition to being acted upon by a radial field the interstellar electrons will move under the influence of equivalent electric fields at right angles to the radial direction in planes parallel to the plane of the magnetic equator. There results a continuous series of spherical shells of current, concentric with the earth, of current density proportional to the cosine of the latitude. If cosmic rays consist only of positively charged particles these current shells produce a magnetic field which augments the earth's field. Hence, if cosmic-ray intensity is changed by anything other than terrestrial magnetic disturbance, this change will *produce* a magnetic disturbance at the earth's surface. It is shown that the ratio $(\Delta I/I)/(\Delta H/H)$ for this type of simultaneous change in cosmic-ray intensity and horizontal component of the earth's field is positive and of the same order of magnitude as observed experimentally.

19. The Mercury Arc Cathode. CHARLES G. SMITH, *Raytheon Mfg. Co., Newton, Mass.*—Conduction electrons in the liquid at the arc spot are considered to be selectively heated to about 4000°K by electronic bombardment from the vapor while the atomic structure is at about 150°C. Thermionic emission yields the arc current plus the return current from the vapor. Observations upon velocity of an arc spot pushed around a circular mercury track by a radial magnetic field show that for fields below approximately 5000 gauss, velocity is proportional to field, is in a direction opposite to the ponderomotive force, and has a negative temperature coefficient. The phenomena are interpreted as due to the Righi-Leduc effect operative in the thin layer of hot conduction electrons of the liquid. The velocity was calculated and the vertical thermal gradient deduced treating the Righi-Leduc effect as a thermomotive force. Arcs were extinguished by current pulses of 10^{-7} sec. superposed upon and in the same direction as the arc current. From these observations the energy content of the excited layer of electrons was evaluated, and therefrom the thermal gradient found. The independent estimates reveal it to be about 4×10^{8} degrees per cm. The Thomson heat counteracts losses along this gradient.

20. Pressures and Temperatures in High Pressure Mercury Lamps. CARL KENTY, *Lamp Development Laboratory, General Electric Company.*—Operating pressures in the H-type mercury lamps have been measured under a variety of conditions with quartz membrane manometers.[1] If L is the input to the lamps in watts per centimeter of arc length, m is the weight of Hg per centimeter in milligrams, and d is the diameter in millimeters, the observed pressure P in atmospheres can be represented approximately by the formula $P\leqq 95(m/d^2)(L^{\frac{1}{4}}/d^{0.1}m^{0.1})$. The average temperature, T_a, of the vapor being proportional to P and inversely to m/d^2 can be represented by $T_a \leqq 1800(L^{\frac{1}{4}}/d^{0.1}m^{0.1})$. Knowing the radial temperature distribution of a single lamp,[2] the values of T_a for other lamps, permits the approximation of their radial temperature distribution, and hence, also of their light and current distributions.

[1] Carl Kenty, Rev. Sci. Inst. **11**, 377 (1941).
[2] Carl Kenty and W. J. Karash, Phys. Rev. **60**, 66A (1941).

21. Self-Broadening and Foreign Gas Broadening in the Infra-Red Absorption Spectrum of HCN. H. M. FOLEY, *University of Michigan.*—The shapes of twenty lines in the 14μ absorption band of HCN have been examined with high resolution at a series of pressures up to 58 cm Hg. With 2-cm pressure of HCN the lines have also been measured with pressures of HCl present as a foreign gas perturber. In both cases the perturbing interaction is between polar molecules of known dipole moments, and thus form an especially favorable case for comparison of the observed absorption coefficient with the values given by the theory of pressure broadening. The observed intensity of transmission through the gas, $I(\nu)$, is related to the absorption coefficient, $\alpha(\nu)$, by

$$I(\nu)=\int_{-\infty}^{+\infty} d\nu' \rho(\nu-\nu') e^{-\alpha(\nu')l},$$

where l is the path length in appropriate units, and $\rho(\nu-\nu')$ is a function giving the spreading effect of the slit width. By numerical solution of this integral equation the absorption coefficient was obtained as a function of the frequency. The shapes of the lines and the shifts are compared with the theoretical results derived by Dr. D. M. Dennison and the author.

22. A Comparison of Certain Infra-Red Bands in C_2H_6, C_2D_6 and C_2H_5D. L. R. POSEY AND E. F. BARKER, *University of Michigan.*—The low frequency perpendicular fundamental in C_2H_6 which occurs at 821 cm^{-1} consists of a sequence of Q branches spaced approximately 2.6 cm^{-1} apart. Except for slight variations due to proton spin the intensities decrease regularly in either direction from the strongest line at 822 cm^{-1}. The corresponding band in C_2D_6 is found near 595 cm^{-1} with a spacing of about 1 cm^{-1} between lines. In C_2H_5D, due to the departure from axial symmetry, the degeneracy is removed and the band pattern is very different. A strong central maximum appears at about 804 cm^{-1} with a set of Q branches on either side having rather low intensities near the center. A second perpendicular band in C_2H_6 occurs at 1463 cm^{-1}. The analogue in C_2D_6 is found at about 1065 cm^{-1}, with a more intense parallel band superposed upon it. The latter has a remarkably broad central maximum extending from 1060 to 1078 cm^{-1}. In C_2H_5D the corresponding perpendicular band is split into two rather widely separated components, of which the more intense lies near 1450 cm^{-1}. The less intense component appears at approximately 1300 cm^{-1}, and it also is partially obscured by a parallel band whose strong Q branch is observed at 1301 cm^{-1}.

23. Fluorescence and Absorption Spectra of Hydrogenated Chlorophyll *a*. H. V. KNORR AND V. M. ALBERS, *Antioch College.*—A solution prepared by dissolving 13.8 mg of chlorophyll *a* in 60 cc of ether, with an additional 100 mg of platinic oxide, was hydrogenated under an average pressure of 48 lbs./in.[2] The hydrogenation extended over a twenty-four hour period. The fluorescence spectrum of the hydrogenated chlorophyll *a* in ether and under an atmosphere of hydrogen was photographed by a method previously described.[1] The positions and relative intensities of the principal bands have been measured. There are three principal bands located at 687, 662, and 628 mμ. The band at 628 mμ vanishes after three hours of irradiation when an additional band located at 620 mμ appears and gradually increases in intensity during the remainder of the twenty-five hours of irradiation. The 687-mμ band decreases in intensity and vanishes after ten hours of irradiation when a new band appears at 690 mμ. During the remainder of the irradiation period the intensity of the long wave-length bands decrease. Absorption curves were obtained for the original hydrogenated chlorophyll *a*, and for the final photodecomposed product.

[1] H. V. Knorr and V. M. Albers, Cold Spring Harbor Symposia on Quantitative Biology **3**, 98–107 (1935).

24. The Problem of Determining a Standard for Chlorophyll Preparations. V. M. ALBERS AND H. V. KNORR, *Antioch College.*—In order to maintain proper controls in experiments using chlorophyll in medicine and other applications, it is desirable to have some convenient means of determining the concentration of the chlorophyll components in a given preparation and also of determining whether the chlorophylls present in two different preparations are actually the same. Absorption coefficient data published by different observers show wide divergence, but the methods of preparation used by these observers have also been different. Few of these observations have been accompanied by any chemical analyses and only one has been accompanied by a complete chemical analysis. A large number of chlorophyll preparations have been made in our laboratory by using different methods of preparation of the pure components. The results of the studies on these preparations indicate that samples on which absorption coefficient measurements are to be made should be subjected to careful chemical analyses to determine the percentage composition of carbon, hydrogen, nitrogen, and magnesium and also to be certain that part of the magnesium has not been replaced by another metal.

25. Valence and Central Forces in the Water Vapor Molecule. ROBERT R. NEWTON AND W. H. SHAFFER, *Ohio State University.*—Appropriate generalized coordinates have been selected for describing the vibrations of bent symmetrical XY_2 molecules for valence and central forces. In terms of these coordinates the most general forms of the quadratic and cubic parts of the potential energy function have been set up and relations have been obtained giving the force constants in these expressions in terms of those occurring in the corresponding normal coordinate expressions. These relations are applied to the data obtained by Darling and Dennison[1] on the water vapor molecule and the values of the force constants have been computed for both valence and central force type functions. The results indicate that the usual valence force approximation is better in the case of H_2O than the central force approximation as regards both the quadratic and the cubic terms in the potential energy function. The results also suggest a possible type of approximation which could be made to reduce the number of constants occurring in the cubic part of the potential function of a polyatomic molecule.

[1] B. T. Darling and D. M. Dennison, Phys. Rev. **57**, 128 (1940).

26. Bond Energies in COOH and COHN Dimers, Indicated by Ultraviolet Absorption Bands. GLADYS A. ANSLOW, *Smith College.*—The interpretation of ultraviolet absorption bands in organic molecules follows from assumption of dimer structure for some of the carboxylic and $-COHN-$ molecules with the consequence that dissociation is affected by the rupture of two dimer bonds in a single photon hit. Resulting spectroscopic values of bond energies agree with thermochemical and emission band values for dissociation. Thus, the 230–200-mμ absorption by aliphatic amino acids[1] results from breaking an O−H bond and an O···H bridge. In COHN dimers the two bands near 280 mμ[2] may result from a 2 C−N and a C−N and C−C combination, the energies indicating stretching of the bonds. The C−C bond energies in the tyrosine and tryptophane rings correspond to longer bond lengths than in the C_6H^5's of phenylalanine and COHN dimers or in aliphatic chains. Alkaline solvents

decrease the O−H···O energy in carboxylic dimers and the C−C energies in tyrosine, but not materially the C−N and C−C energies in tryptophane, phenylalanine and the COHN dimers. C−O, N−H, C−H, S−H and S−S bond energies have been identified.

[1] G. A. Anslow and M. L. Foster, J. Biol. Chem. **97**, 37 (1932); G. A. Anslow, M. L. Foster, and C. Klingler, *ibid.* **103**, 81 (1933).
[2] G. A. Anslow and S. C. Nassar, J. Opt. Soc. Am. **31**, 118 (1941).

27. Bond Energies in Some Protein Fabrics and Side Chains. GLADYS A. ANSLOW, *Smith College.**—The lower energy component of the peptide bands[1] may be caused by the rupture of two C−N bonds by a single photon. The low energy side of the other component may result from the dissociation of a C−N and a C−C bond, the other side to two C−C's. Strong absorption in all proteins studied at 242 mμ may indicate the dissociation of C−H···O groups, existing between side chains and the solvent. Absorption near 230 m is attributed to C−O accompanied by C−C ruptures. These absorption regions are shifted to lower energies in alkaline solvents. Since two of the C−N and C−C bonds are broken simultaneously, a fabric structure theory of the protein is more probable than a long chain polypeptide chain theory. The original Wrinch[2] cyclol fabric theory appears to be supported by the alkaline shift of the peptide bands, the existence of C−O bonds, and the probable non-existence of a N−H group. If the latter exists, C−N bands should not show alkaline shifts, (compare tryptophane and COHN dimer effects[3]), and a narrow band, found at 339 mμ in COHN dimers, should appear.

* To be called for after Paper No. 26, Session C.
[1] G. A. Anslow and S. C. Nassar, J. Opt. Soc. Am. **31**, 118 (1941).
[2] D. Wrinch, Proc. Roy. Soc. **A160**, 59 (1937).
[3] Paper No. 26.

28. The Performance and Calibration of a Recording Infra-Red Spectrometer. ROBERT A. OETJEN, CHAO-LAN KAO AND H. M. RANDALL, *University of Michigan.*—This infra-red spectrograph was described by Randall and Strong in 1931. The collimating mirror has a focal length of 50 cm and the faces of the 60° NaCl prism are 80 by 100 mm. The spectrum of the 10μ NH_3 band shows that those fine structure lines having separations of 3 cm^{-1} are resolved, but lines are unresolved where the separation drops to 1.8 cm^{-1}. Judged by this practical test its resolution equals that of any prism recorder so far described. Sharp symmetrical lines can be located with a reproducibility of 0.003μ at 5μ to 0.001μ at 15μ if appropriate corrections for changes in temperature of the prism are made. The bands of water vapor at 6μ, of ammonia at 10μ, and CO_2 at 15μ have been completely remeasured with a grating instrument of high precision, whose resolution is made to equal that of the prism recorder in each of the three regions. For the purpose of calibration, over 150 standard absorption lines quite uniformly distributed between 5 and 15μ are thus obtained, which leads to an accuracy of measurement by the prism recorder essentially equal to that of the grating measurement, 0.005μ at 5μ and 0.003μ at 15μ.

Author Index to Abstracts of the Michigan Meeting

Albers, V. M.—see Knorr, H. V.
—— **and H. V. Knorr**—No. 24
Anslow, Gladys A.—Nos. 26 and 27
Anthony, R. L.—see Caston, R. H.
Barker, E. F.—see Posey, L. R.
Bessey, R. J.—No. 13
—— see Uhlenbeck, G. E.
Bethe, H. A.—see Blanch, G.
Blanch, G., A. N. Lowan, R. E. Marshak and H. A. Bethe—No. 10
Broxon, James W.—No. 17
Caston, R. H., R. L. Anthony, and E. Guth—No. 2
DeWire, J. W., M. L. Pool and J. D. Kurbatov—No. 14
Evans, Foster—No. 18
Fajans, Kasimir—No. 6
Feshbach, H.—No. 11
Foley, H. M.—No. 21
Gehman, S. D.—No. 1
Greene, J. B. and Millard F. Manning—No. 4
Guth, E.—see Caston, R. H.
—— see Mullin, Charles J.
Kao, Chao-Lan—see Oetjen, Robert A.
Kenty, Carl—No. 20
Knauss, Harold P.—see Weimer, David K.
Knorr, H. V.—see Albers, V. M.
—— **and V. M. Albers**—No. 23
Kurbatov, J. D.—see DeWire, J. W.
Landé, Alfred—see Thomas, L. H.
—— **and L. H. Thomas**—No. 8
Lowan, A. N.—see Blanch, G.
Manning, Millard F.—No. 5
—— see Greene, J. B.
Marshak, R. E.—see Blanch, G.
Mullin, Charles J. and Eugene Guth—No. 3
Newton, Robert R. and W. H. Shaffer—No. 25
Oetjen, Robert A., Chao-Lan Kao and H. M. Randall—No. 28
Pool, M. L.—see DeWire, J. W.
Posey, L. R. and E. F. Barker—No. 22
Randall, H. M.—see Oetjen, Robert A.
Schwarz, W. M.—No. 15
Shaffer, W. H.—see Newton, Robert R.
Smith, Charles G.—No. 19
Thomas, L. H.—see Landé, Alfred
—— **and Alfred Landé**—No. 9
Uhlenbeck, G. E. and R. J. Bessey—No. 12
Wang, Ming-Chen—No. 7
Weimer, David K. and Harold P. Knauss—No. 16